COLLEGE OF AGRICULTURE, ENGINEERING AND SCIENCE

IMPLEMENTATION OF CFD AND REMOTE SENSING TECHNOLOGY TO INVESTIGATE THE SUITABILITY OF TELECOMMUNICATION MAST FOR WIND RESOURCE ASSESSMENT IN SOUTHERN AFRICA

Maduako Emmanuel Okorie

211560648

Thesis submitted in fulfilment of the requirements of the award of the degree of Doctor of Philosophy in Mechanical Engineering

Supervisor

Prof. Freddie L. Inambao

15th December 2021

Supervisor's Declaration

"As the candidate's academic supervisor, I agree to the Submission of this Thesis."

Prof. Freddie L. Inambao ----- -----

Name of Supervisor Signature

Declaration 1 – Plagiarism

I, Maduako Emmanuel Okorie, declare that.

1. The research reported in this thesis, except where otherwise indicated, is my original research.

2. This thesis has not been submitted for any degree or examination at any other university.

3. This thesis does not contain other persons' data, pictures, graphs, or other information, unless specially acknowledged as being sourced from other persons.

4. This thesis does not contain other persons' writing, unless specially acknowledged as being sourced from other researchers. Where other written sources have been quoted, then:

    a. Their words have been re-written, but the general information attributed to them has been referenced.

    b. Where their exact words have been used, then their writing has been placed in italics and inside quotation marks and referenced.

5. This thesis does not contain text, graphics of tables copied and pasted from the internet, unless specially acknowledged, and the source being detailed in the thesis and in the reference's sections.

Signed: . . . ……Date …15/12/2021

Student No: 211560648

Declaration 2- Publications

The following papers have been published in the South African Department of Higher Education (DoHET) accredited journals.

1. M. E. Okorie and F. L. Inambao, "Tower wake distortion effect: A comprehensive review of methods and applications," *International Journal of Engineering Research and Technology*, vol. 13, no. 12, p. 17, 2020. http://www.irphouse.com/ijert20/ijertv13n12_02.pdf

2. M. E. Okorie and F. L. Inambao, "Identification of tower and boom-wakes using collocated anemometers and LiDAR measurement," *International Journal of Mechanical Engineering and Technology*, vol. 10, no. 6, pp. 72–94, Sep.2019.https://iaeme.com/MasterAdmin/Journal_uploads/IJMET/VOLUME_10_ISSUE_6/IJMET_10_06_005.pdf

3. M. E. Okorie and F. Inambao, "Prediction of the impact of tower shading on resource parameters and performance by using LiDAR," *International Journal of Engineering Research and Technology*, vol. 13, no. 11, p. 3125, Nov. 2020, doi: 10.37624/IJERT/13.11.2020.3125-3144. http://www.irphouse.com/ijert20/ijertv13n11_05.pdf

4. M. E. Okorie and F. L. Inambao, "Angle dependence of tower wake distortion: A parametric study," *International Journal of Mechanical and Production Engineering Research and Development*, vol. 11, no. 3, pp. 481–498, 2021, doi: 10.24247/ijmperdjun202138. http://www.tjprc.org/publishpapers/2-67-1621862211-IJMPERDJUN202138.pdf

5. M. E. Okorie and F. L Inambao, "Local wind flow modifications within the vicinity of a communication tower," *International Journal of Mechanical and Production Engineering Research and Development*, vol. 11, no. 3, pp. 421–440, 2021, doi: 10.24247/ijmperdjun202135.http://www.tjprc.org/publishpapers/2-67-1621326533-IJMPERDJUN202135.pdf

6. M. E. Okorie and F. L. Inambao, “Impact of freestream turbulence on the boom length,” *International Journal of Mechanical and Production Engineering Research and Development*, vol. 11, no. 4, pp. 341–354, 2021, doi:10.24247/ijmperdaug202126. http://www.tjprc.org/publishpapers/2-67-1626785833-IJMPERDAUG202126.pdf

In all the above listed papers, the candidate is the main author, while Prof. Freddie L. Inambao is the supervisor.

Signed: . . . . . .

Acknowledgements

Praise be to God Almighty for His kindness and love demonstrated upon my life. His grace is indeed sufficient for me and my family throughout the ups and downs encountered during my study.

My special thanks go to my supervisor Professor Freddie L. Inambao of the Discipline of Mechanical Engineering at the University of KwaZulu-Natal under who's supervision this research work was done. He is an easy-going person with great drive and initiative. His attitude, technical expertise and motivation has been a great inspiration to me. It is a great privilege to know him and to work under him. I lack the requisite words to express the depth of my gratitude. May God bless you and your family.

Most importantly my special gratitude goes to my ailing mother Christiana N. Okorie; My wife Chinonyelum Okorie; My sons: Chukwumerenka, Ogechukwu and Ihechukwu and all my siblings for their patience, love and support. Special thanks to my wife who put her own career on hold to take care of the boys freeing time for me to engage in my study. May God bless all of you.

I want to thank my employer, the Namibia University of Science and Technology for use of the university facilitates and resources for my research. I want to thank the Namibia Energy Institute (NEI), the Namibia Power Cooperation Limited (NamPower) and the Mobile Telecommunication Limited (MTC) for availing the resources needed for the National Wind Resource Assessment Project (NWRAP) of Namibia. I wish to thank my colleagues in the Department of Mechanical and Marine Engineering and colleagues from the Namibia Energy Institute for your supports. Thanks to Dr Richard Steele for proofreading and editing all the published journal articles.

Last but not the least, the support I received from the administrative staff of the Faculty of Engineering of the University of KwaZulu-Natal cannot go unnoticed. Thank you for the professionalism you have always demonstrated in dealing with distance learning students.

Abstract

The National Wind Resource Assessment Project (NWRAP) of Namibia is so far the most comprehensive wind measurement campaign in the country. Cost reductions and timescale for commencement of the project meant that the benefit afforded by the already existing lattice triangular communication towers belonging to Mobile Telecommunication Limited (MTC) Namibia was utilized. The towers were instrumented for wind data collection. Holistic evaluation of a site's winds (statistics and risk) requires placement of speed sensors at some intermediate heights of the tower. This arrangement introduces non-negligible errors to the reading of speed sensors due to tower shadowing, even where a dedicated mast erected for wind measurement is used. A lot of advances have been made with a well formulated mathematical expression by the International Electrotechnical Commission (IEC). The centreline velocity deficit expression guides the anemometer-to-tower separation distance in order to achieve the recommended industry-accepted accuracy of < 1 % errors of the free stream velocity. The method and assumptions used in deriving this expression is an impediment to its universal applicability to towers with different boom arrangements and construction details, especially when bulky communication towers with numerous secondary support structures are deployed for wind measurement. However, the angle dependence of tower shadowing, the impact of secondary support structures, the exact impact of free stream turbulence on boom lengths and the concept of safe angle range (i.e., the incident wind angles for which the boom length computed based on the IEC standard configuration [$\theta = 0°$] can effectively keep the speed sensors out of the tower wakes for winds that arrive at the tower within that defined angle range) are not yet fully resolved. This thesis combines field experimentations (anemometer and LiDAR measurement), numerical analysis (CFD derived flow distortion around the tower) and physical modelling of the tower structure to reasonably address the identified challenges to gain insight regarding the requisite instrumentation details in order to use the readily available communication towers for accurate wind measurement. To take a spot check on the resource at hub-height of interest, reduce shear extrapolation bias and uncertainty and enable independent description of the tower wake boundaries, a ground-based wind profiler Light Detecting and Ranging (LiDAR) was deployed. Also, to capture local flow modifications within the vicinity of the tower, the level of flow interference engendered by the presence of secondary support structures and evaluate the exact impact of the freestream turbulence on the boom lengths, CFD flow simulation over the complex 3D geometry of the towers were performed. Different approaches and parameters were used to identify the waked

direction sectors. The study revealed that the coefficient of determination (R^2) of turbulence intensities (TI) of the collocated speed sensors appear to be a better descriptor of the wake boundaries when compared to the commonly used traditional speed ratio approach. The study established that time series wind shear coefficient (WSC) computed from wind data measured at two intermediate heights (binned in ≤ 5° bin of the wind direction interval) located at approximately the same azimuth from the north, is enough to describe tower wake boundaries accurately without the need for a collocated speed sensor. A new approach to accurately calculate the solidity and the thrust coefficient is proposed based on the physical modelling of the tower structure. This study further combined physical modelling and numerical simulations to derive the values of thrust coefficient (C_{Ti}) and leg length (L_i) at different incident wind angles. The derived values of the parameters were incorporated into the IEC centreline velocity deficit expression to arrive at a modified speed deficit expression that can be used to predict the booms lengths at incident wind angles other than the IEC reference direction (θ = 0°). The study also proposed a safe angle range of θ = < ± 70º with respect to the boom configuration reference direction. This is applicable to the IEC standard boom configuration (i.e., θ = 0º) and when the boom is placed parallel to the face of the tower.

The study concludes that freestream turbulence does not have any significant impact on the boom length required to keep the speed sensors out of the tower wakes. However, it makes flow interference more complex within the regions near the wall of the tower, increases the drag on the tower, and engenders visible inhomogeneity on the flow parameters in the wakes of the tower. An accurate correction method that removes the need to discard wind data in the wake affected direction sectors during wind analysis is proposed. Finally, the study concludes that accurate tower instrumentation for wind measurements requires a combination of physical and numerical study, good understanding of the concept of safe angle range for proper boom installation, and knowledge of prevailing wind patterns at the site. The method proposed in this thesis may be applied successfully to accurately instrument lattice triangular towers of different construction details for wind measurement.

Key wards: Tower shadow, solidity, freestream turbulence, speed deficit and wind speed

Table of Contents

List of Figures

List of Tables

CHAPTER 1: INTRODUCTION

1.1 General introduction

The traditional approach to wind measurement requires the use of instrumented masts (lattice or tubular) for wind data collection. To evaluate the site shear trend, and by extension the envisaged project risk, the location of speed sensors is not confined to the top of the tower (preferred choice) (IEC standard), with some being placed at intermediate heights. Speed sensors located thus are inevitably exposed to tower shadowing, a phenomenon that is known to contribute a non-negligible uncertainty to the measured wind data [1]–[5]. As documented in [6], different methods have been applied to identify and define tower waked boundaries. IEC 61400-12-1 standard [1] contains a well-defined mathematical expression (the centreline velocity deficit expression) that enables the computation of boom lengths required to keep the speed sensors out of the tower wakes. The derivation of the mathematical expression was based on the standard boom configuration ($\theta = 0°$), i.e., a boom that is mounted perpendicular to the tower face. This implies that the incident winds are considered perpendicular to the same mast face, giving rise to velocity deficit values that are predicted using the upstream contour profiles of the modified flow along the same line with the boom. However, the common boom arrangement in many operational towers has been to fix the boom parallel to the face of the mast/tower. This means that wake distortion effects of winds that arrive at the tower at angles other than the reference direction ($\theta = 0^{o}$) may not be properly characterised. Again, instrumentation based on the [1] reference direction does not guarantee that wind observation is accomplished within the recommended industry-accepted accuracy of < 1 % errors between 0° and 360°. This points to a range of angles as it relates to the prevailing wind direction, for which the boom length obtained based on the IEC standard boom configuration ($\theta = 0^{o}$) is sufficient to keep the speed sensors out of the tower wakes.

This thesis combines wind data obtained from site experimentations (speed sensors and LiDAR measurement), CFD flow simulation and physical modelling of the communication tower to study wind flow characteristics around the tower in order to minimise error readings captured due to tower shadowing on the speed sensors mounted on them. Analysis of the observed data enables comparison, validation, identification, and description of the tower waked direction sectors, and the impact of tower shadowing on wind resource parameters and performance. The numerical analysis and physical modelling provide insight into boom length, the effect of secondary support structures, and angle dependence on tower shading. The concept of safe

angle range (the angle range at which boom lengths obtained based on the IEC standard boom configuration [$\theta = 0^{o}$] are long enough to keep the speed sensors out of the tower wakes) and the effect of free stream turbulence on the boom length are required to keep the speed sensor out of the tower wakes.

1.2 Background

The National Wind Resource Assessment Project (NWRAP) of Namibia was tasked with the provision of site representative wind data to enable the evaluation of wind climates of selected sites in Namibia. The formation of NWRAP was meant to bridge the gap that existed due to insufficiency of wind data of required quality and quantity suitable for wind power development. In [7] it was reported that existing wind data in Namibia were mainly for agriculture and meteorology purposes. In other to address the challenges, stakeholders, Mobile Telecommunications Limited (MTC), Gobabeb Research & Training Centre (GRTC), Namibia Power Corporation (NP) and Namibia University of Science and Technology (NUST) assembled under NWRAP in 2008. Between 2010 and 2012 [7], the terms of the cooperation were formalised in a contract. Under this project, wind measurements were done in eleven locations namely Amper-bo (25.354 °S, 18.313 °E), Gobabeb (23.551 °S, 15.051 °E), Helmeringghausen (25.880 °S, 16.828 °E), Kanas (26.775 °S, 17.473 °E), Korabib (28.548 °S, 17.820 °E), Lüderitz (26.709 °S, 15.368 °E), Okanapehuri (21.888 °S, 16.496 °E), Schlip (24.030 °S, 17.131 °E), Terrace Bay (19.993 °S, 13.040 °E), Warmbad (28.472 °S, 18.767 °E) and Walvis Bay (23.041 °S, 14.667 °E). Besides Gobabeb, Lüderitz and Walvis Bay where dedicated tubular masts are used, other NWRAP sites utilized the MTC lattice triangular communication towers of different construction details, instrumented for wind data collocation. Figure 1 is the location of the NWRAP sites. Specific to this study is that the MTC would permit the instrumentation of their existing communication towers for wind measurement and that NUST would manage NWRAP and provide the requisite technical and scientific work. The advantages afforded by the existing communication towers include cost reduction (eliminates cost of building dedicated mast and environmental impact assessment cost), timely commencement of the project (eliminates waiting time for approval by relevant authorities) and security of the equipment against vandalism since they will be located on a stand that is protected by MTC electrified palisade fencing that is remotely monitored [7]. The advantage afforded by these existing communication towers, does, however, come with the price of increased local flow modification within its vicinity. Other secondary support structures i.e., horizontal bracing, cross bracings, communication and lighting cable bundles, lighting, and

communication equipment, climbing ladders, etc, that are unique to the parent towers application, are likely to make flow interference more complex around and through the tower physical structure. Tower induced flow defects contribute a non-negligible uncertainty to the reading of speed sensors mounted. Due to the bulky nature of the tower coupled with numerous discrete members, flow perturbations are likely to be increased. This research study therefore combined different tools and strategies to investigate the suitability of using these communication towers for accurate wind measurement with emphases on tower instrumentation to reduce error readings captured by speed sensors due to their presence.

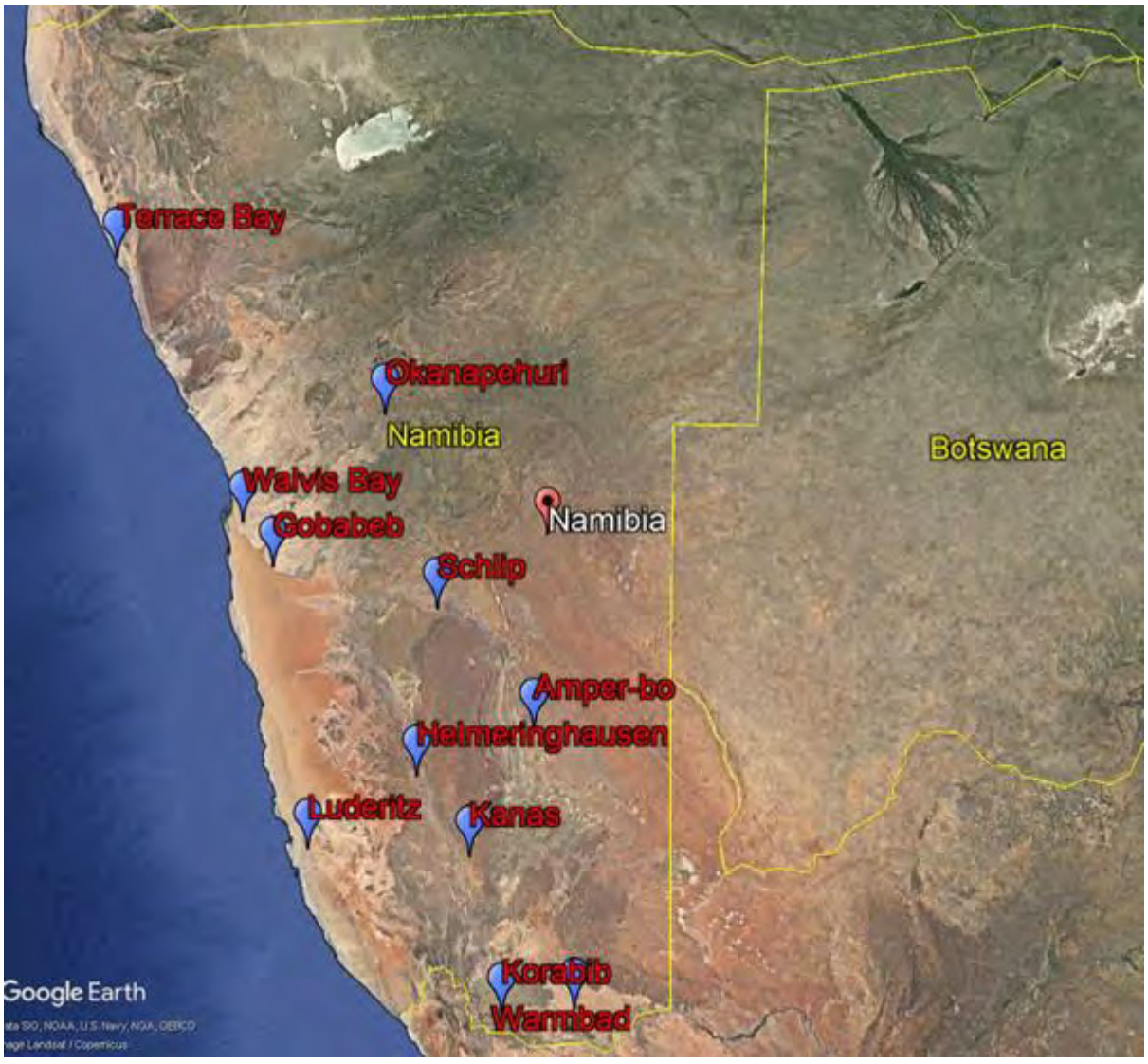

Figure 1. Location of NWRAP sites in Namibia

1.3 Tower Construction Details

The two broad categories of towers investigated were lattice triangular in nature. The locations are Amper-bo (25.354 °S, 18.313 °E), Schlip (24.030°S, 17.131°E) and Korabib (28.548 °S, 17.820 °E). Amper-bo and Schlip sites are desert-like with nearly homogeneous vegetation. They are class A terrain according to Annex B of (IEC 2005) as reported in [2] where brief construction details of the MTC tower used were also presented. The tower at Amper-bo and Schlip have almost the same configuration and are considered to have the same tower induced flow defects. Figure 1 shows the construction details of the tower at Amber-bo. The tower is 120 m high and L_m (centre-to-centre) of 1.10 m throughout the height. It is guyed and has an equilateral triangular cross-section with three vertical tubular mild steel rods of 100 mm external diameter (OD). The vertical tubular rods from repeating construction units which are joined end-to-end by flanged connections. Each construction unit is approximately 3.5 m, and each contains four modules of height 0.89 m. The network of small angular cross bracings made from 45 mm x 45 mm x 5 mm angle bars are bolted to a flat plate (0.045 m x 0.07 m) that is welded to the tubular rods. The boom has an OD of 50 mm and wall thickness of 2 mm and extends approximately 2.56 m away from the tower. The cable ladders and the cable bundles which cover almost half of the W to N (clockwise) facing side of the tower are some of the secondary support structures considered in this work.

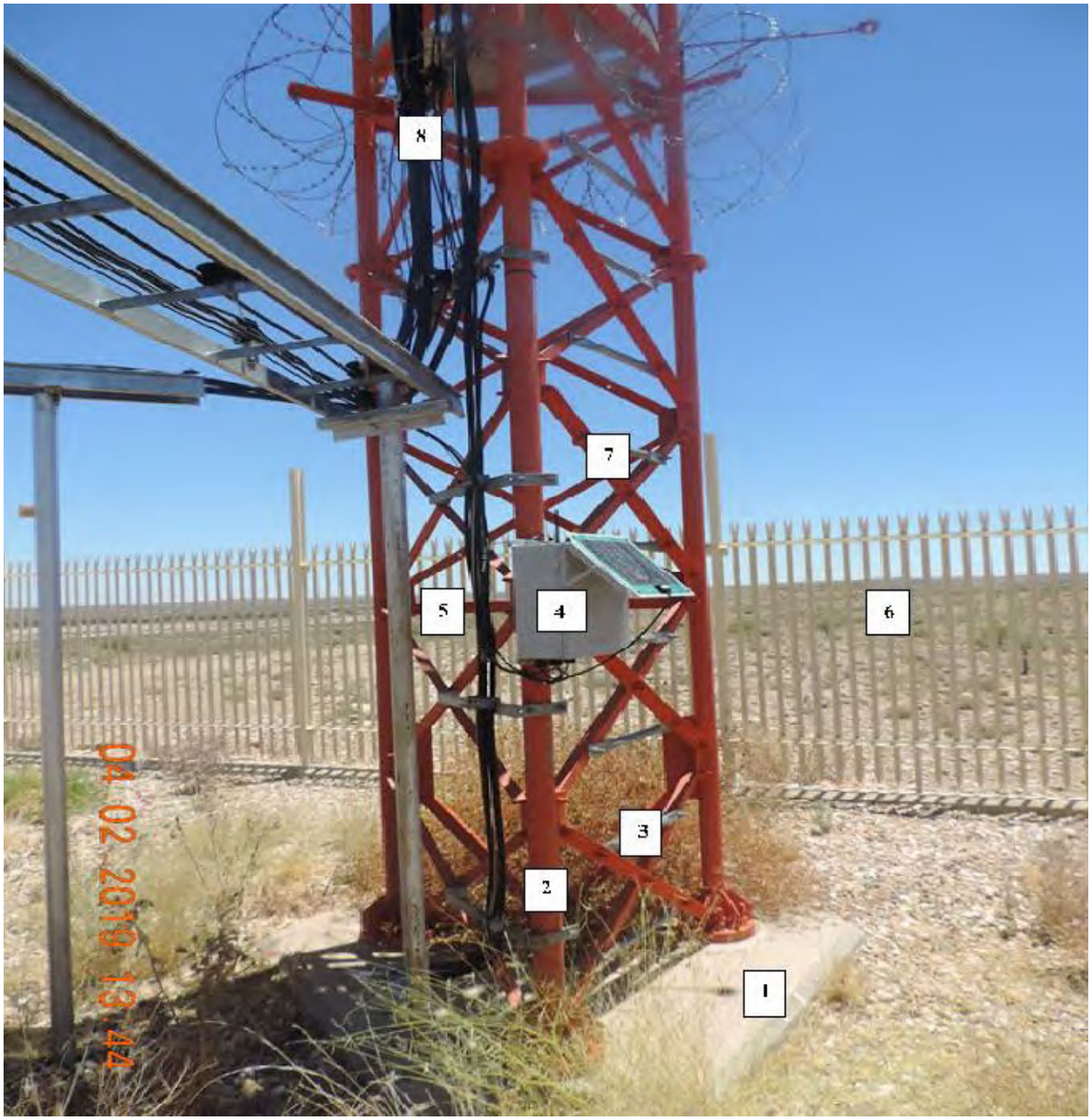

Figure 2. Construction detail of the lattice triangular communication tower used for wind measurement at Amper-bo. 1-Concrete base, 2-Vertical tubular rod, 3-Climbing ladder, 4-Data logger, 5-Horizontal bracing, 6 Palisade fence, 7-Cross bracing, 8-Communication, and lighting equipment cable bundles.

The tower at Korabib is guyed (Figure 2). It is 120 m high and L_m (edge-to-edge) is 1.320 m all through the height. It has an equilateral triangular cross-section with three vertical angle bars (70 mm x 70 mm x 6 mm) made from mild steel. The 70 mm x 70 mm x 6 mm angle bars form repeating construction units which are bolted together using flat plate connections (Figure 2). Each construction unit is 3.024 m, and each contains two modules of height 1.512 m. The network of small angular horizontal and cross bracings made from 60 mm x 60 mm x 5 mm

angle bars are bolted to a flat plate (0.144 m x 0.26 m) that is fixed to the vertical angle bar. The detail of the boom construction and the separation distance from the tower is the same at Amper-bo. The cable bundles and ladder located W to N (clockwise) on the facing side of the tower are the secondary support structures.

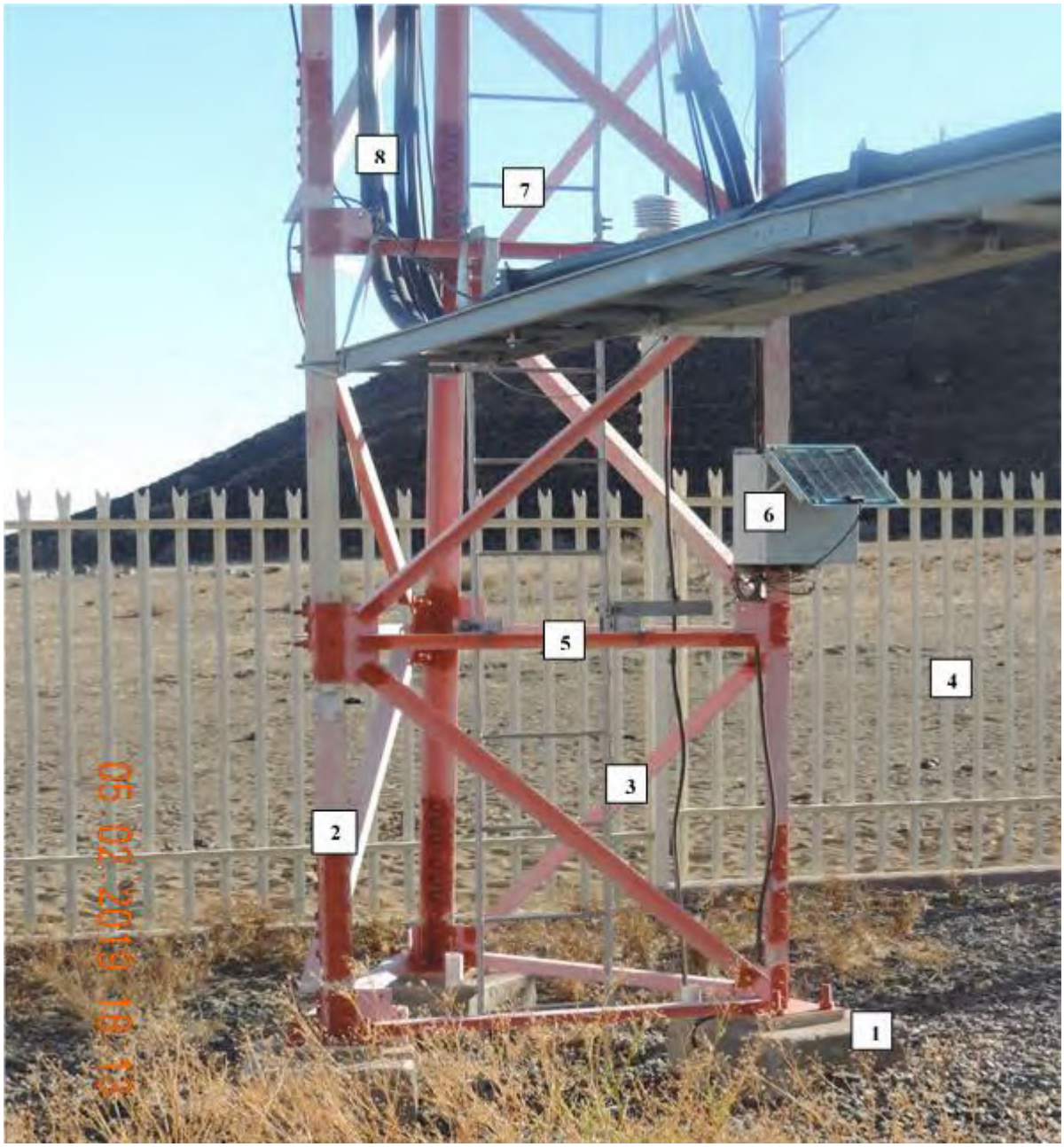

Figure 3. Construction detail of the lattice triangular communication tower us for wind measurement at Korabib. 1-Concreting base, 2-vertical angle bar, 3-Cross bracing, 4-Palisade fence, 5-Horizontal bracing, 6-Data logger, 7-Climbing ladder and 8-Communication, and lighting equipment cable bundles.

The IEC 61400-12-1 standard [1] prescribes a standard boom configuration (θ = 0°) i.e., a boom that is located perpendicular to the tower face. The centreline velocity deficit expression which enables the computation of the requisite boom length was derived on this premise. The implication is that the incident wind is considered perpendicular to the same mast face, giving rise to velocity deficit values that are predicted using the upstream contour profiles of the modified flow around the tower. Contrary to the IEC recommendations, the booms that hold the speed and direction sensors at sites of this study were fixed parallel to the face of the tower (Figure 3).

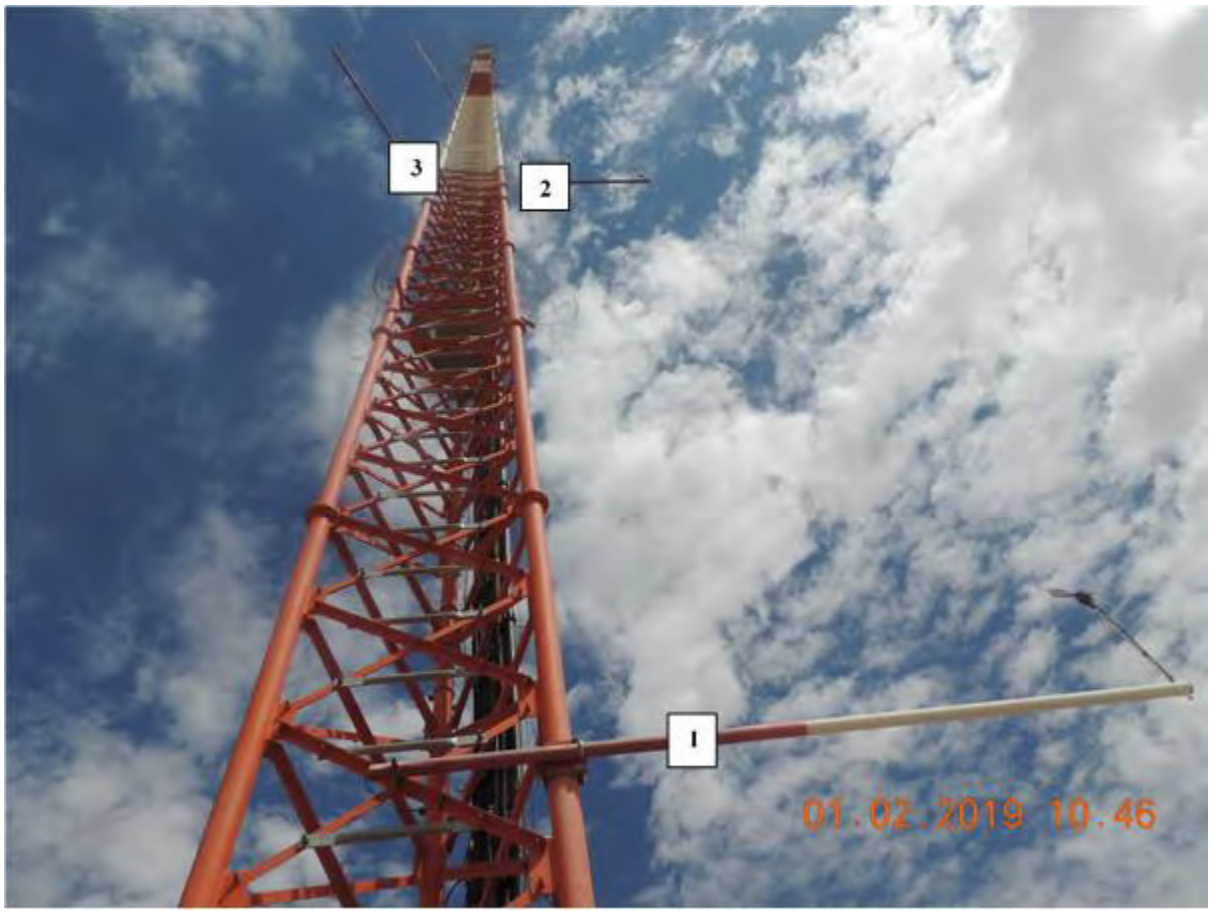

Figure 4. Common boom arrangement of the communication towers investigated. The booms are mounted parallel to the face of the tower. 1-wind direction sensor boom, 2-and 3-Collected speed sensors at some intermediate height.

1.4 Light Detecting and Ranging (LiDAR)

To take a spot check on the resource (wind speed, wind shear, veer, turbulence etc.) at any hub-height of interest and to reduce shear extrapolation bias and uncertainty, a ground-based wind profiler Light Detecting and Ranging (LiDAR) was deployed. The deployment of LiDAR enabled independent verification of the boundaries of tower waked direction sectors in this context. QinetiQ Ltd (UK) ZelphIR (Z300) LiDAR was provided by Masdar Institute of Technology Abudabi, United Arab Emirates (UAE), through the International Renewable Agency (IRENA) Abudabi. Concerns of vandalism and damage by wild animals constrained the installation of LiDAR to the fenced area. It was placed approximately 2.4 m away from the foot of the tower. The instrument used was a homodyne continuous wave (CW) Doppler wind LiDAR system with 10 user programmable heights (beside a pre-fixed height of 38 m) up to 200 m, though 300 m may be selected. The minimum measurement height is 10 m. The Z300 is specifically designed for autonomous wind assessment campaign purposes where wind speed is measured by doppler shift effect [8]. Figure 4 shows the Z300 used for wind measurement and Figure 5 shows the scanning technique [9].

Table 1 is a summary of the specifications of the Z300 with emphasis on operation, performance, and safety.

Figure 5. Z300 deployed for wind measurement.

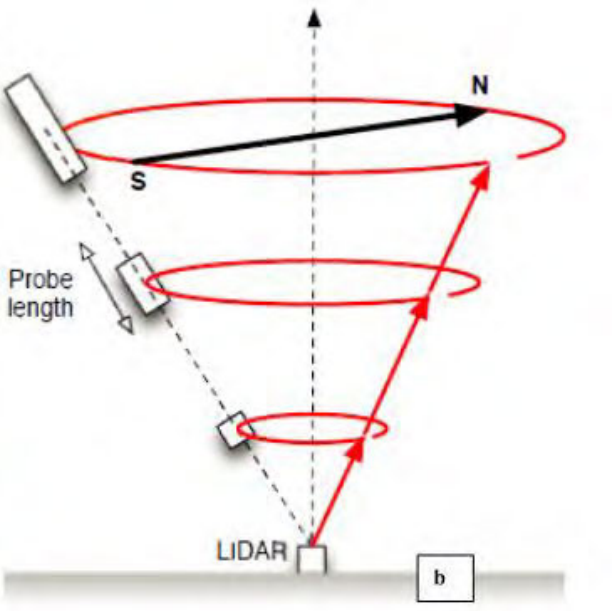

Figure 6. The scanning technique of Z300 LiDAR [10]. 1-Meteorogical station, 2-Automatic moisture sensor, 3-Wiper, 4-Z300 leg, 5-Z300 insulated body pod, 6-Lifting rope, 7-Leg release mechanism.

Each rotation of Z300 LiDAR at every height takes 1 s, in which 50 line-of-sight (LoS) measurements (i.e., 20 milliseconds (ms) sample rate) are taken.

Table 1. summary of the specifications of Z300 with emphasis on the operation, performance, and safety.

Parameter	Range and accuracy
Operation	
Operating temperature	-40 °C to +50 °C
AC power consumption	83 W - Standard climate (-15 °C to -22 °C)
DC power consumption (average wattage)	72 W - Standard climate (-15 °C to +22 °C) 94 W -Hot climate (+23 °C to +50 °C) 119 W-Cold climate (-15 °C to -16 °C)
Impute power range.	100 v to 250 v AC and 9.5 v to 13.5 v DC.
Weight of Z300 Pod	55 kg
Weight of Z300 leg and foot castings	8 kg
Performance	
Measurement height range	10 m to 200 m, extended range 300 m
Focus heights	10 user programable (besides a pre-fixed height of 38 m) heights up to 300 m
Prob length	0.7 m at 10 m and 7.7 m at 100 m
Wind data averaging period	1s (average)
10 minutes wind speed average	80 kB/day
Wind speed range	<1m/s to 70 m/s
Line of sight (LoS) per scan	50 LoS/Scan
Sampling rate	50 Hz
Scanning cone angle	30°
Wind speed accuracy	<0.5 %
Wind direction accuracy	<0.5°
Safety	
Laser classification	Class 1 laser product
Laser peak power consumption	< 1W (70 mm aperture)
Laser wavelength	1560 nm to 1565 nm
Eye safety standard	IEC/EN60825-1 compliance
Ingress protection rating (IP)	IP67

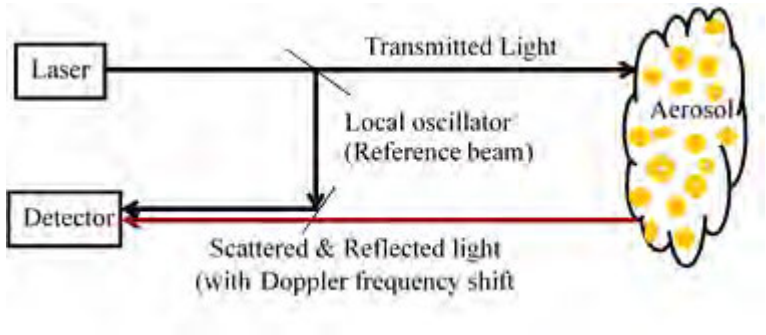

Figure 7. Generic bistatic LiDAR system [11]

The wind parameters extracted from each LoS measurement are horizontal wind speed, vertical wind speed and the wind direction [11]. The wind parameters captured are normally averaged

through 10 minutes to enable resource planning and energy evaluation. Z300 is monostatic in nature (i.e., the transmitted and received path shear common optics) but for easy visual comprehension, are normally represented by a generic bistatic LiDAR system (Figure 6) that simplifies anemometry principles used by coherent laser radar (CLR).

Z300 emits laser radiation in a circular pattern by reflecting the laser beam off a spinning optical wedge, via the Velocity Azimuth Display (VAD) scanning technique [8]. The emitted laser beam hits the aerosol in the atmosphere and scatters in-elastically. The detector records information about the return signal by coherent detection method and creates an electric signal that is digitally sampled for determining the Doppler shifted frequency of the return light by comparing it to the transmitted laser. The Doppler shifted frequency gives an idea of the wind speeds carrying the aerosols [12].

The LiDAR observed wind data assisted in further identification and independent description of the boundaries of the tower and boom wakes but were not suitable to predict the minimum boom length, wind flow characteristics around and through the 3D complex structure of an operational tower, flow interferences engendered by the presence of secondary support structures, and the true impact of freestream turbulence on tower shading. The identified shortfalls regarding site experimentations necessitated the use of computational fluid dynamics (CFD) for further evaluation of the suitability of using towers of this configuration for wind data measurement.

1.5 Numerical Method

1.5.1 Governing Equation

Fluid flow was governed by the conservation of mass (continuity) and conservation of momentum (RANS equations) as shown in equation 1 and equation 2, respectively [4]. Steady, incompressible, and isothermal flow was assumed.

$$\frac{\partial \overline{U}_\iota}{\partial x_j} = 0 \tag{1}$$

$$\frac{\partial\left(\overline{\mathrm{U_I}}\overline{\mathrm{U_J}}\right)}{\partial \mathrm{x_j}} = -\frac{\partial \overline{\mathrm{P}}}{\partial \mathrm{x_i}} + \frac{\partial}{\partial \mathrm{x_j}}\left[\nu_{\mathrm{T}}\left(\frac{\partial \overline{\mathrm{U_I}}}{\partial \mathrm{x_j}} + \frac{\partial \overline{\mathrm{U_J}}}{\partial \mathrm{x_i}}\right) - \rho\overline{\mathrm{u_I'}}\overline{\mathrm{u_j'}}\right] \tag{2}$$

The variable $\bar{u}$ is the Reynolds-averaged velocity, $\bar{P}$ is the averaged pressure, ν_T is the eddy viscosity and $\overline{u_i' u_j'}$ is the Reynolds stress tensor. The presence of the stress terms introduces more variables than may be fully resolved with the available equations, hence the closure problem. Turbulence models often used in external aerodynamics study as described below were used to resolve the closure problem.

1.5.2. Spalart-Allmaras One-Equation Turbulence Model

This turbulence model was designed for aeronautic application, and this makes it suitable for external flow simulation. It solves one equation: as result, it is faster than its two-equation counterparts. For wall-bounded attached flow with adverse pressure gradient, the model performs well but demonstrates weakness in the region where flow separation occurs. In this model the transport equation is solved for $\tilde{\nu}$, a variable that behaves like the turbulent kinematic viscosity (ν_T) far away from the wall but remains linear close to the wall [13]. The transport equation contains primarily the temporal derivative and the convection terms, production, destruction, and diffusion terms as shown in equation 4. The eddy viscosity of this model is computed thus:

$$\nu_T = \tilde{\nu} f_{v1}, \quad f_{v1} = \frac{\chi^3}{\chi^3 + C_{v1}^3}, \quad \chi = \frac{\tilde{\nu}}{\nu} \tag{3}$$

$$\underbrace{\frac{\partial \tilde{\nu}}{\partial t} + U_j \frac{\partial \tilde{\nu}}{\partial x_j}}_{TC} = \underbrace{C_{b1} \tilde{S} \tilde{\nu}}_{Production} - \underbrace{C_{\omega 1} \left(\frac{\tilde{\nu}}{d}\right)^2}_{Destruction\ term} + \underbrace{\underbrace{\frac{1}{\sigma} \frac{\partial \tilde{\nu}}{\partial x_k} \left[(\nu + \tilde{\nu}) \frac{\partial \tilde{\nu}}{\partial x_k} \right]}_{linear} + \underbrace{\frac{C_{b2}}{\sigma} \frac{\partial \tilde{\nu}}{\partial x_k} \frac{\partial \tilde{\nu}}{\partial x_k}}_{nonlinear}}_{Diffusion\ term} \tag{4}$$

The variable t is the time, u is the velocity field, x_j is the cartesian coordinate and d is the distance from the closest surface. The term TC found in the left-hand side is common to all transport equations and it is the temporal derivative and the convention terms. Within the region of high shear stress, there is production of turbulence which relates to the shear rate tensor ($\tilde{S}$). The destruction terms enable the inviscid blocking of the pressure gradient near the wall while the viscous damping is catered for by equation 3. The diffusion terms enable the spread out from the regions of high concentration to those of low concentration. The spreading of the wake profile in this model is controlled by the nonlinear portion of the diffusion term [13]. The closure coefficients and the auxiliary relations are found in [14].

1.5.3 The $k-\epsilon$ Turbulence Model

The $k-\epsilon$ turbulence model (Launder & Sharma 1974)[14] appears to be the most popular turbulence model used in the field of external aerodynamics study. The two transport equations (equations 5 and 6) are solved to obtain the values of the turbulent kinetic energy (k) and that of turbulent dispassion rate (ϵ), respectively. The calculated values of k and ϵ are plugged into equation 7 to compute the value of the kinematic eddy viscosity (ν_T). The value of ν_T computed is substituted back into the momentum equation (equation 2), making the system fully closed. With the closure problem fully resolved, the RANS equation can be solved [15].

$$\underbrace{\frac{\partial k}{\partial t}}_{time} + \underbrace{U_j \frac{\partial U_i}{\partial x_j}}_{convection} = \underbrace{\frac{\partial}{\partial x_j}\left[(\nu + \nu_T/\sigma_k)\frac{\partial k}{\partial x_j}\right]}_{diffusion} + \underbrace{\tau_{ij}\frac{\partial U_i}{\partial x_j} - \epsilon}_{souces+sinks} \tag{5}$$

$$\underbrace{\frac{\partial \epsilon}{\partial t}}_{time} + \underbrace{U_j \frac{\partial \epsilon}{\partial x_j}}_{convection} = \underbrace{\frac{\partial}{\partial x_j}\left[(\nu + \nu_T/\sigma_k)\frac{\partial \epsilon}{\partial x_j}\right]}_{diffusion} + C_{\epsilon i}\frac{\epsilon}{k}\underbrace{\tau_{ij}\frac{\partial U_i}{\partial x_j} - C_{\epsilon 2}\frac{\epsilon^2}{k}}_{souces+sinks} \tag{6}$$

$$\nu_T = C_\mu k^2/\epsilon \tag{7}$$

The closure coefficients as reported in [14] are as follows: $C_{\epsilon 1} = 1.44$, $C_{\epsilon 2} = 1.92$, $C_\mu = 0.09$, $\sigma_k = 1.0$, $\sigma_k = 1.0$. This model, however, is not suitable for predicting boundary layers with adverse pressure gradients. In the context of this thesis, the model may not be the most suitable model to characterise the drag on the walls of the discrete members of the tower geometry during flow simulation.

1.5.4 The $k-\omega$ Turbulence Model

The $k-\omega$ turbulence model is also a two-equation model that has been extensively used in aerodynamics and turbomachinery studies. The two transport equations (equation 8 and 9) are solved to obtain the values of the turbulent kinetic energy (k) and that of the specific turbulent dispassion rate (ω), respectively [14]. Like its two-equation counterpart ($k-\epsilon$), the computed values of k and ω are plugged into equation 10 to compute the value of the kinematic eddy viscosity (ν_T). The value of ν_T computed is subsequently substituted back into the momentum

equation (equation10) to resolve the closure problem. With the closure problem fully resolved, the RANS equation can be solved [16].

$$\underbrace{\frac{\partial k}{\partial t}}_{time} + \underbrace{U_j \frac{\partial U_i}{\partial x_j}}_{convection} = \underbrace{\frac{\partial}{\partial x_j}\left[(\nu + \nu_T/\sigma_k)\frac{\partial k}{\partial x_j}\right]}_{diffusion} + \underbrace{\tau_{ij}\frac{\partial U_i}{\partial x_j} - \beta^* k\omega}_{souces+sinks} \quad (8)$$

$$\underbrace{\frac{\partial \omega}{\partial t}}_{time} + \underbrace{U_j \frac{\partial \omega}{\partial x_j}}_{convection} = \underbrace{\frac{\partial}{\partial x_j}\left[(\nu + \nu_T/\sigma_k)\frac{\partial \omega}{\partial x_j}\right]}_{diffusion} + C_{\epsilon i}\frac{\omega}{k}\underbrace{\tau_{ij}\frac{\partial U_i}{\partial x_j} - C_{\epsilon 2}\frac{\omega^2}{k}}_{souces+sinks} + \frac{\sigma_d}{\omega}\frac{\partial k}{\partial x_j}\frac{\partial \omega}{\partial x_j} \quad (9)$$

$$\nu_T = \frac{k}{\omega} \quad (10)$$

The Wilcox $k-\omega$ model demonstrates superior performance for wall-bounded flows with adverse project gradient when compared to it two equation counterparts ($k-\epsilon$), but it is highly dependent on the freestream turbulence and may not accurately describe flow within that region. The closure coefficients and auxiliary relations are found in [14].

1.5.5 The Shear Stress Transport Model ($k-\omega SST$)

Menter [17] developed this model in 1993 by combining the unique advantages inherent to $k-\epsilon$ and $k-\omega$ models. The shear stress transport ($k-\omega SST$) turbulence model uses the blending function (F_1) to activate the $k-\omega$ model near the wall and $k-e$ model in the freestream region. Equations 11 and 12 are the transport equations for computing k and ω, respectively. The computed parameters are used in equation 13 to calculate the eddy viscosity which was then used to close the momentum equations to enable solution of the RANS equations.

$$\underbrace{\frac{\partial k}{\partial t}}_{time} + \underbrace{U_j \frac{\partial U_i}{\partial x_j}}_{convection} = \underbrace{\frac{\partial}{\partial x_j}\left[(\nu + \nu_T/\sigma_k)\frac{\partial k}{\partial x_j}\right]}_{diffusion} + \underbrace{min\left(\tau_{ij}\frac{\partial U_i}{\partial x_j}, 10\beta^* k\omega\right) - \beta^* k\omega}_{souces+sinks} \quad (11)$$

$$\underbrace{\frac{\partial \omega}{\partial t}}_{time} + \underbrace{U_j \frac{\partial \omega}{\partial x_j}}_{convection} = \underbrace{\frac{\partial}{\partial x_j}\left[(\nu + \nu_T/\sigma_k)\frac{\partial \omega}{\partial x_j}\right]}_{diffusion} + \underbrace{\alpha S^2 - \beta\omega^2}_{souces+sinks} + \underbrace{2(1-F_1)\sigma_{\omega 2}\frac{1}{\omega}\frac{\partial k}{\partial x_i}\frac{\partial \omega}{\partial x_i}}_{blending\ function} \quad (12)$$

The turbulent eddy viscosity (ν_T) is expressed thus:

$$\nu_T = \frac{\alpha_1 k}{max(\alpha_1 \omega, SF_2)} \tag{13}$$

The blending function F1 is defined by:

$$F_1 = \tanh\left\{\left\{\min\left[\max\left(\frac{\sqrt{k}}{\beta^* \omega y}, \frac{500\nu}{y^2 \omega}\right), \frac{4\rho\sigma_{\omega 2} k}{CD_{k\omega} y^2}\right]\right\}^4\right\} \tag{14}$$

The model coefficients and auxiliary relations are found in Menter 1994 [4], [17].

The shear stress transport ($k - \omega SST$) turbulence model was adopted for the flow analysis in this thesis unless where sensitivity analysis with other turbulence models is performed. The $k - \omega SST$ enables accurate analysis of flow interferences and drag near the tower wall and at the same time captures the boom length at a desired distance upstream from the tower surface.

1.6 Problem Statement

Namibia depends greatly on energy imports to meet local demand. Data available from the public utility Namibia Power Cooperation (NamPower) clearly indicates a steady increase in energy imports from Southern Africa Power Pool (SAPP). Between 2013 and 2019, the country's energy import stood at approximately 60 % on the average. As of 2020, as reported in [18], the energy import dropped to 53 % due to 11 % that was added to the grid locally. Demand for energy will however continue to increase if sustainable economic growth continues. In [19] Namibia energy consumption pattern was deemed unfeasible, though it has been sustained through imports, leaving the country with an unfavourable trade balance and this may constitute a strategic security supply risk. To reduce energy dependence, Namibia, in view of its geographical location is oriented to development of renewable sources of energy of which wind and solar are the most promising. Namibia is perceived to have great wind energy potential. This perceived wind energy potential will not be properly utilized unless accurate, reliable, and dependable wind data is available. Data of this type will enable stakeholders to make informed decisions in terms of site energy output and project associated risks if wind energy technology is deployed. However, industrial best practice of installing dedicated masts for wind measurement on the sites is cost intensive and requires lengthy approval processes from the relevant authorities. Thus, the National wind Resource Assessment Project (NWRAP), in 2012 utilized the advantages afforded by the existing communication towers for wind data collection. The Mobile Telecommunication Limited (MTC) towers were

instrumented with the booms placed parallel to the tower face for wind measurement. The instrumentation as reported in [7] was according to [20]. As earlier stated, in contrast, the IEC standard prescribes a standard boom configuration (θ = 0°) i.e., a boom that is mounted perpendicular to the tower face. The centreline velocity deficit expression which enables the computation of the requisite boom length was derived on this premises. The implication is that the incident wind is considered perpendicular to the same mast face, giving rise to velocity deficit values that are predicted using the upstream contour profiles of the modified flow around the tower [6]. Regarding boom installation, [1] suggested that the best option was to mount the anemometer on the top of the tower to avoid tower induced flow perturbation. This option was not possible due to the presence of lighting and communication equipment on top of the tower. Also, wind shear pattern that is needed to gain insight on some aspect of the sites risk, in a situation where wind turbine is deployed, necessitated the installation of the booms at intermediate heights of the tower. This type of boom arrangement would inevitably expose the speed sensor mounted on it to the wake distortion effect of the tower. As reported in the previous studies that utilized site experimentation [21] [22] and numerical approach [4][23], tower shadowing contributes a non-negligible uncertainty to the readings of the speed sensors mounted on them. Application of the previous studies to a tower that has a different construction detail and located in different atmospheric condition in the boundary layer are limited. With the bulky nature of the MTC towers used and the presence of secondary support structures thereof, flow interferences around and through them are more complex. It is against this backdrop that LiDAR measured wind data, CFD derived flow distortion around the tower and physical modelling of the tower structure were combined to investigate the suitability of deploying available communication towers for wind measurement. The identified knowledge-gap and the limitations to the universal application of the relevant standards formed the key area that this study investigated.

1.7 Research Motivation

Namibia is the driest country in sub-Saharan Africa with a climate that is highly variable and unpredictable and vulnerable to desertification and frequent incidences of severe droughts [24]. Globally, climate change and environmental degradation are traceable to excessive emission of greenhouse gasses [25], [26], resulting from the use of conventional energy sources. Global efforts point towards attitudinal change; energy must be sourced from a more sustainable and environmentally friendly way. Being a net importer of energy [18], the cost of energy in Namibia will continue to increase due to population growth, urbanization, and the quest for

industrialization. These trends will continue if unmitigated. One way to mitigate high energy costs and environmental degradation is to improve the local energy mix by utilizing available renewable energy resources. In the Namibian context, wind and solar are dominant among renewable energy resources. To improve the local energy mix using wind generated power requires assessment of the resources as the first and most important step in planning and development of a wind power project [27]. Site wind resources properly characterised can provide the requisite parameters to evaluate wind power project economic viability and risks. Investment in capital intensive projects such as micro-siting or development of a wind farm requires relative certainty in wind measurements [27]. It will only be possible if there is reliable, dependable, and bankable wind data. In recent times, lenders or financial institutions are increasingly depending on the combination of anemometer measurement, ground profiling of wind data (using LiDAR) and computer modeling of wind flow characteristics on the site for decision making rather than the traditional approach of using only an anemometer mounted on the mast [28]. In line with the current global trend, this research work combines data obtained from the traditional approach (anemometer-to-mast arrangement), LiDAR observed wind data, and CFD that accounts for tower wind interaction and physical modelling of the tower structure to fully assess the suitability of using MTC communication towers that are not built according to IEC standard [1] for wind measurement in Namibia and other Southern African countries. Proper characterisation of wind flow around and through these operational towers is a key factor in boom installation to reduce tower wake distortion effect. This means that wind data captured is site representative and can be used for wind power development. The holistic approach adopted ensures that terrain influence in the form of atmospheric turbulence effect is duly captured and that all the limitations inherent with the use Annex G of IEC 61400-12-1 standard [1] regarding boom installations are reasonably resolved. The study provides confidence in installation and utilization of communication towers of different construction details scattered all over Namibia and other Southern African countries for wind measurement.

1.8 Aims and Objectives

The aim of this thesis was to combine field experimentations (anemometer and LiDAR measurement), numerical analysis (CFD derived flow distortion around the tower) and physical modelling of the tower structure to ascertain the suitability of using the Mobile Telecommunication Limited (MTC) of Namibia communication towers scattered all over the

country for accurate wind measurement. To realise this aim, the following specific objectives were implemented:

- To perform field experimentation to capture site wind data using the speed sensors mounted on the communication towers and the ground profiler (LiDAR) for validation and comparison.
- To perform data analysis in other to accurately define the tower wake boundaries and to evaluate the impact of tower shadowing on resource parameters and performance.
- To combine CFD derived flow simulation around the tower and physical modelling approach to understand the angle dependence of tower wake distortion effect. This objective helps to modify the existing velocity deficit expression prescribed in the relevant standards.
- To perform a full 3D CFD study to understand flow characteristics around and through the tower structure. This will enhance understanding of the minimum boom length for achieving 99 % to 101 % (-1% to +1 % speed deficits) of the free stream speed at all direction especially when the boom is in the wake of the tower. This objective will also enable the evaluation of the influence of the secondary support structures, understand the concept of safe angle range and the influence of atmospheric turbulence on tower shadowing.
- To employ a suitable statistical tool/model to compare, combine and validate data captured using different techniques in order to formulate a correction method for removing the effect of tower induced flow perturbation on the observed wind data.

1.9 Significance of the Research Work

Being the driest country in sub-Saharan Africa, Namibia has a climatic condition that is highly variable and unpredictable. The vulnerability of the country to desertification and frequent incidences of severe droughts is a source of great concern [24]. Namibia is also a net importer of energy, and this has resulted in an unfavourable trade balance and constitutes a strategic security supply risk. Not only that, the country's biggest local generator (the Ruacana Hydropower station) a run-of-river system, depends on the amount of rainfall received each year. With its unpredictable weather pattern, there is an urgent need to improve the local energy mix in a sustainable manner by utilizing available renewable energy sources. To improve the local energy mix using wind generated power requires assessment of the resources as the first and most important step in planning and development of the wind power project [27]. Site wind

resources properly characterised can provide the requisite parameters to evaluate a wind power project's economic viability and risks.

Against this backdrop, this research work combines field experimentation (anemometer and LiDAR measurement), numerical (CFD flow analysis) and physical modelling to ascertain the suitability of using the MTC communication towers scattered all over the country and other southern African countries for wind measurement. The holist approach adopted in this work and the output thereof will ensure that wind data captured using these communication towers are site representative. This is because the identified limitations to the universal applicability of the relevant standards regarding tower instrumentation for wind measurement perspective are reasonably resolved. With the realistic site wind characterisation, investment into wind power project will not only improve the contribution of renewable energy to the local energy mix but will also attract much-needed foreign direct investment. This will offset the country's energy trade deficit, guarantee security of supply, and improve the local economy through job creation.

1.10 Thesis Outline

This thesis comprises eight chapters, and is structured thus:

Chapter 1 introduces the tower wake distortion effect. A brief background of the NWRAP project and the need for the thesis was presented. The wind measurement site description and communication towers construction details were covered. The specifications of the LiDAR and the numerical model used and the need for their application were briefly highlighted. The chapter ended with a layout of the content of the report documenting the following subheadings: problem statement, research motivation, significance of the thesis work, general organisation, and scope of the thesis.

Chapter 2 is a comprehensive review of the relevant literature regarding the evaluation method of tower wake distortion effect and their applications. The state of the art and best practice to define, describe and minimise tower wake distortion effects for both lattice (triangular and rectangular) and cylindrical (tubular and rod) towers are fully accounted for based on relevant literature i.e., journal articles, conference papers, standards, books, and reports that are published between 1941 to 2019. The key findings, conclusions, and knowledge gaps identified are documented.

Chapter 3 documented the extensive investigation on the various methods/approaches to identify and accurately define tower wake boundaries using wind data obtained from anemometers collocated at the same intermediate height but of different azimuth from the north. The LiDAR observed wind data enabled independent and accurate verification of the tower and boom wake boundaries. Methods explored include the traditional speed ratio, the coefficient of determination (R^2) of wind speed, the root mean square errors (RMSE) of wind speed, the coefficient of determination (R^2) of turbulence intensities (TI) which appears to be the better descriptor of the wake boundaries when compared to the commonly used traditional speed ratio approach.

Chapter 4 fully answered the question "If the wake affected direction sectors are not corrected or discarded during data analysis, what impact would that have on the resource and performance?". This chapter motivates the need for accurate definition of tower wake boundaries and explains the key features of wake affected direction sectors where collocated sensors are not available. It further proposes a new and a simpler approach to using time series WSC computed from wind data measured at two different intermediate heights, located at approximately the same azimuth from the north to identify the wake affected sectors without the need for collocated sensors.

Chapter 5 combines physical modelling of the tower structure and CFD flow simulation to perform a parametric study in order to investigate the angle dependence of the tower wake distortion effect. The controlling parameters (thrust coefficient [C_T] and the leg length [Lm]) in the centreline velocity deficit expression prescribed in IEC 61400-12-1, varies with incident wind angle. This chapter incorporated the (thrust coefficient [C_{Ti}] and the leg length [L_i]) obtained at different incident wind angles into the IEC centreline velocity deficit expression to obtain a modified speed deficit expression used to predict the booms lengths at incident wind angles other than the IEC reference direction ($\theta = 0°$).

Chapter 6 describes a full 3D CFD flow simulation on the complex 3D geometry of the communication towers and proposes a safe angle range. This aspect of the study is necessary because the boom length computed using the centreline velocity deficit expression found in IEC standard does not guarantee that wind observation is accomplished within the recommended industry-accepted accuracy of < 1 % errors between 0° and 360°. With safe angle range of $\theta = < \pm 70^o$ with respect to each boom arrangements reference direction (i.e., $\theta = 0^o$), the boom lengths obtained based on the IEC standard boom configuration ($\theta = 0^o$) are

long enough to keep the speed sensors out of the tower wakes. Winds that arrive at the tower at other angles outside this range will likely induce error readings on the speed sensor and this explains why towers instrumented according to the IEC standard still fall short of the 1 % speed deficit recommended.

Chapter 7 Explores the impact of freestream turbulence on the boom length required to keep the speed sensor out of tower wakes by comparing the CFD flow simulation results that capture the site's realistic freestream turbulence parameters to the simulation results obtained from standard external flow analysis. Extreme case of laminar flow was also computed and compared with the models that have different turbulence parameters. The chapter concludes that freestream turbulence does not have any significant impact on the boom but makes flow interference more complex within the regions near the wall of the tower. It also increases the drag on the tower and engenders visible inhomogeneity in the flow parameters in the wake of the tower.

Chapter 8 is the summary of the conclusions collected from the entire thesis and recommendations for future work.

1.11 Scope of the Study

The focus of this thesis was to combine wind data obtained from site experimentations (speed sensors and LiDAR measurement), CFD flow simulation and physical modelling of the communication tower to study wind flow characteristics around them in other to minimise error readings captured by speed sensors mounted on them. Analysis of the observed data enables comparison, validation, identification, and description of the of tower waked direction sectors and the impact of tower shadowing on wind resource and performance. The numerical analysis and physical modelling provide insight on the boom lengths, angle dependence of tower wake distortion effect, the concept of safe angle range (the angle range at which boom lengths obtained based on the IEC standard boom configuration [$\theta = 0^{o}$] are sufficient to keep the speed sensors out of the tower wakes) and the effect of free stream turbulence on the boom length required to keep the speed sensor out of the tower wakes. However, the study did not investigate the impact of boom vibration on the captured wind speeds and the impact of freestream turbulence on boom vibration and its associated errors regarding anemometer readings.

1.12 References

[1] International Electrotechnical Commission (IEC), "Wind energy generation systems – Part 12-1: Power performance measurements of electricity producing wind turbines," International Electrotechnical Commission (IEC), IEC Central Office 3 rue de Varembé CH-1211 Geneva 20, Switzerland, International Standard IEC 61400-12-1:2017-03(en-fr), Mar. 2017. Accessed: Oct. 15, 2018. [Online]. Available: https://webstore.iec.ch/publication/26603

[2] M. E. Okorie and F. Inambao, "Identification of tower and boom- wakes using collocated anemometers and lidar measurement," *International Journal of Mechanical Engineering and Technology*, vol. 10, no. 06, pp. 72–94, 2019.

[3] S. Orlando, A. Bale, and D. Johnson, "Experimental study of the effect of tower shadow on anemometer readings," *Journal of Wind Engineering and Industrial Aerodynamics* vol. 99, pp. 1–6, Jan. 2011, doi: 10.1016/j.jweia.2010.10.002.

[4] S. Fabre, M. Stickland, T. Scanlon, A. Oldroyd, D. Kindler, and F. Quail, "Measurement and simulation of the flow field around the FINO 3 triangular lattice meteorological mast," *Journal of Wind Engineering and Industrial Aerodynamics*, vol. 130, pp. 99–107, Jul. 2014, doi: 10.1016/j.jweia.2014.04.002.

[5] M. Stickland, T. Scanlon, S. Fabre, A. Oldroyd, and D. Kindler, "Measurement and simulation of the flow field around a triangular lattice meteorological mast," *Energy and Power Engineering, vol. 5, no. 10, 2013.*

[6] M. E. Okorie and F. L. Inambao, "Angle dependence of tower wake distortion: A parametric study," *International Journal of Mechanical and Production Engineering Research and Development*, vol. 11, no. 3, pp. 481–498, 2021, doi: 10.24247/ijmperdjun202138.

[7] E. B. J. Siepker and T. M. Harms, "The national wind resource assessment project of Namibia," *R&D Journal*, vol. 33, pp. 105–116, 2017.

[8] A. Pena and C. B. Hasager, "Remote sensing for wind energy," Risø National Laboratory for Sustainable Energy, Technical University of Denmark. Risø-I No. 3184(EN.

[9] International Energy Agency, *IEA Wind RP 15. Ground-based, vertically-profiling remote sensing for wind resource assessment*, First edition. Colorado USA, 2013. [Online]. Available: https://community.ieawind.org/HigherLogic/System/DownloadDocumentFile.ashx?DocumentFileKey=7492ade3-03e1-419f-466f-4b6aacc271df

[10] International Energy Agency, “IEA recommended practices for wind turbine testing. Part 11: Wind speed measurements and use of cup anemometer,” Technical Report. Accessed: May 19, 2018. [Online]. Available: https://community.ieawind.org/HigherLogic/System/DownloadDocumentFile.ashx?DocumentFileKey=dcf4afa1-ee68-3111-0ac5-c235d2f2bc16&forceDialog=0

[11] C. Slinger and M. Harris, “Introduction to continuous-wave Doppler lidar,” 2012. Available: http://breeze.colorado.edu/ftp/RSWE/Chris_Slinger.pdf

[12] D. Jaynes, J. Manwell, J. McGowan, W. Stein, and A. Rogers, “MTC final progress report: LIDAR,” Renewable Energy Research Laboratory, Department of Mechanical and Industrial Engineering, University of Massachusetts, 2007.

[13] Fluid Mechanics 101, *[CFD] The Spalart-Allmaras turbulence model*, (Feb. 2020). Accessed: Jul. 03, 2021. [Online Video]. Available: https://www.youtube.com/watch?v=Xivc0EIGFQw&t=299s

[14] D. Wilcox, *Turbulence modeling for CFD (Third Edition) (Hardcover)*, Third edition. California USA: DCW Industries, Inc., 2006. [Online]. Available: file:///C:/Users/OKORIE%20M.E/Desktop/2021-S1/Turbulence%20Modeling%20for%20CFD%20(Third%20Edition)%20(%20PDFDrive%20).pdf

[15] Fluid Mechanics 101, *[CFD] The k - epsilon turbulence model*, (Jun. 15, 2019). Accessed: Jul. 03, 2021. [Online Video]. Available: https://www.youtube.com/watch?v=fOB91zQ7HJU

[16] Fluid Mechanics 101, *[CFD] The k-omega turbulence model*, (Jun. 24, 2020). Accessed: Jul. 03, 2021. [Online Video]. Available: https://www.youtube.com/watch?v=26QaCK6wDp8&t=735s

[17] F. R. Menter, “Two-equation eddy-viscosity turbulence models for engineering applications,” *AIAA Journal*, vol. 32, no. 8, pp. 1598–1605, Aug. 1994, doi: 10.2514/3.12149.

[18] Namibia Power Cooperation, “NamPower annual report 2020,” Windhoek, Namibia, 2020. Accessed: Jul. 03, 2021. [Online]. Available: https://www.nampower.com.na/public/docs/annualreports/NamPower%20Annual%20Report%202020.pdf

[19] M. E. Okorie, F. L. Inambao, Z. Chiguvare, and S. Alfeus, “Renewable energy and African industrialization: A participatory integrated approach in assessing concentrated

solar power potential in Namibia," *International Journal of Mechanical Engineering and Technology*, vol. 9, no. 12, p. 16, Dec. 2018.

[20] International Electrotechnical Commission (IEC), "Wind energy generation systems – Part 12-1: Power performance measurements of electricity producing wind turbines," International Electrotechnical Commission (IEC), IEC Central Office 3 rue de Varembé CH-1211 Geneva 20, Switzerland, International Standard IEC 61400-12-1:2005(E), Dec. 2005.

[21] K. McCaffrey *et al.*, "Identification of tower-wake distortions using sonic anemometer and lidar measurements," *Atmospheric Measurement Techniques; Katlenburg-Lindau*, vol. 10, no. 2, pp. 393–407, 2017, doi: http://dx.doi.org/10.5194/amt-10-393-2017.

[22] J. E. Cermak and J. D. Horn, "Tower shadow effect," *Journal of Geophysical Research (1896-1977)*, vol. 73, no. 6, pp. 1869–1876, 1968, doi: 10.1029/JB073i006p01869.

[23] M. Tusch, C. Masson, and P. Héraud, "Modeling of turbulent atmospheric flow around tubular and lattice meteorological masts," *Journal of Solar Energy Engineering*, vol. 133, no. 1, p. 011011, Feb. 2011, doi: 10.1115/1.4003293.

[24] Republic of Namibia, Ministry of Environment & Tourism, Department of Environmental Affairs, *Third National Action Plan for Namibia to Implement the United Nations Convention to Combat Desertification, 2014-2024*, 2014.

[25] B. K. Sovacool, "Environmental issues, climate changes, and energy security in developing Asia," Social Science Research Network, Rochester, NY, SSRN Scholarly Paper ID 2479725, Jun. 2014. doi: 10.2139/ssrn.2479725.

[26] İ. Dinçer and C. Zamfirescu, "Renewable energies," in *Sustainable Energy Systems and Applications*, İ. Dinçer and C. Zamfirescu, Eds. Boston, MA: Springer US, 2012, pp. 283–387. doi: 10.1007/978-0-387-95861-3_9.

[27] B. H. Bailey, S. L. McDonald, D. W. Bernadett, M. J. Markus, and K. V. Elsholz, "Wind resource assessment handbook: Fundamentals for conducting a successful monitoring program," NREL/SR--440-22223, ON: DE97000250, 486127, Apr. 1997. doi: 10.2172/486127.

[28] Asian Development Bank, "Guidelines for wind resource assessment: Best practices for countries initiating wind development," Mandaluyong City Philippines, TIM146446, May 2014. [Online]. Available: https://www.adb.org/sites/default/files/publication/42032/guidelines-wind-resource-assessment.pdf

CHAPTER 2: TOWER WAKE DISTORTION EFFECT: A COMPREHENSIVE REVIEW OF METHODS AND APPLICATIONS

This chapter presents a comprehensive review of the relevant literature on the evaluation method of tower wake distortion effect and their application. The state of the art and best practice to define, describe and minimise tower wake distortion effects for both lattice (triangular and rectangular) and cylindrical (tubular and rod) towers were fully accounted for based on the relevant literature i.e., journal articles, conference papers, standards, books, and reports that are published between 1941 to 2019. The methods used, key findings, conclusions, and knowledge gaps identified, were documented.

CHAPTER 1: **Cite this article:** M. E. Okorie and F. Inambao, "Tower wake distortion effect: A comprehensive review of methods and applications," *International Journal of Engineering Research and Technology*, vol. 13, no. 12, p. 17, 2020.

Link to the article:

http://www.irphouse.com/ijert20/ijertv13n12_02.pdf

International Journal of Engineering Research and Technology. ISSN 0974-3154, Volume 13, Number 12 (2020), pp.

Tower Wake Distortion Effect: A Comprehensive Review of Methods and Applications

Maduako E. Okorie
Namibia University of Science and Technology, Windhoek, Namibia.
PhD student, University of KwaZulu-Natal, Durban, South Africa.
E-mail: mdkemmanuel@yahoo.com

Freddie Inambao*
University of KwaZulu-Natal, Durban, South Africa.
ORCID: 0000-0001-9922-5434 (Freddie Inambao)
**Corresponding author.*
E-mail: inambaof@ukzn.ac.za;

Abstract

Literature on the evaluation methods for tower wake distortion effect based on the wind measurement is reviewed, including 50 peer reviewed journal articles, conference papers, standards, thesis and reports published between 1941 and 2019. A review of the literatures published prior to 2005 sets the foundation for a critical review of the International Electrotechnical Commission (IEC) 2005 standard. Thereafter, literature published between 2006 and 2017 is reviewed as the basis for a review of the IEC 2017 standard. A review of literature published post IEC 2017 provides insight into current trends. Considering the current published literature, the shortcomings of IEC 2005 and IEC 2017 standards are identified and discussed and areas for future work noted. The reviewed literature is organised according to the method and tower type used and the purpose and major findings. Prior to 2005, field and wind tunnel experiments were the dominant research approach while field measurement and computational fluid dynamics (CFD) dominated the research methods used between 2006 and 2017. Post-2017 saw an increase in the use of ground profile (LiDAR) for tower shadow evaluation. In field observation there is an unwritten consensus that collocating anemometers at some intermediate height of the tower provides enough information for anemometer consistency checking and tower wake evaluation. Previous studies have agreed that three dimensional (3D) CFD analysis is better suited to characterise flow through the complex nature of an operational lattice tower than the 2D actuator disc approach of IEC 2005 and IEC 2017. It is hoped that this paper can meet the needs of researchers for easy reference to methods of evaluating tower shadowing and hence promote future work on the verification of the remaining shortcomings of IEC 2005 and IEC 2017. While that work is ongoing, these two standards should be regarded a guideline rather than a precise description of flow interference effects through an operational tower.

Keywords: Tower wake distortion; speed deficit; wind direction dependency; secondary support structures; free stream turbulence

I. INTRODUCTION

Wind resource assessment involves the use of various techniques to capture site wind data for analysis to aid informed decision making. Traditionally, wind measurement utilises latticed or tubular towers with boom-mounted sensors attached to the towers. Consideration of other resource parameters that assist in further evaluation of the site's overall suitability necessitates installing speed and direction sensors at some intermediate heights of the tower. Arrangements of this sort inevitably expose the instrumentation to the wake distortion effect of the tower, a phenomenon that is known to introduce a non-negligible error in the wind data observed using anemometers placed on the tower [1]–[8]. Previous works on tower shadow effects have found a 35 % to 50 % wind speed reduction which is known to depend on the tower configurations and boom arrangements [5], [11]–[14]. Such observations have been supported by the computational fluid dynamic (CFD) approach [1], [2], [4], [15]. Furthermore, wind speed error is known to propagate into the power output estimates. Accurate wind speed measurement is therefore a prerequisite for improved wind power prediction and evaluation of a site's techno-economic feasibility [16]. Over the last 74 years the scientific literature has devoted much attention to understand tower wake distortion and in recent times, due to the growing contribution of wind energy to the global energy mix, tower wake effects and their impact on resource parameters has been considered a vital component of research work in wind measurement campaigns. Previous studies have suggested that the phenomenon depends on the tower configuration and the anemometer arrangement on it. However, application of these studies to towers of different structural configurations and different sites' atmospheric conditions in the boundary layers is limited.

To the knowledge of the authors, there is no evidence of published papers on the analytical overview of literature on the tower shadow effect. A study of this kind contributes to reviewing and categorisation of the various methods used to identify, define and correct tower induced flow defects and to reveal some grey areas and knowledge gaps that may require further investigation. In this regard, the authors present a comprehensive literature review of selected literature from scientific papers that have addressed tower distortion effects from the wind measurement perspective. In order to account

for the past and present trends this review focuses on peer reviewed journal articles, conference papers, standards, theses and reports published between 1941 and 2019. The state of the art and best practice to define and minimise tower wake effects for both lattice (triangular and rectangular) and cylindrical (tubular and rod) towers are fully accounted for in the 50 items of literature reviewed.

II. BRIEF OVERVIEW OF TOWER SHADOW EFFECT

The tower shadow effect describes the uncertainty introduced to wind data captured using boom mounted anemometers placed at some intermediate heights (Fig.2) because of tower induced flow modifications. These modifications are evident in the underprediction of the local wind speeds in the wake and associated speed-ups in the upwind side of the tower. a Tower construction details showing boom arrangement and secondary support structures. b. Ratio WS4/WS4B plotted on a sector-wise basis binned in 5° bins of wind direction intervals

Fig. 1. A section of the tower at Amper-bo showing the boom arrangement and some secondary support structures.

Figure 2 illustrates the tower induced error readings on a pair of collected anemometers represented here as WS4 and WS4B. The speed ratio (WS4/WS4B) binned in 5° wind direction intervals and drawn as a function of the wind direction clearly shows the severity and boundaries of the waked regions (doted oval shaped). At approximately 60° (75° to 135°), WS4 was under tower shading hence the reduction in wind speed captured. Approximately in the (210° to 260°) wind direction sector, tower induced flow perturbation was captured by WS4B. The unsymmetrical pattern of the waked regions may be attributed to the prevalent clockwise wind direction at the site [11].

Tower induced flow perturbations differ through the different planes (Fig. 3a and Fig. 4b) of each module of the lattice triangular tower investigated. Fig. 3a and Fig 3b are computational fluid dynamics (CFD) derived flow showing local wind flow modifications within the vicinity of the tower.

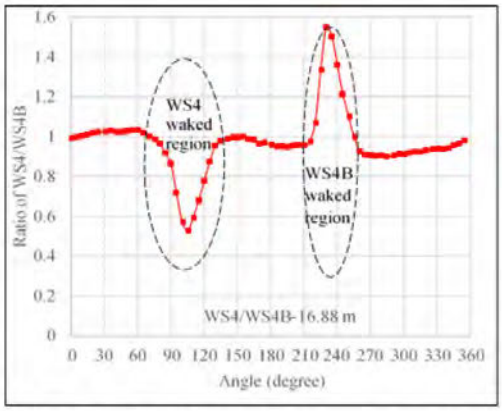

Fig. 2. Ratio of WS4/WS4B plotted on a sector-wise basis binned in 5° wind direction intervals showing waked regions.

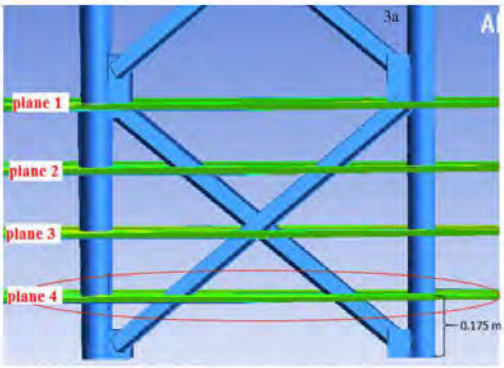

Fig.3a. Convenient plane for positioning the anemometer in the module of the lattice triangular tower at Amper-bo.

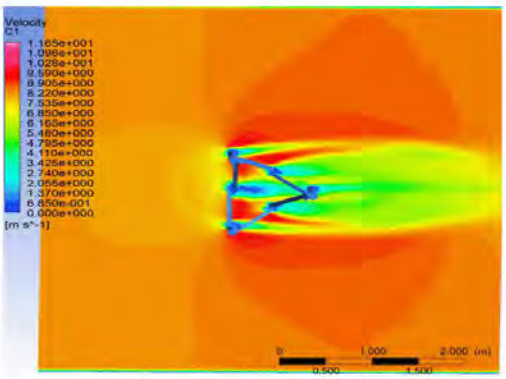

Fig. 3b. 3D CFD flow simulation through a plane of the lattice tower module at Amper-bo (Fig. 3a).

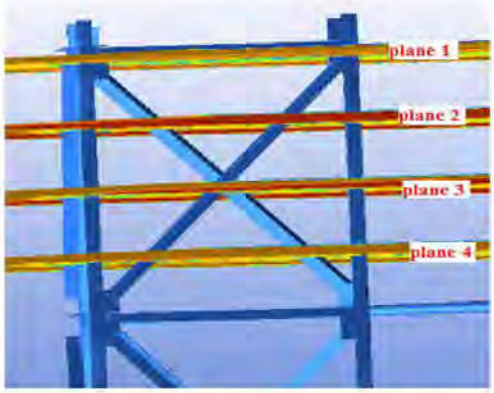

Fig.4a. Convenient plane for positioning the anemometer in the module of the lattice triangular tower at Korabib.

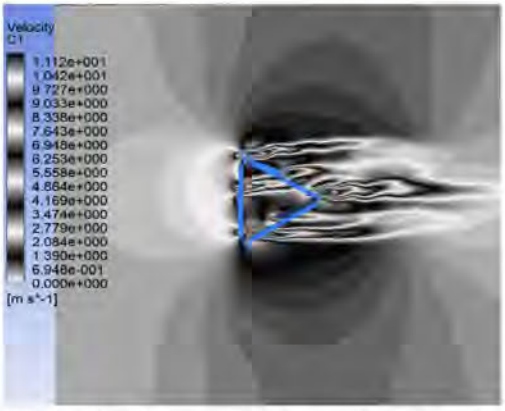

Fig. 4b. 3D CFD flow simulation through a plane of the lattice tower module at Korabib (Fig. 4a).

The flow characteristics differ in each of the planes, an indication that the most convenient plane is the plane with least flow distortion. The optimum boom location for minimum flow distortion is shown in Fig. 3b and 4b with the boom in Fig. 4b directly pointing at the zone of least distortion.

III. METHODS

This study involves an extensive literature review based on the relevant international standards, peer reviewed journal articles, conference papers, reports and theses that have addressed tower induced flow defects in relation to wind measurement. Various methods and approaches used to identify, define and correct tower induced error readings on anemometers have been reviewed. 1941 was chosen as a starting data because it was the year the first article was published that provided a descriptive account of the flow mechanics in the wakes, with emphasis on important parameters such drag, turbulent mixing and vortex shading [17]. The present study, therefore, is based on the review of most relevant literature published from 1941 to 2019, organised systematically to reveal methods used, tower types investigated, purpose of each study and the major findings. The length of period covered in this study is also a testament to the fact that literature on this subject is relatively sparse, so the current study is meant to provide deeper insight into the methods so far used.

For clarity of purposes, the literature is grouped in four major sections around the International Electrotechnical Commission (ICE) standards [3] and [4]. Literature published prior to 2005 is discussed first, setting the foundation for critical review of the (IEC 2005) standard [3]. Thereafter, literature published between 2006 and 2017 is reviewed leading to a review of the (IEC 2017) standard [4]. Articles published post [4] are reviewed to gain insight into the trends, current status and future prospects of this work, which is the core objective of this study.

IV. REVIEW OF LITERATURE

A. Prior to IEC2005 - Tower Wake Effects

Wind energy conversion using windmill technology is centuries old. Due to environmental and sustainability concerns regarding fossil dominant global energy, attention has gradually shifted towards sourcing and using energy in a sustainable manner, but only in the 1980s and 1990s did large-scale utility wind farms start being constructed. Thereafter, wind energy took off and has grown into a multibillion-dollar industry. By 1997, the total global installed capacity of wind power was 7.6 GW, and this grew to a total capacity of 59.2 GW in 2005 i.e. almost 8 times the 1997 global capacity [18]. However, the global consumption of wind energy prior to 2005, evidenced by the global installed capacity, was low when compared to the present time, as was the research on wind energy. The huge investment in the industry necessitated a stringent approach to ensure that quality and accurate data can be measured at a site of interest. Top among the concerns is the placement of instruments on the meteorological (met) mast to minimise the size of the errors associated with the tower induced flow defects.

Research activities in this regard prior to 2005 was dominated by field and wind tunnel experimentation. The oldest scholarly article was published in 1941. Isolated scaled down stack and station models were tested in a wind tunnel experiment and the results provided a good descriptive account of the flow mechanics in the wake, with important parameters such drag, turbulent mixing and vortex shading discussed [17]. A pragmatic and more practical approach to the problem was adopted, by conducting field measurements on lattice towers using test and redundant anemometers [8], [19]. Reference [8] reported speed deficit in the range of 25 % to 50 % and wind direction deviations of about 11 %. Reference [19] reported 30 % deficit upwind and 70 % deficit downwind due to tower wake distortion and both studies suggested a minimum boom length to minimise the effect of tower shadow. Using

anemometers located 120° and placed at some intermediate height of a lattice triangular met mast at Brookhaven National Laboratory, USA, [14] reported a 35 % speed deficit and 19 % speed-ups and a waked region covering an arc of approximately 60°. In [20], a combined double theodolite pilot balloon and instrumented television tower were used in Oklahoma City to evaluate tower shading effect. The study reported a 7 % underestimation of mean wind speed for an anemometer located 3 m upwind of the tower. Further experimental work revealed the influence of tower secondary support structures on the wind speed captured using a Kansas meteorological mast [21], [22]. In [23], a 232 m lattice tower of the Sicily-Calabria power line in Italy was instrumented for measurement. Findings show a speed deficit of 15 % and 80 % on the upwind side and lee side of the tower respectively due to tower shading. Again, several field experiments using tilt-up tubular tower have been conducted, including [24]. The study concluded that side mounted booms that are sufficiently long enough to remove the anemometer away from the tower shadowing are preferred to a top mounted boom. A 20 % maximum speed deficit and a wake boundary covering about 50° in the waked region of the tower were reported. In an attempt to predict the minimum boom length, it was reported in [25] that significant errors occurred on the lee-side of a cylindrical obstruction for which wind tunnel experiment was performed on its scaled down model. Similarly [24] approached the problem experimentally using a 1:4 scale model of a lattice tower in a wind tunnel to ascertain how increase in turbulence level of the oncoming air stream affects the tower induced perturbations. The study reported that the increase in turbulence level resulted in a 2 % speed defect and stressed that perturbations of the wind-field are chiefly caused by tower configuration and sensor arrangements. Reference [26] used a two-pronged approach (field and wind tunnel experiment) to evaluate tower shading. Reference [27] studied a cylindrical tower and observed a suppressed speed on the lee-side of flow and 3 % discrepancies between the up- and down-stream wind speeds. References [28] and [13] each investigated 1:4 scale models of a 150 m lattice equilateral triangular tower in a wind tunnel experiment. When the result from the two experiments were compared, a 10 % speed deficit occurred in the waked zone of the [28] study, and a speed deficit range of 10 % to 40 % confined to the 30° sector was reported by [13]. Work by [29] showed that a tunnel flow simulation performed on a 1:8 scale model of a 150 m NASA lattice tower predicted shadowing effects reasonably when compared with field observation. In [30], wind tunnel and field measurements found that the boom and its actual placement disturbed the flow seen by the anemometer. In their work as reported in [14] Borovenko et al. explored the use of potential flow solution validated with field experiments. The study showed that 75 % of the readings of the anemometer located upstream of the tower fell within ± 5 % of the potential value and least wake distortion was evidenced at ± 45°, providing useful insight on the possible boom orientation in a cylindrical tower. Using a similar approach, [31] concluded that observed upwind pattern around a cylindrical obstacle (oil drums) is well represented by the potential solution around it, whereas the waked region was asymmetrical. Isopleth diagrams of the speed ratios showed a 6 % and 40 % speed reduction in the upwind and downwind side of the cylinder respectively and a 5 % speed-up at the side of the tower. Further potential flow approaches to the problem revealed a maximum speed deficit of 27 % when compared with field experiments performed on a 150 m NASA tower Computing stream function about the same tower with and without catwalk revealed a speed-up of 3.5 % and 4.5 % respectively, providing insight on the influence of tower secondary support structures. Reference [32] reported that potential flow around a tilt-up cylindrical mast with tapered cross-section predicated disturbed flow due to tower structure reasonably well when compared to observed flow around the same mast at different angles of attack. Rather controversially though, the study opined that the magnitude of the disturbances around the tower exhibits no obvious relation to the geometry of the tower, rather such disturbance is Reynolds number dependent. The study concludes that symmetrical mounting of the booms at both sides of the tower may help to identify the tower induced flow distortion. As reported in [33], a lattice tower was modelled as an actuator disc to estimate its shadowing effect on the readings of the speed sensors mounted on it. The CFD result agreed with field observation performed using the mast at Tjcereborg after both tower and boom induced errors were removed. In a similar approach, [34] assessed the wake distortion effect of a lattice tower of square cross section. The study reported a 19 % mean speed reduction and an increase in turbulence spectra in the waked region of the tower. Reference [35] used a computational approach and experimentation to verify the wake impact of the ship's structure on the shipborne instruments [35]. The CFD result agreed with the observed speed except when the anemometer was in the wake of an upstream obstacle Table I and Table II summarise the above studies in tabular form.

TABLE I. SUMMARY OF THE METHODS AND TOWER TYPES FOR WIND ASSESSMENT BEFORE IEC 2005

Methods and Tower types						
	Field measurement	***Wind tunnel experiment***	***Potential flow solution***	***Computational fluid dynamics***	***Tower types***	
					Lattice tower	***Cylindrical tower***
Sherlock & Stalker (1941)		✓				
Sanuki et al. (1955)		✓				✓
Rider (1960)	✓	✓				✓
Moses & Daubek	✓				✓	

(1960)						
Thornthwaite et al. (1962)	✓					
Borovenko et al. (1963)	✓		✓			✓
His & Cermak (1966)		✓			✓	
Hathorn (1968)	✓	✓			✓	
Gill et al. (1967)		✓			✓	
Cermark & Horn (1968)	✓	✓			✓	
Dabberth (1968a)	✓				✓	
Dabberth (1968b)	✓		✓			✓
Camp & Kaufman (1970)	✓	✓			✓	
Angell & Bernstein (1976)	✓				✓	
Wucknitz (1977)	✓		✓			✓
Lavagnin et al. (1988)	✓				✓	
Pedersen et al.1992	✓	✓			✓	
Hansen & Pedersen (1999)	✓			✓	✓	
Barthlott & Fiedler (2003)	✓		✓		✓	
Yelland et al. (2002)	✓				✓	
Klein (2002)	✓			✓		✓

TABLE II. SUMMARY OF THE PURPOSE AND FINDINGS FROM LITERATURES PUBLISHED BEFORE IEC 2005

Author(s) and Year	Purpose of the study	Major Findings
Sherlock & Stalker (1941)	Causes and remedies to downwash	Causes of downwash of stack gases and remedies
Sanuki et al. (1955)	Evaluation of errors due to cylindrical obstruction	Minimum boom length to keep sensors in the lee and windward sides out of tower wake distortion
Rider (1960)	Evaluate flow distortion of 2.5 cm diameter cylindrical mast	3 % difference in the up and downstream speeds. Speed deficit on the lee side of the tower were evident
Moses & Daubek (1960)	Investigate shadow effect of lattice rectangular tilt-up mast	Speed deficit range (25 % to 50 %), speed-ups and flow deviations and angular dependency of wake effects
Thornthwaite et al. (1962)	Investigate the disturbance of the platform to wind flow.	Minimum boom length, 30 % and 70 % speed deficits for up and downstream directions respectively
Borovenko et al. (1963)	Investigate-wake effect of 300 m long tower of 2.4 m diam.	The study provides insight on the possible location of the boom on a cylindrical tower (±

		45°)
His & Cermak (1966)	TI influence on tower produced perturbations	TI increases tower induced perturbation by only 2 %. Shadow effect depends on tower configuration
Hathorn (1968)	Influence of NASA 150 m lattice tower on wind measurement	Speed deficit of 27 % due to tower shadow. Secondary support structure influence noted
Gill et al. (1967)	Investigate shadowing effects of triangular lattice tower	The study suggests possible boom lengths to keep the sensors away from the wake effect of the tower
Cermak & Horn (1968)	Investigate tower shadow effect of a met tower	Speed deficit range 10 % to 40 % for a boom length of 3.6 m and confined to 30° sector in the tower wake
Dabberth (1968a)	Investigate tower wake effects of a lattice triangular tower	The study defines wake boundaries. Speed deficit of 35 % and speed-up of 19 % are evident
Dabberth (1968b)	Investigate shadowing effects of a cylindrical drum	Speed deficit in the upwind and downwind side of 6 % and 40 % respectively. 5 % speed-up evident
Camp & Kaufman (1970)	Investigate the shadowing effect of 150m NASA tower	Result from both experiments correctly defines the boundary of the tower wakes
Angell & Bernstein (1976)	Investigate flow modification around a television tower	7 % speed deficit as a result of tower wake is evident
Wucknitz (1977)	Investigate flow disturbance of a cylindrical tower	Placement of booms symmetrically at both sides of the tower may help to identify wake boundaries
Lavagnin et al. (1988)	Investigation of tower wake of a disused powerline in Italy	Upwind speed deficit of 15 % and lee side speed deficit of 80 % are recorded
Pedersen et al. (1992)	Investigate anemometer arrangement to reduce error	Suitable position for anemometer location to minimise errors due to tower induced disturbances
Hansen & Pedersen (1999)	CFD approach to investigate tower shadow effect	Minimum boom length and suitable boom orientation for lattice and tubular specified
Barthlott & Fiedler (2003)	Investigate the turbulence structure in the waked region	Speed deficit of 19 % and increase in turbulence spectra in the waked region of a lattice tower
Yelland et al. (2002)	Investigate air flow distortion over a research ship	Modelled errors agreed with anemometer reading except in the upstream of the ship
Klein (2002)	Investigate air tower shadowing effect of a tubular tower	A 20 % maximum speed deficit and a wake boundary covering about 50° in the waked region of the tower

B. The Provisions of IEC 2005 and the Shortcomings

Globally, knowledge and guidelines on tower instrumentation are found in standards and research studies, the most prominent of which is the International Electrotechnical Commission (IEC) standard IEC 614200-12-1 Wind turbines–Part 12-1: Power performance measurements of electricity producing wind turbines [3], whose Annex G is the portion of interest. Before the 2017 amended edition [4], the 2005 edition was the internationally accepted guideline for both tubular and lattice tower instrumentation. From the literature (i.e. [4], [11], [12], [36], [37]) it is evident that towers used for wind measurement have a variety of other applications which the standards and available studies did not address in terms of their physical nature and the related effect on wind energy observation. In the context of this study, towers belonging to the mobile telecommunication company MTC of Namibia was instrumented according to [3] for wind measurement. In this regard, [3] was critically reviewed to ascertain its wider applicability to operational towers.

Annex G of [3] specifies three mounting strategies including: a top mounted anemometer, a side-by-side top-mounted anemometer and a side-mounted anemometer. In the top mounted position, the anemometer is placed on the top of the met mast using a vertical tubular rod of specified cross section

and length. It is a preferred option contrary to [24]. Top mounted arrangement may eliminate tower shadowing effect but lack enough information for robust anemometer consistency checking with another similar or lower elevation anemometer which enables the evaluation of the site wind shear trend. Better consistency checking may be achieved with side-by-side top-mounted anemometers provided the sectors affected by tower and boom wake effects are identified and eliminated. Consistency checking for lower level anemometers and shear trend evaluation requires that booms be placed at some intermediate height. Anemometers placed at such intermediate heights are exposed to the shadowing effect of the tower. Reference [3] provides recommendations on the minimum boom length to reduce speed deficit to 0.5 %, but wind flow at any site is not constrained to a specified direction; as result, anemometers might be in the tower's wake at some point. The standard further stated that shadowing effects of the tower depends on its solidity, the drag of individual members, direction of the wind and separation of the measurement point from the mast. Plan views of iso-speed lines of normalised flow within the vicinity of both tubular and lattice meteorological towers are presented. The standard further provides a mathematical expression for estimating centreline velocity deficit upstream of the mast given as a function of the thrust coefficient which depends upon the solidity of the meteorological mast and the normalised leg distance. Based on the Annex G of [3], a user may easily estimate the velocity deficit if the tower dimensions are provided.

Based on detailed analysis, it may appear as if [3] has addressed all the problems regarding tower instrumentation for wind observation. However, the standard has limitations resulting from either the factors considered or not considered, or the method of obtaining the information presented. Some of the shortcomings are briefly discussed here and they agree with the findings in [15].

1) Assumed incident wind direction: The mathematical expression that captures the velocity deficit is assumed to be on the axes that pass through the mast centre and perpendicular to the mast face. The implication is that the incident wind is considered perpendicular to the same mast face, giving rise to velocity deficit values that are predicted using the upstream contour profiles of modified flow within the vicinity of the mast. In most cases, this arrangement does not correspond to the anemometer placements in many wind campaign sites, more especially where communication towers are instrumented for wind assessment. For one reason or the other the most prevalent practical mounting arrangements have been to place the boom parallel to the faces of the mast which then becomes perpendicular to [3] reference direction and this is the boom and anemometer arrangement used in Amperbo, Schlip and Korabib, three southern inland locations in Hardap and Kharas regions of Namibia, where wind observations are currently taking place.

2) Universal applicability: In [3], the range of solidity ratio and by extension the thrust coefficients for lattice meteorological masts of different configurations to be used in the mathematical expression of the velocity deficit are specified. For the communication towers investigated in this study and many other operational towers, the values of the solidity ratio and thrust coefficients are outside the specified range in [3] and vary greatly when different incident wind angles are considered. Having thoroughly investigated this concept accurately in this work, one may question how universally applicable the velocity deficit expression is.

3) Numerical method: Two-dimensional Navier-Stokes numerical computation were used to draw the iso-speed plots of local wind flow modification within the vicinity of the met mast. The numerical computation was based upon a combination of actuator disc and Navier-Stokes theory and analysis [3], as in [33]. This approach oversimplifies the problem in terms of the geometry and flow field and may constitute a major source of uncertainty in its application. As opined in [15], this approach may reasonably describe flow around a cylindrical tower but not for a more complex lattice type of tower.

4) Influence of the secondary support structure: As earlier mentioned, lattice towers used in wind data observation are deployed for other uses as well. As a result, the majority of them have discrete members such as cross and horizontal bracings, cable ladders, cable bundles and attachment brackets etc., which produce discrete wakes which result in a more complex flow interference contrary to the idealised mast configuration as presented in [3]. Tthe guideline presented in [3] neither acknowledges the obvious presence of secondary support structures nor suggests an approach to estimate errors due to their presence.

5) Impact of free-stream turbulence: The maximum height of atmospheric boundary layers which occur at late afternoon are around 1500 m [38]. Experimental results show that wind speed varies with height and so does the free-stream turbulence. Instruments located at different heights of the mast may be exposed to different atmospheric conditions [15]. The standard [3] does not consider the impact of free-stream turbulence on flow distortion within the vicinity of the tower.

6) Wind direction dependency: In [3] incident wind angle was considered to be perpendicular to a face of the lattice met mast, along the same line to the speed sensor and all information available in the standard is based on that assumption. The standard justifies this choice of boom and anemometer arrangement on the premise that local flow distortion within the vicinity of the tower is least within the 90° measurement sector.

V. Review of Literature Published Between 2005 and 2017

Rapid evolution of CFD techniques and decreasing computer hardware costs accompanied by faster processing times [39] have increased the versatility of application of CFD in various fields of learning. CFD study combined with field observation have been used for predicting flow around and through towers deployed for wind measurement. While [40] gave an account of the minimum boom length and how a tower's surface irregularities contribute to flow perturbations, [41] found that an increase in the vertical separation distance of the top mounted anemometer results in less error readings and concluded that free-stream turbulence has negligible impact on

tower induced flow distortion, agreeing with [26]. Reference [42] approached the problem as per [3] where a lattice triangular tower was modelled as an actuator disc. Using the CFD model and varying the solidity and Rd/Lm ratios, a correction factor which provides a qualitative good fit between simulated and observed was derived. In a further computational approach [43] performed CFD analysis of tubular and lattice masts modelled as actuator discs, similar to the approach adopted in literature such as [3], [4], [42] and [44]. Using the k-ω SST two equation RANS model for flow analysis and validating the flow simulation with the field observed data, a correction mechanism for detecting incorrectly mounted booms was suggested. The study by [43] predicted higher flow distortion than [3] and [4] and attributed such to free-stream turbulence that was factored in during the CFD flow simulation. Using the CFD approach, [37] studied the shadowing effect of a lattice triangular communication tower and its secondary support structures and reported that [3] overpredicted the minimum boom length required to place the anemometer away from the tower wakes. Similarly, [1] and [2] performed 3D CFD simulation verified by comparison with 1:20 scale models of FINO 3 lattice towers. While both studies predicted shorter boom lengths at various incident wind directions, [1] reported that one-equation Spalart-Almaras performs surprisingly well compared with its more sophisticated two-equation counterparts k-ε and k-ω SST, based on the sensitivity analysis of the three turbulence models often used in external aerodynamic study. Using CFD flow simulation and wind tunnel measurement, an improved methodology of evaluating shadowing effect of a lattice tower was suggested by [15]. Listing some of the shortcomings of Annex G of [3], as discussed in this present work, the study concluded that tower shadow study is an atmospheric flow problem that requires realistic free-stream boundary conditions corresponding to ABL profiles during computational analysis. Reference [6] proposed a numerical model that combines a potential flow solution in the region outside the tower wake, and a two-dimensional Gaussian turbulent wake within the wake, for the purpose of correcting anemometer readings to remove error due to the shadowing effect of the tower. The study acknowledged the limitation of the model's application due to oversimplification involved in its derivation. As a result of field experimentation, a formula and an in-field calibration for wind speeds and directions measured using booms collocated at 80 m AGL and placed 60° apart in a lattice triangular tower was proposed by [45]. The proposed method extracted direction dependent errors and shadowing effect of the tower to an uncertainty of less than 0.5 %. Similarly [46] clearly shows the severity and boundaries of tower wakes when the speed ratio of collected anemometers placed on an 80 m tilt-up tubular tower was computed. References [47] and [48] approached the problem experimentally using field measurements. Applying different data filtering methodologies, [47] identified and treated the shadowing effect of the tubular tower and proposed two additional methods and correction factors. Using the Levenberg-Marquardt algorithm, measurement from one anemometer was used to recreate data from an anemometer placed at the same intermediate height on the opposite side of a rectangular lattice tower that had failed [48]. Speed ratios plotted as a function of the wind direction clearly revealed the direction sectors and the severity of the tower wake effects. Wind speed deficit in different incident wind directions around a tubular tower was evaluated experimentally by [7], using full-scale wind tunnel testing. A speed deficit of 18 % and 35 % for higher and lower wind speeds was reported in the waked region of the tower and the study concluded that tower wake intensity was speed dependent. Flow induced perturbations of a BT tower building and lattice mast placed on the top of it were investigated [49]. When the results from both experiments were compared, an upward flow deflection due to tower building was evident and uncertainties in speed and direction and speed-ups are all associated with the mast shadowing effect. In [11] and [50], it was reported that higher and lower values of tower distortion factor (TDF) and scatter factor (SCF) are associated with tower waked regions. Table III and Table IV summarise the above studies in tabular form

TABLE III. SUMMARY OF THE METHODS AND TOWER TYPES FOR WIND ASSESSMENT BETWEEN 2005 AND 2017

Methods and Tower types						
Author(s) and Year	***Field measurement***	***Wind tunnel experiment***	***Potential flow solution***	***Computational fluid dynamics***	***Tower types***	
					Lattice tower	***Cylindrical tower***
Filippelli & Mackiewicz (2005)	✓			✓		✓
Perrin et al. (2007)	✓			✓		
Sadoud (2012)	✓			✓	✓	
Tusch et al. (2011)	✓			✓	✓	✓
Bezrukovs et al. (2017)				✓	✓	
Stickland et al. (2013)		✓		✓	✓	
Fabre et., al (2014)		✓		✓	✓	

Lofti et al. (2015)		✓		✓	✓	
Lubitz (2009)	✓		✓			✓
Lindelöw et al. (2010)	✓				✓	
Lang & McKeogh (2011)	✓					✓
Farrugia & Saint (2014)	✓					✓
Farrugia & Sant, (2013)	✓				✓	
Orlando et al. (2011)		✓				✓
Barlow et al. (2011)	✓	✓			✓	
Rehman (2014)	✓					✓

TABLE IV. SUMMARY OF THE PURPOSE AND FINDINGS FROM LITERATURES PUBLISHED BETWEEN 2005 AND 2017

Author(s) and Year	Purpose of the study	Major Findings
Filippelli & Mackiewicz (2005)	Investigate shadowing effect of a tubular tower	Minimum boom length was recommended. Flow perturbation caused by surface irregularities
Perrin et al. (2007)	Investigate flow defect of speed sensor on top of a tubular tower	5 tower diameter vertical distance results in error of less than 1 %. Free-stream turbulence has negligible impact
Sadoud (2012)	Using CFD to investigate the shadowing effect of 134 m lattice tower	A correction factor which provides a qualitative good fit between simulated and observed was derived
Tusch et al. (2011)	CFD to investigate wake effects of tubular and lattice towers	Correction mechanism for detecting incorrectly mounted booms. Free-stream turbulence impact was investigated
Bezrukovs et al. (2017)	CFD to investigate the shadowing effect of lattice triangular communication tower	An attempt to investigate the impact of some secondary support structures
Stickland et al. (2013)	Using CFD to investigate shadowing effect of FINO3 lattice tower	Shorter boom lengths predicted at all incident wind directions
Fabre et al. (2014)	Using CFD to investigate shadowing effect of FINO3 lattice tower	Shorter boom lengths predicted at all incident wind directions. k-ω SST the most suitable turbulence model
Lofti et al. (2015)	Impact of freestream turbulence on tower shadowing effect. A CFD study	Tower shadowing effect is an atmospheric flow problem
Lubitz 2009	Using numerical model and field observation to evaluate tower shadow	Correction factor with limited application due to oversimplification involved was proposed
Lindelöw et al. (2010)	Investigate a methodology to extract tower shadow effect of a lattice tower	Proposed formula for extracting direction dependent errors and tower shadowing effects was proposed
Lang & McKeogh (2011)	Investigating the tower shadow of a tubular tower	Tower wake boundary and intensity are identified

Farrugia & Saint (2014)	Investigating the tower shadow effect of a tubular tower	Proposed two methods for data filtering and correction factors
Farrugia & Sant, (2013)	Investigate tower shadow and method of correction of failed anemometer	Method of recreating lost data from failed anemometer given the data from the opposite anemometer
Orlando et al. (2011)	Using tunnel testing to study tower showing effect of a tubular tower	High wind speeds lead to less speed deficit (18 %) and low wind speeds lead to high speed deficit (35 %)
Barlow et al. (2011)	Investigate flow perturbation of a BT tower and lattice mast on top of it	Speed and direction correction measures were proposed. Flow induced defects from building and mast were evident
Rehman (2014)	Investigate wake effect of a tubular tower by computing the TDF and SCF	Higher values of TDF and SCF in the wake affected regions. Lower values of TDF and SCF in the regions without wake

VI. REVIEW OF IEC 2017

The 2017 edition [4] of the standard acknowledged some of the limitations of the earlier edition discussed above and found in [15]. For instance, on the assumed incident wind direction, the standard (IEC 2017), still uses the same expression for the centre line velocity deficit and its associated uncertainties, as discussed earlier. On the universal applicability, the range of solidity ratio remains as prescribed in [3]. The errors inherent in the use of this expression for operational towers whose solidity ratios are outside the range specified [3] still exist in [4]. Again, the numerical model (combination of actuator disc and two-dimensional Naiver-Stokes theory) used to draw the iso-speed plots of tower induced flow perturbation was carried forward to the newest edition [4]. The standard indicates zones of high accuracy upstream of the mast based on the iso-speed plots on both cylindrical and lattice towers. Furthermore, [4] acknowledges that secondary support structures (cross and horizontal bracings, cable ladders, cable bundles and attachment brackets etc.) produce discrete wakes which make flow interference significantly more complex within the vicinity of the tower, however the standard does not suggest any practical approach to evaluate their contribution to tower induced flow defects. Further comparison of [3] and [4] shows that the 2017 edition of the standard did not also consider whether the free-stream turbulence would affect tower induced perturbations. Finally, on the wind direction dependency, the 2017 edition justifies the choice of boom and anemometer arrangements on the premise that local flow distortion is least within 90° measurement sector and provided that the anemometer is placed a distance Rd > 2 times the met mast leg distance. The 2017 edition further suggests that that flow induced perturbations, having met the stated requirements, are negligibly affected by the met mat orientation (whether the corner or face is oriented into the wind), and as such can be assumed to be the same [4]. The 2017 edition [4] of the standard went a step further and performed a CFD derived flow showing the relative position and hence influence of a secondary support structure on the flow distortion changes with height. Two sets of CFD flow simulation were performed using incident wind at 90° and another at angle less than 90°, both on the same mast face resulting in a distortion that is asymmetric but shows that the optimum location for minimum flow distortion is still within the 90° sector to the flow direction, thereby further reinforcing Annex G of [4]. The standard however acknowledged that winds approaching at an incident angle greater than 100° from the anemometer boom orientation would result in higher flow distortion, though no further explanation was given in that regard.

VII. REVIEW OF LITERATURE PUBLISHED AFTER IEC 2017

Recent advances in the wind energy industry have seen the deployment of light detecting and ranging (LiDAR) and sound detecting and ranging (SODAR) for ground profiling of wind. The shadowing effect of a lattice tower was evaluated through combination of experimental data captured with sonic anemometers, staring and profiling LiDAR [5]. The study reported a maximum speed deficit of up to 50 %, an order of increase in turbulent kinetic energy (TKE), a decrease in wind speed correlation in wake affected direction sectors, and flow deflection due to tower physical structure. Adopting a similar approach, the wake distortion effect of a lattice communication tower was evaluated by analysing and comparing data measured using collocated anemometers and LiDAR [11], [12]. The study reported a maximum speed deficit of 49 %, a decrease in speed and TI correlation in the waked sectors, and an order of increase in turbulence intensity (TI) in the waked zones. The study concluded that TI analysis may be a better predictor of tower wake distortion when compared with the traditional speed ratio approach [11]. Reference [51] in a CFD study developed a correction method that reduced tower induced error readings from 4.1 % to 0.8 % in a field experiment, where four anemometers installed on booms mounted parallel to the four sides of a rectangular lattice tower was proposed. In [52], a study that paralleled [6] was conducted. A preliminary model to remove tower shading and to correct data from pairs of anemometers in which one fails was proposed, though the author acknowledged the limitation of the model's application due to the oversimplification involved in its derivation. Table VI and Table VII summarise the above studies in tabular form.

TABLE V. SUMMARY OF THE METHODS AND TOWER TYPES FOR WIND ASSESSMENT BETWEEN 2017 AND 2019

Methods and Tower types							
Author(s) and Year	*Field measurement*	*Wind tunnel experiment*	*LIDAR measurement*	*Potential flow solution*	*Computational fluid dynamics*	*Tower types*	
						Lattice tower	*Cylindrical tower*
McCaffrey et al. (2017)	✓		✓			✓	
Lubitz & Michalak (2018)	✓			✓			✓
Nishio (2018)	✓				✓	✓	
Okorie & Inambao (2019)	✓		✓			✓	
Okorie & Inambao (2019)	✓		✓			✓	

TABLE VI. SUMMARY OF THE PURPOSE AND FINDINGS FROM LITERATURES PUBLISHED BETWEEN 2017 AND 2019

Author(s) and Year	Purpose of the study	Major Findings
McCaffrey et al. (2017)	Investigate shadowing effect of a BAO lattice tower	Accurate definition of wake boundaries, speed deficits and speed-ups. Decrease in correlation and tower flow deflection
Lubitz & Michalak (2018)	Investigate speed averaging in the measured magnitude in the wake	A preliminary model to remove wake effects from sensor data and to correct data from a pair of sensors if one fails
Nishio (2018)	Using CFD to investigate and correct the shadowing effect of a rect. lattice tower	Proposed a correction method that reduces tower induced error readings from 4.1 % to 0.8 % using CFD analysis
Okorie & Inambao (2019)	Field and LiDAR observation to investigate wake effects of a lattice communication tower	Wake boundaries defined, speed deficits, decrease in correlation. TI analysis a better tower wake predictor
Okorie & Inambao (2019)	Field and LiDAR observation to investigate wake effects of a lattice communication tower	Wake boundaries accurately defined using collocated anemometers. Speed up of up to 49 % reported.

VIII. RESULTS AND DISCUSSION

A. *Distribution of Method of Investigation and Tower Type used*

As earlier stated, the length of time covered in this review is a testament that research publications on the theme is very sparse. Between 1941 to 2004, 21 studies that provided insight into tower shadowing effect were reviewed. While Table I provides the summary of the methods and tower configurations used, Table II summarises the purpose and major findings of each study. Field and wind tunnel experiments were the dominant approaches to the problem, accounting for 51.13 % and 28.12 % respectively of the methods used. Numerical approach (potential flow solution) accounts for 12.5 % and CFD for 6.25 % of the methods used. For validation purposes, two or three of the methods are combined (Table I). Moreover, 17 (68.42 %) lattice tower (triangular and square) were examined while 6 (31.58 %) cylindrical (tubular and rod) were studied. Between 2005 to 2017, 16 studies were reviewed. Table III is a summary of the methods and tower configurations used and Table IV summarizes the purpose and major findings of each study. Rapid evolution of CFD techniques and decreasing computer hardware costs accompanied by faster processing times have increased the versatility of the application of CFD in various fields of learning [35]. CFD study and field observation were the dominant research approach, and accounts for 32 % and 44 % respectively of the methods used. Wind tunnel experiments accounted for 20 % while the potential solution approach accounted for 4 % of the methods used. Lattice towers (triangular and square) investigated accounts for 56.75 % while

cylindrical towers (tubular and rod) accounted for 43.75 %. Five papers were reviewed that we written between 2017 and 2019. In Table VI, we find a summary of the method and the tower configurations used while Table VII summarises the purpose and the major findings. The experimental methods used were field measurements (50 %) and LiDAR (30 %). Potential solution and CFD simulation accounted for 10 % each. Lattice towers (triangular and square) accounted for 80 % while cylindrical towers (tubular and rod) accounted for 20 %.

The three mounting strategies specified by Annex G of [3] and [4] included top mounted anemometer, side-by-side top-mounted anemometer and side-mounted anemometer. The standards considered top mounted as the preferred option contrary to [24]. Previous literature such as [5], [8], [11], [12], [45]–[47] and [51]–[53]) used collocated anemometers where one serves as the test and the other the redundant. This arrangement provided enough information for better sensor consistency check [4] and site shear trend evaluation. However, there was no consensus on the angle of separation between the booms. On the computational model, literatures such as [1], [2], [15], [37], [43] and [51] agreed that the 3D CFD approach was better suited for modelling flow around and through an operational lattice tower structure than the numerical approach prescribed in [3] and [4].

The identified limitations were further discussed considering the current literature regarding identified areas that needed improvement. The issues of secondary support structures, free-stream turbulence, wind direction dependency and tower shadow impacts on other resource parameters were discussed.

B. Secondary Support Structures

Concerns about stability coupled with the variety of other applications on the towers has made secondary support structure a critical component of today's operational towers. In [36] it was reported that a 1 % increase in speed-ups in a150 m NASA lattice tower was due to the presence of a catwalk. The IEC (2017) standard acknowledged that secondary support structures could produce discrete wakes which would make flow interference significantly more complex within the vicinity of the tower. However, the standard did not suggest any practical approach to evaluate their contribution to the overall wake distortion effect. The only literature that considers wake influences of secondary support structures as a research component in modelling flow through an operational tower is [37]. However, the inconsistencies in determining the solidity ratio of the tower, the contribution of the secondary support structures and the thrust coefficient are sources of concern. Models used in the literature to study the secondary support structures are oversimplified and the centreline velocity deficit expression proposed by the IEC standard has still been used to compute the value of R, meaning that the inherent uncertainties mentioned earlier in [3] and [4], on how the expression was derived and used, are also applicable to [37]. Further investigation is therefore required to improve the method of assessment and to estimate the magnitude of perturbations due to secondary support structures.

C. Free-Stream Turbulence

Both editions of the standards are silent on the impact of free-stream turbulence on tower induced flow perturbations. In the earlier literature (i.e. [26], [41]) it was suggested that free-stream turbulence and turbulence level increase do not have any significant impact on the tower induced flow defect. On the contrary, [15] did a comparative study on the choice of boundary conditions used in literatures for free-stream turbulence analysis and found that tower shadowing effect should be treated as an atmospheric flow problem by setting the free-stream boundary conditions that corresponds to atmospheric boundary conditions (ABL) during the flow analysis rather than treating it as an arbitrary external flow problem as previous studies have done. The result of this study by [15] was in agreement with [43] which reported higher flow distortion than [3] and attributed this to free stream turbulence that was considered during the CFD flow simulation. However, there is a limitation in the application of previous studies on towers of different configurations and different site atmospheric conditions in the boundary layer. In the context of the present work, further investigation is needed to estimate possible speed-ups upstream of the tower due to free-stream turbulence using LiDAR captured wind speed that is considered to be undisturbed.

D. Wind Direction Dependency

The idealised tower and boom arrangement whereby predominant wind speed is always perpendicular to the face of the lattice tower is rare in a typical field measurement. Incident wind may arrive at the tower at an angle less or more than 90°. In the context of the present study, the lattice towers investigated were not originally designed and erected for wind measurement purposes. The prevailing wind pattern in terms of predominant direction at the host sites were not known before they were erected. More so, the booms holding the anemometers were placed parallel to the face of the tower while the incident wind angle was not perpendicular to the tower face. Thus, the incident winds arrive at the tower at angles that are not 90°. As the incident wind angle varies, the assumed tower leg length, solidity ratio and in extension thrust coefficient changes as shown in Fig. 5a-5c and Fig. 6a-6c. If the centreline velocity deficit expression derived from the standard mast configuration (Ø = 0°) is the only criterion for quantifying tower flow distortion, the concern about its universal applicability arises again. For this reason, the velocity deficit expression may not precisely predict flow distortion at different incident wind angles. Previous literature (i.e. [1], [2], [15], [37], [40]) that adopted the computational approach to the problem agreed that tower induced flow distortion is angle dependent. However, none of the previous studies had attempted or suggested an approach to modify the velocity deficit expression to truly capture flow distortion at different incident wind angles other than 90° as prescribed in [3] and [4].

Fig. 5 and Fig. 6 are the relationship between parameters of interest derived from the analysis of tower modules (Fig. 3a and Fig. 5b). The variation of incident wind angle with the tower leg length (module face width) for a module 0.890 m and 1.052 m high respectively are clearly illustrated (Fig. 4a and

Fig 5a). The information available in [3] and [4] assume constant leg length but this is not true. Wind incident angle of less or more than 90° on the same tower face will be exposed to a different tower projected area, hence different leg lengths (face width). At each incident wind angle the projected area differs, hence the solidity ratio (Fig. 5b and Fig. 6b). Least flow distortion would occur at angles (30°, 90°, 150°, 210°, 270° and 330°) corresponding to higher solidity ratio and vice versa. Similar results are found in [15]. Figures 5c and Fig. 6c are the solidity ratios. drawn as a function of the tower leg lengths.

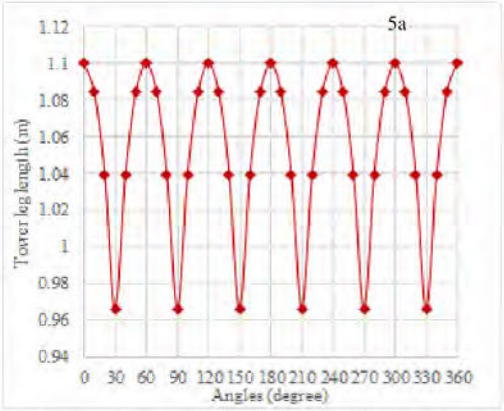

Fig. 5a. Tower leg length (face width) variation with incident wind angle for the module of the tower at Amper-bo (Fig. 3a and Fig.3b).

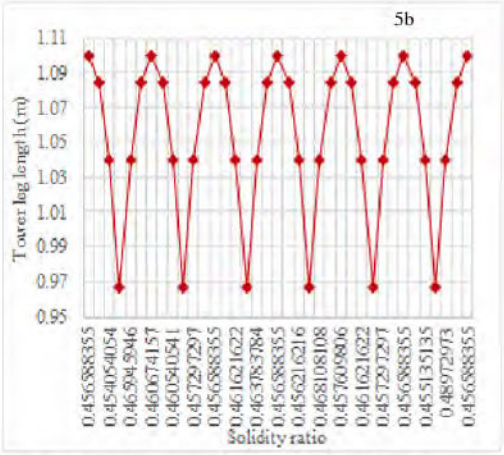

Fig. 5b. Tower leg length (face width) variation with solidity for the tower module of the tower at Amper-bo (Fig. 3a and Fig. 3b).

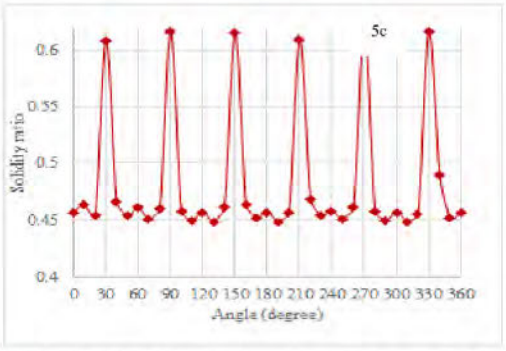

Fig. 5c. Solidity ratio variation with incident wind angle for the tower module of the tower at Amper-bo (Fig. 3a and Fig. 3b).

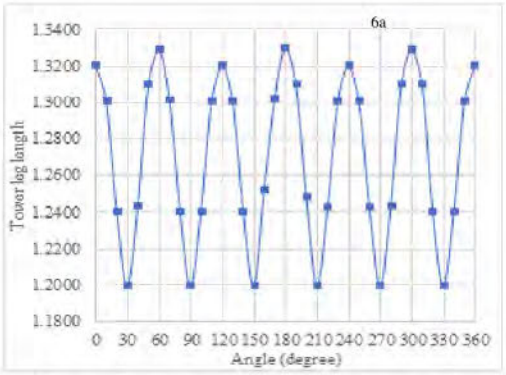

Fig. 6a. Tower leg length (face width) variation with incident wind angle for the module of the tower at Korabib (Fig. 4a and Fig. 4b).

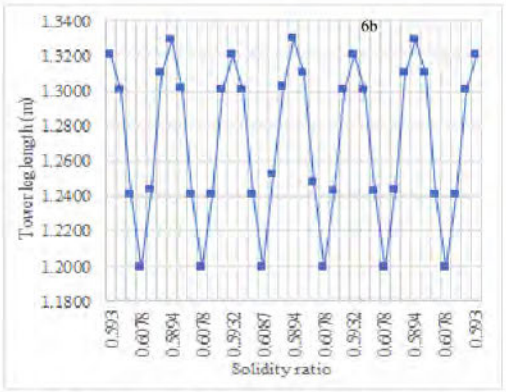

Fig. 6b. Tower leg length (face width) variation with incident wind angle for the module of the tower at Korabib (Fig. 4a and Fig.4b).

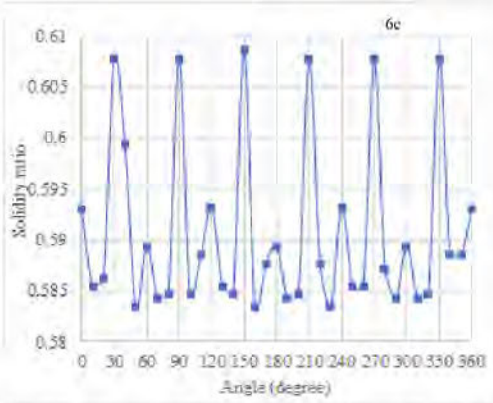

Fig. 6c. Solidity ratio variation with incident wind angle for the tower module of the tower at Korabib (Fig. 4a and Fig. 4b).

The graphs of leg length versus solidity ratio have the same pattern with the graphs of incident wind angles versus leg length. This is well understood because the solidity ratio and the leg length (tower face width) are all computed based on the incident wind angle.

The two lattice triangular towers exhibit rotational symmetry at 120°. Further details of this analysis will be available in future work. Since the two key parameters in the velocity deficit expression (thrust coefficient which depends on the solidity ratio and the tower leg length) are angle dependent, therefore, tower induced flow perturbations are also angle dependent. The universality of application and the assumed incident wind direction based on the recommendations of the standards [3] and [4] are not necessarily true. Again, towers instrumented according to the IEC standards do not guarantee the required 1 % accuracy in waked regions [37]. Based on the critical review of the IEC standards, it is safe therefore, to treat the (IEC 2005 and 2017) as a guideline rather than a document that precisely describes the instrumentation of a typical operational tower. There is a need for a centreline velocity deficit expression that captures variations in solidity ratio and the tower leg lengths to precisely define flow distortions at various incident wind angles around an actual operational tower. There is also a need to improve the method of calculating the solidity ratio, the leg length, and the thrust coefficients, the reduction in porosity due to secondary support structures at any given angle and planes (Fig. 3a and Fig. 4a), and, ultimately, to incorporate wind incident angles into the velocity deficit expression to account for tower wake distortion at such an angle. This may require a parametric approach to the study.

E. Tower Shadow Impact on Resource Parameters

Tower wake distortion is majorly associated with speed deficits and speed-ups. This is evident in all the literature reviewed. Validating field observation with LiDAR captured data, an order of increase in TKE and TI due to tower shading was reported in [5] and [11]. The precise impact of tower shadowing on other resource parameters of interest such as wind shear coefficient, Weibull parameters etc. are not known. For cases where there are no collocated speed sensors, two or three speed sensors are placed at different heights (AGL) but on the same azimuth from the north, but no literature has addressed a method of detecting tower induced flow perturbations to the reading of the sensors. The need to use the undisturbed LiDAR data to quantify the impact of the phenomenon on other resource parameters of interest therefore exists.

IX. CONCLUSION

The current study is a presentation of an extensive review of literature on tower wake distortions and evaluation of methodologies for wind measurement. The best practices to identify, define and minimise tower wake effects for both lattice (triangular and rectangular) and cylindrical (tubular and rod) towers were fully accounted for in 48 of the studies reviewed. The literature was reviewed and organised according to the method and tower type used and the purpose and major findings of each study. Between 1941 and 2004, field and wind tunnel experiments were the dominant approaches to the problem, but from 2005 to 2017 field observation and CFD flow analysis dominated the research approach used. Beyond 2017, field experiments (anemometer and LiDAR) were combined to evaluate tower induced flow defects. Literatures published prior to 2005 was discussed setting the foundation for critical review of the IEC (2005) standard. Thereafter, literature published between 2006 and 2017 was reviewed setting the foundation for further review of the IEC (2017) standard. Finally, literature published post IEC (2017) was reviewed. Arising from this extensive literature, the following grey areas exist for future academic research work:

- (IEC 2017) acknowledged that secondary support structures could produce discrete wakes which would make flow interference significantly more complex within the vicinity of an operational tower. In [37], an attempt was made but there exist inconsistences on how the solidity ratio was evaluated. The model that described the secondary support structures was also over-simplified. Further investigation, especially of towers of different configurations, is therefore required to improve the method of assessment and to estimate the impact of these discrete structures on porosity.
- (IEC 2005) and (IEC 2017) did not assess the impact of free-stream turbulence on tower induced flow perturbations. There exists no consensus on the impact of this phenomenon on tower wake distortion. Some studies opined that free-stream turbulence impact is negligible, while others acknowledged it to be an atmospheric flow problem. Towers of different configurations located at different sites in different atmospheric conditions in the boundary layer requires further verification.

- On the wind direction dependency, relevant literatures published after IEC 2005 have consistently questioned the universality of the application of the centreline velocity deficit expression derived from a standard incident wind angle (Ø = 0°) as prescribed by the standard. The two key parameters in the expression (thrust coefficient which depends on the solidity ratio and the tower leg length) are all angle dependent. Tower wake distortion is therefore angle dependent. Expression that precisely captures tower induced flow perturbations at various incident wind angles is needed.
- Beside speed deficit, speed-ups and order of increase in TI and TKE reported in the literature, there exists a need to use undisturbed LiDAR observed data to further evaluate the exact impact of tower shadowing on other resource parameters of interest such as wind shear coefficient, Weibull parameters etc. A combination of the knowledge of the resource parameters and the two observation techniques, coupled with the knowledge of CFD, will assist greatly in arriving at the most accurate correction factor for each tower configuration.

The identified limitations suggest that further and continuous studies are needed. Application of previous studies to towers of different configurations located at different sites in different atmospheric conditions in the boundary layer are limited. IEC (2005 and 2017) therefore serve as a guideline rather than a precise description of local flow modification around and through an operational tower instrumented for wind measurement.

ACKNOWLEDGEMENT

Funding for this project was provided by the Ministry of Foreign Affairs of Denmark, Ministry of Foreign Affairs of Finland, United Kingdom Department for International Development, Austrian Development Agency and Namibia Power Corporation. Invaluable support is provided by Namibia Energy Institute under Namibia University of Science and Technology.

REFERENCES

[1] S. Fabre, M. Stickland, T. Scanlon, A. Oldroyd, D. Kindler, and F. Quail, "Measurement and simulation of the flow field around the FINO 3 triangular lattice meteorological mast," *J. Wind Eng. Ind. Aerodyn*., vol. 130, pp. 99–107, Jul. 2014, doi: 10.1016/j.jweia.2014.04.002.

[2] M. Stickland, T. Scanlon, S. Fabre, A. Oldroyd, and D. Kindler, "Measurement and simulation of the flow field around a triangular lattice meteorological mast," *Energy Power Eng*., vol. 5, Oct. 2013.

[3] International Electrotechnical Commission (IEC), "Wind energy generation systems – Part 12-1: Power performance measurements of electricity producing wind turbines," International Electrotechnical Commission (IEC), IEC Central Office 3 rue de Varembé CH-1211 Geneva 20, Switzerland, International Standard IEC 61400-12-1:2005(E), Dec. 2005.

[4] International Electrotechnical Commission (IEC), "Wind energy generation systems – Part 12-1: Power performance measurements of electricity producing wind turbines," International Electrotechnical Commission (IEC), IEC Central Office 3 rue de Varembé CH-1211 Geneva 20, Switzerland, International Standard IEC 61400-12-1:2017-03(en-fr), Mar. 2017.

[5] K. McCaffrey *et al.*, "Identification of tower-wake distortions using sonic anemometer and lidar measurements," *Atmos. Meas. Tech.,* vol. 10, no. 2, pp. 393–407, 2017, doi: http://dx.doi.org/10.5194/amt-10-393-2017.

[6] [6] W. D. Lubitz, "Effects of Tower Shadowing on Anemometer Data," in *11th Americas Conference on Wind Engineering*, San Juan, Puerto Rico USA, 2009.

[7] S. Orlando, A. Bale, and D. A. Johnson, "Experimental study of the effect of tower shadow on anemometer readings," *J. Wind Eng. Ind. Aerodyn*., vol. 99, no. 1, pp. 1–6, Jan. 2011, doi: 10.1016/j.jweia.2010.10.002.

[8] H. Moses and H. G. Daubek, "Errors in wind measurements associated with tower-mounted anemometers," *Bull. Amer. Meteor. Soc.*, vol. 42, no. 3, pp. 190–194, Mar. 1961, doi: 10.1175/1520-0477-42.3.190.

[9] J. E. Cermak and J. D. Horn, "Tower shadow effect," *J. Geophys. Res.*, vol. 73, no. 6, pp. 1869–1876, Mar. 1968, doi: 10.1029/JB073i006p01869.

[10] W. F. Dabberdt, "Tower-induced errors in wind profile measurements," *J. Appl. Meteorol*., vol. 7, no. 3, pp. 359–366, Jun. 1968, doi: 10.1175/1520-0450(1968)007<0359:TIEIWP>2.0.CO;2.

[11] M. E. Okorie and F. Inambao, "Identification of tower and boom- wakes using collocated anemometers and LiDAR measurement," *Int. J. Mech. Eng. Technol.,* vol. 10, no. 06, pp. 72–94, 2019.

[12] M. E. Okorie and F. Inambao, "Identification of tower-wake distortion using LiDAR measurement," *Procedia Manuf.*, vol. 35, pp. 704–710, Jan. 2019, doi: 10.1016/j.promfg.2019.06.012.

[13] J. E. Cermak and J. D. Horn, "Tower shadow effect," *J. Geophys. Res*., vol. 73, no. 6, pp. 1869–1876, 1968, doi: 10.1029/JB073i006p01869.

[14] W. F. Dabberdt, "Tower-induced errors in wind profile measurements," *J. Appl. Meteorol. (1962-1982)*, vol. 7, no. 3, pp. 359–366, 1968.

[15] M. Lotfi, "Atmospheric Wind Flow Distortion Effects of Meteorological Masts," Master's Thesis, FEUP, Porto, Portugal, 2015.

[16] O. Rodríguez, J. A. del Río, O. A. Jaramillo, and M. Martínez, "Wind power error estimation in resource

assessments," *PLOS One*, vol. 10, no. 5, p. e0124830, May 2015, doi: 10.1371/journal.pone.0124830.

[17] R. H. Sherlock and E. A. Stalker, *A study of flow phenomena in the wake of smokestacks*. printed by the George Banta Publishing Company, 1941.

[18] O. Karin *et al.*, "GWEC-GlobaWind Report 2018," GWEC-Global Wind Energy Council, Brussels Belgium, Technical report GlobaWind Report 2018, Apr. 2019.

[19] C. W. Thornthwaite, W. J. Superior, and R. T. Field, "Evaluation of an Ocean Tower for the Study of Climatic Fluxes," p. 79. Available: https://apps.dtic.mil/dtic/tr/fulltext/u2/401471.pdf

[20] J. K. Angell and A. B. Bernstein, "Evidence for a reduction in wind speed on the upwind side of a tower," *J. Appl. Meteorol. (1962-1982)*, vol. 15, no. 2, pp. 186–188, 1976.

[21] J. Wieringa, "A revaluation of the Kansas mast influence on measurements of stress and cup anemometer overspeeding," *Boundary Layer Meteorol.*, vol. 18, pp. 411–430, Jun. 1980, doi: 10.1007/BF00119497.

[22] G. C. Gill, L. E. Olsson, J. Sela, and M. Suda, "Accuracy of wind measurements on towers or stacks," *Bull. Am. Meteorol. Soc.*, vol. 48, no. 9, pp. 665–674, 1967.

[23] A. Lavagnini, S. Argentini, and R. Carullo, "Wind field modifications due to an anemometer tower," *Il Nuovo Cimento C*, vol. 11, no. 5–6, pp. 619–627, Sep. 1988, doi: 10.1007/BF02507005.

[24] J. Kline, "Effects of Tubular Anemometer Towers on Wind Speed Measurements," RAM Associates, Brentwood, USA.

[25] M. Sanuki, S. Kimura, and S. Toyama, "Anemometer reading in the presence of nearby obstacle," *Pap. Met. Geophys.*, vol. 6, no. 2, pp. 140–143, Dec. 1955, doi: 10.2467/mripapers1950.6.2_140.

[26] G. Hsi and J. E. Cermak, "Meteorological-Tower Induced Wind- Field Perturbations (Supplement)," Technical report CER6 6GH-JEC26, May 1966.

[27] N. E. Rider, "On the performance of sensitive cup anemometers," 1960.

[28] G. C. Gill, "Comments on 'A revaluation of the Kansas mast influence on measurements of stress and cup anemometer overspeeding,'" *J. Appl. Meteor.*, vol. 21, no. 3, pp. 437–440, Mar. 1982, doi: 10.1175/1520-0450(1982)021<0437:COROTK>2.0.CO;2.

[29] D. W. Camp and J. W. Kaufman, "Comparison of tower influence on wind velocity for NASA's 150-meter meteorological tower and a wind tunnel model of the tower," *J. Geophys. Res.*, vol. 75, no. 6, pp. 1117–1121, 1970, doi: 10.1029/JC075i006p01117.

[30] B. Maribo Pedersen, K. S. Hansen, S. Øye, M. Brinch, and O. Febian, "Some experimental investigations on the influence of the mounting arrangements on teh accuracy of cup-anemometer measurements," *J. Wind Eng. Ind. Aerodyn.*, vol. 39, no. 1, pp. 373–383, Jan. 1992, doi: 10.1016/0167-6105(92)90561-N.

[31] W. F. Dabberdt, "Wind disturbance by a vertical cylinder in the atmospheric surface layer," *J. Appl. Meteor.*, vol. 7, no. 3, pp. 367–371, Jun. 1968, doi: 10.1175/1520-

[32] J. Wucknitz, "Disturbance of wind profile measurements by a slim mast," *Boundary-Layer Meteorol.*, vol. 11, no. 2, pp. 155–169, Mar. 1977, doi: 10.1007/BF02166802.

[33] M. O. L. Hansen and B. M. Pedersen, "Influence of the meteorology mast on a cup anemometer," *J. Sol. Energy Eng.*, vol. 121, no. 2, p. 128, 1999, doi: 10.1115/1.2888150.

[34] C. Barthlott and F. Fiedler, "Turbulence structure in the wake region of a meteorological tower," *Boundary-Layer Meteorol.*, vol. 108, no. 1, pp. 175–190, Jul. 2003, doi: 10.1023/A:1023012820710.

[35] M. J. Yelland, B. I. Moat, R. W. Pascal, and D. I. Berry, "CFD model estimates of the airflow distortion over research ships and the impact on momentum flux measurements," *J. Atmos. Oceanic Technol.*, vol. 19, no. 10, pp. 1477–1499, Oct. 2002, doi: 10.1175/1520-0426(2002)019<1477:CMEOTA>2.0.CO;2.

[36] J. W. Hathorn, "Wind tower influence study /For NASA's 150-meter meteorological tower at Kennedy Space Center, Florida/," Kennedy Space Center, Flortda USA, NASA CR-61242, 1968.

[37] V. Bezrukovs, V. Bezrukovs, S. Upnere, D. Bezrukovs, and A. Sauhats, "The assessment of wind speed distortions in a simulated flow around a lattice cellular communication mast," in *2017 European Conference on Electrical Engineering and Computer Science (EECS)*, 2017, pp. 421–428, doi: 10.1109/EECS.2017.84.

[38] T. T. de A. T. Neves and G. Fisch, "The daily cycle of the atmospheric boundary layer heights over pasture site in Amazonia," *American J. Environ. Eng.*, vol. 5, no. 1A, pp. 39–44, 2015.

[39] G. H. Yeoh, C. Liu, J. Tu, and V. Timchenko, "Advances in computational fluid dynamics and its applications," *Modell. Simul. Eng.*, vol. 2011, 2011, doi: 10.1155/2011/304983.

[40] [40]M. Filippelli and P. Mackiewicz, "Experimental and computational investigation of flow distortion around a tubular meteorological mast," in *CanWEA's 21. Annual Conference and trade show 2005*, Toronto Canada, 2005, vol. 1, pp. 11–18.

[41] D. Perrin, N. McMahon, M. Crane, H. J. Ruskin, L. Crane, and B. Hurley, "The effect of a meteorological tower on its top-mounted anemometer," *Appl. Energy*, vol. 84, pp. 413–424, 2007.

[42] M. Sadoud, "Lattice Tower Shadow Investigation," National Renewable Energy Laboratory (NERL), Ottawa, Ontario Canada, Technical Note Draft 800113-CAMO-T-01, May 2012.

[43] M. Tusch, C. Masson, and P. Héraud, "Modeling of turbulent atmospheric flow around tubular and lattice meteorological masts," *J. Sol. Energy Eng.*, vol. 133, no. 1, p. 011011, Feb. 2011, doi: 10.1115/1.4003293.

[44] [44] M. O. L. Hansen and B. M. Pedersen, "Influence of the meteorology mast on a cup anemometer," *J. Sol. Energy Eng.*, vol. 121, no. 2, p. 128, 1999, doi: 10.1115/1.2888150.

[45] P. Lindelöw-Marsden, T. F. Pedersen, J. Gottschall, A. Vesth, R. W. U. Paulsen, and M. S. Courtney, "Flow distortion on boom mounted cup anemometers," Risø National Laboratory for Sustainable Energy. Technical University of Denmark, DK-4000 Roskilde Denmark, Risø-R-Report Risø-R-1738(EN), Aug. 2010.

[46] S. Lang and E. McKeogh, "LIDAR and SODAR measurements of wind speed and direction in upland terrain for wind energy purposes," *Remote Sensing*, vol. 3, no. 9, pp. 1871–1901, Sep. 2011, doi: 10.3390/rs3091871.

[47] R. N. Farrugia and T. Sant, "Modelling wind speeds for cup anemometers mounted on opposite sides of a lattice tower: A case study," *J. Wind Eng. Ind. Aerodyn.*, vol. 115, pp. 173–183, Apr. 2013, doi: 10.1016/j.jweia.2012.11.006.

[48] R. N. Farrugia and T. Sant, "Wind speed measurements in the vicinity of a tubular mast : influence of data selection methods on wind speed average determination," *Wind Eng.*, vol. 38, no. 2, 2014. https://doi.org/10.1260/0309-524X.38.2.147

[49] J. F. Barlow, J. Harrison, A. G. Robins, and C. R. Wood, "A wind-tunnel study of flow distortion at a meteorological sensor on top of the BT Tower, London, UK," *J. Wind Eng. Ind. Aerodyn.*, vol. 99, no. 9, pp. 899–907, Sep. 2011, doi: 10.1016/j.jweia.2011.05.001.

[50] S. Rehman, "Tower distortion and scatter factors of co-located wind speed sensors and turbulence intensity behavior," *Renewable Sustainable Energy Rev.*, vol. 34, pp. 20–29, Jun. 2014, doi: 10.1016/j.rser.2014.03.007.

[51] N. Nishio *et al.*, "A study on wind speed correction method of lattice tower mast using CFD simulation," *Transactions of the JSME (in Japanese)*, vol. 84, no. 862, pp. 18-00042-18–00042, 2018, doi: 10.1299/transjsme.18-00042.

[52] W. D. Lubitz and A. Michalak, "Experimental and theoretical investigation of tower shadow impacts on anemometer measurements," *J. Wind Eng. Ind. Aerodyn.*, vol. 176, pp. 112–119, May 2018, doi: 10.1016/j.jweia.2018.03.012.

[53] J. Wieringa, "A revaluation of the Kansas mast influence on measurements of stress and cup anemometer overspeeding," *Boundary-Layer Meteorol.*, vol. 18, no. 4, pp. 411–430, Jun. 1980, doi: 10.1007/BF00119497.

CHAPTER 3: IDENTIFICATION OF TOWER AND BOOM-WAKES USING COLLOCATED ANEMOMETERS AND LIDAR MEASUREMENT

This chapter documented extensive investigation on the various methods/approaches to identify and accurately define tower wake boundaries using wind data obtained from anemometers collocated at the same intermediate height but of different azimuth from the north. The LiDAR observed wind data enabled independent and accurate verification of the tower and boom wake boundaries. Methods explored include the traditional speed ratio, the coefficient of determination (R^2) of wind speed, the root mean square errors (RMSE) of wind speed, the coefficient of determination (R^2) of turbulence intensities (TI) which appear to be the better descriptors of the wake boundaries when compared to the commonly used traditional speed ratio approach.

CHAPTER 2: **Cite this article**: M. E. Okorie and F. L. Inambao, "Identification of tower and boom-wakes using collocated anemometers and Lidar measurement," *International Journal of Mechanical Engineering and Technology*, vol. 10, no. 6, pp. 72–94, Sep. 2019.

Link to the article:

https://iaeme.com/MasterAdmin/Journal_uploads/IJMET/VOLUME_10_ISSUE_6/IJMET_10_06_005.pdf

International Journal of Mechanical Engineering and Technology (IJMET)
Volume 10, Issue 06, June 2019, pp. 72-94. Article ID: IJMET_10_06_005
Available online at http://iaeme.com/Home/issue/IJMET?Volume=10&Issue=6
ISSN Print: 0976-6340 and ISSN Online: 0976-6359

IDENTIFICATION OF TOWER AND BOOM-WAKES USING COLLOCATED ANEMOMETERS AND LIDAR MEASUREMENT

Maduako E. Okorie
Namibia University of Science and Technology, Private Bag 3388, Windhoek 9000, Namibia

Freddie Inambao
University of KwaZulu-Natal Durban 4041, South Africa

ABSTRACT

In this study the extent of tower and boom wake distortions were evaluated using collocated anemometers and Lidar measurement based on wind data from Amperbo, Namibia, where an existing latticed equilateral triangular communication tower was instrumented according to IEC specifications. Wind data analysed was 10-minute averaged, captured over a period of nine months (May to Sept. 2014). To enable further and independent investigation of flow modification within the vicinity of the tower, ZephIR 300 wind Lidar was installed at about 5.4 m from the foot of the tower. Wind data from pairs of collocated cup anemometers located at 16.88 m and 64.97 m above ground level (AGL) were analysed and compared to identify the range of directions that were affected by the waking of the entire tower physical structure. Mean speed and turbulence intensity (TI) were used in quantify the wake impact on the wind data observed using cup anemometers, showing a speed deficit of up to 49 % and order of magnitude increase in the TI for all the regions within the wake of the tower. Comparison with ZephIR 300 observed mean speed resulted in a speed deficit of up to 50 % which further confirmed the extent of tower distortion and wake boundaries. The Lidar also confirmed the speed-up effects and the asymmetric nature of the wake boundaries associated with the mounting booms. The results show that TI analysis has the potential to more accurately define the wake boundaries and wake distortion than traditional speed ratios analysis. The study shows that the severity of tower wake effects varies seasonally with winter months (June and July) recording the highest speed deficit when compared to December, a summer month. Root Mean Square Errors (RMSE) were further computed to ascertain the similarity degree of resource parameters from the two measurement techniques, resulting in peak values of RMSE in the wake affected regions. The TI approach consistently predicted larger wake boundaries than speed ratio analysis. Wind direction analysis clearly showed the 180° ambiguity of ZephIR 300 and the extent of deflection of the winds around the tower structure. Preliminary evaluation of wake impact on the resource parameter shows that removing the sectors affected by tower wakes leads to an increase in mean wind speed and a decrease in TI values.

Keywords: Tower wake, flow distortion, speed ratios, wind speed, speed deficit.

Cite this Article: Maduako E. Okorie and Freddie Inambao, Identification of Tower and Boom-Wakes Using Collocated Anemometers and Lidar Measurement, *International Journal of Mechanical Engineering and Technology*, 10(6), 2019, pp. 72-94.
http://iaeme.com/Home/issue/IJMET?Volume=10&Issue=6

1. INTRODUCTION

Wind data for wind resource assessment in Namibia has been collected over the years by The National Wind Recourse Assessment Project (NWRAP). Cost reduction and urgent commencement of the project necessitated the use of existing communication towers for the experiment. Towers belonging to Mobile Telecommunication Limited (MTC) were utilized. The lattice equilateral triangular communication towers with boom-mounted anemometers attached it were instrumented according to the IEC61400-12-1:2005(E) standard. Traditional wind speed and directional measurement utilizes latticed or tubular towers with boom-mounted anemometers attached to them. The best option [1], [2] would have been to mount the anemometers on top of the tower to avoid any local wind flow modification by the tower structure. This may not be a perfect option either because knowledge of the site shear trend is needed to reduce project risk; as a result, booms are often placed below the tower top. The obvious implication is that such an arrangement will inevitably expose the anemometer to the flow distortion influence of the tower structure. Since the local wind flow at any site is not constrained to a direction, the sensor at one time or the other might be directly in the tower's wake. Speed and direction sensors used at Amperbo, Namibia, are located below the top of the tower. According to [3]– [6], arrangement of this sort exposes the speed sensors to tower shadow effects. The tower induced flow modification, according to literature, contributes non-negligible uncertainty on the wind data observed. This level of error is not acceptable in the wind energy industry, where accuracy in wind measurement is needed for investment decision making and project risk analysis. Previous works on tower shadow effect have found a 35 % to 50 % wind speed reduction and the severity is known to be directly related to different configurations of the tower structure [7]– [10]. Such observations have been supported by computational fluid dynamic approaches (CFD) [2], [6], [11]. According to [1], [2], for a triangular lattice mast with thrust coefficient (C_T) of 0.5, and 99.5 % centreline wind speed deficit, R_d is 5.7 times the width (L_m) of the tower phase. However, application of these studies to towers of different structural configurations and possible different site atmospheric conditions in the boundary layers are limited. The MTC tower at Amperbo has a unique geometry and boom arrangement with numerous secondary support structures such as cross and horizontal bracings, cable ladders, cable bundles and attachment brackets, which may contribute to making flow around and through the tower more complex; a situation that necessitates further investigation of the tower under consideration. To further identify the boundaries of tower and boom wakes on the wind speed observed by the cup anemometer, an additional independent instrument was used, namely, a continuous wave (CW) ground-based profiling Lidar (Light Detection and Ranging) located about 5.4 m away from the foot of the tower. This study utilized different approaches and various methodologies to identify the extent of the tower and boom-wake distortion on the wind data measured with collocated anemometers and the Lidar, by: (1) performing regression analysis, (2) comparing the speed ratios (3) evaluating the Root Mean Square Errors (4), evaluating the tower distortion and scatter factors and (5) analysis of wind direction differences for the concurrently observed wind data.

2. BACKGROUND

2.1. Site Description and Experimentation

Amperbo is a settlement in the Hardap region in Namibia, situated at 1152 m above sea level (ASL). It is located at latitude 18.313°E and longitude 25.354°S. The test site is flat, and the orography is gentle which qualifies the site as class A terrain according to Annex B of [2]. The communication tower used belongs to the Mobile Communication Company (MTC) of Namibia, the construction details of which are discussed in subsection 2.2 below. A QinetiQ Ltd (UK) ZephIR Z300 Lidar (Light Detection and Ranging) provided by Masdar Institute of Technology Abudabi, United Arab Emirates (UAE) was installed close to the foot of the tower. Concerns on vandalism and damage from wild animals justified the placement of the Lidar in a fenced area, although this raised the concern that the Lidar emitted laser might intersect the guy wires at some heights. It is a homodyne continuous wave (CW) Doppler wind Lidar system with 10 user programmable heights (besides a pre-fixed height of 38 m) up to 200 m, though 300 m can be selected, with a minimum measurement height of 10 m. The probe length is designed to increase quadratically with height. At 10 m, the probe length is 0.07 m, whereas at 200 m, it is 30 m. The technical specification of the equipment indicates wind speed and wind direction accuracies as < 0.1 m/s and < 0.5°, respectively [12–16]. It is a monostatic coaxial system where emitted and backscattered light share common optics [17]. As a result of the monostatic nature of ZephIR 300 and homodyne detection, meaning that only the absolute value of the Doppler-shift is measured, there is 180° ambiguity in the measured wind direction [16]. To resolve this issue and provide an estimate of the site wind direction, ZephIR 300 has an inbuilt meteorological station which measures other resource parameters, including wind direction [14]. Each rotation of Lidar at every height takes 1 s, in which 50 measurements of 20 ms are taken, from which the 3D (i.e. horizontal and vertical wind speed, horizontal wind direction) are generated. Lidar is specifically designed for autonomous wind assessment campaign purposes where wind speed is measured by doppler shift effect. Z300 emits laser radiation in a circular pattern by reflecting the laser beam off a spinning optical wedge, via the Velocity Azimuth Display (VAD) scanning technique. The emitted laser beam hits the aerosol in the atmosphere and scatters in-elastically. The detector records information about the return signal by a coherent detection method and creates an electric signal that is digitally sampled for determining the Doppler shifted frequency of the return light by comparing it to the transmitted laser. The Doppler shifted frequency gives an idea of the wind speeds carrying the aerosols [14], [17]

2.2. Tower Construction Detail and Instrumentation

The 120 m high guyed tower has an equilateral triangular cross-section with three vertical tubular mild steel rods connected with a network of small angular cross bracings made from 45 mm x 45 mm x 5 mm angle bars. The leg distance or sides are 1.1 m throughout the height and the vertical tubular rod each have a diameter of 100 mm. The boom has an outside diameter of 50 mm and wall thickness of 2 mm. The boom protrudes 2.56 m from the tower. Each discrete member of the lattice tower generates a discrete wake which modifies local wind flow through and around the tower structure (Figure 2a). Figure 2b is the top view of the boom arrangement on the tower for the collocated speed sensors at 16.88 m and 64.92 m. L_m is leg distance or phase width of the tower, R_d is the distance from the center of the communication tower, the point of wind data observation, whereas $\boldsymbol{a}$ is the minimum boom length. The thrust coefficient (C_T) of the tower is approximately 0.4495. The thrust coefficient may vary slightly depending on the exact section of the tower considered. This was verified (Figure 2d) by a preliminary computational fluid dynamic (CFD) study on the most convenient plane for positioning the

anemometer in the tower to ensure minimum flow distortion. For the C_T of approximately 0.45 and 99 % centerline wind speed deficit, R_d is 3.74 times the width (L_m) of the tower phase. Other secondary support structures such as ladder, cable bundles and attachment brackets were not considered in estimating C_T.This agrees with [2]. For a triangular lattice mast with thrust coefficient (C_T) of 0.5 and 99 % centerline wind speed deficit, R_d is 3.7 times the leg length of the tower.

a

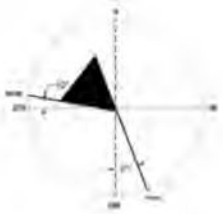

b

Figure 1. (a). Photograph of the MTC tower at Amperbo, looking up at the north facing side. The WS_4 boom, WS_{4B} boom and boom mounting of the wind vane are pictured extending out at 16.88 m (AGL). The faces housing the climbing ladder and the cable bundles are shown. (b) The plan view schematic of the tower showing the layout of the WS_4 and WS_{4B} booms shown at about 159° and 278° respectively

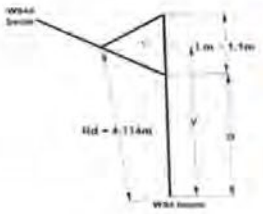

c

d

Figure 1. (c) The plan view schematics of the tower showing the configurations of the speed sensor booms and associated dimensions. (d) Preliminary CFD study revealing the most suitable plane for location of the speed sensors. Each plan presents slightly different porosity and wake effect

Further study using CFD will enable an evaluation of the amount of wake effects induced by the secondary parameters on the wind data measured. Table I, is a summary of the detailed speed and direction sensors installed on the tower. The speed and direction sensors are labeled with a numerical suffix that increases with increase in installation height. As indicated on Table I, on March 27th, 2014, the two lower anemometers initially installed in August 2012 were removed from their initial lower heights and reinstalled at 16.88 m and 64.92 m AGL. The pair of the collocated anemometers at 16.88 m and 64.92 m are 120° apart. The new arrangement was to enable an evaluation of the extent of the tower and boom's wake distortion effect on the data measured by each anemometer. The hub heights indicated in the table were determine by Namibia University of Science and Technology (NUST) students using a total survey station. The boom orientations indicated in Table I were determined from GPS readings of the positions of the waypoints that are located at the intersection of a circle of radius of approximately 50 m centered on the mast center and the forward and rearward extensions of the centerlines of the

installed booms as determined by line of sight and parallax as reported in [18]. Though efforts were made at the time of installation of direction sensors, there is always an uncertainty of several degrees in the absolute north of such sensors [19] and this is taken into consideration in this work.

Table I Sensor Instrumentation details at Amperbo

	August 2012 Arrangement		**March 27, 2014 Arrangement**	
Sensor	Height (m)	Angle (ϕ) degree	Height (m)	Angle (ϕ) degree
WS_1	3.38	159		
WS_2	4.88	159	-	-
WS_3	8.68	159	8.68	159
WS_4	16.88	159	16.88	159
WS_{4B}	-	-	16.88	159
WS_5	32.68	160	32.68	160
WS_6	64.92	160	64.92	160
WS_{6B}	-	-	64.92	278
WS_7	120.38	159	120.38	159
WD_1	4.88	38	4.88	38
WD_2	16.88	38	16.88	38
WD_3	64.92	38	64.92	38
WD_4	120.38	279	120.38	279

3. METHOD

To understand the wake distortion effect, two pairs of wind speed sensors collocated at 16.88 m and 64.92 m were analyzed and compared. To further evaluate the extent of the wake distortions, and to know if the wake identified by the anemometers are caused by the tower or booms attached to the tower, in-situ and ZephIR 300 concurrently observed wind data were used. The Lidar was placed about 5.4 m away from the foot of the tower sequel for the reasons mentioned earlier. The wind speed measured by the Lidar was considered site representative because the effect of volume averaging, a major source of uncertainty in Lidar measurement, was negligible because of the gentle orography of the terrain [14], [20]. To verify if there was a significant influence of the guy wires or the tower itself on the wind data recorded by the ZephIR 300, wind data measured at 150 m and 200 m (AGL) were analyzed and compared with the data observed at other lower heights. Wind data analyzed were 10-minute averaged, concurrently measured using anemometers and ZephIR 300 for a six-month period (01/04/2014 to 30/09/2014). In the analysis, different approaches where utilized: the ratios of the mean speeds and the turbulence intensities (TI) recorded by both data acquisition techniques were evaluated to give insight on which parameter better defines the boundaries of the wake affected regions. The traditional approach (speed ratios) often used in tower shadow identifications (Figure 2), has an inverse effect on the boundaries of the wake regions [7]. To precisely define the sectors affected by the tower wake and its severity on data measured, a second approach which utilises how related the parameters observed are, in this case the coefficient of determination, R^2, was used. When the R^2 values are close to 1, it is an indication of a strong positive relation and the reverse is the case. Further investigation required evaluation of the similarity degree of the concurrently observed data. In this case, the root means square error (RMSE) was computed. Regions that show less similarity indicate tower physical structure influence on the observed parameters. The tower distortion factor (TDF) and the scatter factor (SCF) were computed based on the wind data observed. Regions with high TDF and SCF are

notable in a tower wake [21]. Finally, wind direction measured using wind vane and ZephIR 300 was analysed and possible flow deflection around the tower physical structure was identified.

4. DATA ANALYSIS COMPARISONS AND DISCUSSIONS

4.1. Tower wake Identification: Collocated Anemometer Comparison

The wake effect of the tower is illustrated in Figure 2, which shows the ratio of raw wind speeds from the collocated anemometers at 16.88 m and 64.92 m as a function of the wind direction measured by a wind vane. The ratio of each pair of the collocated anemometers for the six months where data were concurrently observed in 2014, are binned in 5° wind direction intervals. The graphs reveal the wind speed deficits recorded in each collocated anemometer at the azimuths of their respective mounting booms. The affected angle range for both pairs of collocated anemometers at 16.88 m and 64.92 m was approximately between 60° and 65°. The most affected regions differed in terms of severity of tower distortion effect as evidenced by the amount of speed deficit encountered. At 16.88 m and 64.92 m speed deficit was more pronounced in WS_{4B} (peak at 235°) and WS_{6B} (peak at 250°) compared to WS_4 (peak at 110°) and WS_6 (peak at 120°). At 235°, the peak speed deficit for WS_{4B} was 35 % whereas the average for the affected sectors was 16 %, whereas at 110° the peak and average for the affected sectors was 49 % and 20 %, respectively, for WS_4. Similar comparison resulted in a peak and affected sector average of 29 % and 10 % for WS_{6B} and a peak and affected sector average of 40 % and 18 % for WS_6, respectively. The peak value of speed deficit in the severely affected regions was slightly higher than the findings in the literature (e.g. [3] and [7]). The difference may be traceable to many secondary support structures such as ladders and cable bundles (Figure 2a) which were not considered when the tower was instrumented. Again, if the two anemometers were positioned at different plans (Figure 1d); they would inevitably experience different wake distortion effects as suggested by CFD study of the flow distortion around the tower, agreeing with [2]. However, the observations are valid since wind speed ratio in the other sectors that were not affected appeared to be similar. It also shows that there was no external structure within the vicinity of the tower that affected data collected apart from the tower structure itself. The plot of the ratio of WS_{6B}/WS_6 against the wind direction measured by a wind vane shows similar patterns in Figures 2a and 2b, an indication that the booms' influence and speed up around the tower were not succinctly captured by the current speed sensor arrangement. The slight shift to the right on the graph of WS_6/WS_{6B} (Figure 2a and b) is an indication of veer effect between 16.88 m and 64.92 m. The wind coming from the South East experienced approximately 10° veer whereas the North West bound wind experienced close to 15° veer between the two heights. Figure 2b shows clearly how the range of winds coming from the North West covering 265° to 330° (green shade) produced a wake in wind speed captured by WS_4 in the the South East location (angle range under tower wake 85° to 145°), whereas the winds ranging from 40° to 100° coming from the North East (blue shade) produced a wake for wind speed captured by $WS4_B$ in the the South West (angle range under tower wake 220° to 280°) location.

Using the three subdivisions found in Figure 2a (i.e. the two regions affected by the waking of the tower and the undisturbed regions), Figures 3a and 3b show WS_4 and WS_{4B} at 16.88 m, and WS_6 and WS_{6B} at 64.92 m compared in the three directional sectors to enable the evaluation of how the wind speeds measured by the pair of the anemometers agreed. The shades of orange and green (Figures 3a and 3b) indicate the magnitude of disagreement in the measurements of each pair of the collocated anemometers. These show speed reduction because of waking of the entire tower structures on WS_4 and WS_{4B} and WS_6 and WS_{6B}, respectively, while the middle

region (shade of dark blue) shows where the two anemometers agree when not in the wake of the tower.

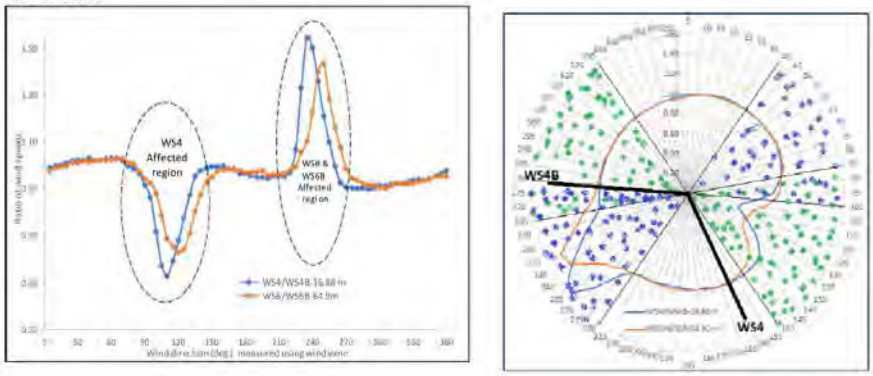

A b

Figure 2a and b. Ratio of 10-minute average WS_4 versus WS_{4B} and WS_6 versus WS_{6B} plotted on a sector-wise basis binned in 5° bins of wind direction intervals measured using a wind vane for the full six months data at 16.88 m and 64.92 m

This agrees with the findings in [7]. The R^2 values for the undisturbed regions for the two anemometers at 16.88 m and for the two at 64.92 m were 0.99 and 0.97 respectively, a clear indication of a positive and strong relationship between the wind speed measured by each pair of the anemometers.

Figure 4 is the monthly variation of the tower wake effect as illustrated by the graph of ratio of WS_4/WS_{4B} binned in 5° wind direction intervals and drawn as a function of the wind direction measured by a wind vane. Wind speeds used were measured between April 1 to December 31, 2014. The two dashed vertical lines indicate the position of the booms at approximately 159° (WS_4) and 278° (WS_{4B})

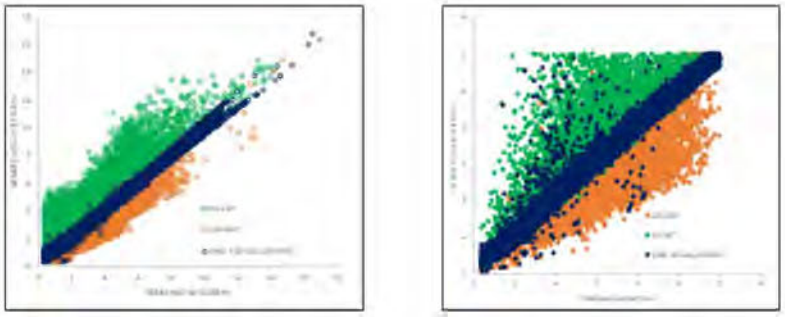

a b

Figure 3. (a). Ten-minute average WS_4 versus WS_{4B} at 16.88 m in three bins containing WS_4 wake, about (81° to 150°, green), WS_{4B} wake, about (220° to 280°, orange), and the non-waked regions (0° to 80°, 150° to 220°, 281° to 360°, dark blue). (b) Ten-minute average WS_6 versus WS6B at 64.92 m in three bins containing WS_6 wake, about (81V to 160°, green), WS_{4B} wake, about (221° to 290°, orange), and the non-waked regions (0° to 80°, 161° to 220°, 291° to 360°, dark blue)

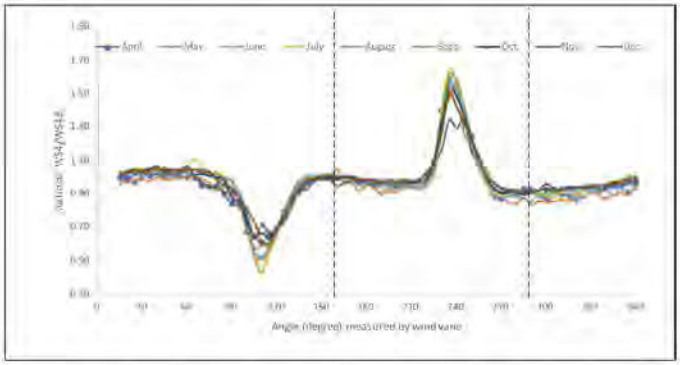

Figure 4 Seasonal variation of tower distortion effect illustrated by plotting the ratio of 10-minute average WS_4 and WS_{4B} on a sector-wise basis binned in 5° bins of wind direction intervals measured using a wind vane from April to December 2014 using data collected at 16.88 m

The range of angles affected (85° to 145°) were the same as those in Figure 2b. The pattern and angle range covered by wake effect of the tower is expected because the position of the tower structure is fixed. However, the severity in the speed deficit in the wake affected regions for each month differs. Considering WS_4, June and July (winter months) recorded the highest speed deficits of 55 % and 56 % respectively between 110° and 115° whereas in December (a summer month) the smallest value of 40 % at the same angle range was recorded. Similar results were obtained using WS_{4B}, where the peak speed deficits of 33 % and 35 % respectively were recorded in June and July between 235° and 240°. Once again, December accounted for the smallest value of 23 %. The speed deficit appears to relate directly to the wind speed. Both speed sensors recorded highest monthly mean wind speeds and highest values of speed deficit due to tower wakes in June and July. The reverse is the case in the month of December.

Wind speed ratio is often employed in tower shadow identifications (Figures 2a and 2b) and is known to have an inverse effect on the boundaries of the wake regions [7]. The inverse effect is not noticeable in this experiment which is possibly due to the length of the boom. To precisely define the sectors affected by the tower wake, a second approach which utilises how WS_4 and WS_{4B} are related; in this case the coefficient of determination, R^2, was used. The R^2 between the WS_4 and WS_{4B} as drawn as a function of the wind direction was measured using a wind vane, evaluated in 1° bins and smoothed with 2° running average (Figure 4). A result with R^2 values close to 1 would indicate a strong positive relation between WS_4 and WS_{4B} when neither speed sensors are in the wake of the tower structure. The areas between the vertical lines with decreased correlation are the areas under the influence of the tower wake.

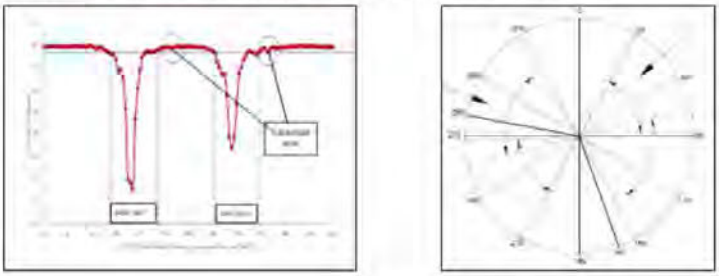

a b

Figure 5 (a) Coefficient of determination of WS_4 and WS_{4B} averaged in 10-minute intervals at 16.88 m for six months with data binned into 1°wind direction intervals for directions measured using a wind vane and smoothed with a running average of 2°. It identifies the peak value wake for WS_4 at 110° and that for WS_{4B} at 240°. (b) The angle extent covered is identified by the analysis inFigure 5a. The thick black lines show the boom orientations while the two arrows indicate the direction of winds that are modified by the tower structure.

The mean values of the standard deviations of R^2 values in the three identified non-wake regions (0° to 75°, 141° to 207° and 270° to 360°), were 0.990, 0.990 and 0.992 respectively. The boundaries of the tower wakes were identified to be the direction sectors which have R^2 values that were less than 2 standard deviations of the mean values of the three non-waked regions. The intersections of the vertical and the horizontal dashed lines clearly show the boundaries of the wakes. This approach enabled the understanding of how a range of winds coming from 256° to 321°produced a wake around WS_4 located in the South East (angle range under tower wake 76° to 145°), whereas winds ranged from 28° to 88° coming from the North East produced a wake around WS_{4B} which is located in the North West (angle range under tower wake 208° to 268°), as shown in Figure 5a. The wind speed deficit was more pronounced in WS_4 (between 76° and 141°) and slightly lower in WS_{4B} (between 220° and 260°). The range of angles affected are shown in Figure 5b. The difference is traceable to some secondary support structures and possibly the location of the anemometers at different planes of the tower (Figure 2d) as discussed in section 3.1. This is because each plane presents different tower porosities which results in different wake patterns [2]. However, the observations are valid since wind speed ratio in other sectors that were not affected appeared to be similar. This result reinforces the previous ones which show that there was no external structure within the vicinity of the tower that affected data collected apart from the entire tower structure itself. The arrangement of the collocated anemometeres (WS_4 and WS_{4B}) at 16.88 m and 64.92 m (Figure 2a) was not adequate enough to predict the wake effects of the booms. The booms are shown with the two thick black lines located nearly at 159° and 278° (Figure 5b). The obvious implication is that if the boom is located in the tower wake regions, the wake effect of the booms are masked entirely by the tower wakes.

4.2 Tower wake effects: Turbulence Intensity as a Predictor

Turbulence intensity (TI) is calculated thus:

$$TI = \frac{\sigma}{\bar{U}} \tag{1}$$

where σ is the standard deviation and the $\bar{U}$ is the mean wind speed.

Turbulence is an undesirable parameter in wind resource evaluation which is expected to increase in the wake region of the tower. Using a similar approach to that taken in section 4.1, the TI for each collocated anemometer at 16.88 m (AGL) was computed and compared, to indentify increases in TI due to tower wakes. The ratio of turbulence intensities (TI_{WS4}/TI_{WS4B}) binned in 5° wind direction intervals (ordinate) plotted against the wind direction measured by a wind vane (abscisa), is illustrated in Figure 6a and 6b. The graphs have the same pattern but are directly opposite to the ratio of the wind speeds (Figure 2a and 2b), and clearly show the variations of TI for the months of April to December, 2014.

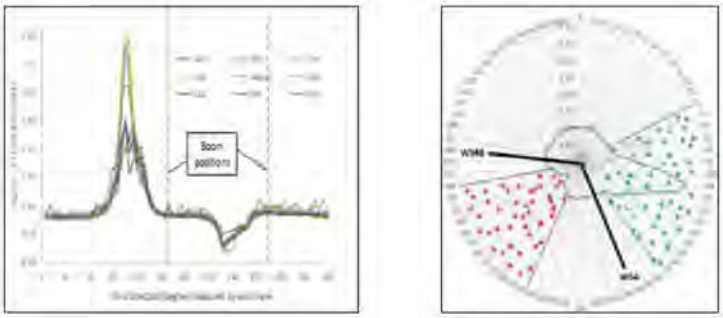

a b

Figure 6. (a) Seasonal variation of tower distortion effect illustrated by plotting the ratio of 10-minute interval average TI_{WS4} and TI_{WS4B} on a sector-wise basis binned in 5° wind direction intervals from April to December 2014 using data collected at 16.88 m (AGL). (b) Average TI_{WS4}/TI_{WS4B} ratio plotted on a sector-wise basis binned in 5° wind direction intervals for the full six months data at 16.88 m(AGL). WS_4 is waked in the region with green harsh and WS_{4B} in the regions with red harsh.

As earlier indicated, the two vertical dashed lines are the booms' positions approximately at 159° (WS_4) and at 278°(WS_{4B}) and are shown with the thick dark lines in Figure 6b. The TI analysis reveals that the angle ranges affected were slightly higher than the ranges predicted by the mean speed ratios. The shades of green and blue show the affected sectors in WS_4 and WS_{4B} respectively. The affected angle span was up to 76° in WS_4 while in WS_{4B}, where the shadow effect was less, the angle span was approximately 65°. The higher values of angle range recorded by the TI analysis may not be unconnected with higher perturbations in the wake as a result of the tower structure. The TI approach may prove valuable in capturing the boundaries of the tower wakes around and through the tower structure. In agreement with the analysis in Figure 4, the tower wake influence varied in severity in months/season of the year. In June and July, the peak winter months, the ratios of TI varied from 1 to 4.09 and 4.16 respectively at 110° wheras in December, a summer month, the range was from 1 to 1.8 at the same angle range. A similar result was obtained for WS_4 where the ratio of TI varied from 0.40 to 1 and 0.41 to 1 respectively between 230° and 240°. Once again, the TI ratio was the smallest in December, with values of 0.72 to 1. The higher range of values recorded indicates higher turbulence and higher wake influence as a result. The trend is that higher wind speed produce higher turbulence; hence, a higher wake distortion effect that was noticed in WS_4 (South East), where the range of winds coming from the North West produced a higher wake downstream of the tower for winds out of the South East. The range of winds coming from the North East produced a wake downsream of the tower for winds out of the South West where where speed captured by WS_{4B} is is affected.

Further analysis for precise definition of the angular extent affected by tower wakes was again undertaken but this time using the coefficient of determination (R^2) between TIs (TI_{WS4} & TI_{WS4B}) computed from the 10-minute interval averages for WS_4 and WS_{4B} measured at 16.88 m. The R^2 between the TI_{WS4} and TI_{WS4B} drawn as a function of the wind direction that was measured using a wind vane, binned in 1° wind direction intervals and a smoothed over a 4° running average (Figure 7a). The R^2 values that are close to 1 show a strong positive relation between TI_{WS4} and TI_{WS4B} where neither anemomters are in the wake of the tower structure. The sectors between the vertical lines with decreased correlations are the regions under the influence of the tower wake. The mean values of R^2 in the three identified non-wake regions (0° to 72°, 148° to 207° and 269° to 360°) were 0.99, 0.98 and 0.99. The boundary of the tower

wakes was identified to be the direction sectors which had R^2 values less than 2 standard deviations of the mean values of R^2 of the three non-waked regions. The intersections of the vertical and the horizontal dashed lines clearly show the boundaries of the wakes. This approach shows how a range of winds coming from 252° to 328°produced a wake around WS_4 located in the South East (angle range under tower wake 72° to 148°) whereas winds ranging from 28° to 88° coming from the North East produced a wake around WS_{4B} located in the North West (angle range under tower wake 208° to 268°) as shown in Figure 7b. The R^2 values for the regions under the influence of tower wakes shows differences in severity with TI_{WS4} being the most severely affected. The difference is traceable to secondary support structures and possibly the location of the anemometers in different planes (Figure 2d), as earlier stated. The observations are valid since the TI ratio in the other sectors that are not affected appear to be similar. The result reinforces the previous assumption that there was no external structure within the vicinity of the tower that affected data collected apart from the entire tower structure itself. The larger angular extent predicted by TI analysis in general may be a good indication that TI may be a better predictor of the boundaries of wake affected regions in tower wake distortion analysis.

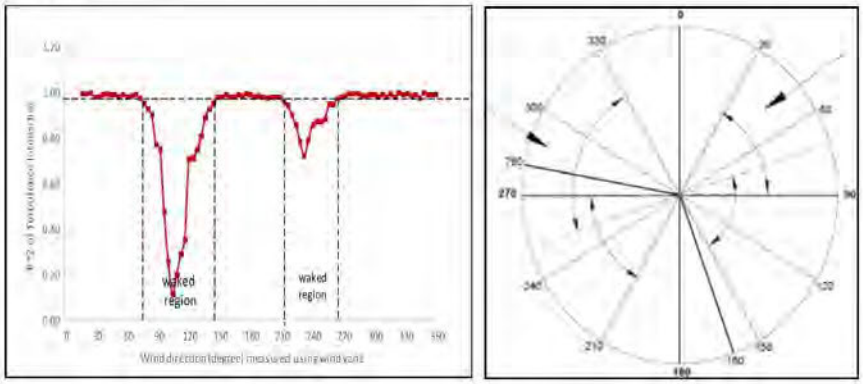

a b

Figure 7. (a). Coefficient of determinationon of TI_{WS4} and TI_{WS4B} averaged in 10-minute intervals at 16.88 m for six months data binned into 1° wind direction intervals for directions measured using a wind vane and smoothed with a running average of 4°. It identifies the peak value wake for TI_{WS4} at 110° and that for TI_{WS4B} at 240°. (b) The angle extent covered as identified by Figure 7a analysis. The thick black lines show the boom orientations while the two arrows indicate the direction of winds that are modified by the tower structure.

Further evaluation and verifications required that the three subdivisions (i.e. the two regions affected by the waking of the tower structure and the undisturbed regions) found in Figure 6, and Figure 7 were analysed and compared in three wind direction sectors to understand how the pair of the computed TIs from WS_4 and WS_{4B} agreed.

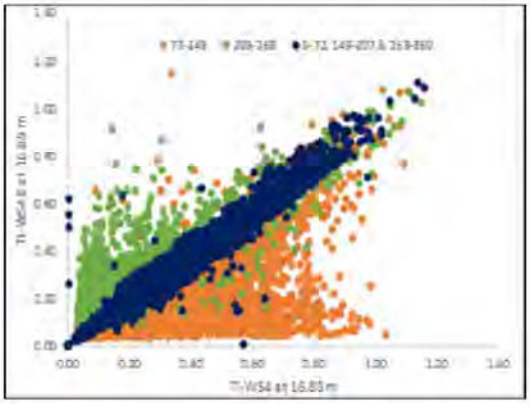

Figure 8 Ten-minute intervals average TIWS4 versus TIWS4B at 16.88 m in three bins containing WS4 wake (73° to 148°, orange), WS4B wake (208° to 268°, green), and the non-waked regions (0° to 72°, 149° to 207°, 268° to 360°, dark blue)

Similar analysis (Figures 3a and 3b) yielded the same results, where the shades of orange and green (Figure 8) indicate that the magnitude of disagreement in the computed pair of TIs (TI_{WS4} and TI_{WS4B}) was due to being in the tower wake, while the middle region (shade of dark blue) where TI values agree was not in the wake of the tower. This agrees with the findings in [9]. Tower waking reduces wind speeds, leading to an increase in standard deviation and turbulence intensities. The R^2 values of TI for the undisturbed regions was 0.97, an indication of a positive and strong relationship between the TI_{WS4} and TI_{WS4B}.

5. EVALUATIONOF THE INFLUENCE OF THE GUY WIRES: LIDAR MEASURMENTS COMPAIRED

To ensure that the data used was quality checked, several data cleaning procedures regarding wind data measured using the ZelphIR 300 and the cup anemometers were undertaken. For the Lidar observation, 37 025 data points collected between 16/02/2014 and 30/09/2014 were analysed and compared. The data was 10-minute averaged, collected at hub heights of 16 m, 32 m, 64 m, 74 m, 90 m, 120 m, 150 m and 200 m. The ZephIR 300 observed data at those heights below the top of the tower are suspected to have intersected the guy wires due to placement close to the foot of the tower. These sets of data were therefore subjected to further verification before comparing them with the data obtained using the cup anemometers. The guy wires are located approximately at 70°, 190° and 310°, separated by approximately 120°, which in each case is approximately at 30° clockwise away from the positions of the three vertical tubular rods that define the equilateral triangular nature of the lattice tower. To verify if there was a significant influence of the guy wires, the ratios of wind speeds measured by Lidar at 150 m and lower heights were computed and plotted against the wind directions recorded by the Lidar at each lower height (Figure 9).

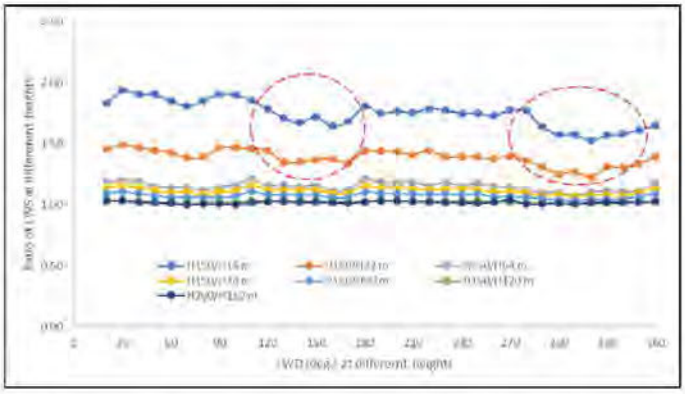

Figure 9 Ratio of Lidar wind speeds (LWS) at all heights binned in 10° wind direction intervals and plotted against wind direction captured using Lidar at Amperbo for six months

The ratio of each two-height was binned in 10° wind direction intervals and evaluated for the period when the equipment was in operation. The ratios of data observed at heights 200 m and 150 m (H200/H150) and those of 150 m and 120 m (H150/H120), (ASL) as a function of the wind direction at the lower height revealed a relatively horizontal line, as expected. Wind speed measured using ZephIR 300 at these heights was entirely out of the influence of the tower structure. The ratios of some lower heights as a function of the lower Lidar wind direction, such as H150/H90, H150/H75 and H150/H65, that were below the top of the tower, maintained a similar pattern but were not as flat as those heights that were above the tower. The guy wires' influence at 90 m, 75 m and 65 m was insignificant and the inconsequential difference may also be attributed to veer and shear due to altitude difference. At 32 m and 16 m, similar patterns which can be attributed to the tower structure are noticeably evident, and the most severely affected regions are highlighted with dashed red circle (Figure 9). The vertical height of the lowest guy wires on the tower are above 16 m (AGL); as a result, the guy wires did not influence wind speed measured at 16.88 m and at any other heights for the period of the campaign. Analysis (Figure 9) clearly shows that the ZephIR 300 measured data is not in any way affected by the guy wires although measurements at height ≤ 32 m (AGL) were minimally affected by the tower wakes.

5.1. Tower and booms' wake Identification: Anemometer versus lidar Measurement

As noted in the in section 4.1, the arrangement of the booms on the tower at Amperbo did not provide enough information to enable the identification of the boom wake effect on the data measured by the anemometers. To enable further evaluation of the boundaries of tower and boom wakes on the wind speed observed by the cup anemometer, discussed in section 4.1, an additional independent instrument in the form of a ground-based continuous wave profiling lidar located 5.4 m from the foot of the tower was used. 25 567 data points collected between 01/04/2014 and 30/09/2014 were analysed and compared. The lidar measures wind at 16 m (AGL). The 10-minute averaged wind speeds concurrently measured by both types of equipment were evaluated in order to identify the period when the cup anemometers on each boom measured substantially lower wind speeds compared to the Lidar, and to find out if the waking effect was due to tower or boom influence or both combined.

The ratio of wind speeds (WS_4/LWS and WS_{4B}/LWS) drawn as a function of wind direction measured by a wind vane is shown in Figure 10a and b. Based on the speed ratios, the Lidar

measured data correctly predicted the tower wake effects which agreed with the result obtained from the collocated anemometers at 16.88 m AGL. The waked regions are the dashed black circles (Figure 10a). The shade of green and blue illustrates the sectors affected by the tower wakes in WS_4 and WS_{4B} respectively (Figure 10b). Wind speed deficit was prominent in WS_4 and WS_{4B} between 85° and 145° and 220° and 270° respectively. The affected angle range for WS_4 and WS_{4B} was approximately 60°, agreeing with the result obtained from the pair of the collocated anemometers, as reported in section 3.1. WS_4, WS_{4B} and LWS were binned in 5° wind direction intervals to enable the estimation and comparison of the peaks and average speed deficits with those of the collocated anemometers in section 3.1. For WS_4, the peak speed deficit (at 110°) was 50 % whereas the average for the affected region was 23 %. Similar comparisons resulted in a peak and regional average of 40 % and 22 %, respectively, for WS_{4B}.

To understand the contribution of the booms to the wake effect, similar analysis to section 3.2 was repeated but in this case the wind speed ratios (WS_4/LWS and WS_{4B}/LWS) are illustrated (Figure 11 a and 11b) as a function of wind direction measured using wind ZephIR300. The thick black lines in Figures 11a and 11b show the positions of the booms of WS4 (South East) and WS4B (North West) approximately at 159° and 278° respectively. The ratio of WS_4/LWS binned in 10° wind direction intervals, plotted as a function of the lidar wind direction (LWD) (Figure 11a) clearly identifies the regions (green shade) where the mounting boom's influence was felt. The largest wind speed deficit was reported around 165° in relation to the South East anemometer (WS_4). The speed deficit at the peak was about 47 % less than the Lidar wind speed.

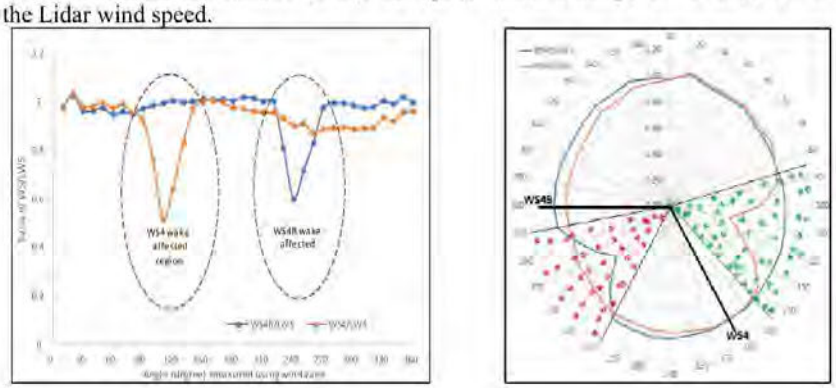

a b

Figure 10a and 10b. Ratio of WS_4 and LWS (orange line) and WS_{4B} and LWS (blue line) plotted on a sector-wise basis binned in 10° wind direction intervals, using wind direction captured with an anemometer for full six months data. Regions with green and red hatches (Figure 10b) indicate wake affected sectors of WS_4 and WS_{4B} respectively

The peak boundaries of the boom's effect were asymmetrical and cantered at a clockwise orientation from the boom orientation, which was consistent with the earlier observation that winds at Amperbo predominantly blow in a clockwise direction. Similar analysis (Figure 11b) for WS_{4B} shows that the peak speed deficit was around 285°. The speed deficit at the peak was about 32 % less than the Lidar wind speed. An asymmetrical pattern of the boom effect was evident but centered at a clockwise orientation from the boom orientation, which is consistent with the earlier observation regarding predominantly clockwise wind directions at the site.

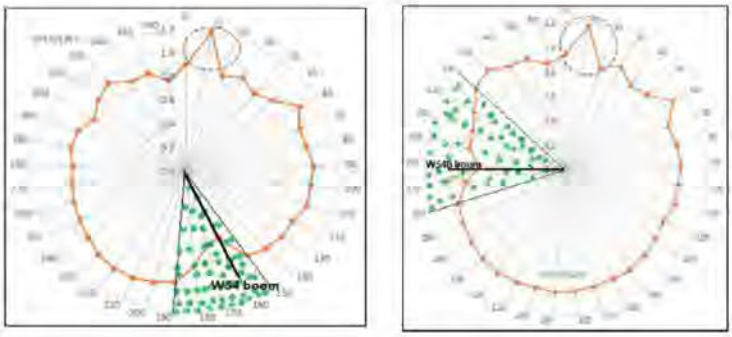

a b

Figure 11a and 11b. Ratio of WS_4 and LWS and WS_{4B} and LWS plotted on a sector-wise basis binned in 10° wind direction intervals, using wind direction captured with ZephIR 300 for full six months data at 16.88 m. Regions with green hatch (Figure 10a and b) indicate boom wakes affected sectors of WS_4 and WS_{4B}.

The asymmetric nature of the boom wakes around the boom may also be attributed to the parallel installation of the boom (Figure 1a) to the face of the tower, compared to having the boom placed perpendicular to the face of the tower as recommended by [2]. The dashed circles on both graphs between 0° to 20° with a peak at about 10° may be due to speed ups as a result of the interaction of the winds and the tower structures and it is about 5 % of ZephIR free stream velocity for both speed sensors.

6. TOWER WAKE IDENTIFICATION: ROOT MEANS SQUARE ERROR APPROACH

To evaluate the similarity degree of both collocated anemometers at 16.88 m and the measurements obtained from cup anemometers and the Lidar observed data, the root means square errors (RMSE) was computed. Computing the overall RMSE value of the unfiltered data for wind data obtained between 01/04/2014 and 30/09/2014 using the collocated anemometers yielded a value of 0.8312 m/s. The value seems high considering the orography of the terrain which is flat. To further understand the impact of tower wake on the collocated anemometers, the RMSE was computed using WS_4 and WS_{4B} and their TI (TI_{WS4} and TI_{WS4B}) as illustrated in Figure 12. The RMSE values for both parameters were drawn as a function of wind direction obtained using a wind vane and binned in 10° wind direction intervals. Two regions where the RMSE values peaked are noticed. The result is consistent with what was reported in sections 3, 4 and 5, clearly showing the regions affected by the tower wake. The similarity degree further confirms the severity of the wake influence on both speed sensors. The analysis for both wind speeds and TIs (Figure 12) revealed that tower distortion was more pronounced in WS_4 than WS_{4B}, agreeing with the previous approaches (sections 3, 4 and 5). Using the wind speeds, the peak RMSE value was 2.63 m/s and 1.39 m/s for WS_4 and WS_{4B} whereas TI gave 0.35 m/s and 0.14 m/s for WS_4 and WS_{4B} respectively. The TI approach consistently predicted larger wake boundaries than did speed ratio analysis.

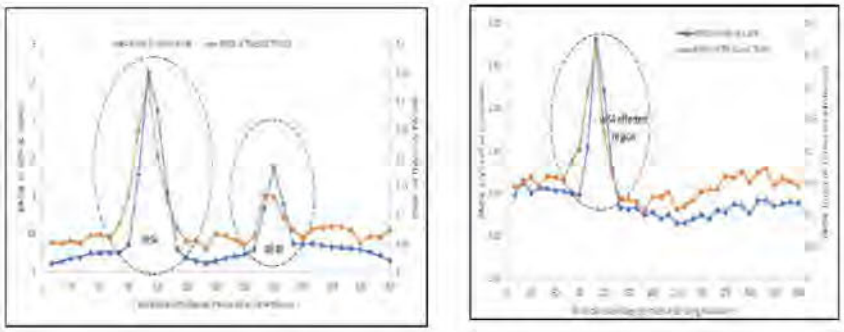

a b

Figure 12 (a) RMSE of WS_4 and WS_{4B} and TI_{WS4} and TI_{WS4B} binned in 10° wind direction intervals and drawn as a function of wind direction measured using a wind vane. (b). RMSE of WS_4 and LWS and TI_{WS4} and TI_{LWS} binned in 10° wind direction intervals and drawn as a function of wind direction measured using awind vane

As earlier stated, TI may be a better predictor of the boundaries of wake affected regions in tower wake distortion analysis. Further evaluation of RMSE by comparing WS_4 and LWS and their turbulence intensities (Figure 12b) showed a pattern consistent with Figure 12a and the previous sections. The amount of data in each wind direction bin did not have any noticeable effect on the RMSEs computed.

7. TOWER DISTORTION AND SCATTER FACTORS

The local wind flow modification caused by the physical structure of the tower to the speed sensors attached to it is referred to as the tower distortion. To detect and minimise its effect, wind speed measured using the collocated anemometers at 16.88 m and LWS concurrently observed at about the same height were further analysed and compared. Tower distortion factor (TDF) measures the tower shadowing effect by comparing the outputs of the collocated sensors and was computed using Eq. 2 [21].

$$TDF = \frac{\sum_1^n |1 - \eta_i| m_i}{\sum_1^n m_i} \tag{2}$$

The scatter factor (SCF) used Eq. 2 to enable the evaluation of the spread in the ratio of the WS_4 and WS_{4B}, WS_4 and LWS, and WS_{4B} and LWS.

Where n (wind direction sector) is 72 in this case because it is binned in 5° wind direction intervals, η_i is the median value of the ratio of speed sensors binned in the wind direction sector i, and m_i is the number of records in each direction sector. Three subdivisions (i.e. the two regions affected by the waking of the tower structure and the undisturbed regions) were identified when the ratio of WS_4 and WS_{4B} was computed, agreeing with the results obtained from the previous sections. The overall tower distortion factor was 0.1. The TDF for the undisturbed regions was 0.336. In the regions where WS_4 and WS_{4B} were under wake of the tower structure, the TDFs were 0.180 and 0.209 respectively. Similar analysis was performed using WS_4 and LWS. Two subdivisions (one region affected by waking of the tower structure and the undisturbed region) were identified. The overall TDF was 0.092. The TDF for the undisturbed region was 0.055 and 0.193 for the wake affected region. Again, using WS_{4B} and LWS yielded an overall TDF of 0.064. The TDF for the wake free region was 0.033 and 0.213

for the waked region. A TDF of zero is an indication that the sensors are measure the same wind speed in each wind direction sector. A larger value of TDF indicates a higher variation between the wind speed observed by the sensors. As expected, the regions under the tower wake for the three different analysis clearly revealed that TDF values were higher in the wake affected zones. The LWS consistently recorded higher TDF values compared to the collocated anemometers themselves.

$$SCF = \frac{\sum_1^n \sigma_i m_i}{\sum_1^n m_i} \tag{3}$$

Where n (wind direction sector) is 72 in this case, because it is binned in 5° wind direction intervals, σ_i is the standard deviation of the ratio of speed sensors binned in the wind direction sector i, and m_i is the number of records in each direction sector. The overall values of the SCF for the collocated anemometers (WS_4 and WS_{4B}) at 16.88 m AGL was 0.709. The scatter factor for the undisturbed region was 0.542 whereas at the regions where WS_4 and WS_{4B} were under tower wakes, SCF values were 0.745 and 1.02. Considering WS_4 and LWS, two subdivisions (one region affected by waking of the tower structure and the undisturbed region) were identified. The overall SCF was 0.258. The SCF value for the undisturbed region was 0.211 and 0.275 for the wake affected region. In the case of WS_{4B} and LWS, the overall SCF was 0.447. The SCF for the wake free region was 0.432 and 0.697 for the waked region. The result agrees with [21], indicating that the regions under the tower wake for the three different sets of wind speed comparisons yielded higher SCF values in the wake affected sectors.

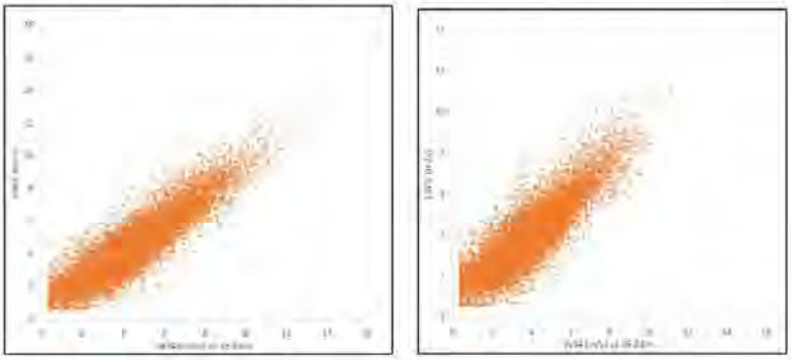

a b

Figure 13 a and 13b. Wind speed correction between WS4, WS4B and LWS at 16.88 m (AGL)

This work has extensively described different approaches/methodologies to understand the extent of the influence of tower structure on the wind data collected using cup anemometers mounted on a boom attached to a communication tower. The sectors that were affected by the wakes were excluded, resulting in WS_4 and WS_{4B} showing a strong positive relation with the LIDAR observed wind speed (Figure 13 a and 13b). The R^2 values for WS4 and WS4B were 0.76 and 0.80 respectively for the six months data compared.

8. DATA QUALITY CHECK-WIND DIRECTION ANALYSIS

Figure 14 shows the plot of the wind direction measured using a wind vane at 16.88 m against wind direction measured using lidar at 16 m (AGL). Irrespective of the wide spread of data that could mislead, a pattern is noticed. Figure 14 shows a positive relationship with the data points

concentrated in 5 major zones though symmetrical. The regions around the blue circles (located in the left upper corner and right lower corner) indicate that when one instrument measured values close to 360° at one moment the other instrument recorded values close to 0° at the same time. The two portions marked with green dash circle lie around ±180° deviation, which is traceable to the 180° ambiguity issue of the ZephIR 300 as mentioned earlier. The central portion of the data which lies on the diagonal indicates a region where both instruments measured relatively the same wind direction. The wind directions and time for a typical day, on 1 April 2014, is illustrated from 00:00 hour to 24:00 hours (Figure 15a). The dashed horizontal line shows the angle of the wind vane's boom orientations from the north. The lidar and the vane see the wind almost from the same angle between 21:10 hours to 11:30 hours. Between 11:30 to 16:30 hours, the direction recorded by the vane appeared to be under tower influence, hence the unexplained irregular pattern which is different from the more regular pattern recorded by the Lidar observation. Within the same period, the 180° ambiguity issue of the ZelphIR 300 is noticed. The Lidar observation is 170° to 180° higher than that of the wind vane and a similar pattern occurred between 16:30 to 21:10 hours when the Lidar recorded wind direction that was between 170° to 180° less than that of the vane.

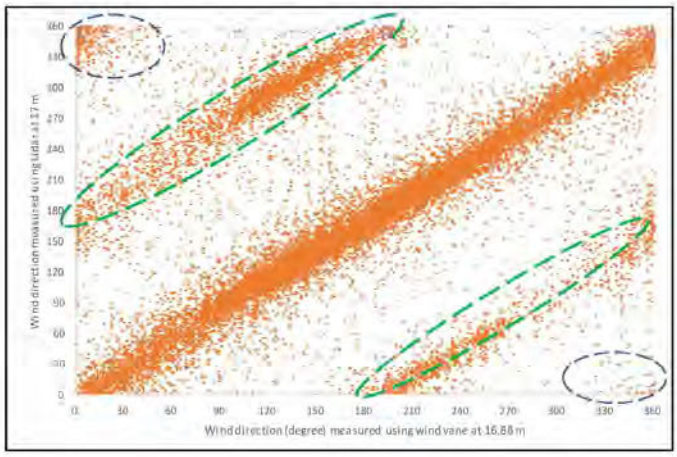

Figure 14 Wind direction correction between wind direction captured using a wind vane and ZephIR 300 at 16.88 m

To further evaluate this, Figure 15b illustrates the plot of the wind direction difference between the Lidar and wind vane, binned in 10° wind direction intervals and drawn as a function of the wind direction measured using Lidar (blue line) and wind vane (orange line). The two graphs are the same, but one is the reverse of the other. In the 1st and 2nd quadrants, the wind vane measured higher wind direction than the lidar whereas the reverse is the case in the 3rd and 4th quadrants. The sum of the differences (thick black line) exhibits a sine-function characteristic between 70° and 270° and a difference up to 34° is noticed in the regions around 70° to 180° and 190° to 270°. The result reveals that winds coming from between approximately 250° and 360° were deflected up to 34° away from the tower structure as recorded by the wind captured by the vane between approximately 70° and 180°. Similarly, observation shows that winds coming between approximately 10° to 90° were deflected by the tower structure as captured by the wind vane records between approximately 190° to 270°.

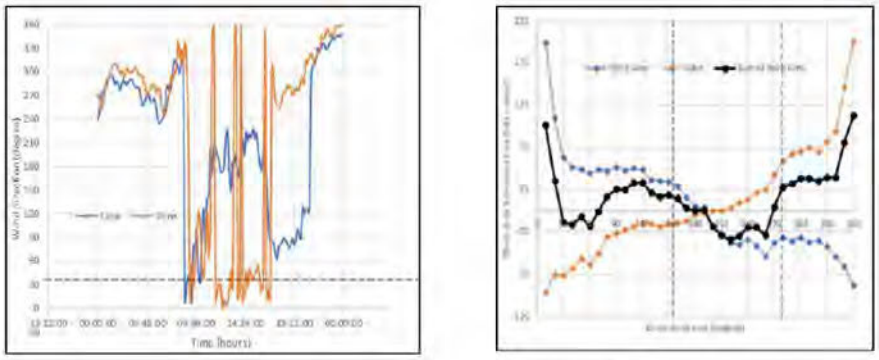

a b

Figure 15 (a) Time series 10-minute wind direction intervals observed using ZephIR 300 and a wind vane on 1 April 2014. (b) Shows wind direction differences binned in 10° wind direction intervals and plotted against wind directions captured by ZelphIR 300 (orange line) and a wind vane (blue line). The thick black line is the sum of the differences.

Figure 16 shows the correlation of wind direction measured by a wind vane against wind direction measured using ZephIR 300 wind lidar for data sets where the absolute value of the wind direction difference was 90°. The non-symmetrical nature of the deflections in the two regions can be attributed to the tower and support structures encountered by the winds in the upstream direction of the tower (Figure 1b). Wind direction correction was implemented by applying four filters according Figure 14 and other filters regarding the wind speeds. This aspect is not discussed further in this work. Again, excluding data points (Figure 14) where the ZelphIR 300 ambiguity issue is noticed, wind direction difference in the range $-90 \leq x \leq 90$, that is evaluating the number of events where the absolute value of the deviation is 90, yielded the graph in Figure 16, with an R^2 value of 0.95.

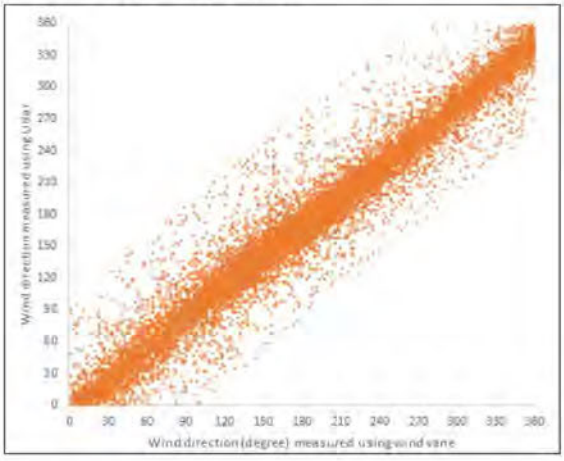

Figure 16 The correlation of wind direction measured by a wind vane against wind direction measured using ZephIR 300 wind lidar for data sets where the absolute value of the wind direction difference is 90°

On the wakes' impact on some selected resource parameters, removing the sectors within the waked zone will inevitably reduce the number of available records thus affecting the data recovery rate (DRR). Based on the boundary defined by speed ratios, DRR for WS_4 decreased by 18.8% and that of WS_{4B} by 15.1%. Similar analysis based on the boundary defined by TI_{WS4} and TI_{WS4B} found that DRR decreased by 23% and 19.1%, respectively. With the percentages computed, the representativeness of the data captured is likely compromised. Wake impact on resource parameters and methods of waked data replacement are not fully explored in this paper, nonetheless, removing wind speeds that fall within the wake boundary for WS_{4B} and WS_4 lead to slight improvements in the mean wind speeds computed for the full six months data. For WS_{4B} and WS_4, there was a 4.17 % and 0.24 % increase after removing the wake affected regions. An 11 % decrease of mean value of TI_{WS4} and a 3.4 % decrease for TI_{WS4B} was computed.

9. CONCLUSION

The data analysed and compared are data from 10-minute average intervals collected over a period of six months (01/04/2014 to to 30/09/2014), being the period when the collocated anemometers at 16.88 m and 64.97 m (AGL) concurrently captured wind data together with ZephIR 300. To enable an evaluation of the seasonal variations of tower wake effect, the data from the collocated anemometers captured between May 01 to Dec. 31, 2014, were used. Different approaches/methodologies were used in identification and evaluation of the extent of tower and boom wake effects. The traditional speed ratio approach compared the wind speeds captured for each pair of collocated anemometers (located 120° apart) at 16.88 m and 64.97 m (AGL) which had been placed on the MTC communication tower at Amperbo. This arrangement clearly reveals the effect of tower wake on the downstream speed sensors, resulting in wind speed deficits of up to 49 %. The affected angle range for both pairs of collocated anemometers at 16.88 m and 64.92 m was approximately between 60° and 65°. The ratio of turbulence intensities (TI_{WS4}/TI_{WS4B}) reveals that the affected angle span was aproximately between 65° and 76°, which is higher than the range predicted by mean speed ratio. The range of angles and extent of wake distortion predicted by TI analysis was not unconnected with higher perturbations in the wake of tower, and may well prove very valuable in strictly defining the wake boundries. The severity of wakes on the collocated anemometers differs, a situation that can be attributed to the presence of secondary support structures and possible positioning of the speed sensors on different planes (Figure 1d) of the tower, which inevitably presents different tower porosities and different flow modifications in the vicinity of the tower.

To avoid inverse effects of the speed ratio approach, and to precisely define the wake affected sectors, the coefficient of determination, R^2, was used. The R^2 between the WS_4 and WS_{4B} were evaluated in 1° bins of wind vane direction and smoothed with 2° running average. The boundary of the tower wakes were identified to be the direction sectors which had R^2 values that were less than 2 standard deviations of the mean values of the three non-waked regions identified. The affected angle in this case were approximately between 60° and 69°. Similar analysis using TI shows that the R^2 between the TI_{WS4} and TI_{WS4B} binned in 1° wind direction intervals and smoothed overs 4° running averages, predicted the wake boundary as the direction sectors which had R^2 values that were less than 2 standard deviations of the mean values of R^2 of the three non-waked regions. The range of angle affected was beween 60° to 76°. The correlation analysis shows that the R^2 values for mean speeds and TI for the undisturbed regions were 0.99 and 0.97 respectively, an indication of positive and strong relationship between the resource parameters from the collocated speed sensors at 16.88 m (AGL).

The variations of wake distortion effects by seasons was evaluated using speed and TI ratios. For WS_4, the winter months (June and July) recorded the highest speed deficits of 55 %

and 56 % respectively between 110° and 115° whereas in December (the summer month) the smallest value of 40 % at the same angle range was recorded. Considering WS_{4B}, the peak speed deficits of 33 % and 35 % were recorded in June and July respectively, between 235° and 240°. December accounted for the smallest value of 23 %. In agreement with the speed ratio analysis, tower wake influence varied in intensity in seasons of the year. In June and July, the peak winter months, the ratios of TI varied from 1 to 4.09 and 4.16 respectively at 110° wheras in December, a summer month, the range was from 1 to 1.8 at the same angle range as WS_{4B}. Similar result were obtained for WS_4 where the ratio of TI varied from 0.40 to 1 and 0.41 to 1 respectively between 230° and 240°. In December the TI ratio was the smallest with values of 0.72 to 1. The speed deficit and increase in TI appeared to be directly related to the wind speed. Arrangement of the collocated anemometers appeared not to be adequate to investigate the booms and possible speed up effects on the free stream winds captured by any of the speed sensors.

ZephIR 300 enabled the identification of the tower wakes, boom wakes and possible speed ups effects. The ratio of wind speeds (WS_4/LWS and WS_{4B}/LWS) were analysed, drawn as a function of wind direction measured using a wind vane and then compared. For WS_4 and WS_{4B}, speed deficits up to 50 % and 40 %, respectively were recorded. To identify boom wakes and speed effects, the speed ratios (WS_4/LWS and WS_{4B}/LWS) were drawn as a function of wind direction measured using ZephIR 300. The speed deficit of up to 47 % less than the Lidar observed speed was computed around 165° for the South East anemometer (WS_4). For WS_{4B}, speed deficit of up to 32 % less than the lidar wind speed was computed around 285°. The boundaries of the boom's wake for both speed sensors were asymmetrical and cantered at a clockwise orientation from the boom orientation, an indication that winds at Amperbo predominantly blow in a clockwise direction. For both WS_4 and WS_{4B}, a 5 % speed up effect was noticed between 5° and 20° with a peak at 10°.

Further investigation required the computation of the Root Mean Square Errors (RMSE) to ascertain the similarity degree of resource parameters. Considering the wind speeds, the peak RMSE values for the waked regions were 2.63 m/s and 1.39 m/s for WS_4 and WS_{4B}, whereas TI provided 0.35 m/s and 0.14 m/s for WS_4 and WS_{4B} respectively. The TI approach consistently predicted larger wake boundaries than speed ratio analysis. The Tower Distortion Factor (TDF) and the Scatter Factors (SCF) were consistent with findings in literatures, with TDF and SCF being higher at wake affected sectors when compared with the undisturbed regions.

Wind direction analysis clearly revealed the 180° ambiguity ZephIR 300 and possible deflection of winds. Winds coming from between approximately 250° to 360° were deflected up to 34° away from the tower structure as recorded by the wind captured by t wind vane between approximately 70° to 180°. Similar observation showed winds coming from between approximately 10° and 90° were deflected by the tower structure as captured by the wind vane records between approximately 190° and 270°.

Wake impact on resource parameters and methods of waked data replacement are not fully explored in this paper, however, removing wind speeds that fall within the wake boundary for WS_{4B} and WS_4 led to slight improvements in the mean wind speeds computed for the full six months data. For WS_{4B} and WS_4, there was a 4.17 % and 0.24 % increase in mean wind speed after removing wake affected regions. There was a 11 % decrease of mean value of TI_{WS4} and a 3.4 % decrease for TI_{WS4B}.

Finally, different approaches/methodologies were used in identification of tower wake distortion and definition of wake boundaries from the MTC communication tower used for wind data collection at Amperbo. Flow modification within the vicinity of the tower due to the tower's physical structures and other secondary support structures have significant influence on the wind speed, turbulence intensity and wind directions. For stringent evaluation of the wake

influence, the results show that TI analysis has the potential to accurately define the wake boundaries and the extent of wake distortion.

ACKNOWLEDGEMENTS

Funding for this project was provided by the Ministry of Foreign Affairs of Denmark, Ministry of Foreign Affairs of Finland, United Kingdom Department for International Development, Austrian Development Agency and Namibia Power Corporation. Invaluable support is provided by Namibia Energy Institute under Namibia University of Science and Technology.

REFERENCES

[1] International Electrotechnical Commission (IEC), Wind Energy Generation Systems – Part 12-1: Power Performance Measurements of Electricity Producing Wind Turbines. International Electrotechnical Commission (IEC), IEC Central Office 3 rue de Varembé CH-1211 Geneva 20, Switzerland, International Standard IEC 61400-12-1:2005(E), Dec. 2005.

[2] International Electrotechnical Commission (IEC), Wind Energy Generation Systems – Part 12-1: Power Performance Measurements of Electricity Producing Wind Turbines. International Electrotechnical Commission (IEC), IEC Central Office 3 rue de Varembé CH-1211 Geneva 20, Switzerland, International Standard IEC 61400-12-1:2017-03(en-fr), Mar. 2017.

[3] Orlando, S., Bale, A. and Johnson, D. Experimental Study of the Effect of Tower Shadow on Anemometer Readings, *Journal of Wind Engineering and Industrial Aerodynamics*, **99**, 2011, pp. 1–6.

[4] Lubitz, W. D. and Michalak, A. Experimental and Theoretical Investigation of Tower Shadow Impacts on Anemometer Measurements, *Journal of Wind Engineering and Industrial Aerodynamics*, **176**, 2018, pp. 112–119.

[5] Hansen, M. and Pedersen, B. M. Influence of the Meteorology Mast on a Cup Anemometer, *Journal of Solar Energy Engineering*, **121**(2), 1999, pp. 128–131.

[6] Stickland, M., Scanlon, T., Fabre, S., Oldroyd, A. and Kindler, D. Measurement and Simulation of the Flow Field Around a Triangular Lattice Meteorological Mast, *Energy and Power Engineering*, **5**(10), 2013.

[7] McCaffrey, K. *et al.*, Identification of Tower-Wake Distortions using Sonic Anemometer and Lidar Measurements, *Atmospheric Measurement Techniques; Katlenburg-Lindau*, **10**(2), 2017, pp. 393–407.

[8] Dabberdt, W. F. Tower-Induced Errors in Wind Profile Measurements, *Journal of Applied Meteorology*, **7**(3), 1968, pp. 359–366.

[9] Orlando, S. Bale, A. and Johnson, D. A. Experimental Study of the Effect of Tower Shadow on Anemometer Readings, *Journal of Wind Engineering and Industrial Aerodynamics*, **99**(1), 2011, pp. 1–6.

[10] Cermak J. E. and Horn, J. D. Tower Shadow Effect, *Journal of Geophysical Research*, **73**(6), 1968, pp. 1869–1876.

[11] Fabre, S., Stickland, M., Scanlon, T., Oldroyd, A., Kindler, D. and Quail, F. Measurement and Simulation of the Flow Field Around the FINO 3 Triangular Lattice Meteorological Mast, *Journal of Wind Engineering and Industrial Aerodynamics*, **130**, 2014, pp. 99–107.

[12] ZelphIR Lidar, ZP300 Operations & Maintenance Manual, QinetiQ Ltd (UK) ZelphIR (Z300) Lidar, Uk, Technical report, Feb. 2013.

[13] ZelphIR Lidar, Guidelines for Siting and Comparison of ZephIR Against a Meteorological Mast, QinetiQ Ltd (UK) ZelphIR (Z300) Lidar, UK, Technical report, Nov. 2013.

[14] Pena A. and Hasager, C. B. Remote Sensing for Wind Energy, Risø National Laboratory for Sustainable Energy, Technical University of Denmark., Risø–I–3184(EN), May 2011.

[15] Knoop, S., Koetse, W. and Bosveld, F. Wind LiDAR Measurement Campaign at CESAR Observatory in Cabauw: preliminary results, *arXiv:1810.01734 [physics]*, Oct. 2018.

[16] Jaynes, D., Manwell, J., McGowan, J., Stein, W. and Rogers, A. MTC Final Progress Report: LIDAR, Renewable Energy Research Laboratory, Department of Mechanical and Industrial Engineering, University of Massachusetts, 2007.

[17] Siepker, E. and Harms, T. The National Wind Resource Assessment Project of Namibia, R & D Journal of the South African Institution of Mechanical Engineering **33**, 2017, pp. 105-116 .

[18] Schmidt, M., Trujillo, J. J. and Kühn, M. Orientation Correction of Wind Direction Measurements by Means of Staring Lidar, *Journal of Physics: Conference Series*, **749**, 2016.

[19] Jaynes, D. W., McGowan, J. G., Rogers, A. L. and Manwell, J. F. Validation of Doppler LIDAR for Wind Resource Assessment Applications, AWEA Windpower2007 Conference, Los Angeles, CA, 2007, p. 16.

[20] Rehman, S. Tower Distortion and Scatter Factors of Co-Located Wind Speed Sensors and Turbulence Intensity Behavior, *Renewable and Sustainable Energy Reviews*, **34**, 2014, pp. 20–29.

CHAPTER 4: PREDICTION OF THE IMPACT OF TOWER SHADING ON RESOURCE PARAMETERS AND PERFORMANCE BY USING LIDAR

This chapter reasonably answered the question "If wake affected direction sectors are not corrected or discarded during data analysis, what impact would that have on the resource and performance?". This chapter motivates the need for accurate definition of tower wake boundaries and explains the key features to identify wake affected direction sectors where collocated sensors are not available. It further proposes a new and a simpler approach of using time series WSC computed from wind data measured at two different intermediate heights, located at approximately the same azimuth from the north to identify the wake affected sectors without the need for collocated sensors.

Cite the article: M. E. Okorie and F. Inambao, "Prediction of the impact of tower shading on resource parameters and performance by using LiDAR," *International Journal of Engineering Research and Technology*, vol. 13, no. 11, p. 3125, Nov. 2020, doi: 10.37624/IJERT/13.11.2020.3125-3144.

Link to the article:

http://www.irphouse.com/ijert20/ijertv13n11_05.pdf

International Journal of Engineering Research and Technology. ISSN 0974-3154, Volume 13, Number 11 (2020), pp.

Prediction of the Impact of Tower Shading on Resource Parameters and Performance by Using LiDAR

Maduako E. Okorie
Namibia University of Science and Technology, Windhoek, Namibia.
PhD Student, University of KwaZulu-Natal, Durban, South Africa
E-mail: mdkemmanuel@yahoo.com

Freddie Inambao*
University of KwaZulu-Natal, Durban, South Africa.
ORCID: 0000-0001-9922-5434 (Freddie Inambao)
**Corresponding author.*
E-mail: inambaof@ukzn.ac.za;

Abstract

Accurate identification and definition of tower wake boundaries for wind measurement is crucial for site representative wind characterization and economic evaluation. Besides computational and wind tunnel approaches, other methods utilized in field experiments to identify tower waked direction sectors are traditional speed ratio and the coefficient of determination (R^2) of turbulent kinetic energy (TKE), and turbulence intensity (TI) of collocated sensors. In a situation where collocated sensors are not available, and wind data are collected from two intermediate heights with the same azimuth angle from the north, typical of majority of the National Wind Resources Assessment Project (NWRAP) wind measurement sites, the traditional approaches are limited in their applications. Therefore, in this current study, a new, simpler, and more useful approach to identifying and defining waked boundaries is proposed. In this approach, time series wind shear coefficients (WSCs) are computed, binned in appropriate wind direction bins ($\leq 5°$ to reduce averaging effect) and drawn as a function of wind direction. At Amper-bo, time series WSC computed between the height intervals 8.68 m to 16.88 m, 16.88 m to 32.68 m, 16.88 m to 64.92 m and 32.68 m to 64.92 defined wake boundaries covering an angle of approximately 60° each, when compared with time series WSC calculated using undisturbed LiDAR data at corresponding height intervals, and this is in agreement with the approximately 60° span defined by the traditional approach. Similarly, at Schlip, time series WSC computed between 20.63 m to 49.9 m defined a wake boundary of approximately 70° and the result is again supported the traditional speed ratio approach that defined a wake boundary of approximately 70°. Two statistical models (Weibull and Raleigh) could not properly characterize the wake affected zones and the mean value of Weibull c were found to be in the range of 12 % to 14 % higher than the observed mean speed at both sites. Furthermore, wind power density (WPD) was found to be grossly underpredicted in the wake affected direction sectors. At Amper-bo, the WPD obtained showed a consistent underestimation, > 95 % for the observed and for the models in the severely affected direction sectors. At Schlip, WPD also showed a consistent underprediction of > 73 % for the observed and the models in the severely affected direction sectors. When the wake affected direction sectors were removed, the mean speed, mean value Weibull c and the mean WPD improved. Finally, insight gained from thorough description of the wind rose shows that wake affected sectors are characterized with disproportionally higher percentages of low wind regimes when compared to other sectors and this is contrary to the LiDAR observation in the corresponding sectors.

Keywords: Tower shading, resource parameters, wind shear coefficients, wind power density and Weibull models

I. INTRODUCTION

'Tower wake distortion effect' describes the uncertainty introduced to wind data captured using boom mounted anemometers placed on the top or at some intermediate heights of a tower, due to tower induced flow modifications which result in the underprediction of the local wind speeds in the wake and associated speed-ups in the upwind side of the tower. Previous literature [1]–[10] has reported tower induced flow defects in the form of wind speed deficits in the waked regions and speed-ups in the upwind side of the tower. Using computational fluid dynamics (CFD) flow analysis and wind tunnel experiments, literature such as [4] and [11]–[14] have revealed an order of increased turbulence intensity (TI) and impact of freestream turbulence in tower shadings. Some of the studies, however, opined that an increase in upstream turbulence intensity (TI) and freestream turbulence do not significantly affect flow modification within the vicinity of the tower. Studies that have validated in-situ with light detection and ranging (LiDAR) captured data [2], [15] also reported an order of increase in turbulent kinetic energy (TKE) and TI due to tower wake effects.

Besides the obvious speed deficit, speed-ups and increase in TI and TKE reported, there is a need to further characterize the exact impact of tower wake distortion effects on these parameters and other resource parameters of interest against the undisturbed LiDAR observed data. This study, therefore, investigated the impact of tower wake distortion on resource parameters and performance. The tower shadow impact on wind shear trend and coefficients, and other site-specific statistics predicted with probability density functions (Weibull and Rayleigh), were quantified and compared with undisturbed LiDAR data. Besides the common and universally accepted approach of filtering and discarding wind data in the wake affected regions, the current work proposes a new approach to identifying and removing wake affected direction sectors where collocated sensors are not available and wind data are collected from two intermediate heights, with the boom

orientation on the same azimuth from the north. This approach leverages on the relationship between the observed wind speed and other resource parameters.

The impact of tower wake on the selected parameters were further evaluated and compared to the LiDAR for performance evaluation, with the aim of understanding how the tainted data propagates into the wind power density (WPD). This study contributes to literature and further reveals why stringent/strict best practices and approaches must be adhered to in placing instruments for wind measurement on operational towers of any configuration to minimize or remove entirely the effect of tower shading. Finally, the study will answer the question "what are the performance implications of not removing wake affected direction sectors?".

II. BACKGROUND

As part of the National Wind Resource Assessment Project (NWRAP) of Namibia, two study areas where wind data were concurrently being acquired (2014) using anemometers mounted on communication towers and LiDAR are analyzed and reported. The first site (25.354°S, 18.313°E) is an inland farm settlement called Amper-bo in the Hardap region of southern Namibia. It is 1152 m above sea level. The terrain is flat, and the orography gentle so can be classified as class A terrain according to Annex G of [16], [17]. The tower is a 120 m lattice triangular communication tower belonging to the Mobile Telecommunication Limited (MTC) of Namibia and is heavily instrumented with a huge number of sensors at various heights. The brief construction detail is found in [2], [18]. A ground profiler, QinetiQ Ltd (UK) ZephIR Z300 LiDAR was installed at approximately 5.4 m from the foot of the tower to enable data comparison and tower shadow identification. It is a homodyne continuous wave (CW) Doppler wind LiDAR system with 10 user programmable heights (besides a pre-fixed height of 38 m) up to 200 m, with a minimum measurement height of 10 m was operational from 16th Jan. 2014 to 30th Sept. 2014. The brief detailed specifications and operation of ZephIR Z300 LiDAR is found in [18]. The second site (24.030°S, 17.131°E) is located near Schlip, a farm settlement in the Rehoboth rural constituency in the Hardap region of central Namibia. Wind speeds were measured at two intermediate heights (20.63 m and 49.90 m) but at the same azimuth from the north (Table IV) on the 80 m high communication tower. The construction details are the same as the tower at Amper-bo as reported in [2]. The LiDAR was moved from Amper-bo and was operational from 31st Sept. 2014 to 24th Dec. 2014 at Schlip site. The results from the analysis of the two data sets are reported in this work.

III. METHODS

To investigate the relationship between wind speed and WSC and to enable its use for identification and definition of tower waked regions, the shear trend and WSC for both sites were carefully studied and reported. To enable performance evaluation of the waked regions, the probability density functions often used (Weibull and Rayleigh models) to describe a site wind statistic were computed in reference to the observed data (in-situ and LiDAR).

A. Wind Shear Trend and Coefficients

Accurate site wind speed characterization is the basis for wind power project economic projection and overall site suitability. The growing height of modern-day wind turbines makes it impossible for wind data to always be measured at the hub height of interest, necessitating hub height extrapolation based on wind speeds measured at lower reference heights. Literature (such as [19]–[21]) has reported that shear extrapolation introduces non-negligible errors to the predicted wind speed. The accuracy of the predicted hub height speed depends wholly on how the model used can accurately predict the velocity profile at the site. In the context of this study, three methods were adopted for computing WCS to permit hub height extrapolation. They are one-point theoretical log law, two points power law and multi-points fitted power law.

B. The Two-Point Power Law

The power law is the model commonly used for wind speed extrapolation. With two wind speeds measured at two different heights, the power law exponent is obtained which is subsequently used in conjunction with a power law to extrapolate to the hub height of interest. A commonly used version of the Hellmann's power law (1) is:

$$v_2 = v_1 \left(\frac{h_2}{h_1}\right)^{\alpha} \tag{1}$$

Where wind speed v_1 is known at a reference height h_1 and required at a desired height h_2. Solving for α yields (2).

$$\alpha = \frac{\ln(v_2)-\ln(v_1)}{\ln(h_2)-\ln(h_1)} \tag{2}$$

The exponent (α), is the WSC considered to be site, time, and height interval dependent [19], [22]. Application of (1) and (2) requires confidence in the observed wind speed. A multi-point fitted power law profile can also be fitted to measurements where three or more heights are available in order to obtain the power law exponent that can be used to predict wind speed at the hub height of interest.

C. One Point Theoretical Log Law

The log law originates from boundary layer fluid mechanics. A simpler and a more practical model of the one-point theoretical law derived under the neutral stability assumption (i.e. vertical wind flow in the atmosphere without excitation), (3) utilizes only theoretical considerations to extrapolate a single wind speed from a lower reference height to wind speeds at other hub heights of interest.

$$v_2 = v_1 \frac{ln(h_2/Z_0)}{ln(h_1/Z_0)} \tag{3}$$

where wind speed v_1 is known at a reference height h_1 and required at a desired height h_2. The surface roughness is (z_0). The simplified version of (3) limits its application to terrain of

flat and homogenous orography in practice. Worthy of note, however, is that the log law becomes mathematically undefined at two heights when v_1 at h_1 is equal to v_2 at h_2. On the other hand, a decrease in wind speed with height will give a z_0 value that is high but unrealistic. Solving (1) and (3), by eliminating v_1 and v_2, provides a formula for calculating z_0 as reported by Gualtieri and Secci [21].

$$z_0 = \exp\left[\frac{h_2^{\alpha}\ln(h_1) - h_1^{\alpha}\ln(h_2)}{h_2^{\alpha} - h_1^{\alpha}}\right] \quad (4)$$

D. The Multi-Point Fitted Log Law

This approach requires fitting a logarithmic profile to measurements where three or more heights are available. The fitted profile is used to predict wind speed at the hub height of interest. According to [23], a good test of how well this approach performs is the correlation coefficient. A good practice is that heights with erroneous data must be removed provided three measurement heights are still available.

E. Turbulence Intensity (TI)

Turbulence intensity is the ratio of the standard deviation (σ) over the mean wind speed (u) as shown in (5):

$$TI = \sigma/u \ (5) \quad (5)$$

F. Wind Power Density (WPD)

Wind power density (WPD) is a vital resource parameter that provides an indication of the wind power potential of a site as it enables the estimation of how much energy per unit of time and swept area of the blades is available if wind conversion technology is deployed. It is directly related to the specific site air density and to the cube of the wind speed, computed, thus:

$$\mathrm{WPD} = \frac{1}{n}\sum_{i=1}^{i=n}\frac{1}{2}\rho u_i^3 \quad (6)$$

Where u_i [m/s] and $\bar{u}$ are the mean wind speed for the data record i and the total number of data records in that time series respectively, ρ [kg/m^3] is the air density which is a function of function of ambient temperature T [°C] and pressure (P), both parameters are known to vary with height above sea level Z [24]. For wind potential estimation at a given hub height, the corresponding ρ is evaluated using (8) as reported in [24]:

$$\rho = \rho_0\frac{T_0}{T}\left(1 - \frac{\Gamma_0 Z}{T_0}\right)^{\frac{g}{TR}} \quad (7)$$

Where g + 9.81 m/s is the gravitational acceleration, T is the temperature in Kelvin [K], R = 287.08 J/kgK, is the gas constant,

$T_0 = 288.15\ \mathrm{K}\ (= 273.15 + 15)$

$T_0 = 288.15\ \mathrm{K}\ (= 273.15 + 15)$ is the vertical temperature gradient, $T_0 = 288.15\ \mathrm{K}\ (= 273.15 + 15)$, $\rho_0 = 1.225\ \mathrm{kg/m^3}$. Parameters with subscript 0 are obtained from the standard atmospheric conditions.

G. Weibull distribution of Wind Speed

In wind data analysis for power potential estimation, it is ideal to have a few parameters that can satisfactorily describe the generally wide range of wind data captured by various wind observation techniques. Time and resources being of the essence in the majority of the wind assessment projects, a set of statistical functions was employed to describe such variations in wind speed. Probability functions, of which the most used are the Weibull and Rayleigh Probability density functions, are the industry wide accepted statistical approaches [24]–[27]. Probability density function and cumulative distribution F(v) are the two-parameter functions used by the Weibull approach to describe wind speed variation, typical of actual site observed wind data. The f(v) is the frequency of occurrence of wind speed (v) in a frequency distribution. Its expression is given by:

$$f(v) = \frac{k}{c}\left(\frac{v}{c}\right)^{k-1} \times \exp\left[-\left(\frac{v}{c}\right)^{k}\right] \quad (8)$$

Where k is the empirical Weibull shape factor which captures the spread of the wind speed, and c [m/s] is the empirical Weibull scale factor which shows how windy a site is. As a continuous distribution F(v) of the wind speed (v) is the integral of the F(v) and it gives the probability that the wind speed is ≤ v. It is calculated thus:

$$F(v) = 1 - \exp\left[-\left(\frac{v}{c}\right)^{k}\right] \quad (9)$$

Several methods have been used to determine the Weibull c and k to enable proper description of the site wind regime [28]. In this study, a graphical approach which leverages on the transformation of the cumulative distribution function into a linear form by taking double logarithm of equation of equation 9 was adopted, and it follows that:

$$\ln\{-\ln[1 - F(v)]\} = k\ln(v) - k\ln(c) \quad (10)$$

The graphical representation of ln(v) and ln{-ln[1-F(v)]} yields a straight line with a slope of k and intercept with the abscissa of (-kln(c)). The values of k and c are obtained by the slope of the line of best fit to the straight line graph and the intercept with the ordinate respectively.

According to [25], the WPD for Weibull function is calculated thus:

$$\mathrm{WPD} = \frac{1}{2}\rho c^3\Gamma\left[1 + \frac{3}{k}\right] \quad (11)$$

IV. DATA DESCRIPTION

At both sites, the wind data concurrently observed in 2014 by the two measurement techniques were analyzed and reported. At Amper-bo the LiDAR observed data was for 8.4 months (16th Jan. 2014 to 30th Sept. 2014) and at Schlip for nearly 3 months (31st of Sept. to 24th of Dec. 2014). The operating range and accuracy of the sensors are summarized in Table I. Table II shows the sensor arrangement details at the Amper-bo site. Table III gives a summary of the mean speed captured by the

LiDAR from the 10 user programmed heights at a pre-fixed height of 38 m. The wind speed captured by LiDAR at Amper-bo is denoted as LiDAR wind speed (LWS) and at Schlip, it is denoted as Schlip LiDAR wind speed (sLWS). The brief operating range and accuracy of the LiDAR is reported in [2].

TABLE I. OPERATING RANGES AND ACCURACIES OF VARIOUS SENSORS USED FOR DATA ACQUISITION

S. no	Parameter	Sensor type	Operating range	Accuracy
1	Wind speed	NRG#40 Maximum anemometer	1.0 - 96 m/s	0.1 m/s
2	Wind vane	NRG#200P Wind direction vane	0 - 360°.	1°
3	Temperature	NRG#110S with solar radiation shield	-40 - 52.5 °C	± 1.78°C
4	Relative Humidity	RH-5 Relative humidity sensor	5 -95%	± 5% RH
5	Pressure	NRG#BP20 Barometric pressure sensor	15 - 115 kPa	± 1.5 kPa

TABLE II. INSTRUMENTATION DETAILS OF AMPER-BO EXPERIMENT IN 2014

	August 2012 Arrangement		March 27, 2014 Arrangement	
Sensors	*Heights (m)*	*Angle (ϕ) degree*	*Height (m)*	*Angle (ϕ) degree*
WS1	3.88	159	-	-
WS2	4.88	159	-	-
WS3	8.68	159	8.68	159
WS4	16.88	159	16.88	159
WS4B	-	-	16.88	278
WS5	32.68	160	32.68	160
WS6	64.92	160	64.92	160
WS6B	-	-	64.92	278
WS7	120.38	159	120.38	159
WD1	4.88	38	4.88	38
WD2	16.88	38	16.88	38
WD3	64.92	38	64.92	38
WD4	120.38	279	120.38	279

TABLE III. MEAN SPEED CAPTURED BY THE LIDAR AT AMPER-BO IN 2014

Height (m/s)	10	17	33	38	49	65	75	90	12	150	200
Sensor	LWS1	LWS2	LWS3	LWS4	LWS5	LWS6	LWS7	LWS8	LWS9	LWS10	LWS11
Mean speed (m/s)	3.73	4.26	5.21	5.46	5.81	6.25	6.46	6.73	7.09	7.33	7.54

At Schlip, wind speeds were measured at two intermediate heights and Table IV is a summary of the sensor instrumentation detail and mean speed using the communication tower. Table V summarizes the mean speed captured by the LiDAR from the 8 user programmed heights and a pre-fixed height of 38 m. Wind speed increases with heights as expected (Table III, Table IV and Table V).

TABLE IV. INSTRUMENTATION DETAILS AT SCHLIP IN 2014

Sensors	Heights (m)	Angle (ϕ) degree	Mean speed (m/s)
WS8	20.63	161	4.66
WS9	49.90	163	5.31
WD5	49.90	283	-

TABLE V. MEAN SPEED CAPTURED BY THE LIDAR AT SCHLIP IN 2014

Height (m/s)	10	20	38	52	80	100	120	150
Sensor	sLWS1	sLWS2	sLWS3	sLWS4	sLWS5	sLWS6	sLWS7	sLWS8
Mean speed (m/s)	3.73	4.26	5.21	5.46	5.81	6.25	6.46	6.73

V. DATA RECOVERY RATE

Data recovery rate expresses the percentage of the valid data points to the possible data points. The recovery rate of the in-situ measurement at Amper-bo and Schlip evaluated for this study was 100 %. At Amper-bo, the LiDAR recorded a consistent data recovery rate at all heights > 95 %, except the two topmost heights (150 m and 200 m) where the data availabilities were 94.86 % and 81.47 % respectively (Fig. 1a).

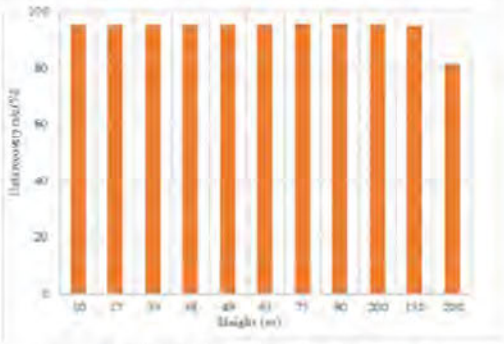

Fig. 1a LiDAR data recovery rate at Amper-bo.

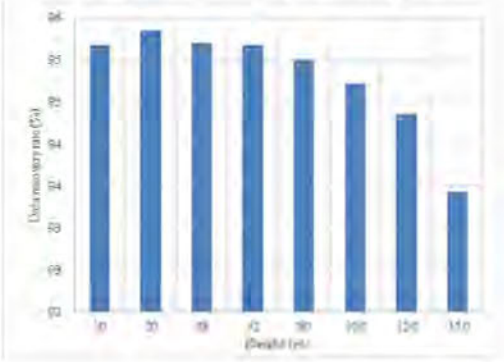

Fig. 1b. LiDAR data recovery rate at Schlip.

Similar data availability patterns were recorded when the ground profiler was installed at Schlip with recovery rates at all heights > 95 %, except the three topmost heights (100 m, 120 m and 200 m) where the recovery rates were 94.86 % and 81.47 % respectively (Fig. 1b). This trend may be attributed to weak backscatter signal which is difficult for the LiDAR to detect due to large beam waist radius and measurement probe depth at such heights [29]. Data losses within the first four months of the campaign at Amper-bo was mainly due to power failure.

VI. WIND ROSE AND SITE CHARACTERISTICS

Fig. 2 shows the wind rose diagrams from the Amper-bo and Schlip experiments. The terrains of both sites are relatively flat, therefore the influence of the orography is not detected; hence the similarity in distribution of winds captured by the two observation techniques. At Amper-bo, the wind pattern of WS6 and WS4 captured by the in-situ method are the same (Fig. 2a and Fig. 2b). Similar behavior is evident with LWS6 and LWS2 captured by LiDAR (Fig. 2c and Fig. 2d). At 64.92 m (WS6), the predominant range of mean speed was 5 m/s to 10 m/s (52.27 %), followed by 0 m/s to 5 m/s (40.1 %) and 10 m/s to 15 m/s (7.48 %) (Fig. 2a), whereas at 16.88 m (WS4) the dominant range was 0 m/s to 4 m/s (51.28 %), followed by 4 m/s to 8 m/s (45.03 %) and 8 m/s to 12 m/s (3.54 %) (Fig. 2b). Again, at 64.92 m (Fig. 2a), a most frequent SE-SSE is recorded (8.41 %), while NNW-N (8.34 %) and SW-WSW (8.06 %) are the second and third predominant directions respectively.

Also, at 16.88 m (Fig. 2b), a prevalent SE-SSE occurs (8.55 %), while NNW-N (7.88 %) and SSE-S (7.76 %) are the secondary predominant directions. The strongest wind from WS6 (64.92 m) and WS4 (16.88 m) are from the SE-SSE direction sectors. At Amper-bo, for the LiDAR observation, at 65 m (LWS6), the predominate range of mean speed was 5 m/s to 10 m/s (52.33 %), followed by 0 m/s to 5 m/s (36 %) and 10 m/s to 15 m/s (9.56 %) (Fig. 2c), whereas at 17 m (LWS2) the dominant range was 4 m/s to 8 m/s (51.05 %), followed by 0

m/s to 4 m/s (45.6 %) and 8 m/s to 12 m/s (3.24 %) (Fig. 2d).

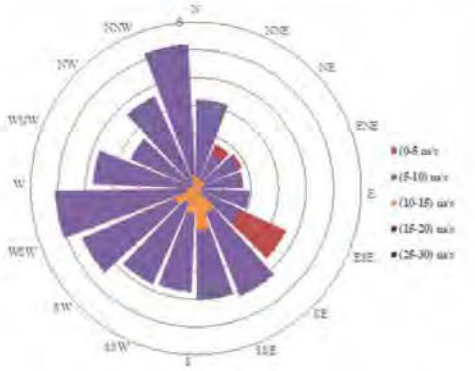

Fig. 2a. Wind rose of WS4 (16.88 m) measured at Amber-bo.

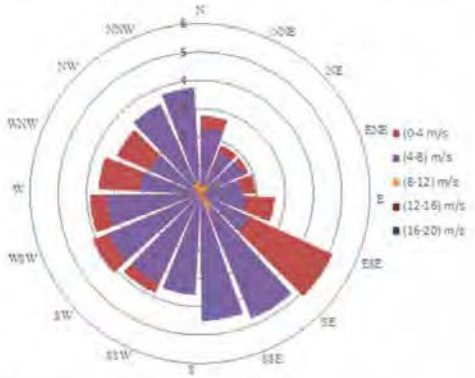

Fig. 2b. Wind rose of WS6 (64.92 m) measured at Amber-bo.

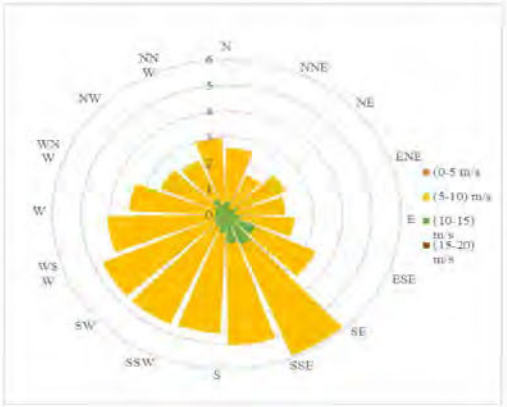

Fig. 2c. Wind rose of LWS6 (65 m) measured at Amper-bo.

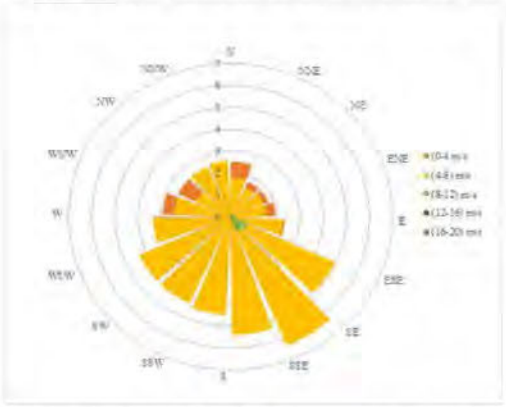

Fig. 2d. Wind rose of LWS2 (17 m) measured at Amper-bo.

Again, at 65 m (Fig. 2c), a most frequent SE-SSE is recorded (10.12 %), while SSE-S (9.36 %) and SW-WSW (9.09 %) are the second and third predominant directions respectively. Also, at 17 m (Fig. 2d), a prevalent SE-SSE occurs (10.38 %), while SSE-S (9.31 %) and SSW-SW (8.61 %) are the secondary predominant directions. The strongest wind from 65 m (LWS4) and 17 m (LWS2) are also from SE-SSE direction sectors. However, in the direction sector where tower shadow influence is most severe (ESE-SE), the percentage of wind speed between 0 m/s and 4 m/s is disproportionally high (65.38 %) for WS6 and (71.99 %) for WS4 compared to other wind regimes in the other direction sectors, which is contrary to the undisturbed LiDAR observation within ESE-SE.

At the Schlip experiment, similar evaluations were performed based on WS9 (49.9 m) and sLWS4 (65 m) and the results were as follows: the pattern of distribution of winds for the two acquisition systems were the same.

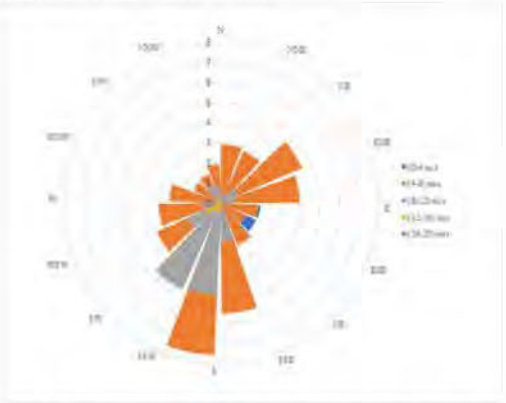

Fig. 2e. Wind rose of sLWS4 (52 m) measured at Schlip.

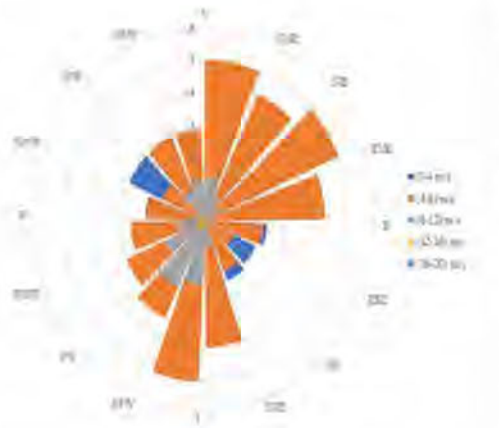

Fig. 2f. Wind rose WS9 (49.9 m) measured at Schlip.

At 49.9 m (WS9), the range of mean speed that occur most is 4 m/s to 8 m/s (51.07 %), followed by 0 m/s to 4 m/s (33.68 %) and 8 m/s to 12 m/s (13.82 %) (Fig. 2f), while, at 52 m (sLWS4) the dominant range is 4 m/s to 8 m/s (51.61 %), followed by 0 m/s to 4 m/s (26.04 %) and 8 m/s to 12 m/s (19.56 %) (Fig. 2e). At 49.9 m (Fig. 2f), the most frequent S-SSW was recorded (9.49 %), while N-NNE (8.84%) and NE-ENE (7.88%) were the second and third predominant directions respectively. Also, at 51 m (Fig. 2e), a prevalent S-SSW occurs (14.78%), while SSW-SW (10.98%) and SSE-S (10.06%) are the secondary predominant directions. The strongest wind from 49.9 m (WS9) and 52 m (sLWS4) were from the S-SSW direction sector. The direction sector (S-SSW) was severely affected by the tower shading, recording disproportionately high (65.15%) wind speed between 0 m/s and 4 m/s for WS9 when compared to other wind regimes in the other direction sectors which was contrary to the undisturbed Lidar observation withing ESE-SE.

VII. WIND SHEAR TRENDS AND COEFFICIENTS

At Amper-bo the multi-point fitted power and log law profiles for the 11 different hub heights where LiDAR captured data yields WSCs (power law exponent) and surface roughness of 0.243 m and 0.626 m respectively. Using the in-situ data for the following heights 8.68 m, 16.88 m, 32.68 m and 64.92 m, multi-point fitted power and log law profiles give WSCs (power law exponent) and surface roughness of 0.259 m and 0.494 m respectively. WSC calculated using average wind speeds observed at 16.88 m and 64.92 m (Table II) is 0.279 (2). Again, the time series WSC between 16.88 m and 64.92 m was calculated and averaged, yielding a WSC value of 0.275 m (2). At Amper-bo, based on the in-situ observation, the WSC was calculated using average wind speed at two reference heights (16.88 m and 64.92 m) is 7.17 % and 1.43% higher than values obtained from the multi-point and time series approach respectively. This implies that the magnitude of the WSC obtained was dependent on the computation model applied. The computed roughness lengths appeared higher than normal when compared to values reported for terrains of such orography [19]–[21]. At Schlip a similar approach (multi-point fitted power and log laws) yielded a WSC of 0.135 and z0 of 0.0225 m using the three months LIDAR data captured there. For the same data set, using two-point power law, the WSC computed using average wind speeds at 20 m and 52 m (Table V) was 0.181. The time series WSC between 20 m and 52 m was further computed and averaged, resulting in a WSC value of 0.143. Again, using the in-situ measurements performed at two heights (Table IV), in 2014, the multipoint fitted approach gave a WSC of 0.150 and z0 of 0.0397 m. For the same data set, using the two-point power law, the WSC computed based on the average wind speeds at 20.63 m and 49.9 m (Table IV) was 0.148 (2). The time series WSC between 20.63 m and 49.9 m was further computed and averaged, resulting in a WSC value of 0.170 (2). At Schlip, based on the in-situ observation, the WSC computed from the time series approach from two reference heights (20.63 m and 49.9 m) was 11.76 % and 12.94 % higher than the values obtained from the multi-point and hub heights average wind speed approach, respectively.

In terms of the monthly variation of WSC for both measurements techniques at the two sites, the winter months (May, June and July) accounted for the highest values whereas the summer months (January and December) recorded the lowest values (Fig. 3a and Fig. 3b). This agrees with the findings in the literature review (such as [19]–[21]). This trend is due to thermal stratification of the atmospheric body at both sites [22], [30]. At Amper-bo, both observation techniques recorded a WSC value of 0.37 in June. In January, α1 was 0.18 and α2 was 0.17. At Schlip, in June and January, α3 and α4 were 0.184 and 0.113 respectively.

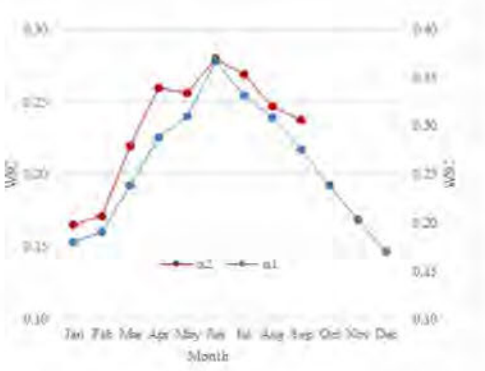

Fig. 3a. Monthly variation of WSC recorded by in-situ (α1) and LiDAR (α2) at Amper-bo in 2014.

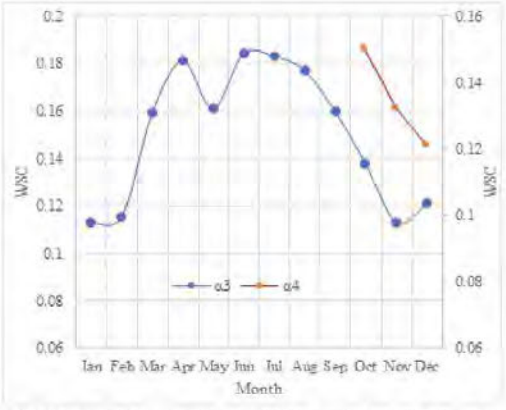

Fig 3b. Monthly variation of WSC recorded by in-situ (α3) and LiDAR (α4) at Schlip in 2014.

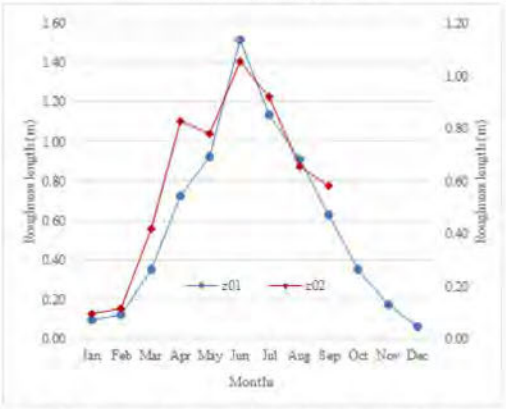

Fig. 3c. Monthly variation of z0 recorded in-situ (z01) and LiDAR (z02) at Amper-bo in 2014.

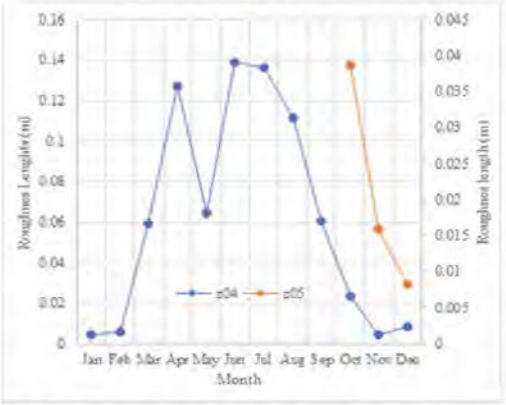

Fig. 3d. Monthly variation of z0 recorded in-situ (z03) and LiDAR (z024) at Schlip in 2014.

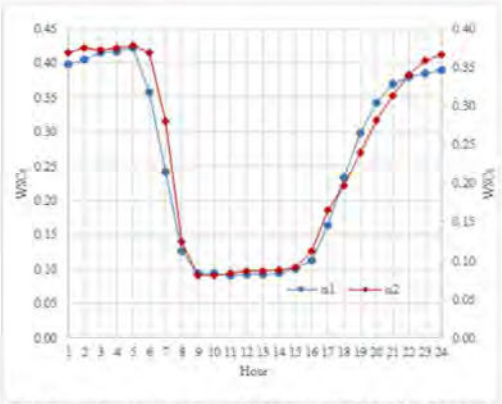

Fig. 3e. Diurnal variation of WSC recorded by in-situ (α1) and LiDAR (α2) at Amper-bo in 2014.

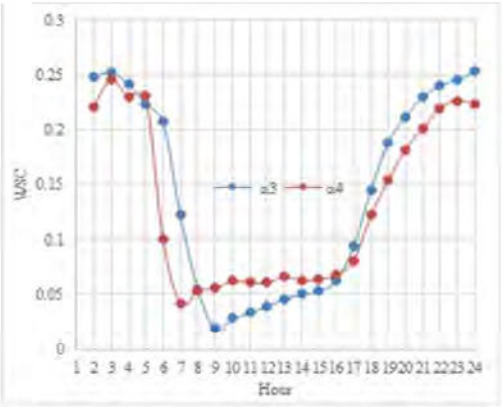

Fig. 3f. Diurnal variation of WSC recorded by in-situ (α3) and LiDAR (α4) at Schlip in 2014.

The month of May 2014 is the least windy and that explains the pattern observed in the monthly variations of the α3 and z03 (Fig. 3b and Fig. 3d). The monthly variation of the roughness length has the same patterns as those of WSC, and it is also attributed to the thermal stratification of the atmospheric body at both Amper-bo and Schlip (Fig. 3c and Fig. 3d). Diurnally, the computed WSC at both Amber-bo and Schlip show evidence of direct correlation to the diurnal heating/cooling cycle of air above the ground, and thus of atmospheric stability. Higher values are recorded in the stable night hours whereas the unstable daylight hours account for the lowest values (Fig. 3d and Fig. 3e). This pattern is in agreement with several authors (e.g. [20], [31]–[33]. A similar explanation also holds for the pattern of hourly variation of the roughness length at Amper-bo and Schlip as captured by the instruments.

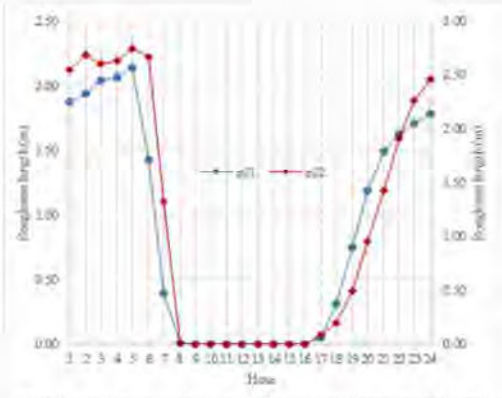

Fig. 3g. Diurnal variation of z0 recorded in-situ (z01) and LiDAR (z02) at Ampber-bo in 2014.

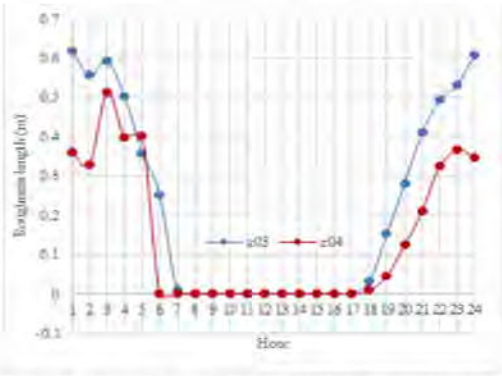

Fig. 3h. Diurnal variation of z0 recorded in-situ (z03) and LiDAR (z04) at Schlip in 2014.

VIII. USING WSC TO DETECT SECTORS AFFECTED BY TOWER WAKES

A universally accepted norm espoused by many authors in the literature review (such as [2], [16], [17], [34], [35]) for tower wake evaluation and accurate definition of the wake boundaries is the computation of the speed ratios of collocated sensors at the same height of the tower. Other parameters such TEK and TI were used by [2] and [15] for tower wake evaluation. Collocated sensors are commonly placed opposite each other (i.e., at 180°) or at 120° and 60° apart on triangular lattice masts. For a square lattice tower, collocated speed sensors are often placed 180° and 90° apart because the booms are placed parallel to the face of the tower, and similarly for the lattice triangular tower arrangement. At the Amper-bo experiment, speed sensors were collocated at 16.88 m and placed 120° apart. Different approaches were used to precisely define the wake boundaries [2]. Fig. 4 is the speed ratio of the collocated anemometers (WS4 and WS4B) drawn as a function of the wind direction. The wake affected direction sector of WS4 and WS4B are shown.

Where there are no collocated speed sensors (anemometers), but two or three speed sensors (anemometers) are placed at different heights above ground level (AGL) but located on the same azimuth from the north, no literature has addressed a method to detect the error readings of the anemometers as result of tower induced flow perturbations. In this study, WSC (α) was computed from time series data using (2) and drawn as a function of the wind direction at the higher height (h2). The graphs, Fig. 5a, Fig. 5b, Fig. 5c and Fig. 5d clearly show that the WSC variation with direction provided enough information to identify the wake affected sectors. The graphs (Fig. 5a, Fig. 5b, Fig. 5c, and Fig. 5d) are the WSCs binned in 5° wind direction intervals and plotted as a function of the wind direction. The speed sensors designated WS3, WS4, WS5 and WS6 were placed on the same tower face (Table II), and each sensor's boom azimuth was approximately 160° from the north. The blue (α1) and dark red (α2) lines are WSC variations with directions for in-situ measurements and the ground profiler (LiDAR) respectively at approximately the same height. It has been reported that factors such as site orography/terrain type, heterogeneity of vegetations, possible presence of obstacles and sea/land breezes may be responsible for WSC variation with direction [19], [20]. However, none of these studies considered the impact of tower shading on WSC. As a result, tower shading impact on the directional variation of WSC has not been properly described, with such influence being rather attributed to the orography of those sites investigated.

At Amper-bo, the terrain is flat, the vegetation is almost homogenous at all seasons and there are no near-by obstacles that could significantly influence or modify local flow within the vicinity of the tower except the physical structure of the tower. This explains why the WSC variations (Fig. 5a, Fig. 5b, Fig. 5c and Fig. 5d) for the in-situ and LiDAR observations maintained similar patterns in all direction sectors except the sectors that were exposed to tower induced flow perturbations. The wake affected direction sectors identified by this approach agree with the direction sectors defined by the traditional speed ratio and the coefficient of determination (R^2) of TI approaches proposed in [2]. Precise definition of wake boundaries and subsequent elimination of the inverse effect of the speed ratio have necessitated the adoption of the R^2 approach as shown in Fig. 4. This is the R^2 of WS4 and WS4B binned in 1° wind direction intervals and smoothed with a running average of 2° and drawn as a function of the wind direction.

The R^2 values close 1 indicates a strong positive relation between WS4 and WS4B when neither speed sensors are in the wake. The areas between the vertical dashed lines (Fig. 4) with decreased correction are the areas under the influence of the tower wake. The tower wake boundaries (Fig. 4) were identified to be the direction sectors with R^2 values that are less than 2 standard deviations of the mean values of the three non-waked regions. The wake boundaries cover an angle of approximately 60°. Strictest measure would be to declare every direction sector that falls within 1 standard deviation of the mean values of the three non-waked regions invalid but doing

so will increase the wake boundaries and reduce the amount of captured data for analysis.

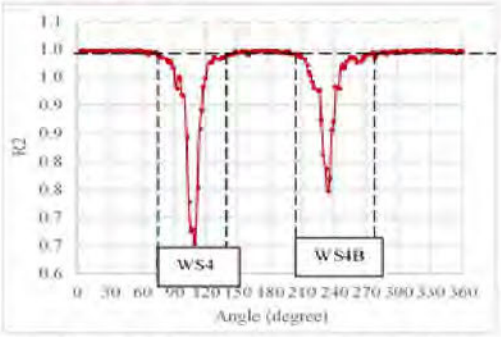

Fig. 4.Coefficient of determination (R^2) of WS4 and WS4B binned in 1° wind direction intervals and smoothed with a running average of 2°.

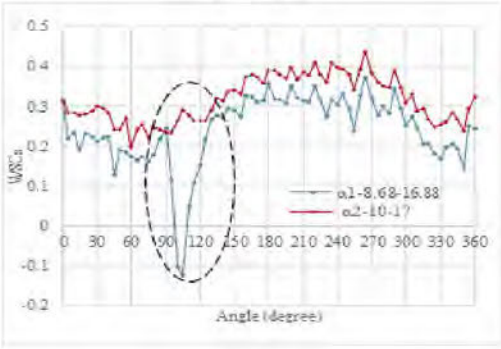

Fig. 5a. Time series WSC calculated for the in-situ (8.88 m to 16.88 m) and for the LiDAR (10 m to 17 m), binned in 5° wind direction intervals and drawn as a function of the wind direction.

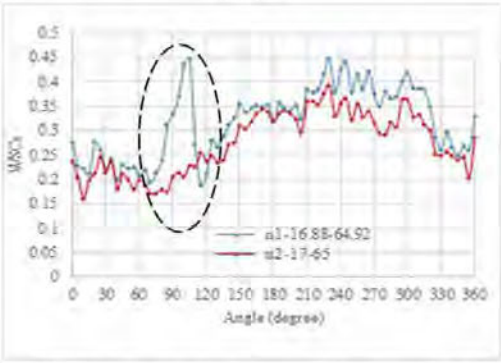

Fig. 5b. Time series WSC calculated for the in-situ (16.88 m to 64.92 m) and for the LiDAR (17 m to 65 m), binned in 5° wind direction intervals and drawn as a function of the wind direction.

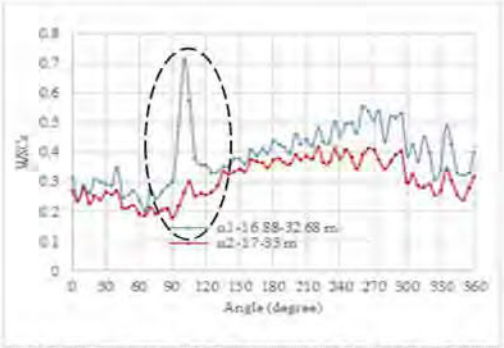

Fig. 5c. Time series WSC calculated for the in-situ (16.88 m to 32.68 m) and for the LiDAR (17 m to 33 m), binned in 5° wind direction intervals and drawn as a function of the wind direction.

The computed WSCs for the in-situ measurement deviate greatly from the LiDAR observations due to tower wakes at all the height intervals considered. The upward and downward displacements noticed (Fig. 5) are directly related to wind speed differences measured by the higher height (hh) and lower height (lh) anemometers. When the higher height anemometer measures wind speeds that are consistently higher than the lower height anemometer, even in the tower waked regions, the deviation is positive from the LiDAR WSC. When speed sensor at lh measures higher speed than the hh speed sensor, which may occur due to severe speed deficit in the hh sensor, the computed WSCs exhibit lower deviation from the LiDAR values at such an angle. The peak speed deficit occurred between 105° and 110°, agreeing with the R^2 of collocated wind speeds (Fig. 4) and R^2 of TI analysis of collocated speed sensors reported in [2]. Time series α1 computed between 8.68 m and 16.88 m (in-situ) was compared with α2 computed between 10 m and 17 m (LiDAR) and a 57.04 % difference existed at the most severely affected direction sectors (Fig. 5a).

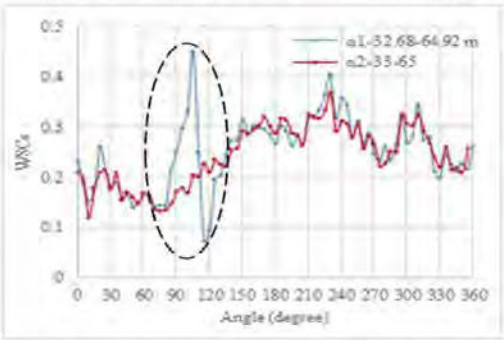

Fig. 5d. Time series WSC calculated for the in-situ (32.68 m to 64.92 m) and for the LiDAR (33 m to 65 m), binned in 5° wind direction intervals and drawn as a function of the wind direction.

Similarly, α1 calculated between 16.88 m and 64.92 m (in-situ) deviated by 48.60 % when compared with α2 calculated between 17 m and 65 m (LiDAR), and α1 and α2 differed by 58.04 % in the peak of the waked region when computed between 16.88 m and 32.68 m (in-situ) and 17 m and 33 m (LiDAR). Further evaluation reveals a difference of 54.04 % between α1 and α2 in the peak of the waked region following computation of WSC from 32.68 m to 64.92 m (in-situ) and from 33 m to 65 m (LiDAR).

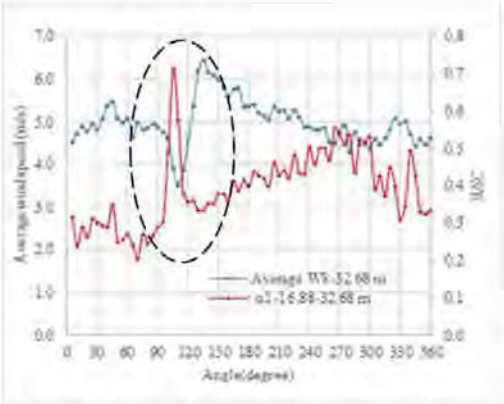

Fig. 6a. Relationship between WS5 and WSC at 32.68 m (in-situ) measurement at Amper-bo.

Fig. 6a and Fig. 6b illustrate the relatedness of WSC and average wind speed at 32.68 m (in-situ) and 33 m (LiDAR) respectively. The two parameters were binned in 5° bins of wind direction intervals. The tower affected sectors (the dashed oval circle) show that a reduction in mean wind speed led to an increase in WSC values. Such abrupt change in the WSC pattern (which occurred consistently at approximately the same angle range with the wind speeds captured using anemometers mounted on the tower) is not noticed in the in the undisturbed LiDAR observed wind data.

Similar analysis performed using data obtained from the Schlip experiment clearly defined the sectors affected by tower shading. The two parameters evaluated (speed ratio and WSC) were binned in 5° bins of wind direction intervals and drawn as a function of the wind direction captured by the in-situ measurements (Fig. 7a and Fig. 7b). The traditional speed ratios (WS8/sLWS2) and (WS9/sLWS4) clearly define the wake boundaries in the affected direction sectors. The affected angle range was approximately 70°, shown in Fig. 7a by the dotted oval shape. Again, time series WSC computed and

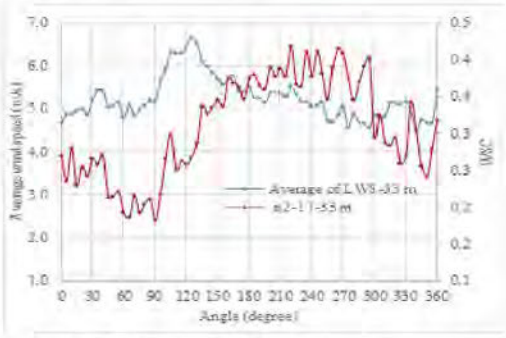

Fig. 6b. Relationship between LWS3 and WSC at 33 m (LiDAR) measurement at Amber-bo.

drawn as a function of the wind direction using WS8 and WS9, located at approximately the same azimuth angle (160°) from the north accurately predicted the waked boundaries, characterized with abrupt change in the WSC pattern. As with the speed ratio approach, the WSC approach captured the affected angle range of approximately 70°, shown in Fig. 7b by the dotted oval shape. Both approaches correctly showed that the most severely affected sectors were between 285° and 290°. The speed deficits at 20.63 m and 49.9 m when compared with LiDAR measurement were 23.04 % and 37.62 % respectively. The regions indicated by the dotted rectangles in Fig. 7 were characterized by speed reduction and marked variation in the WSC. Further reduction in speed encountered by the in-situ measurements (WS8 and WS9) in this region may be traceable to the boom influence or perturbations due to the presence of some secondary support structures, since there were no other sheltering obstacles within the vicinity of the experiment. It is again established that time series WSC computed from wind data measured at two different heights and the same azimuth from the north could be used for identifying the wake affected sectors without the need for a collocated sensor.

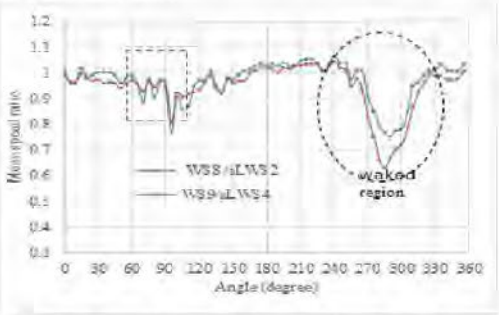

Fig.7a. Ratio of WS8 and sLWS2 and WS9 and sLWS4 plotted on sector-wise basis and binned in 5° wind direction intervals. The oval and rectangular dashed shapes indicate the wake affected direction at Schlip in the course of three months data captured concurrently in 2014.

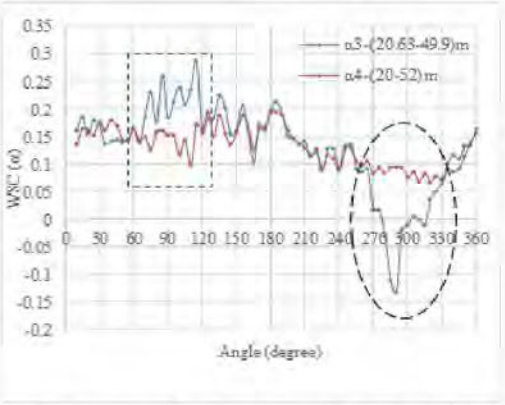

Fig. 7b. Time series WSC calculated for the in-situ (20.63 m to 49.9 m) and for the LiDAR (20 m to 52 m), binned in 5° wind direction intervals. The oval and rectangular dashed shapes indicate the wake affected direction at Schlip in the course of three months data captured concurrently in 2014.

IX. WEIBULL AND WIND POWER DENSITY (WPD): TOWER WAKE DISTORTION CHARACTERIZATION

The two parameter Weibull distribution has been used extensively to describe wind speed variation commonly encountered in the majority of wind assessment projects. However, the Weibull distribution has a limitation in that it does not reveal good conformity for low wind speeds, which is a problem because tower wake distortion is characterized by low wind speed. It becomes interesting to verify how Weibull two parameter functions describe the direction sectors affected by tower shadowing if such sectors were not excluded before analysis.

Time series wind speeds at both sites were binned into 10° wind direction intervals. At Amper-bo, the collocated sensors at 16.88 m were used whereas at Schlip the in-situ measurement at 49.9 m and the LiDAR captured data at 52 m were used. The Weibull k, c, and WPD were calculated over 36° wind direction sectors. The probability density function f(v) and cumulative distribution F(v) were also evaluated.

Fig. 8 illustrates the variation of the Weibull shape factor k with wind direction sectors. At Schlip, the k values obtained from both anemometer and LiDAR have the same pattern (Fig 8a). The mean values of k are 2.38 and 2.67 for WS9 and sLWS4 respectively. At Amper-bo, the k values calculated from the collocated sensors show the same pattern (Fig. 8b). The mean k values for the collocated sensors are 2.27 for WS4 and 2.37 for WS4B. The k values recorded in each 10° wind direction bin depends on the spread of wind speed. Tower shading has no noticeable effect on the k values calculated.

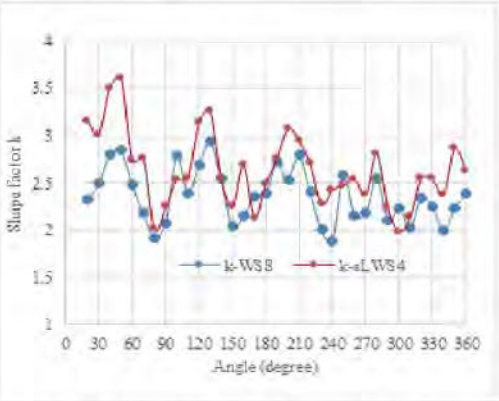

Fig.8a. Weibull k for in-situ (WS9) and LiDAR (WS4) binned in 10° wind direction intervals and drawn as a function of the wind direction at Schip.

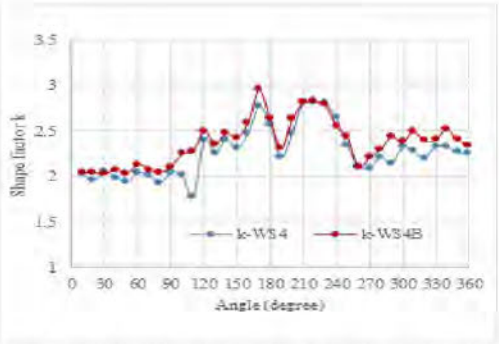

Fig. 8b. Weibull k for in-situ (WS4) and (WS4B) binned in 10° wind direction intervals and drawn as a function of the wind direction at Amper-bo.

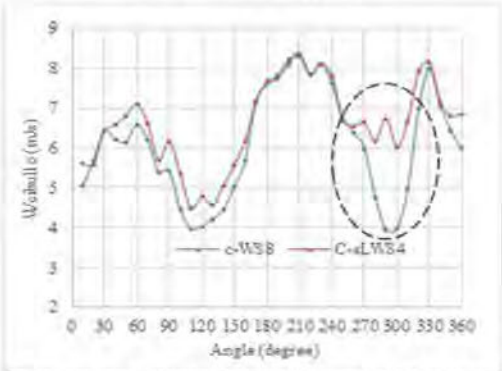

Fig. 8c. Weibull c for the in-situ (WS9) and LiDAR (sLWS4) binned in 10° wind direction intervals and drawn as a function of the wind direction at Schip.

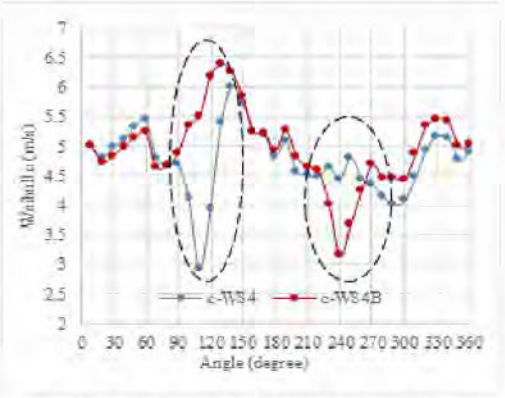

Fig. 8d. Weibull c for the collocated sensors (WS4 and WS4B) binned in 10° wind direction intervals and drawn as a function of the wind direction at Amper-bo.

Fig. 8a and Fig. 8c are the Weibull scale factor (c) which indicates how windy a site is. The parameter is affected by tower induced flow perturbations as indicated with the oval dashed circle. At Schlip, the overall average of c ws 6.09 m/s which was 12.17 % higher than the observed average of WS9. The mean value of c computed from the LiDAR (sLWS4) captured data was 6.59 m/s which was 13.72 % higher than the sLWS4 average. Based on the 10° bin of wind direction intervals used, the sector that was most severely affected by tower induce flow perturbations was 290°. A speed deficit of 37.84 % resulted in a corresponding 41.65 % deficit of Weibull c when the LiDAR (sLWS4) observed data was compared with WS9. Similarly, at Amper-bo, the average of c generated from WS4 was 4.75 m/s which was 12.99 % higher than the mean of WS4. The same was applicable to WS4B where the mean c value (4.96 m/s) was 13.49 % of WS4B mean.

The most severely affected sectors by tower shading were 110° and 240° for WS4 and WS4B respectively. At 110°, WS4 was 44.96 % less than WS4B and c of WS4 was 46.99 % less than c of WS4B. At 240°, WS4B was 32.22 % less than WS4 and c of WS4B was 29.19 % less than c of WS4. The discrepancies in the severity revealed that WS4 was more exposed to the tower shadings than WS4B. Based on the results from the two sites, this study may conclude that the mean values of Weibull c were between 12 % to 14 % higher than the observed mean speed at these two locations.

The probability density function, cumulative frequency, and frequency of occurrence of the observed speed in the severely affected direction sectors are illustrated in Fig.9a to Fig. 9d.

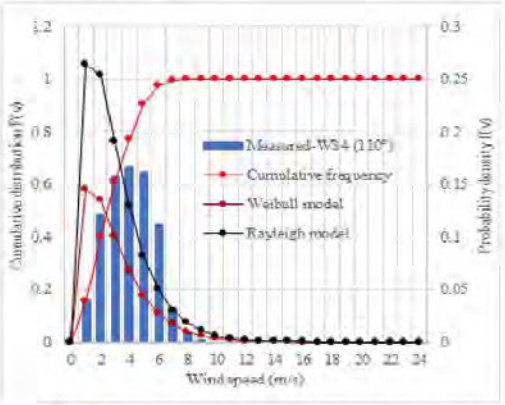

Fig. 9a. Wind speed probability density, cumulative frequency and observed frequency of WS4 obtained from the most severely affected direction sector (110°) at Amper-bo.

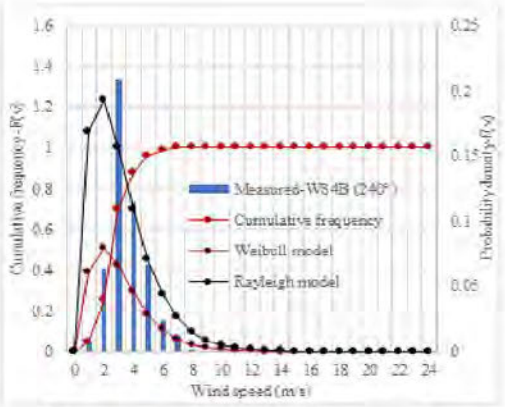

Fig.9b. Wind speed probability density, cumulative frequency and observed frequency of WS4B obtained from the most severely affected direction sector (240°) at Amper-bo.

Fig. 9d is the direction sector where the collocated sensors at Amper-bo were both out of tower wake effect. The direction sectors severely affected were characterized mostly by lower wind speeds and lower spread as well. The distribution models (Weibull and Rayleigh) used demonstrate a measure of weakness, hence, the notable under-prediction of resource parameters evaluated from such direction sector (Fig. 9a, Fig. 9b and Fig. 9c). Further statistics would reveal the most suitable of the two in characterizing resource parameters at both sites.

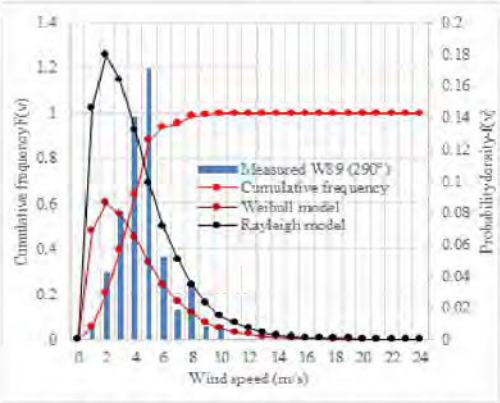

Fig. 9c. Wind speed probability density, cumulative frequency and observed frequency of WS49 obtained from the most severely affected direction sector (290°) at Schlip.

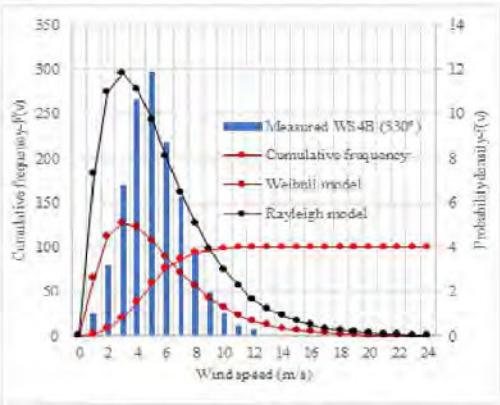

Fig. 9d. Wind speed probability density, cumulative frequency and observed frequency of WS4B obtained from udisturebed direction direction sector (330°) at Amper-bo.

The WPD computed from each 10° bin of the observed (WS4 and WS4B) probability density distributions and the corresponding values obtained from the Weibull and Rayleigh models and the associated errors based on the two models are illustrated in Fig 10. The dashed oval shape represents the direction sectors under the influence of the tower wakes. The sector-wise comparison of the WPD (Fig. 10a and Fig. 10c) affirms that WPD depends on site observed wind speed, with higher values in the direction sectors that are windier.

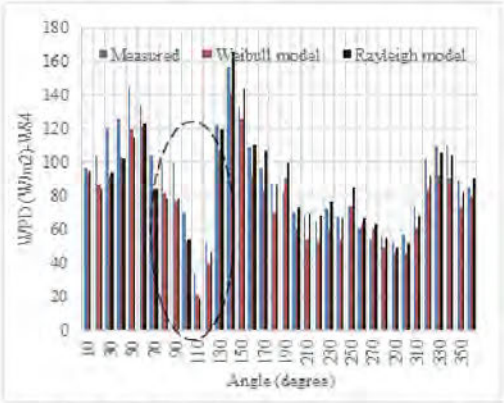

Fig. 10a. WPD of the observed (WS4) compared to those obtained from the Weibull and Rayleigh models at Amper-bo.

Based on the WS4 analysis, the observed average WPD was 90.13 W/m^2. The corresponding values for Weibull and Rayleigh models were 77.36 W/m^2 and 85.48 W/m^2 respectively. These results indicated 14.16 % and 5.16 % underestimation by the Weibull and Rayleigh models respectively. Similarly, the observed average WPD for WS4B was 98.59 W/m^2. The Weibull model yielded 85.41 W/m^2, whereas the Rayleigh model yielded 97.90 W/m^2.

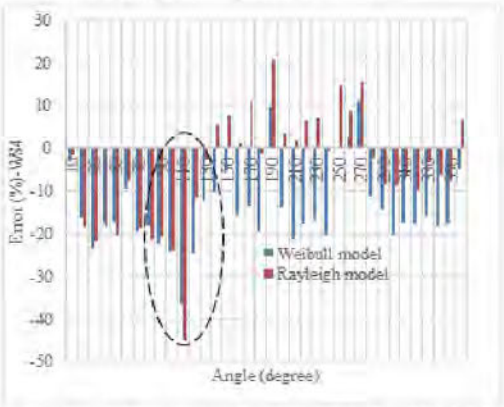

Fig. 10b. WPD values predicted by Weibull and Rayleigh models in reference to the WPD obtained from the observed (WS4) at Amper-bo.

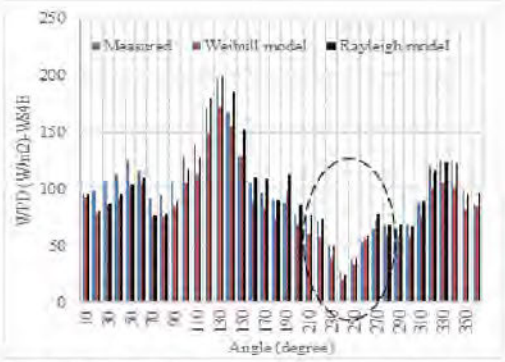

Fig 10c. WPD of the observed (WS4B) compared to those obtained from the Weibull and Rayleigh models at Amper-bo.

The Weibull and the Rayleigh models underpredicted WPD by 13.37 % and 0.70 % respectively. The overall averaging approach, while providing information on the wind power potential of a site, tended to mask the actual characteristics of winds in the direction sectors; hence the sector-wise evaluation. Again, at the WS4 most severely affected sector (110°), the Weibull and Rayleigh models under predicted WPD by 36.61 % and 45 % (Fig. 10b), whereas at 240°, Weibull and Rayleigh models underpredicted WPD by 26.06 % and 9.5 % respectively (Fig. 11d).

The tower shading impact on WPD was examined by comparing data from the collocated sensors (WS4 and WS4B) at the two most severely affected sectors 110° and 240°, respectively. At 110°, WPD (measured) of WS4 was 75.4 % less than WPD (measured) of WS4B, and the Weibull and Rayleigh models of WS4 underpredicted WPD by 80.68 % and 85.11 % when compared to their counterparts in WS4B. Also, at 240°, the WPD obtained from WS4B measured data was 60.99 % less than the WPD obtained from WS4.

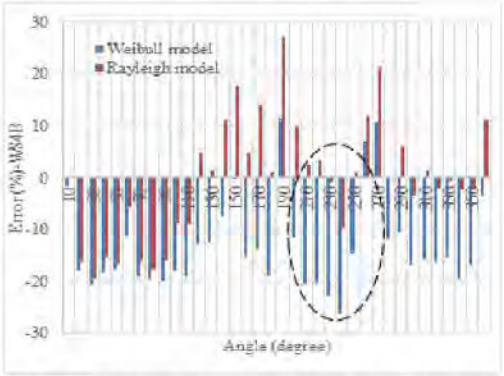

Fig. 10d. WPD values predicted by Weibull and Rayleigh models in reference to the WPD obtained from the observed (WS4B) at Amper-bo.

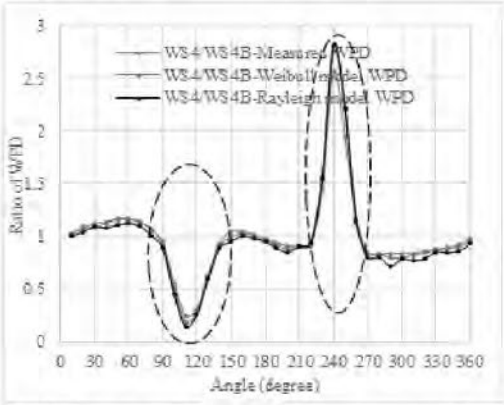

Fig. 11. Ratio of WPD obtained from the observed probability density distribution functions and the corresponding values obtained from the Weibull and Rayleigh models based on the collocated sensors (WS4 and WS4B) at Amper-bo.

The ratios of the WPD obtained from the measured data and from the two models, drawn as a function of the wind direction, are illustrated in Fig. 11. The boundaries of the wake affected regions are defined and indicated by the dashed over shape. The two models captured the waked regions of the two sensors sufficiently. When the affected direction sectors were removed, WS4 saw an improvement of 3.78 % for the WPD obtained from the observed data. WPD from the Weibull and Rayleigh models improved by 4.6 % and 4.87 % respectively. In WS4B, the measured WPD increased by 9.78 %. The Weibull and Rayleigh approaches increased by 9.28 % and 9.03 % respectively.

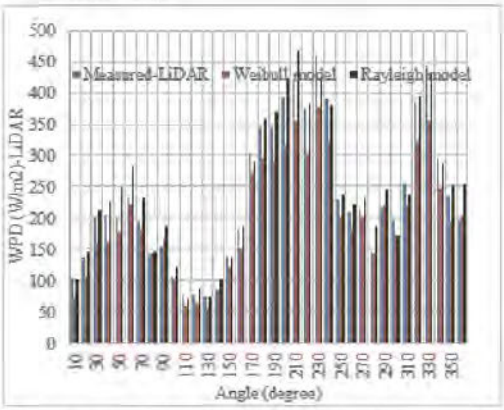

Fig. 12a. WPD of the observed LiDAR (LWS4) compared to those obtained from the Weibull and Rayleigh models at Schlip.

In Schlip, the WPD computed from each 10° bin of the observed (WS9 and sLWS4) probability density distributions and the corresponding values obtained from the Weibull and Rayleigh models and their associated errors when compared to

the observed data are illustrated in Fig. 12. The dashed oval shape represents the direction sectors that were under the influence of tower shading (Fig 12a to Fig. 12d). Analysis of WS9 shows that the observed average WPD was 211.18 W/m^2. The corresponding values for Weibull and Rayleigh models were 181 W/m^2 and 206.28 W/m^2 respectively.

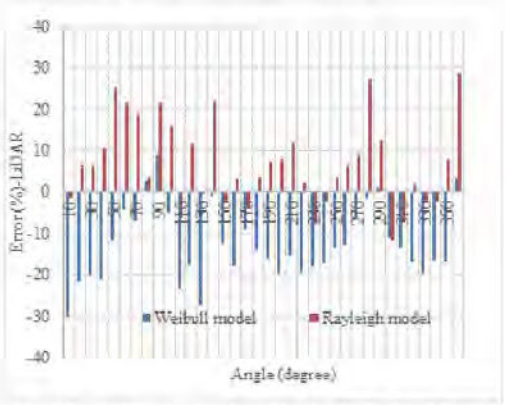

Fig. 12b. WPD values predicted by the Weibull and Raleigh models in reference to the WPD obtained from the observed LiDAR (sLWS4) data at Schlip.

The results represent a 14.29 % and 2.32 % underestimation by the Weibull and Rayleigh models respectively. Similarly, the observed average WPD for the LiDAR (sLWS4) is 232.47 W/m^2. The Weibull model yielded 200.67 W/m^2 and the Rayleigh model yielded 245.16 W/m^2. The Weibull under predicted WPD by 13.68 % while the Rayleigh model overpredicted WPD by 5.46% %. Based on the sector-wise evaluation, at the WS9 most severely affected sector (290°), the Weibull and Rayleigh models under predicted WPD by 21.50 % and 17.11 % (Fig. 12c). The LiDAR observed data was considered undisturbed; as a result, the influence of tower induced flow perturbation was absent.

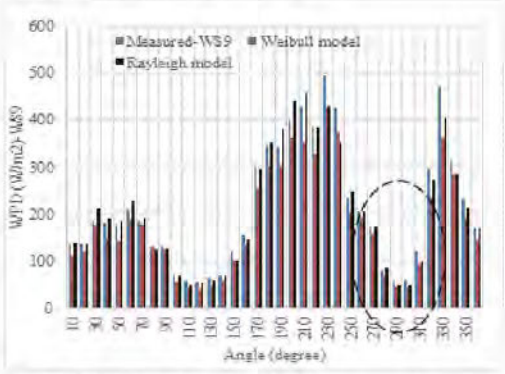

Fig. 12c. WPD of the observed (WS9) compared to those obtained from the Weibull and Rayleigh models at Schlip.

The impact of tower shading on WPD was examined by comparing WS9 and LiDAR (sLWS4) for the three months when the two data acquisition systems concurrently captured wind data. At 290°, the WPD obtained from WS9 was 73.11 % less than the WPD obtained from the measured LiDAR (sLWS4) wind speed. The WPD based on the Weibull and Rayleigh models of WS9 under predicted WPD by 79.09.68 % and 80.13 % respectively when compared to their counterparts obtained based on LiDAR (sLWS4) valuation. The ratios of the WPD obtained from the measured data and from the two models, drawn as a function of the wind direction (Fig. 13), clearly defined the wake boundaries.

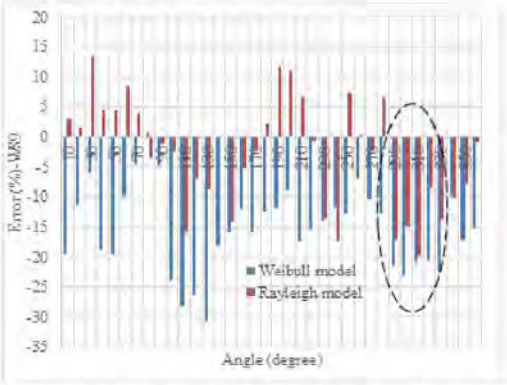

Fig. 12d. WPD values predicted by Weibull and Rayleigh models in reference to the WPD obtained from the observed (WS9) at Schlip.

The two models captured the affected direction sectors sufficiently. When the affected direction sectors were removed, the overall WPD obtained from WS9 improved by 7.79 %. The overall WPD from the Weibull and Rayleigh models improved by 8.07 % and 8.24 % respectively.

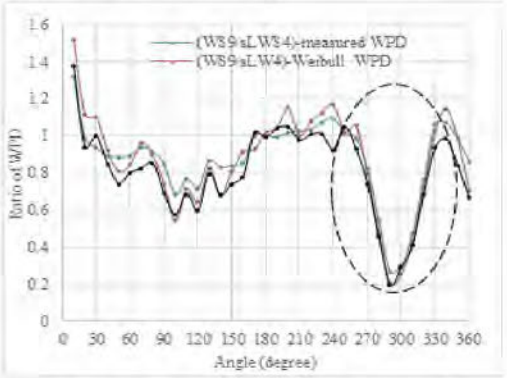

Fig. 13. Ratio of WPD obtained from observed probability density distribution functions and the corresponding values obtained from the Weibull and Rayleigh models based on in-situ (WS9)and LiDAR (sLWS4) that were concurrently captured at Schlip.

X. TEST-OF-FIT USED

The measure of goodness-of-fit of the two statistical models (Weibull and Rayleigh) summarizes the differences between the observed values and the values predicted by the models. The suitability of the models in reference to the observed was determined from the two most applied tests – the root mean square error (RMSE) and the coefficient of determination (R^2). Table VI is a summary the test-of-fit for the distributions (Weibull and Rayleigh) used.

TABLE VI. TEST-OF-FIT FOR WEIBULL AND RAYLEIGH MODELS

Amper-bo				
	Weibull (RMSE)	***Rayleigh (RMSE)***	***Weibull (R^2)***	***Rayleigh (R^2)***
WS4	90.37	74.60	0.9262	0.8428
WS4B	95.65	68.38	0.9445	0.9062
Schlip				
WS9	244.82	152.70	0.9882	0.9621
sLWS4	248.08	148.84	0.9735	0.9627

(R^2) values close to 1 indicate a strong relation between the model values and the observed values. The Weibull model showed a stronger relation than its counterpart (Rayleigh model) but the (R^2) values accounted for only the proportion of the variability explained by the observed data. From the tests (Table VI), the scatter index (SI = RMSE/data mean) of less than one indicates that both models sufficiently describe the observed data set. However, the Rayleigh model returned less error (RMSE), making it the most suitable model of the two for both sites.

XI. CONCLUSION

The wind data analyzed, compared and reported in this study were 10-minute averaged, concurrently observed measurements, using LiDAR and instrumented communication towers in 2014, at Amper-bo and Schlip, two inland locations in southern and central Namibia respectively. At Amper-bo the LiDAR operated for 8.4 months (16th Jan. 2014 to 30th Sept. 2014) and nearly 3 months at Schlip (31st Sept. 2014 to 24th Dec. 2014) where wind data was measured simultaneously at the instrumented lattice triangular communication towers. The in-situ captured data were evaluated in reference to the LiDAR observed to gain insight into the performance implications of not excluding tower waked regions before analysis. Beside traditional speed ratio which is commonly used, and the coefficient of determination (R^2) of turbulent kinetic energy (TKE), and turbulence intensity (TI) of collocated sensors recently proposed, this work suggests a simpler approach to identify tower waked direction sectors where collocated sensors are not available but wind data are collected from two intermediate heights with the same azimuth angle from the north.

The following conclusions based on the specific impact of the tower wake distortion on the in-situ observed data verified by the undisturbed LiDAR observations have been drawn:

- Times series WSC computed, binned in 5° in wind direction intervals and drawn as a function of the wind direction enables the identification and definition of the boundaries of tower waked regions where collocated sensors are not available but wind data are collected from two intermediate heights with the same azimuth angle from the north. The traditional speed ratio approach and the coefficient of determination (R^2) of turbulence intensity (TI) at Amper-bo for the collocated sensors revealed wake boundaries that cover an angle of approximately 60°. Time series WSC computed between the heights 8 m to 16.88 m, 16.88 m to 32.68 m, 16.88 m to 64.92 m and 32.68 m to 64.92 m equally defined wake boundaries covering angles of approximately 60° when compared with time series WSC calculated using undisturbed LiDAR data at corresponding height intervals. Based on the height intervals previously mentioned, at the most severely affected direction sector (110°), the WSC obtained deviated by 57.0 %, 58.04 %, 48.60 % and 54.04 % respectively from their LiDAR counterparts. At Schlip, time series WSC calculated between 20.63 m and 49.9 m defined a wake boundary of approximately 70° when compared with the same evaluation from LiDAR data at the corresponding height interval and the result is again supported by the traditional speed ratio approach which defined a wake boundary of approximately 70°. From this study, it is established that time series WSC computed from wind data measured at two different intermediated heights, located at approximately the same azimuth from the north is sufficient for identifying the wake affected sectors without the need for collocated sensors.

- The two statistical models (Weibull and Rayleigh) demonstrated a measure of weakness in properly characterizing the wake affected zones. Tower shading has no noticeable effect on the k values calculated on the average from the two sites. Results from the two sites revealed that mean values of Weibull c were between 12 % to 14 % higher than the observed mean speed at these two locations.

- The impact of tower shadow on performance was further verified by the following comparisons: Using the collocated sensors at Amper-bo, at 110° (WS4 servery affected direction sector), WPD (measured) of WS4 was 75.4 % less than WPD (measured) of WS4B and the Weibull and Rayleigh models of

WS4 underpredicts WPD by 80.68 % and 85.11 % when compared to their counterparts in WS4B. Also, at 240° (WS4B most servery affected direction sector), WPD obtained from WS4B measured data was 60.99 % less than WPD obtained from WS4. When the affected direction sectors were removed, WS4 saw an improvement of 3.78 % for the WPD obtained from the observed data. WPD from the Weibull and Rayleigh models improved by 4.6 % and 4.87 % respectively. In WS4B, the measured WPD increased by 9.78%. The Weibull and Rayleigh approaches increased by 9.28 % and 9.03 % respectively. Using WS9 and LiDAR (sLWS4) at Schlip, at 290° (WS9) most severely affected direction sector), the WPD obtained from WS9 was 73.11 % less than WPD obtained from the measured LiDAR (sLWS4) wind speed. The WPD based on the Weibull and Rayleigh models of WS9 under predicted WPD by 79.09.68 % and 80.13 % respectively when compared to the results of their counterparts based on LiDAR (sLWS4) valuation. When the affected direction sectors were removed, the overall WPD obtained from WS9 improved by 7.79 %. The overall WPD from the Weibull and Rayleigh models improved by 8.07 % and 8.24 % respectively.

- Regarding data availability at both sites, there was a 100 % data recovery rate (in-situ) and a consistent data recovery at all heights > 95 % (LiDAR), except the three topmost heights where the data availability fell below that. This trend is attributed to weak backscatter signal which is difficult for the LiDAR to detect due to large beam waist radius and measurement probe depth at such heights.

- The wind roses at both sites were thoroughly described and insights gained on the direction sectors where predominant and strongest winds blow. The direction sectors affected by tower shadings at both sites were characterized with disproportionally higher percentages of low wind regimes compared to other sectors and this was contrary to the LiDAR observation within those affected sectors.

- Various models were explored to compute WSC to permit hub height extrapolations and revealed that the magnitude depends on the model applied. On the monthly variation of WSC for both measurement techniques at the two sites, the winter months (May, June and July) accounted for the highest values whereas the summer months (January and December) recorded the least values. The same applied to the monthly variations of the roughness lengths. This trend is due to thermal stratification of the atmospheric body at both sites. Diurnally, the computed WSC at both Amber-bo and Schlip showed evidence of direct correlation to the diurnal heating/cooling cycle of air above the ground, and thus of atmospheric stability. Higher values were recorded in the stable night hours whereas the unstable daylight hours accounted for the lowest values. The same applied to the diurnal variation of roughness length.

Thus, tower shading impact on resource parameters have been examined. From this study, it is established that time series WSC computed from wind data measured at two different intermediate heights, located at approximately the same azimuth from the north can be used for identifying the wake affected sectors without the need for collocated sensors. Regarding the performance implications, failure to address tower distortion effect properly will lead to underpredictions of energy yield. Further statistical review shows that the Rayleigh model performed better than the Weibull model at both sites.

ACKNOWLEDGMENT

Funding for this project was provided by the Ministry of Foreign Affairs of Denmark, Ministry of Foreign Affairs of Finland, United Kingdom Department for International Development, Austrian Development Agency and Namibia Power Corporation. Invaluable support is provided by Namibia Energy Institute under Namibia University of Science and Technology.

REFERENCES

[1] M. Sanuki, S. Kimura, and S. Toyama, "Anemometer reading in the presence of nearby obstacle," *Pap. Meteorol. Geophys.*, vol. 6, pp. 140–143, Jan. 1955, doi: 10.2467/mripapers1950.6.2_140.

[2] M. E. Okorie and F. Inambao, "Identification of tower and boom-wakes using collocated anemometers and lidar measurement," *Int. J. Mech. Eng. Technol.*, vol. 10, no. 06, pp. 72–94, 2019.

[3] M. E. Okorie and F. Inambao, "Identification of tower-wake distortion using LiDAR measurement," *Procedia Manuf.*, vol. 35, pp. 704–710, 2019, doi: 10.1016/j.promfg.2019.06.012.

[4] S. Fabre, M. Stickland, T. Scanlon, A. Oldroyd, D. Kindler, and F. Quail, "Measurement and simulation of the flow field around the FINO 3 triangular lattice meteorological mast," *J. Wind Eng. Ind. Aerodyn.*, vol. 130, pp. 99–107, Jul. 2014, doi: 10.1016/j.jweia.2014.04.002.

[5] M. Stickland, T. Scanlon, S. Fabre, A. Oldroyd, and D. Kindler, "Measurement and simulation of the flow field around a triangular lattice meteorological mast," *Energy Power Eng.*, vol. 5, Oct. 2013.

[6] R. N. Farrugia and T. Sant, "Modelling wind speeds for cup anemometers mounted on opposite sides of a lattice tower: a case study," *J. Wind Eng. Ind. Aerodyn.*, vol. 115, pp. 173-183, 2013, doi: 10.1016/j.jweia.2012.11.006. *Meteorol. Mag.*, vol. 89, pp. 209-215.

[7] N. E. Rider, "On the performance of sensitive cup anemometers," *Meteorol. Mag.*, vol. 89, pp. 209-215. 1960.

[8] B. Maribo Pedersen, K. S. Hansen, S. Øye, M. Brinch, and O. Febian, "Some experimental investigations on the influence of the mounting arrangements on teh accuracy of cup-anemometer measurements," *J. Wind Eng. Ind. Aerodyn.*, vol. 39, no. 1, pp. 373–383, Jan. 1992, doi: 10.1016/0167-6105(92)90561-N.

[9] J. E. Cermak and J. D. Horn, "Tower shadow effect," *J. Geophys. Res.*, vol. 73, no. 6, pp. 1968, doi: 10.1029/JB073i006p01869.

[10] W. F. Dabberdt, "Tower-induced errors in wind profile measurements," *J. Appl. Meteorol.*, vol. 7, no. 3, pp. 359–366, 1968.

[11] N. Nishio et al., "A study on wind speed correction method of lattice tower mast using CFD simulation," Transactions of the JSME (in Japanese), vol. 84, no. 862, pp. 18-00042-18–00042, 2018, doi: 10.1299/transjsme.18-00042.

[12] M. Tusch, C. Masson, and P. Héraud, "Modeling of turbulent atmospheric flow around tubular and lattice meteorological masts," *J. Sol. Energy Eng*, vol. 133, no. 1, p. 011011, Feb. 2011, doi: 10.1115/1.4003293.

[13] V. Bezrukovs, V. Bezrukovs, S. Upnere, L. Gulbe, and D. Bezrukovs, "The use of cellular communication masts for wind share research," *Energetika*, vol. 64, no. 2, Sep. 2018, doi: 10.6001/energetika. v64i2.3780.

[14] M. Lotfi, "Atmospheric Wind Flow Distortion Effects of Meteorological Masts," Annual Conference of the Portuguese Renewable Energy Association (APREN), Lisbon, Portugal, 2016. DOI: 10.13140/RG.2.2.36519.39848

[15] K. McCaffrey et al., "Identification of tower-wake distortions using sonic anemometer and lidar measurements,"*Atmos. Meas. Tech.*, vol. 10, no. 2, pp. 393–407, 2017, doi: http://dx.doi.org/10.5194/amt-10-393-2017.

[16] International Electrotechnical Commission (IEC), "Wind energy generation systems – Part 12-1: Power performance measurements of electricity producing wind turbines," International Electrotechnical Commission (IEC), IEC Central Office 3 rue de Varembé CH-1211 Geneva 20, Switzerland, International Standard IEC 61400-12-1:2005(E), Dec. 2005.

[17] International Electrotechnical Commission (IEC), "Wind energy generation systems – Part 12-1: Power performance measurements of electricity producing wind turbines," International Electrotechnical Commission (IEC), IEC Central Office 3 rue de Varembé CH-1211 Geneva 20, Switzerland, International Standard IEC 61400-12-1:2017-03(en-fr), Mar. 2017.

[18] M. E. Okorie and F. L. Inambao, "Identification of Tower and Boom-Wakes Using Collocated Anemometers and Lidar Measurement," IJMET, vol. 10, no. 6, pp. 72–94, Sep. 2019.

[19] M. E. Okorie, F. Inambao, and Z. Chiguvare, "Evaluation of wind shear coefficients, surface roughness and energy yields over inland locations in Namibia," *Procedia Manuf.*, vol. 7, pp. 630–638, Jan. 2017, doi: 10.1016/j.promfg.2016.12.094.

[20] M. E. Okorie, F. L. Inambao, Z. Chiguvare, and N. A. Kgabi, "Wind shear coefficients and energy yields estimations: Namibia case study of arid coastal and inland locations," *Int. J. Appl. Eng. Res.*, vol. 13, no. 8, pp. 6282-6296, 2018.

[21] G. Gualtieri and S. Secci, "Wind shear coefficients, roughness length and energy yield over coastal locations in Southern Italy," *Renewable Energy*, vol. 36, no. 3, pp. 1081–1094, Mar. 2011, doi: 10.1016/j.renene.2010.09.001.

[22] G. Gualtieri and S. Secci, "Comparing methods to calculate atmospheric stability-dependent wind speed profiles: A case study on coastal location," *Renewable Energy*, vol. 36, no. 8, pp. 2189–2204, Aug. 2011, doi: 10.1016/j.renene.2011.01.023.

[23] A. Derrick, et al., "HAVSNÄS – Pilot project report on cold climate and high hub height on mate and high hub height," Göteborg Sweden, Renewable Energy Systems Ltd/NV Nordisk Vindkraft AB, 2012.

[24] I. Fyrippis, P. J. Axaopoulos, and G. Panayiotou, "Wind energy potential assessment in Naxos Island, Greece," *Appl. Energy*, vol. 87, no. 2, pp. 577–586, Feb. 2010, doi: 10.1016/j.apenergy.2009.05.031.

[25] A. N. Celik, "A statistical analysis of wind power density based on the Weibull and Rayleigh models at the southern region of Turkey," *Renewable Energy*, vol. 29, no. 4, pp. 593–604, 2004.

[26] S. A. Akdağ, H. S. Bagiorgas, and G. Mihalakakou, "Use of two-component Weibull mixtures in the analysis of wind speed in the Eastern Mediterranean," *Appl. Energy*, vol. 87, no. 8, pp. 2566–2573, Aug. 2010, doi: 10.1016/j.apenergy.2010.02.033.

[27] E. K. Akpinar and S. Akpinar, "Statistical analysis of wind energy potential on the basis of the Weibull and Rayleigh distributions for Agin-Elazig, Turkey:," *Proc. Inst. Mech. Eng., Part A*, Jan. 2006, doi: 10.1243/0957650042584357.

[28] P. K. Chaurasiya, S. Ahmed, and V. Warudkar, "Study of different parameters estimation methods of Weibull distribution to determine wind power density using ground based Doppler SODAR instrument," *Alexandria Eng. J.*, vol. 57, no. 4, pp. 2299–2311, Dec. 2018, doi: 10.1016/j.aej.2017.08.008.

[29] A. Pena and C. B. Hasager, "Remote sensing for wind energy," Risø National Laboratory for Sustainable Energy, Technical University of Denmark., Risø–I–3184(EN), May 2011.

[30] G. Gualtieri, "The strict relationship between surface turbulence intensity and wind shear coefficient daily courses: a novel method to extrapolate wind resource to the turbine hub height," *Int. J.Renewable Energy Res.*, vol. 5, no. 1, pp. 183–200, 2015, doi: 10.20508/ijrer.39363.

[31] M. E. Okorie, F. Inambao, and Z. Chiguvare, "Evaluation of Wind Shear Coefficients, Surface Roughness and Energy Yields over Inland Locations in Namibia," *Procedia Manuf.*, vol. 7, pp. 630–638, Jan. 2017, doi: 10.1016/j.promfg.2016.12.094.

[32] G. Gualtieri and S. Secci, "Methods to extrapolate wind resource to the turbine hub height based on power law: A 1-h wind speed vs. Weibull distribution extrapolation comparison," *Renewable Energy*, vol. 43, pp. 183–200, Jul. 2012, doi: 10.1016/j.renene.2011.12.022.

[33] S. Rehman and N. M. Al-Abbadi, "Wind shear coefficient, turbulence intensity and wind power potential assessment for Dhulom, Saudi Arabia," *Renewable Energy*, vol. 33, no. 12, pp. 2653–2660, Dec. 2008, doi: 10.1016/j.renene.2008.02.012.

[34] S. Orlando, A. Bale, and D. Johnson, "Experimental study of the effect of tower shadow on anemometer readings," *J. Wind Eng. Ind. Aerodyn.*, vol. 99, pp. 1–6, Jan. 2011, doi: 10.1016/j.jweia.2010.10.002.

[35] R. N. Farrugia and T. Sant, "Modelling wind speeds for cup anemometers mounted on opposite sides of a lattice tower: a case study," 2013, doi: 10.1016/j.jweia.2012.11.006G.

CHAPTER 5: ANGLE DEPENDENCE OF TOWER WAKE DISTORTION: A PARAMETRIC STUDY

This chapter combines physical modelling of the tower structure and CFD flow simulation to perform a parametric study in order to investigate the angle dependence of tower wake distortion effect. The controlling parameters (thrust coefficient [C_T] and the leg length [L_m]) in the centreline velocity deficit expression prescribed in IEC 61400-12-1, varies with incident wind angle. This chapter incorporated the (thrust coefficient [C_{Ti}] and the leg length [L_i]) obtained at different incident wind angles into the IEC centreline velocity deficit expression to obtain a modified speed deficit expression used to predict the booms lengths at incident wind angles other than the IEC reference direction ($\theta = 0°$).

Cite this article: M. E. Okorie and F. L. Inambao, "Angle Dependence of Tower Wake Distortion: A Parametric Study," *International Journal of Mechanical and Production Engineering Research and Development*, vol. 11, no. 3, pp. 481–498, 2021, doi: 10.24247/ijmperdjun202138.

Link to the article:

http://www.tjprc.org/publishpapers/2-67-1621862211-IJMPERDJUN202138.pdf

International Journal of Mechanical and Production Engineering Research and Development (IJMPERD)
ISSN (P): 2249–6890; ISSN (E): 2249–8001
Vol. 11, Issue 3, Jun 2021, 481-498

TRANS STELLAR
•Journal Publications •Research Consultancy

Original Article

ANGLE DEPENDENCE OF TOWER WAKE DISTORTION: A PARAMETRIC STUDY

MADUAKO E. OKORIE[1] & FREDDIE L. INAMBAO[2]

[1]*Student, University of KwaZulu-Natal, Department of Mechanical Engineering, Durban, South Africa*

[2]*University of KwaZulu-Natal, Department of Mechanical Engineering, Durban, South Africa*

ABSTRACT

The controlling parameters (thrust coefficient (C_T) and the tower leg lengths (L_m)) found in the centreline speed deficit expression provided in the International Electrotechnical Commission (IEC 61400-12-1) standard which derivation was based on the reference direction ($\theta = 0°$) are angle dependent. It is therefore crucial to evaluate and incorporate values of these parameters into the centreline speed deficit expression to account for tower wake distortions at different incident wind angles. In this research, the variation of these parameters with the incident wind angles were investigated using two lattice equilateral triangular communication towers of different configurations, belonging to the Mobile Telecommunication Limited (MTC) of Namibia, located at Amper-bo and Korabib. Physical modelling and computational approaches were utilized to establish the values of these parameters at incident wind angles other than the IEC reference direction. For both towers, deducting a range 2 % to 4 %, 9 % to 13 % and 15 % to 20 % out of the IEC reference value ($\theta = 0°$) will accurately estimate C_T values for winds that arrive at the tower at 10°, 20° and 30°, respectively. An expression of C_T for the tower at Amper-bo is $C_T = 1.27(1 - S)S$ and that at Korabib is $C_T = 1(1 - S)S$, provided winds arrive at the towers at angles $\leq \pm 70°$ with respect to the IEC reference direction ($\theta = 0°$). For winds that arrive at the tower at angles $\geq \pm 70°$, a boom length of $x \geq 7.5\mathrm{m}$ and $x \geq 6.5\mathrm{m}$ at Amper-bo and Korabib respectively is enough to keep the speed sensors out of the tower wakes. Deducting approximately 1.5 %, 5 % and 12 % less of the IEC reference value will reliably estimate L_m values for winds that arrive at the tower at ±10°, ±20°, ±30° and ± 40°, respectively. Again, physical modelling approach enables the computation of the solidity ratio (S) to an accuracy of 0.001 mm, showing an increase in the blockage to wind flow and corresponding increase in boom lengths due to the presence of secondary support structures, while the computational approach illustrates a more complex flow interference around the tower with no appreciable increase in boom lengths. Finally, the thrust coefficient (C_{Ti}) and the leg length (L_i) obtained at different incident wind angles were incorporated into the IEC centreline velocity deficit expression to arrive at a modified speed deficit expression used to predict the booms lengths at incident wind angles other than the IEC reference direction($\theta = 0°$).

KEYWORDS: Tower Wakes, Solidity Ratio, Thrust Coefficient, Boom Length, Speed Deficit & CFD

Received: Feb 03, 2021; **Accepted**: Feb 23, 2021; **Published**: May 21, 2021; **Paper Id.**: IJMPERDJUN202138

1. INTRODUCTION

The angle dependence of tower wake distortion effects was investigated using two lattice equilateral triangular communication towers of different configurations. Guidelines for tower (tubular and lattice) instrumentation for wind measurement perspective has been provided for in Annex G of the International Electrotechnical Commission standards[1], [2].In [3]an expression to evaluate the mast to assess the anemometer separation that is required for a desired maximum flow distortion was also proposed. The two editions of the standards [1]and [2]and the recommended guideline acknowledge that tower shading is angle dependent. Previous literature (i.e. [4] and [5])that

approached the problem using computational fluid dynamics (CFD) agreed with the findings in [1], [2]that tower induced flow perturbation is angle dependent. In most field experiments, practitioners have relied heavily on the centreline velocity deficit expression as prescribed in IEC standard to calculate the sensor separation distance from the tower given the desired measurement accuracy. In most of the instrumented operational wind measurement towers, the household statement "instrumented according to IEC standard", to a large extent, means calculating the boom length using the centre-line velocity deficit expression prescribed in ([1] and [2], without considering the other important and indispensable factors from which the expression was derived. It is apparent that the centre-line velocity deficit expression according to [1] and [2] was derived based on the assumed reference incident wind direction ($\theta = 0°$), where the velocity deficit is assumed to be on the same axis that passes through the mast centre and perpendicular to the mast face. The implication is that the incident wind is considered perpendicular to the same mast face, giving rise to velocity deficit values that are predicted using the upstream contour profiles of modified flow due to tower physical structure. In most cases, this arrangement does not correspond to the anemometer arrangements in field experiments, especially where disused powerlines or communication towers are instrumented for wind assessment. For one reason or the other, the most prevalent practical mounting arrangements have been to place the boom parallel to the face of the mast which then makes the boom to either be at 90° or 30° to the IEC reference direction. Restrictions on further constructions on the Mobile Telecommunication Limited (MTC) of Namibia towers used for the National Wind Resource Assessment Project (NWRAP), meant that the booms are placed parallel to the face of the lattice communication towers instrumented for wind measurement.

In the arrangement of this kind, the incident wind obviously arrives at the tower at an angle that is not perpendicular to the face of the tower. As the incident wind angle varies, so also does the total exposed area of the tower the incident winds encounter. As a result, the two important variables in the velocity deficit expression i.e., the assumed tower leg length (L_m) and the thrust coefficient (C_T) (which depend on the solidity (S)) varies. If the centre-line velocity deficit expression derived from the standard mast configuration ($\emptyset = 0°$) is the only criterion to quantify tower induced flow perturbations at different incident wind angles and for towers of different configurations, it is necessary to verify its universal applicability. For this reason, the IEC velocity deficit expression may not precisely predict flow distortion at different incident wind angles for a typical operational tower. A centre-line velocity deficit expression that captures the variation of $C_T$and $L_m$with incident wind direction to precisely define flow distortions at such incident wind angles is needed. In this study, an improved method of calculating the variables of interest is proposed.

As earlier mentioned, operational towers instrumented for wind measurement are mostly deployed in the first place for a variety of other uses. As a result, the majority of them have discrete members such as cross and horizontal bracings, cable ladders, cable bundles and attachment brackets etc., which produce discrete wakes, resulting in more complex flow interferences contrary to the idealised mast configuration presented in ([1] and [2].The 2017 edition of the standard[2] acknowledged that the presence of secondary support structures makes flow interferences significantly more complex within the vicinity of the tower. However, the standard does not suggest any practical approach to evaluate their contribution toflow defects within the tower vicinity. An attempt was made in [6] to account for the contributions of the secondary support structures to tower induced flow defect. The inconsistencies in estimating the $C_T$values and oversimplified model for studying the secondary support structures place a great limitation on the outcome of the study. Further investigation is therefore required to improve the method of assessment and to evaluate their contributions to wake distortion effects.

Finally, an accurate method of calculating the parameters of interest, and, ultimately, to incorporate the variation of C_T and $L_m$into the velocity deficit expression to account for their angle dependency,is proposed. The outcome of this study will contribute to the body of literature in this field and enable stakeholders in the wind energy industry to properly instrument lattice triangular towers taking into consideration the angle dependency of tower shading.

2. BACKGROUND

Different crude methods have been used to acquired wind data in Namibia, mainly for agricultural and meteorological purposes. Winds obtained based on these crude methods are not suitable for site wind power potential estimation and economic evaluation. In 2008, stakeholders Gobabeb Research & Training Centre (GRTC), Mobile Telecommunications Limited (MTC), Namibia Power Corporation (NP) and Namibia University of Science and Technology (NUST) came together to establish the Namibia Wind Resource Assessment Project (NWRAP) with the overall goal of assessing and provisioning high quality wind data from locations of interest. Cost containment and early commencement of the project being of the essence, MTC permitted the instrumentation of their existing communication towers for NWRAP wind measurement [7]As a result, lattice triangular communication towers of various configurations were instrumented and are being used for wind data observation. This current study therefore investigates their suitability with emphasis on sensor arrangements when the winds arrive at the tower at other angles different from the IEC 2017 reference direction.

3. SITE AND TOWER CONSTRUCTION DETAILS

The two broad categories of towers investigated are lattice with triangular footprint. The locations are Amper-bo (25.354 °S, 18.313 °E) and Korabib (28.548 °S, 17.820 °E). Amper-bo's siteis desert-like with homogeneous vegetation. It is a class A terrain according to Annex B of (IEC 2005) as reported in [8], [9]where brief construction details of the MTC tower used were also presented. Figure 1 shows the construction details. The tower is 120 m high and L_m(centre-to-centre) of 1.10 m, all through the height. It is guyed and has an equilateral triangular cross-section with three vertical tubular mild steel rods of 100 mm external diameter (OD). The vertical tubular rods from repeating construction units which are joined end-to-end by flanged connections. Each construction unit is 3.5 m, and each contains four modules of height 0.89 m. The network of small angular cross bracings made from 45mm x 45 mm x 5 mm angle bars are bolted to a flat plate (0.045 m x 0.07 m) that is welded to the tubular rods. The boom has an OD of50 mm and wall thickness of 2 mm and extends approximately 2.56 m away from the tower. The cable ladders and the cable bundles which cover almost half of the W to N (clockwise) facing side of the tower are the secondary support structures.

Figure 1a: A Section of the Tower at Amper-bo showing the Boom Arrangements and some Secondary Support Structures. Figure 1b: A Section of the Tower at Korabib showing the Boom Arrangements and some Secondary Support Structures.

The tower at Korabib is guyed, 120 m high and L_m(edge-to-edge) of 1.32 m all through the height. It has an equilateral triangular cross-section with three vertical angle bars (70 mm x 70 mm x 6 mm) made from mild steel. The 70 mm x 70 mm x 6 mm angle bars form repeating construction units which are bolted together using flat plate connections (Figure 1b). Each construction unit is 3.024 m, and each contains two modules of height 1.512 m. The network of small angular horizontal and cross bracings made from 60 mm x 60 mm x 5 mm angle bars are bolted to a flat plate (0.144 m x 0.26 m) that is fixed to the vertical angle bar. The detail of the boom construction and the separation distance from the tower is the same at Amper-bo. The cable bundles and ladder located W to N (clockwise) facing side of the tower are the secondary support structures.

4. A BRIEF OVERVIEW OF THE IEC STANDARD IN REFERENCE TO THE CURRENT STUDY

Based on the reference incident wind direction ($\theta = 0°$)(Figure3), Annex G of [1], [2]prescribed a centre-line velocity deficit expression the values of which are obtained along an upstream profile, an indication that the expression is along an axis that passes through the tower centre-line and perpendicular to the face of the tower as well. The centre-line velocity deficit expression (U_d) which gives the normalised velocity profile upstream of the tower face on the wind, is computed as per Equation (1):

$$U_d = 1 - (0.062C_T^2 + 0.072C_T) \cdot \left(\frac{L}{R} - 0.082\right) \quad (1)$$

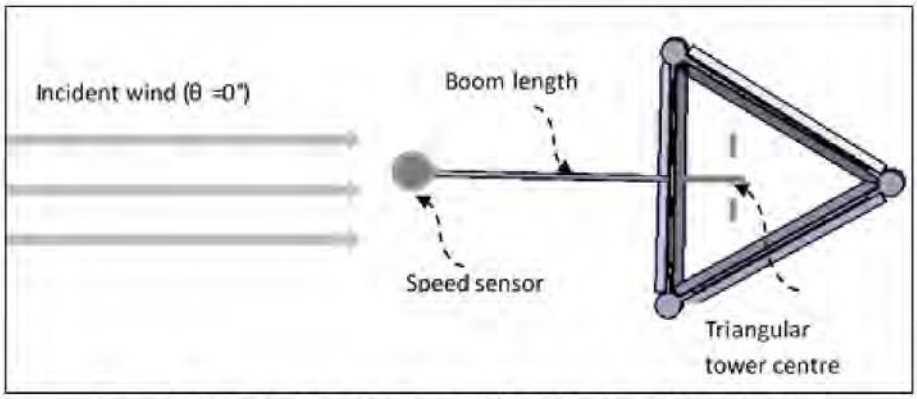

Figure 3: IEC Standard Boom Configuration ($\theta = 0°$) for lattice Triangular Tower.

Solving for R, gives Equation (2) which is of more practical use in field experiments to compute the sensor separation distance from the centre of the tower to keep the speed deviation due to tower induced flow perturbations below 100 ± 1 % of the free stream velocity, according to the standards.

$$R = \frac{L}{\frac{1-U_d}{(0.062C_T^2+0.076C_T)}} \tag{2}$$

where U_d is the centre-line velocity deficit, R [m] is the distance of the speed sensor from the tower centre to the point of observation, L [m] is the face width or tower leg length and C_T is the thrust coefficient.

5. RESULT AND DISCUSSIONS

5.1 Mast Geometry and Properties

At Amper-bo, the module height$h$ is 0.89 m and L_m is 1.1 m, whereas at Korabib, the module height and $L_m$are 1.052 m and 1.320 m, respectively. Each module investigated was modelled in a CAD tool. For each of the modules, 36 independent projected planes, each at 10° were created. The angle of each plane indicates the incident wind angle whereas the corresponding total exposed area projected on the plane represented all the towers' physical structures that the wind at the angle would encounter. Each area projected on the plane was transformed to a two-dimensional structure, properly trimmed, and later transformed back to a three-dimensional structure to enable the computation of the total exposed area. the projected are a being of great significance in the field of external aerodynamics and the solidity ratio to an accuracy of 0.001 mm.

The solidity ratio (S) was therefore defined as the ratio of the projected area (A_p) of all structural members on the side of the meteorological mast normal to the wind direction to the total exposed area normal to the wind direction [1], [2]and was computed thus:

$$S = A_p/A_e \tag{3}$$

Based on the standard incident wind direction ($\theta = 0°$), [1] and [2]prescribed a centre-line velocity deficit expression which presumed a universal applicability. The implication is that the total exposed area is independent of the

incident wind angle. This may not hold since the total exposed area is simply the product of the height and the L_m of the tower.Results from the present study show that when the incident wind angle varied, it resulted in a total exposed area that was dependent on the incident wind angle due to the observed variation of L_m at that angle. The incident wind angle and the projected area at such angle of the instrumented tower are therefore the variable and function thereof respectively. The variations of the S and L_m with respect to θ is illustrated in Figures 4a, 4b and 4c.

The equilateral triangular towers exhibit rotational symmetry with an angle of 120°, with obvious repetition of geometric properties every 120°.

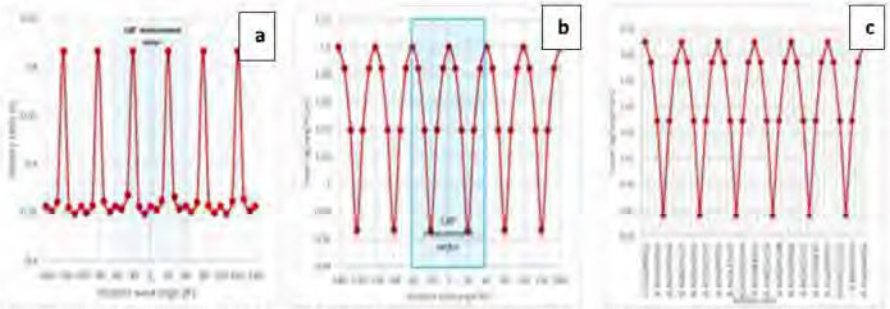

Figure 4a: Graph of Solidity Ratio Versus the incident wind Angles. Figure 4b: Graph of Tower Leg Length Versus the Incident Wind Angle. Figure 4c: The Tower Leg Length Versus the Solidity Ratio Computed at Different Incident wind Angles for the Tower at Amper-bo.

Repetition of values noticed every 60° instead of 120° is attributed to the identical projected area as seen by the incident wind from opposite directions[4].The minimum obstruction (higher value of solidity) is recorded when two of the mast legs align with the wind direction, occurring at angles {-90°, -30°, 30°, 90°}, for a tower that is face-on to the wind, where as maximum obstruction (lower values of solidity is encountered at angles {-40°, -20°, 20°, 40°} and {-50°, -10°, 10°, 50°}is recorded when the legs are slightly moved out of alignment with the adjacent one, thereby increasing the blockage (Figure 4 and Figure 5).

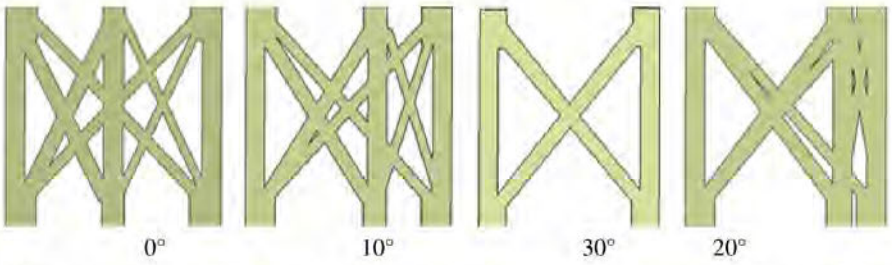

Figure 5: Projected Areas of the Tower at Amper-bo for each of the Indicated Incident Wind Angles.

The variation$S$and L_m with θmaintained a pattern that is consistent with the rotational symmetry of the triangular tower. With the solidity ratio at the standard wind direction ($\theta = 0°$) of 0.4565, adding 0.55 % to 0.56 % of the reference

value to its original value (i.e., $0.4565 + (0.56\% \times 0.4565)$ will yield a good estimate of the solidity at angles {-50°, -10°, 10°, 50°},within a measurement sector of 120°. Similarly, subtracting 0.86% to 0.87% of the reference value from itself gives a reliable value of$S$ at angles (-40°, -20°, 20°, 40°). At angles {-90°, -30° 30°, 90°} where minimum obstruction is encountered due to alignment of the tower legs,S value is reliably estimated by subtracting 33 % to 33.5% of the reference value from itself.As expected,Figure 4c shows that $L_m$and $A_e$are least where minimum$S$is encountered and vice versa.

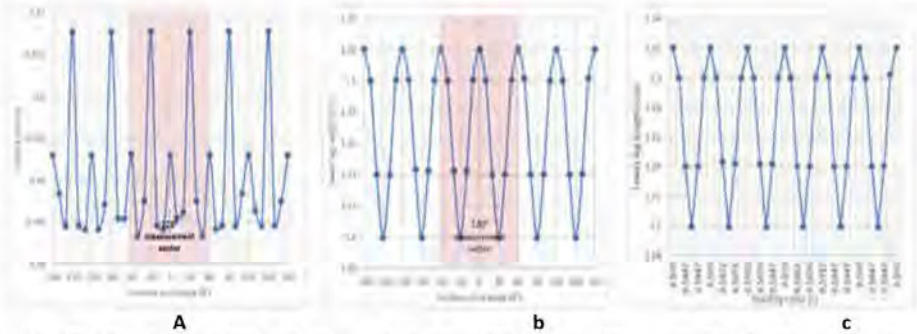

A b c

Figure 6a: The Graph of Solidity Ratio Versus the Incident Wind Angles. Figure 6b: Graph of Tower Leg Length Versus the Incident Wind angle. Figure 6c: The Tower Leg Length Versus the Solidity Ratio Computed at Different Incident Wind Angles for the Tower at Korabib.

At Korabib, apart from the rotational symmetry with obvious repetition of geometric properties every 120°, the tower at Korabib encountered minimum obstruction (higher solidity) when two of the mast legs aligned with the wind direction, recorded at angles {-90°, -30°, 30°, 90), whereas maximum obstruction (lower values of solidity)was recorded at angles {-50 -40°, -20°, 20°, 40° 50°}, when the legs were slightly moved out of alignment with the adjacent one, thereby increasing the blockage (Figure 6 and Figure 7).

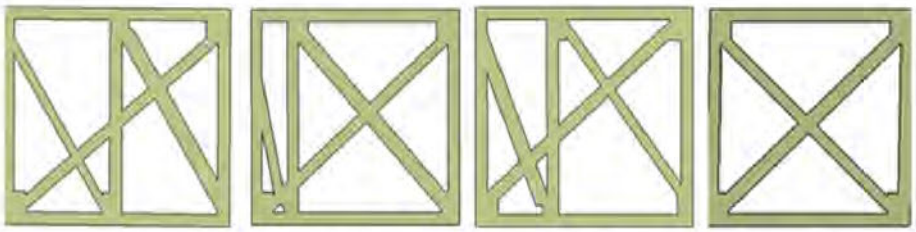

0° 10° 20° 30°

Figure 7: Projected Areas of the Tower at Korabib for each of the Indicated Incident Wind Angles.

Values of C_T and $L_m$are repeated every 60° as reported earlier.At Korabib, the solidity ratio at the standard wind direction ($\theta = 0°$) is 0.593. Adding (1.4 % to 1.5 % of the reference value toitself (i.e., $0.593 + (0.56\% \times 0.593)$gives a good estimate of the solidity at angles (-50°, -10°, 10°, 50°), for a measurement sector of 120°. Also, addingapproximately 1.4%of the reference value to itself gives reliable values of solidity ratios at angles (-20°and 20°), but subtracting 0.90% to 0.92% of0.593 yields reliable values of solidity ratios at angles (-40°, and 40°).At angles {-90°, -30° 30°, 90°} where

minimum obstruction is encountered due to alignment of the tower legs, S value is reliably estimated by subtracting 2.4 % to 2.5% of the reference value from itself.Consistent with the tower at Amper-bo,Figure 6c shows that L_m and A_e are least where minimum S is encountered and vice versa.

With this approach, a practitioner may estimate the Sat other incident wind angles when the value at the reference direction is evaluated. Minimum flow distortion is encountered when the booms are mounted at 30° and 90° from the reference direction ($\theta = 0°$) but on the condition that the incident wind arrives at the tower at the same angle as the speed sensor.

5.2 Impact of Secondary Support Structures

Secondary support structures are critical components of operational towers. They come in different configurations and their sizes and shapes depend on the application of the parent-tower. The presence of these substructures produce discrete wakes, which makes flow interference within the vicinity of the tower more complex, contrary to the idealised mast configuration presented in [1] and [2].In this study, cross and horizontal bracings are considered natural members of an operational tower and are treated as such. However, cable ladders, cable bundles and other substructures provided for safe climbing of the tower are secondary support structures and were investigated. At both sites, cable bundles of diameters approximately 52 mm, 30 mm and 5 mm that covered approximately one-half of the tower phase were investigated. Amper-bo hosts two additional cable ladders of diameter approximately 16 mm in diameter that are fixed on the cross bracings in each tower module. At Korabib, the cable ladder and the structures provided for safe climbing are built (inscribed) inside the tower. Figure 8 and Figure 9 illustrate the relationship between the S andL_m with respect to the incident wind angle at Amper-bo. The minimum obstruction (higher value of solidity) is recorded when two of the mast legs align with the wind direction, occurring at angles {-30° and 30°} (Figure 8) for a tower face on the wind whereas maximum obstruction (lower values of solidity) is recorded at angles {-80°,-40°, -20°, 20°, 40°, 80°}, when the legs are slightly moved out of alignment with the adjacent one, thereby increasing the blockage.

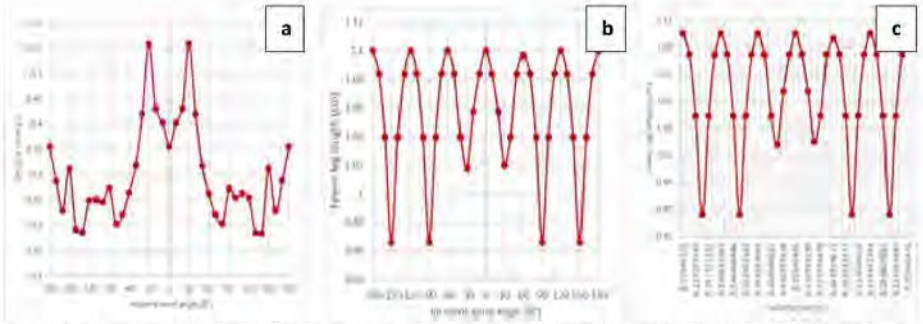

Figure 8a: Graph of Solidity Ratio Versus the Incident Wind Angles. Figure 8b: Graph of Tower Leg Length Versus the Incident Wind Angle. Figure 8c: Tower Leg Length Versus the Solidity Ratio Computed at Different Incident Wind Angle for the Tower at Amper-bo, with the Secondary Support Structure's Influence Captured.

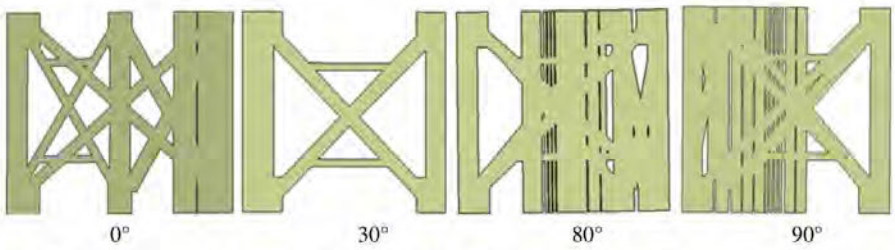

Figure 9: Projected Areas of the Tower at Amper-bo with Secondary Support Structure Influence for each of the Indicated Incident Wind Angles.

Figure 10 and Figure 11 illustrate the relationship between the S and L_m with respect to the incident wind angle at Korabib. The minimum obstruction (higher value of solidity) is recorded at 10° (Figure 10b) for a tower face on the wind whereas maximum obstruction (lower values of solidity) is recorded at angles {-20°, 20°} due to the presence of secondary support structures.

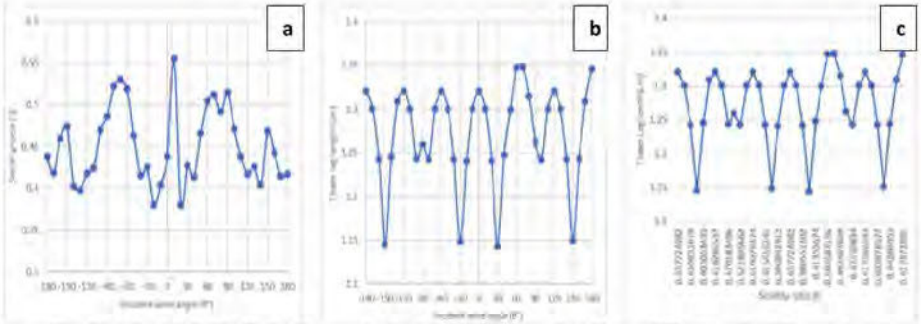

Figure 10a: Graph of Solidity Ratio Versus the Incident Wind Angles. Figure 10b: Graph of Tower Leg Length Versus the Incident wind Angle. Figure 10c: Tower Leg Length Versus the Solidity Ratio Computed at Different Incident wind Angles for the Tower at Korabib, with the Secondary Support Structure's Influence Captured.

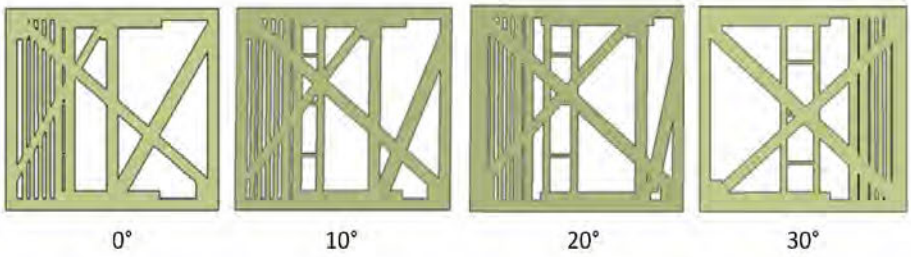

Figure 11: Projected Areas of the Tower at Korabib with Secondary Support Structure Influence Captured for each of the Indicated Incident Wind Angles.

The percentage differences in the $S$of the tower without and the tower with secondary support structures

calculated as a function of the tower without secondary structure and drawn as a function of the incident wind angles are illustrated in Figure 12a and Figure 12b.

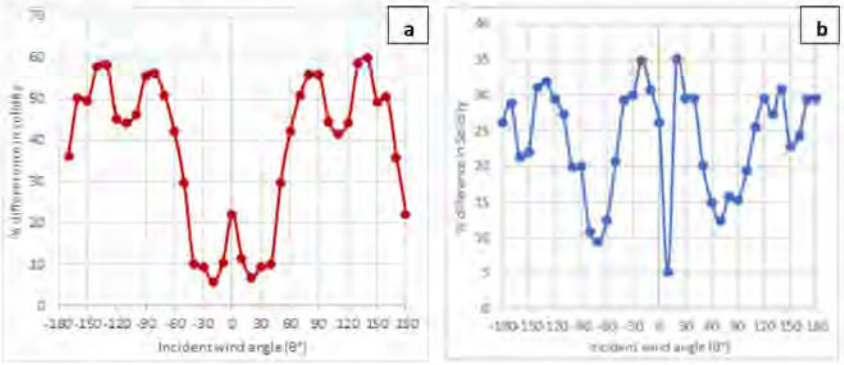

Figure 12a: The Percentage Difference in the Solidity Ratio of the Tower without and the Tower with Secondary Support Structures Versus the Incident Wind Angle for Amper-bo tower. Figure 12b: The Percentage Difference in the Solidity Ratio of the Sower without and the Sower with Secondary Support Structures Versus the Incident wind Angle for Korabib Tower.

The percentage difference in S for the most severely affected direction sectors is approximately 56%, recorded at angles (-90°, -80°, 80°, 90°). The corresponding percentage difference in S for the least affected is approximately 6 % which occurred at angles {-30°, 30°}. Similarly, approximately 35% is recorded at angles (-20°, 20°) being the most severely affected angles whereas 5% difference is encountered at 10°, the least affected. The shape and location of the secondary support structures determine how it induces flow defect.

5.3 Thrust Coefficient

The flow modification within the vicinity of the tower is a function of the thrust coefficient (C_T) which in turns depends on the solidity of the tower. C_T, therefore, is the total drag force per unit length of the tower module divided by the dynamic pressure and the leg distanceL_m(IEC 2005 and 2017). The computational models used are the areaA_c $[m^2]$ $\left(\text{i.e.}, A_c = A_e - A_p\right)$obtained from each tower module (Figure 13), where A_e and A_p are the total exposed area and the projected area, respectively. The computational domain is rectangular in shape and the turbulent model used was the $k-\omega SST$ solved in Ansys Fluent. At the boundaries, the hydraulic diameter of the frontal area of A_c was specified and the simulation result obtained was post-processed by calculating the thrust coefficient (Equation 4) as prescribed in[1] and [2].

$$C_T = \frac{2F_d}{\rho A_c V^2} \tag{4}$$

where F_d is the drag force $[N]$, ρ is the density of air $[kg/m^3]$ and$V$ is the wind velocity $[m/s]$.Standard air density ($\rho = 1.225\ kg/m^3$) was used. The total area on the olive green (Figure 13) is the A_c.

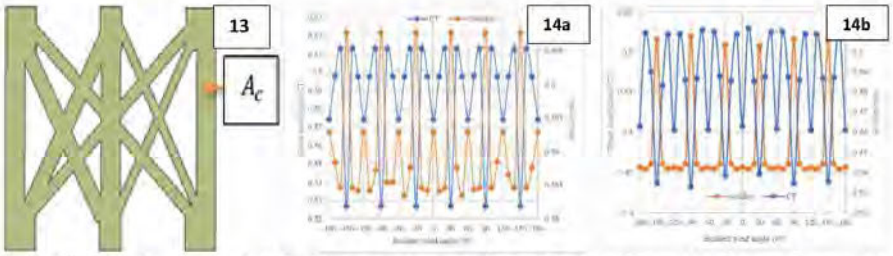

Figure 13: The Frontal Area used in the Flow Simulation for Calculating the Thrust Coefficient. Figure 14a: The Variation of C_T and Sat each Incident Wind Angle at Korabib. Figure 14b: The Variation of C_T and Sat each Incident wind Angle at Amper-bo.

Figure 14a and 14b illustrate the variation of $C_T$and$S$at each incident wind angle at Amber-bo and Korabib. Higher values of $S$are recorded at angles (-30° and 30°) and corresponding lower values of the $C_T$and vice versa.

Based on the centre-line wind speed deficit expression prescribed in [1], [2],(Equation 1), the graph of the nondimensionalise centre line wind speed ($u/UorU_d$) is drawn as a function of the distance to the tower centre divided by tower leg length (R_d/L_m) (Figure 15a). A user may use this expression to evaluate the tower to speed sensor separation required for a desired maximum flow induced error reading when the C_T is known. In this regard, 1% speed deficit will occur at L/R value of approximately 0.25 when the C_T is 0.5. For this level of tower induced flow modification, a boom-mounted anemometer should be placed4 tower leg lengths distance. If the desired speed deficit is 0.5%, the required separation will be 7 tower leg distance.

Based on the procedure recommended in[3]the centre-line wind speed deficit ($\Delta = 1 - u/U$) was drawn as a function of L_m/R_d for various thrust coefficients (Figure 15b) and the slope of each line was further drawn as a function of the corresponding C_T (Figure15 c). The curve fitting Figure 15b and Figure 15c yields Equation 5 for estimating the centre line velocity deficit for lattice tower face-on to the incident wind direction [3].

$$\Delta = (0.126C_T - 0.006)\left(\frac{L}{R} - 0.08\right) \quad (5)$$

Sensitivity tests conducted over a range of C_T showed that the equation demonstrated high accuracy for a centre-line speed deficit between 0.001 to 0.02. Beyond this range, there exists inconsistencies in accurately predicting speed deficit using Equation 5. The equation was further modified to predict speed deficit beyond this range, but it served no practical purpose since speed deficit beyond this range is not acceptable in wind measurement.

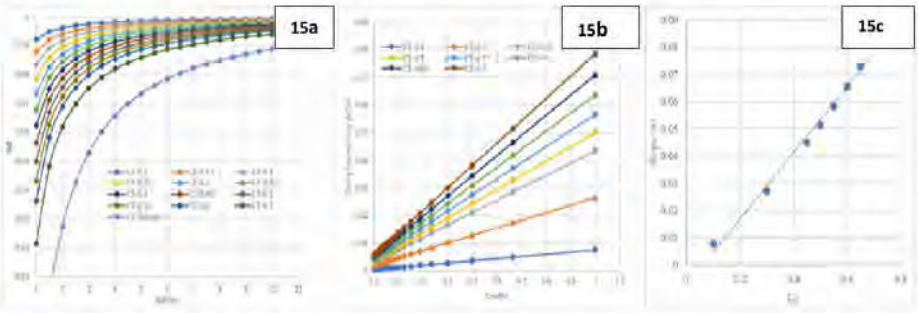

Figure 15a: The Graph of u/U (U_d) Versus R_d/L_m at Various C_T Values. Figure 15b: The Graph of Δ Versus L_m/R_d at Various C_T Values. Figure 15c: The Slope of each line in Figure 15b Drawn as a Function of the Corresponding C_T Value.

6. MODIFICATION OF THE IEC AND IEA CENTRE-LINE WIND SPEED DEFICITS

To incorporate theincident wind angle into the speed deficit expression prescribed in[1]–[3],the $C_T$and L_m values computed at different incident wind angles wereused. At Amper-bo, the $C_T$at the standard incident wind direction ($\theta = 0°$) is 0.6286. Subtractingapproximately2.5% of the reference value from itself (i.e., $0.6286 - 2.2\,\% \times 0.6286$)will yield a good estimate of C_T at angles (-50°, -10°, 10°, 50°) and subtracting approximately 12% of the reference value from itselfwill accurately predict the C_T value at angles (-80, -40, -20, 20, 40, 80). Due to the alignment of the tower legs, minimum obstruction is encountered, evident at angles (--30° and 30°) where the $C_T$are reliably estimated by subtracting approximately 18% of the reference value from itself. The tower at Korabib is made up of members with sharp edges. The large surface area of the angle bar used means that the C_T values obtained in this tower are marginally higher than its counterpart at Amper-bo. At the IEC reference wind direction ($\theta = 0°$), the C_T is 0.9632. Again, subtractingapproximately 3% of the reference value from itself (i.e., $0.9632 - 2.2\,\% \times 0.9632$) yields a good estimate of C_T at angles (-50°, -10°, 10°, 50°) and subtracting approximately 10 % of the reference value from itselfaccurately predicts the C_T value at angles (-80, -40, -20, 20, 40, 80). Due to the alignment of tower legs, minimum obstruction is evident at angles (-30° and 30°) where the $C_T$are reliably estimated by subtracting approximately 16% of the reference value from itself.

Again, the L_m at the standard wind direction ($\theta = 0°$) is 1.1 mm for the tower at Amper-bo. As the incident wind angle changes, the actual$L_m$of the incident wind depends on the total exposed area whichvaries as well. For both tower configurations at both sites, deducting approximately 1.5% of the reference L_m from itself accurately predicts the leg lengths (L_i) at angles (-50°, -10°, 10°, 50°), and approximately 5% less of its original value predicts (L_i) at angles (-40°, -20°, 20°, 40°). As statedearlier, the L_i values at (30° and 30°) are minimal and may be reliably estimated by subtracting approximately 12% of the reference value from itself.Thus, the two centreline speed deficit expressions found in [1]–[3]are modified to incorporate the variation of the key parameters with respect to the incident wind angle.

$$U_{di} = 1 - \left(0.062C_{Ti}^2 + 0.072C_{Ti}\right)\left(\frac{L_i}{R} - 0.082\right) \tag{6}$$

$$\Delta_i = \left(0.126C_{Ti} - 0.006\right)\left(\frac{L_i}{R} - 0.08\right) \tag{7}$$

where $C_{Ti} = C_T - BC_T$ and $L_i = L_m - QL_m$. B and Q are the percentage differences of the C_T and L_m values at standard incident wind direction($\theta = 0°$). The values of the parameters are repeated every 60° based on the reasons mentioned earlier.With this approach, a practitioner may estimate the speed deficit at other incident wind angles when the C_T and $L_m$at the reference direction is evaluated. Minimum flow distortion is encountered when the booms are mounted at angle (-30°, 30°) from the reference direction ($\theta = 0°$).The presence of secondary structures such as cable ladders, cable bundles etc, contribute to a marginal increase in the values of the thrust coefficient. The local flow modification impact of these substructures depends on their position on the parent tower.Therefore, individual assessment of each operational tower to ascertain their impacts is recommended. The obvious implication of their presence is an overall increase in$C_T$values.At Korabib the C_T values increased by approximately 16.2% at standard incident wind angle ($\theta = 0°$) when

compared to a tower without secondary support structures, i.e., for a lattice mast face-on to the wind. At 30°, blockage by the discrete members was least, i.e., approximately 2% higher.and approximately 16.5% higher at 80°. Similar evaluation of the tower at Amper-bo shows that at $\theta = 0°$ the C_T value of the tower with secondary support structures is approximately 18.5% higher than a tower without such structures and approximately 14% higher at 30°.

Basedon the modified centre-line speed deficit expression (Equation 8)Figures 16a and 16bshow the graphsof (U_d) drawn as a function of R_d/L_m taking cognisance of the C_{Ti}obtained at angels 0°, 10°, 20° and 30° for Amper-bo and Korabib, respectively. At Amper-bo, for the reference direction ($\theta = 0°$), a boom-mounted anemometer should be placedapproximately 5 tower leg lengths away for a speed deficit of 1%. At 10°, 20°, and 30°, 10%, 17% and 25% shorter boom lengths respectively are required for 1% speed deficit when compared to the value obtained in the reference direction ($\theta = 0°$). Similarly, at Korabib, a boom-mounted anemometer should be the length of 8.5 tower leg lengths for a speed deficit of 1% in the reference direction. At angle 10°, 20° and 30° respectively, a12%, 18% and 28% less boom length is required for a centreline speed deficit of 1% when compared to the reference wind direction.With this approach and based on the IEC reference wind direction ($\theta = 0°$), C_T for the tower at Amper-bo and Korabib can be estimated: $C_T = 2.53(1 - S)S$ and $C_T = 3.99(1 - S)S$ respectively.It is apparent thatthe resulting boom lengths required to achieve 99% of the freestream velocity are way too long and booms of these lengthsare susceptible to vibration which will further increase error readings of the speed sensors mounted on them. Due to this effect, CFD flow simulation that captures the complex 3D nature of the two towers wasperformed.

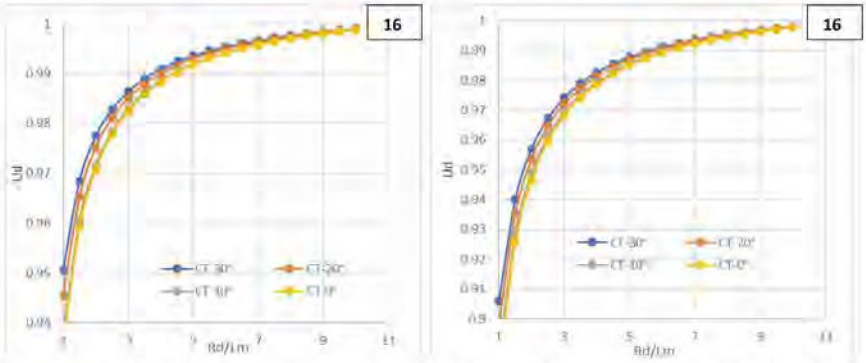

Figure 16a: Graph of U_d Versus R_d/L_m at Various C_T Values for the Modified Centre-Line Speed Deficit at Amper-bo. Figure 16b: The Graph of U_d Versus R_d/L_m at Various C_T Values for the Modified Centre-Line Speed Deficit at Korabib.

7. USE OF COMPUTATIONAL FLUID DYNAMICS

The CFD derived flow around the Amper-bo and Korabib towers is illustrated in Figures 17a and 17b. To further investigate the angular dependence of tower wake distortions, CFD simulation was performed for winds that arrive at the towers at the IEC standard wind direction ($\theta = 0°$), 10°, 20° and 30°. For a wind speed deficit of 99%, corresponding values of R_d/L_m based on the IEC boom configuration for each of the angles were computed (Figures 18a and 18b)and reversed mathematics performed on the IEC centre-line speed deficit expression (Equation 1) to enable the evaluation of the corresponding C_T values for each of the incident wind angles. The graphs of the relative centre-line wind speed (u/U or U_d) drawn as a function of R_d/L_m when the tower is face-on to the wind (i.e., at $\theta = 0°$) based on the CFD flow

simulation are shown in Figures 18a and 18b.The C_T value at $\theta = 0°$ for Amper-bo tower is 0.316. Winds that arrive at the tower at 10°, 20° and 30° with respect to the reference wind direction require 4%, 12% and 22% less of the reference C_T value to achieve 99% of the free stream value. With the C_T of 0.2095 at $\theta = 0°$ for the Korabib tower 5%, 14% and 22% less of the referenceC_T values are required to achieve 99% of the free stream speed when the winds arrive at 10°, 20°and 30° respectively. Further CFD flow simulation around bluff Amper-bo and Korabib towersshows that there is no significant difference in the C_T values and boom lengths when compared with the values obtained from the operational towers with and without secondary support structures.

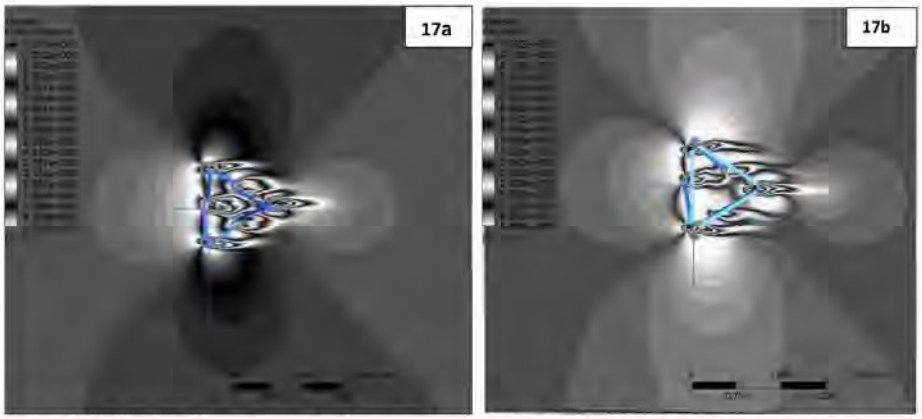

Figure 17a: CFD Derived Flow Around the Tower at Amper-bo. Figure 17b: CFD Derived Flow Around the Tower at Korabib.

Comparing the C_T values and their corresponding boom lengths obtained from the CFD approach to the counterpart values obtained from Equation (1), the study shows boom lengths obtained from one half of the module height at Amper-bo and one fourth of the module height at Korabib are long enough to keep the speed sensors out of the tower induced error readings. With the solidity ratio (S) at each segment of the towers being almost constant, the representative expression ofC_T for the towers at Amper-bo and Korabib are estimated thus,$C_T = 1.27(1 - S)S$ and $C_T = 1(1 - S)S$, respectively. Computed C_T values from both towers show that deducting a range of 2 % to 4 % out of the reference C_T value will accurately estimate the C_T value for winds that arrive at the tower at 10°. For winds that arrive at the tower at 20° and 30°, deducting a range 9 % to 13 % and 15 % to 20 % of the reference values from themselves will reliably predict C_T values respectively at both angles. The C_T expression reported in this section is only valid when the winds arrive at the towers at angles $\leq \pm 70°$ with respect to the IEC reference direction ($\theta = 0°$).

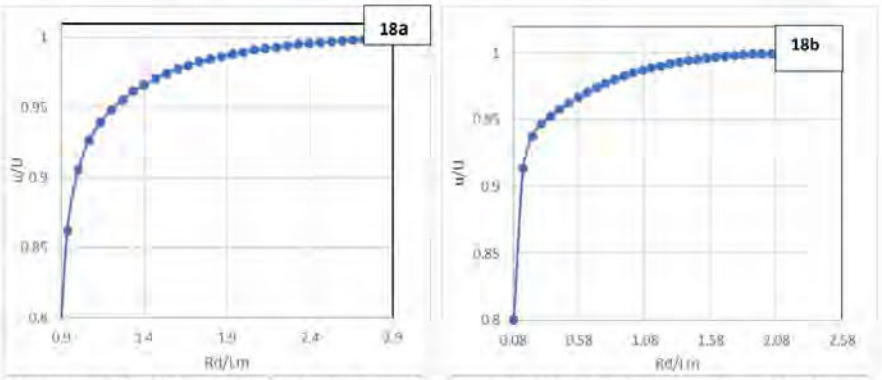

Figure 18a: Graph of u/U Versus R_d/L_m for a Tower Face-on to the Wind at Amper-bo. Figure 18b: Graph of u/U Versus R_d/L_m for a Tower Face-on to the Wind at Korabib.

For Winds that arrive at the tower at angles $\geq \pm 70°$, a boom length of $x \geq 7.5m$ and $x \geq 6.5mm$ at Amper-bo and Korabib respectively is enough to keep the speed sensors out of the tower wakes at all other incident wind angles.

Previous studies concluded that that the IEC speed deficit expression overestimates the boom lengths required to keep the speed sensor out of the wake influence of the tower. This single draw back in the universal application of Equation (1) is traceable to how the C_T values are evaluated and used.The drag on the tower at Korabib with sharp edges islarger than the drag on the tower at Amper-bo and this canbe attributed to the larger surface area presented to the wind, but3d CFD flow simulations around the towers revealed that the tower at Amper-bo neededa longer boom length than its counterpart at Korabib. Using the IEC (Equation 1) and the modified version (Equation 6) of the centre-line speed deficit expression, the tower at Korabib would require longer boom length than the tower at Amper-bo due to higher values of C_T associated with its physical interaction with the winds.In agreement with previous literature (i.e.,]) the study concludes that 3d CFD flow simulations give a better description of local flow modifications around the tower.However, pysical modelling validated using computational approach is necessary for accurate prediction of the boom lengths for each of the incident wind angles.

7. CONCLUSIONS

The variation of tower wake distortioneffects with different incident wind angles was performed by using different approaches to investigate the flow-induced perturbations caused by the physical structure of two lattice equilateral triangular communication towers belonging to the Mobile Telecommunication Limited (MTC) of Namibialocated at a central and southern inland location.Conclusions based on the wind's interaction and itsflow modification within the vicinity of the tower at various incident wind angles are as follows:

- Being of equilateral triangular footprint, the towers exhibited rotational symmetry every 120°, with obvious repetition of geometric properties and repetition of values noticed every 60° instead of 120°,attributed to the identical projected area as seen by the incident wind from opposite directions. The solidity ratio (S) computed from each module of the tower indicates that minimum obstruction (higher value of solidity) is recorded at such incident wind angels (θ) when two of the tower legs align with the wind direction, whereas maximum obstruction

occurs at such incident wind angles when the legs are slightly moved out of alignment with the adjacent one, thereby increasing the blockage. A simpler and more practical approach for calculating the solidity ratio (S) to an accuracy of 0.001 mm is proposed.

- The effective leg length (L_m) that the winds see varies with θ. Based on the IEC arrangement, the width of the tower is the original length. At Amper-bo and Korabib, it is 1.1 m and 1.320 m, respectively. For both tower configurations, deducting approximately 1.5% of the reference value from itself will accurately predict the leg lengths (L_i) at angles (-50°, -10°, 10°, 50°), whereas approximately 5% less of its original value predicts (L_i) at angles (-40°, -20°, 20°, 40°). As stated earlier, the L_i values at (30° and 30°) are minimum and may be reliably estimated by subtracting approximately 12% of the reference value from itself.
- Physical modelling and computational approaches were combined to estimate tower representative C_T values and boom lengths. Analysis of the computed C_{Ti} values from both towers shows that deducting a range 2 % to 4% out of the reference C_T value will accurately estimate C_{Ti} value for winds that arrive at the tower at 10°. For winds that arrive at the tower at 20° and 30°, deducting a range 9 % to 13% and 15 % to 20% of the reference values from themselves will reliably predict C_T values respectively at both angles. The modified controlling parameters (C_{Ti} and L_i) were combined to obtain the modified speed deficit expression. The representative expression ofC_T for the tower at Amper-bo is $C_T = 1.27(1 - S)S$ and that at Korabib is$C_T = 1(1 - S)S$. The C_T expression and the corresponding boom lengths are valid for winds that arrive at the tower at angles $\leq\pm$ 70° with respect to the reference direction.For Winds that arrive at the tower at angles $\geq \pm$ 70°, a boom length of $x \geq 7.5m$ and $x \geq 6.5m$ at Amper-bo and Korabib respectively is enough to keep the speed sensors out of the tower wakes at all other incident wind angles.
- The physical modelling approach shows an increase in the blockage to wind flow and a corresponding increase in boom lengths due to the presence of secondary support structures, while the computational approach illustrates a more complex flow interference around the tower's structure with no appreciable increase in boom length.

The variation of tower wake distortion with different incident wind angles was performed and the controlling parameters in the IEC centreline speed deficit expression (C_T and L_m) modified to capture tower induced flow defects for winds arriving at the tower at other angles besides the IEC reference direction. The study suggested a representative expression for computing C_T and L_m values at other incident wind angles through a combination of physical and computational modelling of the towers' complex 3D structures. Thestudy concludes that shorter boom lengths are needed to keep the speed sensors out of the tower wakesfor winds that arrive at the tower at other angles besides the IEC reference direction if winds arrive at the tower at angles $\leq\pm$ 70° with respect to the IEC reference direction.

REFERENCES

1. *International Electrotechnical Commission (IEC), "Wind energy generation systems – Part 12-1: Power performance measurements of electricity producing wind turbines," International Electrotechnical Commission (IEC), IEC Central Office 3 rue de Varembé CH-1211 Geneva 20, Switzerland, International Standard IEC 61400-12-1:2005(E), Dec. 2005.*
2. *International Electrotechnical Commission (IEC), "Wind energy generation systems – Part 12-1: Power performance measurements of electricity producing wind turbines," International Electrotechnical Commission (IEC), IEC Central Office 3 rue de Varembé CH-1211 Geneva 20, Switzerland, International Standard IEC 61400-12-1:2017-03(en-fr), Mar. 2017.*

Accessed: Oct. 15, 2018. [Online]. Available: https://webstore.iec.ch/publication/26603.

3. *Singh, R. K. "Deviations in Language of Literature." International Journal of English and Literature (IJEL) 3.5 (2013): 43-48.*
4. *IEA, "IEA recommended practices for wind turbine testing. Part 11: Wind speed measurements and use of cup anemometer," Technical Report. Accessed: May 19, 2018. [Online]. Available: https://community.ieawind.org/HigherLogic/System/DownloadDocumentFile.ashx?DocumentFileKey=dcf4afa1-ee68-3111-0ac5-c235d2f2bc16&forceDialog=0.*
5. *M. Lotfi, "Atmospheric wind flow distortion effects of meteorological masts," Master's thesis, University of Porto, Porto, Portugal, 2015.*
6. *S. Fabre, M. Stickland, T. Scanlon, A. Oldroyd, D. Kindler, and F. Quail, "Measurement and simulation of the flow field around the FINO 3 triangular lattice meteorological mast," Journal of Wind Engineering and Industrial Aerodynamics, vol. 130, pp. 99–107, Jul. 2014, doi: 10.1016/j.jweia.2014.04.002.*
7. *Nsaidzedze, IgnatiuS. "Women and Nationalistic Politics in Robert Browning's Poetry: A Feminist Reading of ''Balaustion's Adventure and ''Aristophanes Apology." International Journal of English and Literature (IJEL) 7 (2017): 43-64.*
8. *V. Bezrukovs and S. Upnere, "Effect of the cellular communication mast structure on the wind speed measurement results," International Journal of Contemporary Energy, no. Vol. 3, No. 2, pp. 41–49, Nov. 2017, doi: 10.14621/ce.20170205.*
9. *Seddeek, Abeer M. Refky M. "Combating Conventional Realism and Commodity Fetishism in Representation of Everyday Life: A Study of Ron Silliman's Bart on Bart."International Journal of Linguistics andLiterature (IJLL) 7.5, Aug – Sep 2018; 33-48*
10. *E. Siepker and T. Harms, "The National Wind Resource Assessment Project of Namibia," vol. 33, pp. 105–116, Jan. 2017.*
11. *M. E. Okorie and F. L. Inambao, "Identification of tower and boom-wakes using collocated anemometers and lidar measurement,"International Journal of Mechanical Engineering and Technology, vol. 10, no. 6, pp. 72–94, Sep. 2019.*
12. *Ismail, Mahmud Rasheed, Muhannad Al-Waily, and Ameer A. Kadhim. "Biomechanical Analysis and Gait Assessment for Normal and Braced Legs." International Journal of Mechanical & Mechatronics Engineering IJMME-IJENS 18.03 (2018).*
13. *M. E. Okorie and F. Inambao, "Identification of tower-wake distortion using LIDAR measurement," Procedia Manufacturing, vol. 35, pp. 704–710, 2019, doi: 10.1016/j.promfg.2019.06.012.*
14. *Sharma, Sanjeev, et al. "Temperature Dependence ZnS Based One-Dimensional Photonic Crystals." International Journal of Physics And Research (IJPR) ISSN (P) (2016): 2250-0030.*

CHAPTER 6: LOCAL WIND FLOW MODIFICATIONS WITHIN THE VICINITY OF A COMMUNICATION TOWER

This chapter describes a full 3D CFD flow simulation on the complex 3D geometry of the communication towers and proposes a safe angle range. This aspect of the study becomes necessary because the boom length computed using the centreline velocity deficit expression found in IEC standard does not guarantee that wind observation is accomplished within the recommended industry-accepted accuracy of < 1 % errors between 0° and 360°. With safe angle range of $\theta = < \pm 70^{o}$ with respect to each boom arrangements reference direction (i.e., $\theta = 0^{o}$), the boom lengths obtained based on the IEC standard boom configuration ($\theta = 0^{o}$) are long enough to keep the speed sensors out of the tower wakes. Winds that arrive at the tower at other angles outside this range will likely induce error reading on the speed sensor and this explains why towers instrument according to IEC standard still fall short of the 1 % speed deficit recommended.

Cite this article: M. E. Okorie and F. L Inambao, "Local wind flow modifications within the vicinity of a communication tower," *International Journal of Mechanical and Production Engineering Research and Development*, vol. 11, no. 3, pp. 421–440, 2021, doi: 10.24247/ijmperdjun202135.

Link to the article:

http://www.tjprc.org/publishpapers/2-67-1621326533-IJMPERDJUN202135.pdf

International Journal of Mechanical and Production Engineering Research and Development (IJMPERD)
ISSN (P): 2249–6890; ISSN (E): 2249–8001
Vol. 11, Issue 3, Jun 2021, 421–440

TRANS STELLAR
•Journal Publications •Research Consultancy

Original Article

LOCAL WIND FLOW MODIFICATIONS WITHIN THE VICINITY OF A COMMUNICATION TOWER

MADUAKO E. OKORIE[1] & FREDDIE L. INAMBAO[2]

[1]*Namibia University of Science and Technology, Windhoek, Namibia. Post Graduate student, University of KwaZulu-Natal, Durban, South Africa.*

[2]*University of KwaZulu-Natal, Durban, 4041, South Africa*

ABSTRACT

The boom length obtained from the International Electro technical Commission (IEC 61400-12-1) standard is based on the centreline velocity deficit expression derived on the assumed incident wind that is perpendicular to the tower face, giving rise to a velocity deficit value that is predicted using the upstream contour profile of the modified flow around the tower. The boom length computed thus does not guarantee that wind observation is accomplished within the recommended industry-accepted accuracy of < 1 % errors between 0° and 360°. In this study, the local flow modification around the 3D complex geometry of two communication towers of different construction details located at Amper-bo and Korabib in Namibia were performed using Ansys Fluent flow solver in other to introduce the safe angle range, where boom length computed based on the IEC reference direction (θ = 0°) is long enough to achieve 99 % of the free stream velocity. In this regard, a full 3D CFD flow analysis was performed to obtain the maximum boom length based on the two commonly encountered boom arrangements (perpendicular and parallel to the face of the tower). The boom length obtained based on the IEC standard boom configuration (θ = 0°) is long enough to keep the speed sensors out of the tower wakes if winds arrive at the tower at incident angles θ = < ± 70° with respect to each boom configuration reference direction (i.e., θ = 0°), which defines the safe angle range. Winds that arrive at the tower between ± 90° ≥ x < ± 150° with respect to each boom arrangement reference direction cast their full shadow on the speed sensors. A boom length of approximately x ≥ 7.5 m and x ≥ 6.5 m at Amper-bo and Korabib respectively are needed to keep the speed sensors out of the tower wakes. However, the suitability of a slender boom of this length which is susceptible to vibration and therefore can introduce more errors to the readings of the speed sensors mounted on them is questionable. A shorter boom length of x ≥ 4.5 m to x ≥ 3.5 m or less at Amper-bo and Korabib respectively is needed to keep the sensors out of the tower wakes when the incident wind angles are within the range ± 150° ≤ x ≤ 180° from the reference directions. This type of arrangement is not encouraged because any slight shift in the direction of the upstream wind will cast shadows of the tower on the speed sensors. The study further revealed that the boom length computed based on the two popular boom arrangements is independent of the scale and turbulence models used in CFD flow analysis. Also, complex flow interference was reported around the tower structure with no appreciable increase in boom length due to the presence of the secondary support structures. In the second section of the study, a correction method based on the combined field observed wind data is proposed. Based on the accuracy of the correction method, it may no longer be necessary to discard the tower wake affected direction sectors in wind analysis. Finally, the speed sensor to tower separation distance needed to keep the speed sensor away from the tower-induced flow defect was thoroughly investigated using lattice communication towers of different construction details and booms of different arrangements on the towers. A safe angle range (θ = < ± 70°) was proposed. Winds that arrive at the tower at other angles outside this range will likely induce error readings on the speed sensor mounted on the boom and this explains why most towers instrumented according to the IEC standard still fall short of the 1 % speed deficit recommended.

KEYWORDS: Safe angle Range, Tower Wakes, Speed Deficit, Correction Factor and Boom Length.

Received: Apr 14, 2021; **Accepted**: May 06, 2021; **Published**: May 18, 2021; **Paper Id.**: IJMPERDJUN202135

1. INTRODUCTION

The knowledge and guidelines on tower instrumentation for wind measurement perspective are largely found in research studies and standards, the most prominent of which is the International Electrotechnical Commission (IEC) standard IEC 614200-12-1 Wind turbines–Part 12-1: Power performance measurements of electricity producing wind turbines [1], [2], whose Annex G is of interest [3]. The standard prescribes, among other things, the centreline velocity deficit expression which is based on its standard boom configuration ($\theta = 0^{o}$), derived on the assumed incident wind that is perpendicular to the tower face, giving rise to a velocity deficit value that is predicted using the upstream contour profile of the modified flow around the tower. A user may use this expression to evaluate the tower to speed sensor separation required for the desired maximum flow-induced error reading when the thrust coefficient (C_T) is known. However, the boom length computed using this expression does not guarantee that wind observation is done with the recommended industry accepted accuracy of < 1 % errors between 0° and 360°. This is in agreement with [4], where it was suggested that the choice of boom length based on the IEC recommendations is not a guarantee that measured wind speed between 0° to 360° will always achieve 99% of the free stream velocity. At some incident wind angles, the tower induced error readings on the speed sensor may be > 1 %, bringing into question the universal applicability of the speed deficit expressions at incident wind angles other than the IEC reference direction ($\theta = 0^{o}$) and to other towers of different construction details with a solidity ratio (S) that is way off the values specified in the standard. Other limitations of the IEC standard include insufficiency of the numerical model used to draw the iso-speed plots of locally modified wind flow around a meteorological mast to fully and sufficiently describe wind interaction around a complex operational lattice tower, lack of information on how to account for complex flow interferences occasioned by the presence of other secondary support structures, the inadequacy of the prescribed expression to address the wind direction dependence of tower shadowing, and the exact impact of free-stream turbulence on the specified boom length [3]. Previous authors (e.g., [4]–[7]) have made attempts to address some of the identified limitations, but not all. Investigating the impact of atmospheric turbulence on the local flow modifications using CFD flow simulation, [5], [7] reported higher flow distortion than [1], [2], and [5] concluded that the phenomenon is an atmospheric problem and should be treated as such. In a similar study, [6] reported a shorter boom length when compared with [1], [2] and concluded that 3D CFD flow analysis is better suited to study wind interaction with the 3D complex geometry of an operational lattice mast as against the simplified approach used in the IEC614200-12-1 standard. Further computational approach by [8] attempted to investigate the impact of the secondary supporting structures with an oversimplified model and reported that [1], [2] overpredicted the minimum boom length. Efforts by previous authors to address the identified shortfalls of the IEC614200-12-1 standard are evident but the application of such studies to towers of different configurations located at different sites in different atmospheric conditions in the boundary layer may be limited.

In this study, a 3D CFD study of two lattice communication towers of different construction details was performed, to understand the safe angle range $x = \pm \leq \theta^{o}$, i.e., the incident wind angles for which the boom length computed based on the IEC standard configuration ($\theta = 0°$) can effectively keep the speed sensors out of the tower wakes for winds that arrive at the tower within that defined angle range. The exact impact of the secondary support structures on the boom lengths was further investigated. The second section of the study combined wind data obtained from collocated

speed sensors and Light Detection and Ranging (LiDAR) to develop a correction method for correction of the wake affected direction sectors. The detailed approach adopted in this study provides insight on the best approach to instrument lattice communication towers for wind measurement. Finally, successful implementation of the correction method increased the utilization of observed wind data and enhances wind resource assessment because it may no longer be necessary to discard the tower wake affected direction sectors during site wind resource characterisation.

2. SITE AND TOWER CONSTRUCTION DETAILS

The locations are Amper-bo (25.354 °S, 18.313 °E) and Korabib (28.548 °S, 17.820 °E). Amper-bo site is desert-like with almost homogeneous vegetation. It is a class A terrain according to Annex B of (IEC 2005) as reported in [9]. Figure 1a shows the tower construction details. The tower at Amper-bo is 120 m high and L_m (centre-to-centre) of 1.10 m, all through the height. It is guyed and has an equilateral triangular cross-section with three vertical tubular mild steel rods of 100 mm external diameter (OD). The vertical tubular rods from repeating construction units are joined end-to-end by flanged connections. Each construction unit is approximately 3.5 m, and each contains four modules of height 0.89 m. The network of small angular cross bracings made from 45 mm x 45 mm x 5 mm angle bars are bolted to a flat plate (0.045 m x 0.07 m) that is welded to the tubular rods. The boom has an OD of 50 mm and wall thickness of 2 mm and extends approximately 2.56 m away from the tower surface. The cable ladders and the cable bundles which covered almost half of the W to N (clockwise) facing side of the tower are the secondary support structures. At, Korabib the tower is also guyed, 120 m high and L_m (edge-to-edge) of 1.32 m all through the height. It has an equilateral triangular cross-section with three vertical angle bars (70 mm x 70 mm x 6 mm) made from mild steel. The 70 mm x 70 mm x 6 mm angle bars form repeating construction units which are bolted together using flat plate connections (Figure 1b). Each construction unit is 3.024 m, and each contains two modules of height 1.512 m. The network of small angular horizontal and cross bracings made from 60 mm x 60 mm x 5 mm angle bars are bolted to a flat plate (0.144 m x 0.26 m) that is bolted to the vertical angle bar. The detail of the boom construction and the separation distance from the tower is the same as the tower at Amper-bo. The cable bundles and ladder located W to N (clockwise) facing the side of the tower are the secondary support structures.

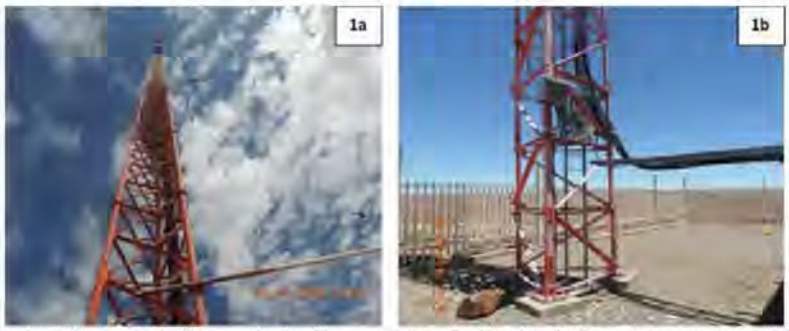

Figure 1a: A Section of the Communication Tower at Amper-bo Showing the Boom Arrangements and Some Secondary Support Structures. Figure 1b. A Section of the Communication Tower at Korabib Showing the Boom Arrangements and Some Secondary Support Structures.

3. METHODS

Local flow modification around the 3D complex geometry of two communication towers was performed using Ansys

Fluent flow analysis. The holistic approach adopted in this work led to the evaluation of the speed sensor to tower separation distance required for the desired maximum speed deficit.

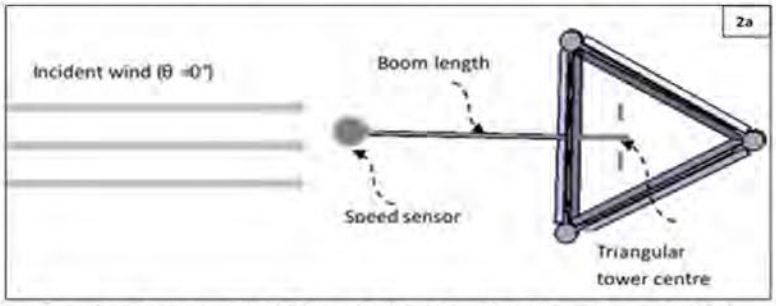

Figure 2a: Illustration of the IEC Boom Configuration with the Tower Face-on the Wind.

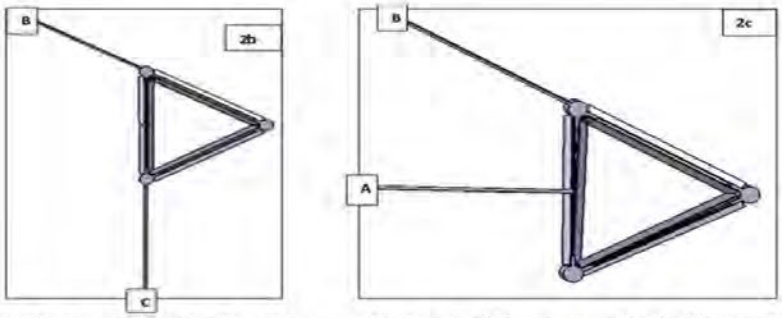

Figure 2b: The Common boom Configurations are used in Operational Towers. Figure 2c. Combination of the Two Boom Configuration Methods.

Two major boom configurations often encountered in lattice tower instrumentation for wind measurement are considered. With the IEC61400-12-1 reference wind direction (θ = 0°), the tower is always face-on to the wind. The velocity deficit is assumed to be on the same axis that passes through the tower centre and perpendicular to the tower face. The incident wind is therefore perpendicular to the same tower face, giving rise to velocity deficit values that are predicted using the upstream contour profiles of modified flow around the tower. Using the IEC standard boom configuration (Figure 2a), CFD flow simulation was conducted over 36 incident wind angles, each at 10°. The boom length was computed with respect to a reference direction (θ = 0°) for each incident wind angle. Similar flow analysis was performed on the second and most common boom arrangement (Figure 2b and Figure 2c), whereby the booms were placed parallel to the face of the tower. For the IEC arrangement, the speed sensors mounted on boom B and boom C are 30° and 90° respectively from the prevailing wind direction (Figure 2b). Based on the IEC standard configuration, a boom length needed to keep the speed sensor A (Figure 2c) out of the tower-induced flow defect was computed and the safe angle range was also defined.

The safe angle range $x = \pm \leq \theta°$ is the incident wind angles for which the boom length computed based on the IEC standard boom configuration can effectively keep the speed sensors out of the tower wakes for winds that arrive at the tower

within that defined angle range. Similar CFD flow analysis was performed to equally establish a safe angle range for booms placed parallel to the face of the tower, i.e., boom B (Figure 2c). The field observed data were combined to establish a correction method for the wake-affected direction sectors.

4. GOVERNING EQUATIONS

The fluid flow is governed by Navier-Stokes's equation and conservation of mass. A steady, incompressible, and isothermal flow was assumed. The flow field is described by the conservation of mass and momentum equations i.e., Eq. (1) and Eq. (2), while the Reynolds Average Navier-Stokes's equations (RANS) take care of the time-average approximations.

$$\frac{\partial \overline{u_i}}{\partial x_i} = 0 \tag{1}$$

$$\frac{\partial \left(\overline{u_i u_j}\right)}{\partial x_i} = -\frac{\partial \overline{P}}{\partial x_i} + \frac{\partial}{\partial x_i}\left\{\mu_t\left(\frac{\partial \overline{u_i}}{\partial x_i} + \frac{\partial \overline{u_j}}{\partial x_i}\right) - \rho \overline{u_i' u_j'}\right\} \tag{2}$$

where $\overline{u}$ is the Reynolds-averaged velocity, $\overline{P}$ is the averaged pressure, μ is the eddy viscosity and $\overline{u_i'}$ is the Reynolds stress tensor which introduces more variables than the number of equations; hence, the closure problem is subsequently resolved using turbulence models. To assess the suitability of each model in the context of this study, common turbulence models often encountered in the aerodynamic of eternal flow, such as the one-equation Spalart-Almaras turbulence model and the two-equation standard k-ε model, the standard k-ω model and k-ω shear stress transport (SST) models, were evaluated and compared.

5. NUMERICAL APPROACH

Ansys Fluent uses finite volume discretization methods to generate a set of linear equations from the partial differential equations, solved by iteration between cell centres in the computational mesh. Velocity and pressure were coupled using the SIMPLE technique in the Ansys fluent solver. Meshing around the tower structure was suitable to properly describe airflow within its vicinity, with velocity inlet and constant pressure outlet boundary conditions applied. Figures 3a, 3b 3c and 3d are the computational domains and surface meshing of the towers at Amper-bo and Korabib, respectively.

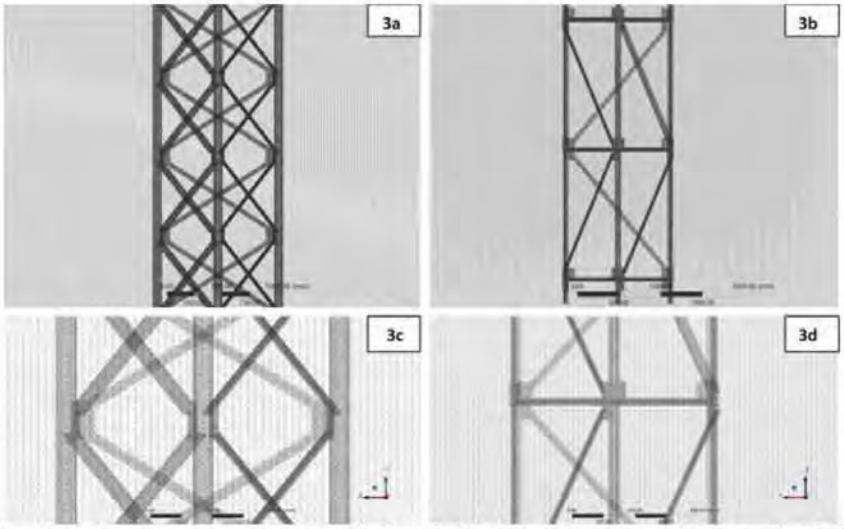

Figure 3a and 3c: Computational Domain and Surface Meshing of the Tower at Amper-bo. Figure 3b and 3d: Computational Domain and Surface Meshing of the Tower at Korabib.

6. Comparison of Velocity Profile for Each Turbulence Model

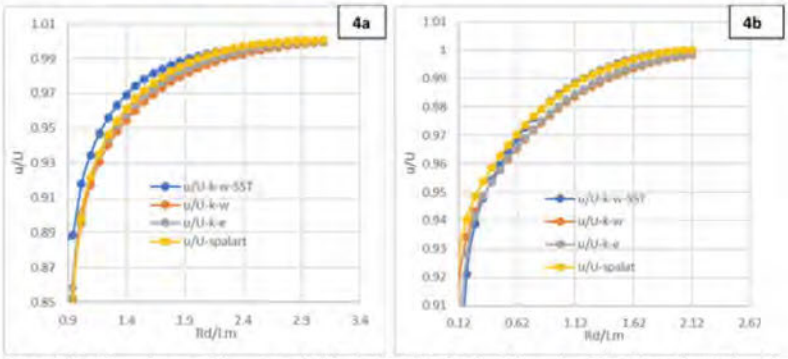

Figures 4a and 4b: Show the non-Dimensional Velocity Profiles Derived from the CFD Flow Simulation along with the IEC Standard Boom Configuration.

Figures 4a and 4b show the non-dimensional velocity profiles derived from the CFD flow simulation around the tower structures using the four turbulence models $k - wSST$, $k - w$ standard equation, $k - e$ and one equation Spalart-Almaras), at Amper-bo and Korabib, respectively.

Using the four turbulence models ($k - wSST$, k-ω standard equation, k-ε and one equation Spalart-Almaras) often used in external aerodynamics study, it is observed that all the models correctly predicted approximately the same minimum boom length required to achieve 99 % of the free stream velocity. This agrees with the findings in [6] where it

was reported that no individual RANS equation may be considered most suitable for the evaluation of the minimum boom lengths. There was also no significant difference in the drag force computed using each turbulence model though the drag force on the tower at Korabib is larger than that of its counterpart at Amper-bo, as expected, due to the larger surface area presented to the wind by the tower at Korabib.

7. SCALE EFFECT

The scale effect was investigated and illustrated in Figure 5. Figure 5a is the non-dimensional velocity profiles drawn as a function of the boom length for wind speeds 20 m/s, 15 m/s and 6 m/s respectively based on the IEC reference direction (θ = 0°), whereas Figure 5b is the speed profiles for boom C (Figure 2b), that is located 30° with respect to the IEC reference direction. Similar analysis (Figures 5c and 5d) are the non-dimensional velocity profiles for wind speeds 20 m/s, 15 m/s and 5 m/s obtained from the tower at Korabib. Wind speeds 6 m/s and 5 m/s are approximately the observed average speed at Amper-bo and Korabib, respectively at about 60 m height. The results agree with previous literature (i.e., [6] which reported the independence of scale to the CFD derived flow).

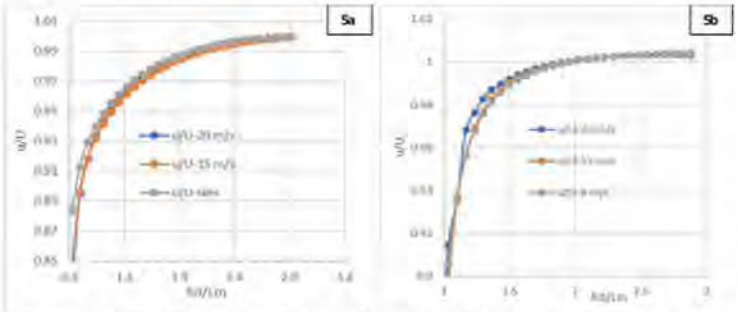

Figure 5a: Scaling Effect: Non-Dimensional Velocity Profile versus R_d/Lm along the Boom Length based on the IEC Standard Configuration (θ = 0°) at Amper-Bo. Figure 5b. Non-Dimensional Velocity Profile versus R_d/Lm along the Boom Length for the Boom Located 30° with Respect to the IEC Standard Configuration at Amper-bo.

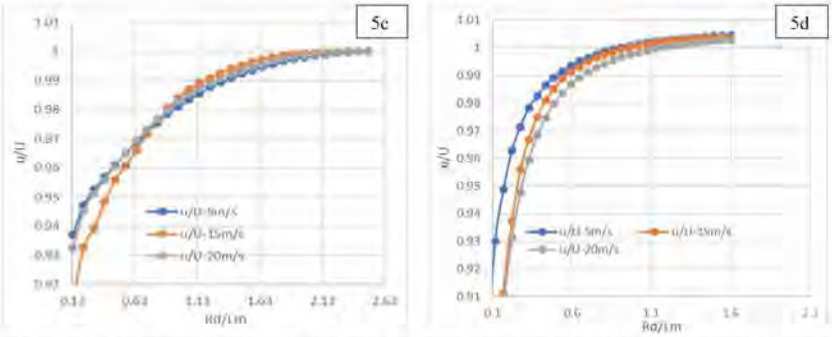

Figure 5c: Scaling Effect: Non-Dimensional Velocity Profile versus R_d/Lm along the Boom Length based on the IEC Standard Configuration (θ = 0°) at Korabib. Figure 5d. Non-Dimensional Velocity Profile Versus R_d/Lm along the Boom Length for the Boom Located 30° with Respect to the IEC Standard Configuration at Korabib.

8. 3D CFD Flow Simulation

The CFD-derived flows around the towers are illustrated in Figure 6. Figures 6a and 6b are modified flow around the towers when they are face-on to the winds (i.e., when $\theta = 0°$) whereas Figures 6c are 6d illustrate flow modification around the towers when the boom is placed at 30° clockwise from the IEC reference direction.

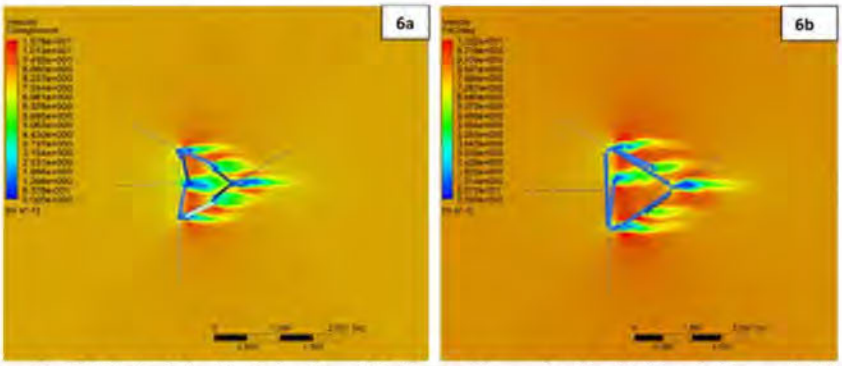

Figure 6a: CFD Derived Flow Simulation Around the Tower at Amper-bo when the Tower is Face-on the Wind. Figure 6b: CFD Derived Flow Simulation Around the Tower at Korabib when the Wind is Face-on the Wind.

From the CFD-derived flows, the minimum boom length required to achieve 99% of the free stream speed for speed sensors mounted on the booms A and B for each of the 12 incident wind directions were computed (Figures 7a and 7b). Figure 7a shows the estimated boom lengths for the tower at Amper-bo and Figure 7b are those of the tower at Korabib. As seen in Figure 2c, earlier discussed, boom A is based on the IEC recommendation whereas boom C is the most common boom arrangement in operational tower instrumentation.

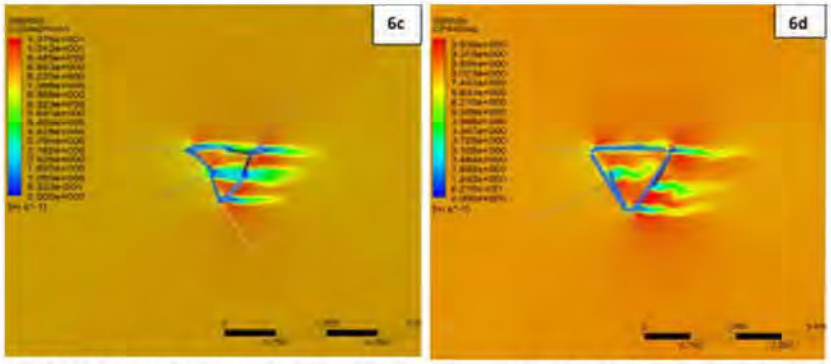

Figure 6c: CFD Derived Flow Simulation Around the Tower at Amper-bo when the Winds Arrive at the tower at 30° Incident wind Angle. Figure 6c: CFD Derived Flow Simulation Around the Tower at Korabib when the Winds Arrive at the Tower at 30° Incident Wind Angle.

At Amper-bo, based on the IEC recommendations (Figure 1), a boom length of 2.4 m protruding from the tower face is required to achieve 99 % of the freestream velocity. The boom lengths computed based on the IEC standard configuration are long enough to keep the speed sensors out of the tower wakes provided that the winds arrive at the tower

at incident angles $\theta = <\pm 70^{o}$ with respect to the reference direction (i.e., $\theta = 0^{o}$). Similar analysis reveals that when the direction of boom B is taken as the reference direction (i.e., $\theta = 0^{o}$), the boom length needed to achieve 99 % of the freestream speed is approximately 1.3 m.

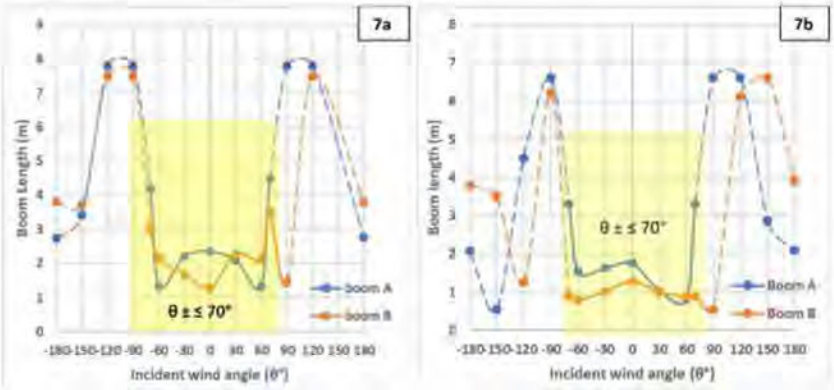

Figure 7a: The Estimated Boom Lengths to Achieve 99% of the Free Stream Speed for the Tower at Amper-bo for 12 Different Incident Wind Angles. Figure 7b. The Estimated boom Lengths to Achieve 99 % of the Freestream Speed for the Tower at Korabib for 12 Different Incident Wind Angles.

The shorter boom length reported is expected due to the minimum obstructions encountered because of the alignment of the tower legs when the tower face is parallel to the incident wind direction. Based on the safe or effective angle range (i.e., $\theta = <\pm 70^{o}$), a boom length of approximately 2.2 m computed when the winds arrive at the tower at 60° is appropriate. For both boom arrangements, the study acknowledges that the boom length computed when the tower is face-on to the wind is long enough to keep the speed sensors out of the tower wakes if winds arrive at the tower within the safe angles range (i.e., $\theta = <\pm 70^{o}$). Similar results were obtained from the tower at Korabib (Figure 7b). In (Figure 2c), a boom length of 1.76 m protruding from the tower face is required for boom A to achieve 99% of the free stream velocity. Again, this boom length computed based on the IEC standard configuration is long enough to keep the speed sensors out of the tower wakes provided that the winds arrive at the tower at incident angles $\theta = <\pm 70^{o}$ with respect to the reference direction (i.e., $\theta = 0^{o}$). Again, when the direction of boom B is taken as the reference direction (i.e., $\theta = 0^{o}$), the incident wind is now parallel to the face of the tower, and a boom length of approximately 1.3 m is needed to achieve 99 % of the freestream velocity. As earlier mentioned in respect to the tower at Amper-bo, a shorter boom length is needed due to the alignment of the tower legs. Considering the safe angle range mentioned earlier (i.e., $\theta = <\pm 70^{o}$), this boom length is long enough to keep the speed sensors out of the tower wakes provided that the winds arrive at the tower at incident angles $\theta = <\pm 70^{o}$ with respect to the reference direction. The safe or effective boom placement angle range observed from the towers investigated is ± 30° less than the range suggested in [2] where it was stated that the speed sensors mounted on a tower based on the IEC standard configuration will only be in the wake of the tower if winds arrive at the mast at angles ($\theta = >\pm 100^{o}$) with respect to the standard incident wind direction ($\theta = 0^{o}$). The proposed safe angle range based on IEC 2017 does not hold on operational towers of the configurations investigated in this work.

For winds that arrive at the tower between $\pm 90^{o} \geq x < \pm 150^{o}$ with respect to the reference direction of each boom

arrangement, will cast their full shadow on the speed sensors. A boom length of approximately $x \geq 7.5$ m and $x \geq 6.5$ m respectively at Amper-bo and Korabib are needed to keep the speed sensors out of the tower wakes. Unfortunately, a slender boom of this length might be susceptible to vibration and will introduce more errors to the readings of the speed sensors mounted on them. A shorter boom length of 3.5 m to 4.5 m for each of the towers is needed to keep the sensors out of the tower wakes when the incident wind angles are within the range $\pm 150^{o} \leq x \leq \pm 180^{o}$. Although the boom length within this range of incident wind angles appears shorter, good practice from a wind measurement perspective may be to consider this arrangement as not the most appropriate because any slightest shift in the wind direction will completely cast its shadow on the speed sensors. It is important to note that booms mounted parallel to the face of the tower require shorter boom lengths to keep the speed sensors out of the tower wakes when compared to their counterparts mounted according to IEC61400-12-1 standard configuration and this is directly related to the thrust coefficient of the towers. To achieve 99 % of the freestream speed or a speed deficit of 1% when the tower is instrumented based on the IEC standard configuration, or based on the approach proposed in this study for booms mounted parallel to the face of the tower, a combination of physical and computational modelling of the tower is required to accurately obtain the relevant parameters especially the controlling parameters of the IEC centreline velocity deficit expression and to understand the prevailing wind pattern of the site. The IEC approach has always resulted in a longer boom length, as is the case in this study, yet towers assumed to have been instrumented based on the standard mostly fall short of the recommended 1 % speed deficit because the relevant parameters in the speed deficit expression are not properly characterized and or the site prevailing wind direction is not taken into consideration during the instrumentation stage.

9. Secondary Support Structures

Secondary support structures are critical components of an operational tower. They come in different configurations and their sizes depend on the application of the parent tower. The presence of these substructures produces discrete wakes, which makes flow interference within the vicinity of the tower more complex, contrary to the idealized mast configuration presented in [1] and [2]. In this study, cross and horizontal bracings are considered natural members of an operational tower and are treated as such. However, cable ladders, cable bundles and other substructures provided for safe climbing and proper instrumentation of the tower are the secondary support structures investigated. Based on the CFD study, complex flow interference was reported within the regions very close to the tower due to the presence of secondary support structures. However, their presence does not result in any appreciable increase in the boom length.

10. Identification and Correction of Tower Waked Direction Sectors

In the field observed data, methods utilized to identify tower waked direction sectors are traditional speed ratio and the coefficient of determination (R^2) of the turbulent kinetic energy (TKE) and turbulence intensity (TI) of the collocated sensors [9], [10]. A new and simpler approach that uses time series WSC for wind data that are collected from two intermediate heights with approximately the same azimuth angle from the north, when speed sensors collocated at the same height are not available, was proposed [11]. In the Amper-bo experiment, speed sensors (WS4 and WS4B) are collocated at 16.88 m and placed approximately 120° apart. WS4 and WS4B are located at approximately 159° and 278° azimuth from the north. The instrumentation details of the communication towers at Amper-bo and Korabib are summarised in Tables 1 and 2. Ten different heights plus the default pre-set height (38 m) where the Lidar measured wind speed is reported in Table 3.

Table 1: Instrumentation Details of the Tower at Amper-bo

	August 2012 Arrangement		March 27, 2014 Arrangement	
Sensors	**Heights (m)**	**Angle (ϕ) degree**	**Height (m)**	**Angle (ϕ) degree**
WS1	3.88	159	-	-
WS2	4.88	159	-	-
WS3	8.68	159	8.68	159
WS4	16.88	159	16.88	159
WS4B	-	-	16.88	278
WS5	32.68	160	32.68	160
WS6	64.92	160	64.92	160
WS6B	-	-	64.92	278
WS7	120.38	159	120.38	159
WD1	4.88	38	4.88	38
WD2	16.88	38	16.88	38
WD3	64.92	38	64.92	38
WD4	120.38	279	120.38	279

Table 2: Instrumentation Details of the Tower at Korabib

Sensors	Heights (m)	Angle (Ø) Degree
WS1K	19.86	168
WS2K	51.11	164
WDK	51.11	287

Table 3: Instrumentation details of the tower at Korabib

Height (m/s)	10	17	33	38	49	65	75	90	12	150	200
Sensor	LWS1	LWS2	LWS3	LWS4	LWS5	LWS6	LWS7	LWS8	LWS9	LWS10	LWS11
Mean speed (m/s)	3.73	4.26	5.21	5.46	5.81	6.25	6.46	6.73	7.09	7.33	7.54

The speed ratio and coefficient of determination (R^2) computed based on the collocated speed sensors at Amperbo are shown in Figure 8 and Figure 9.

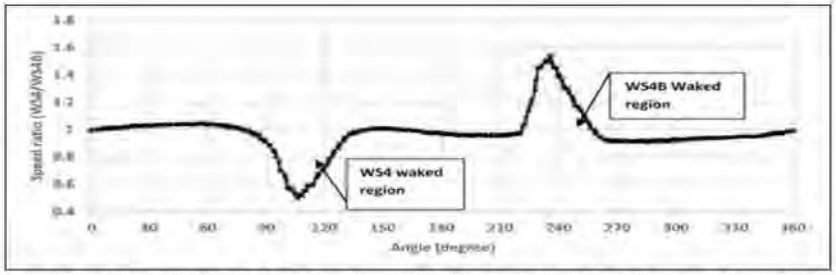

Figure 8: The Ratio of WS4/WS4B Plotted on a Sector-wise Basis Binned in 1° wind Direction Intervals with the Tower Waked Direction Sectors Properly Described.

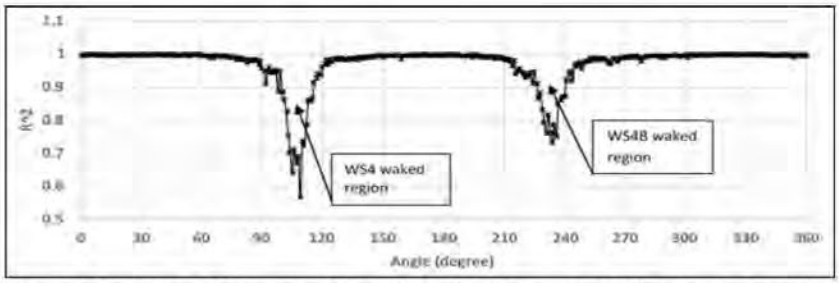

Figure 9: Coefficient of Determination (*R2*) of WS4 and WS4B Binned in 1° Wind Direction Intervals.

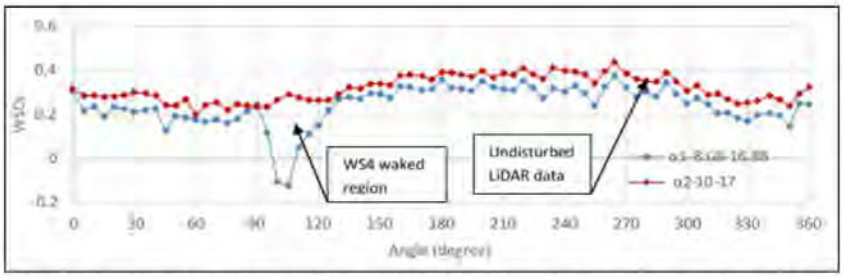

Figure 10: Time Series WSC Calculated for the in-situ (8.88 m to 16.88m) and LiDAR (10 m to 17 m), Binned in 1° Wind Direction Intervals and Drawn as a Function of the Wind Direction at the Same Height.

Figure 11 is a summary of the direction sector selection rule that was used to derive the correction factor for both the collocated speed sensor at 16.88 m (WS4 and WS4B) and the LiDAR observed speed at approximately the same height. The ratios of WS4 and WS4B, WS4 and LWS and WS4B and LWS are plotted on a sector-wise basis and binned in 1° bin of wind direction intervals with the wake affected direction sectors clearly illustrated. The ratio of wind speed in the wake-affected direction sectors (target direction sectors) and the corresponding ratio of wind speed at angles directly opposite the wake-affected direction sectors (reference direction sectors) are evaluated. Based on the direction sectors selected, an expression for correcting the wake affected direction sectors have been proposed, as follows in Eq. (5):

$$C_f = \frac{U_{aff}}{U_{ref}} \tag{5}$$

U_{aff} is the ratio of the time series wind speed recorded in the wake affected direction sectors. It is simply the ratio of the target wind speed to the reference wind speed in the wake-affected direction sector. In this case, WS4 is the target wind speed whereas WS4B is the reference wind speed. Therefore, WS4, $U_{aff} = WS4/WS4B$. The WS4 wake affected direction sector is between 80° and 140° (Figure 11a). Again, $U_{aff} = WS4/WS4B$, for time series wind speed measure between 260° and 320° (Figure 11a). The expression for the correction factor (C_f) is shown in Eq. (6).

$$W_c = \frac{U_{org}}{C_f} \tag{6}$$

where U_{org} is the original or raw wind speed measured in the wake affected direction sector.

Similarly, the correction factor for WS4B's wake-affected direction sectors was computed (Figure 11b) using the collocated wind speed (WS4). Again, using the LiDAR undisturbed wind data, a correction factor for WS4 (Figure 11c) and WS4B (Figure 11d) were computed.

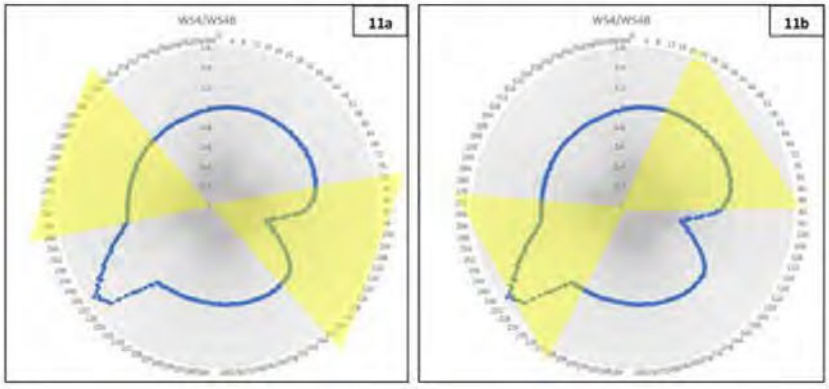

Figure 11a: Selection Rule for the Direction sectors used to Derive the Correction Factor for WS4 using WS4B as Reference. Figure 11b. Selection Rule for the Direction Sectors used to Derive the Correction factor for WS4B using WS4 as Reference.

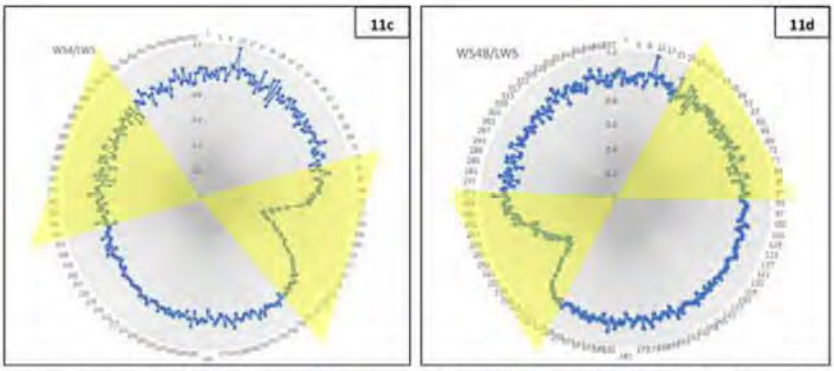

Figure 11c: Selection Rule for the Direction Sectors used to Derive the Correction Factor for WS4 using LWS as Reference. Figure 11D: Selection Rule for the Direction Sectors used to Derive the Correction factor for WS4B using LWS as Reference.

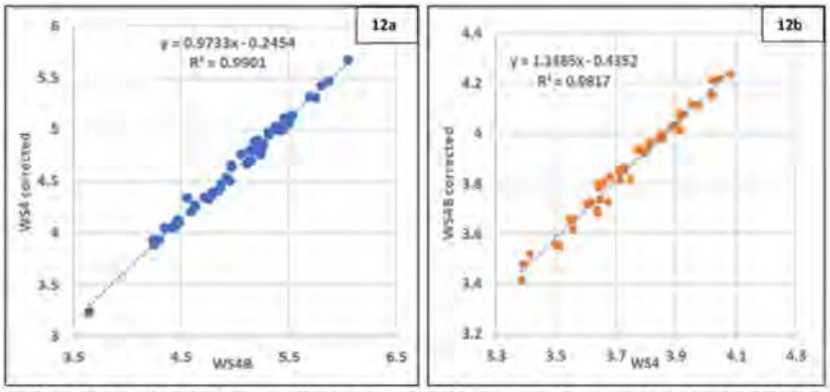

Figure 12a: The Graph of the Reference Winds Speed (WS4B) Versus the Corrected wind Speed (WS4). Figure 12b: The Graph of the Reference Winds Speed (WS4) Versus the Corrected Wind Speed (WS4B).

Figure 12 is the graph of the reference wind speed versus the corrected wind speed. In Figure 12a, WS4 was corrected using WS4B. The coefficient of determination R^2 improves from 0.1281 to 0.9901 after correcting WS4 with WS4B (Table 4a). At 106° (worst affected direction sector), the highest speed deficit of 50.38% was recorded but reduces to 8.1% when the correction factor is applied. Similarly, for WS4B, R^2 improved to 0.9817 from 0.0449 after applying the correction factor. Again, based on the same bin interval, WS4B encountered the higher wake effect at 235° with a speed deficit of 35.26 % when the target (WS4B) was compared to the reference (WS4) which reduced to 4.19% after applying the correction factor (Table 4a). Again, the LiDAR observed speed was used as reference wind speed to derive the correction factor for WS4 (Figure 12c) and WS4B (Figure 12d). The R^2 value obtained when the corrected WS4 was compared to the reference LiDAR wind speed was 0.8897 as against 0.0234 when the raw data were compared. The speed deficit of 52.43 % was computed from the pairs of the raw data at the most severely affected direction sector (107°), which reduced to 16.10 % after applying the correction factor. Similar evaluation with LiDAR data shows that R^2 is 0.8646 after the correction factor was applied as against 0.0226 obtained when the pair of data (corrected WS4B and LiDAR) was compared. There is a drop to 1.32 % from the previous error of 41.27% computed using the pair of the raw data (Table 4b).

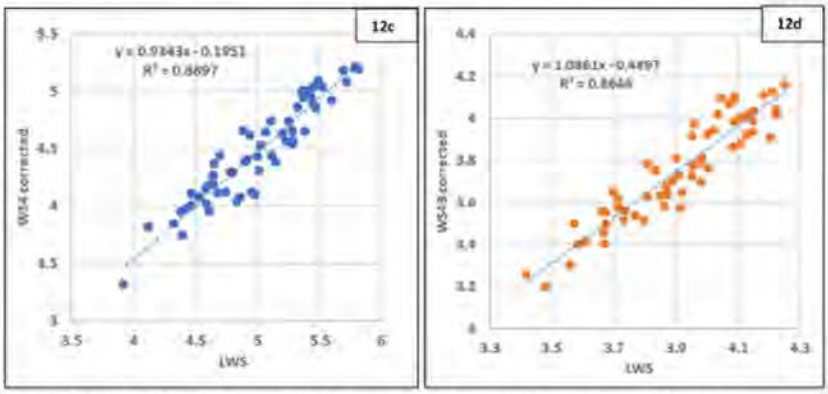

Figure 12C: The Graph of the Reference Winds Speed (LWS) Versus the Corrected wind Speed (WS4). Figure 12d: The Graph of the Reference Winds Speed (LWS) Versus the Corrected Wind Speed (WS4B).

Table 4a: Summary of the Key Parameters used to Illustrate the Efficacy of the Correction Factor.

Parameters of the Wind Measurement				
WS4 = target data; WS4B = reference data				
	Key Parameters of Raw Data (WS4 and WS4B) at WS4 Wake Affected Direction Sector		**Key Parameters (Corrected WS4 and WS4B)**	
R^2	0.1281		0.9901	
RMSE	1.333		0.382	
Wind speed (m/s) at 106°	WS4B	WS4	WS4B	Corrected WS4
	4.44	2.20	4.44	4.08
Average wind speed (m/s) between 80° and 140°	WS4B	WS4	WS4B	WS4
	5	3.97	5	4.63
WS4B = target data; WS4 = reference data				
	Key Parameters of Raw Data (WSB and WS4) at WS4B Wake Affected Direction sector		**Key Parameters (Corrected WS4B and WS4)**	
R^2	0.0449		0.9817	
RMSE	0.756		0.127	
Wind speed (m/s) at 235°	WS4	WS4B	WS4	Corrected WS4B
	3.66	2.44	3.57	3.50
Average wind speed (m/s) between 215° and 265°	WS4	WS4B	WS4	WS4B
	3.87	3.34	3.87	3.76

Table 4b: Summary of the Key Parameters used to Illustrate the Efficacy of the Correction Factor

WS4 = target data; LWS = reference data		
	Key Parameters of Raw Data (WS4 and LWS) at WS4 Wake Affected Direction Sector	**Key Parameters (Corrected WS4 and LWS)**
R^2	0.0254	0.8896
RMSE	1.4215	0.541

Wind speed (m/s) at 107°	WS4	LWS	Corrected WS4	LWS
	2.31	4.86	4.08	4.86
Average wind speed (m/s) between 80° and 140°	WS4	LWS	WS4	LWS
	3.90	5.02	4.49	5.02
WS4B = target data; LWS = reference data				
	Key Parameters of Raw Data (WS4B and LWS) at WS4B Wake Affected Direction Sector		**Key Parameters (Corrected WS4B and LWS)**	
R^2	0.0226		0.8646	
RMSE	0.923		0.189	
Wind speed (m/s) at 235°	WS4B	LWS	Corrected WS4B	LWS
	2.17	3.70	3.65	3.70
Average wind speed (m/s) between 210° and 270°	WS4B	LWS	WS4B	LWS
	3.22	3.92	3.75	3.91

The suitability of the correction method was validated by comparing the percentage difference between pairs of raw WSB and WS4 observed between (80° and 140°), corrected WS4 compared to raw WSB between (80° and 140°) and the undisturbed raw WS4B and WS4 measured between 260° and 320° are illustrated (Figure 13a). Again, a similar percentage difference between pairs of raw WS4 and WS4B observed between (215° and 265°), corrected WS4B compared to raw WS4 between (215° and 265°) and undisturbed raw WS4 and WS4B measured between 35° and 85° are shown in figure 13b. There are no significant difference between the corrected wind speed in the target direction sectors (wake affected region) and the reference direction sectors (opposite the wake affected region). This shows that the percentage difference computed after the correction factor had been applied is due to the difference between raw wind speeds that the speed sensor would have captured if it is not exposed to the tower wakes. This correction mechanism can therefore be applied reliably to correct wind speeds in the wake-affected direction sectors instead of discarding them. In Figures 13a and 13b, the wake-affected direction sectors are clearly illustrated.

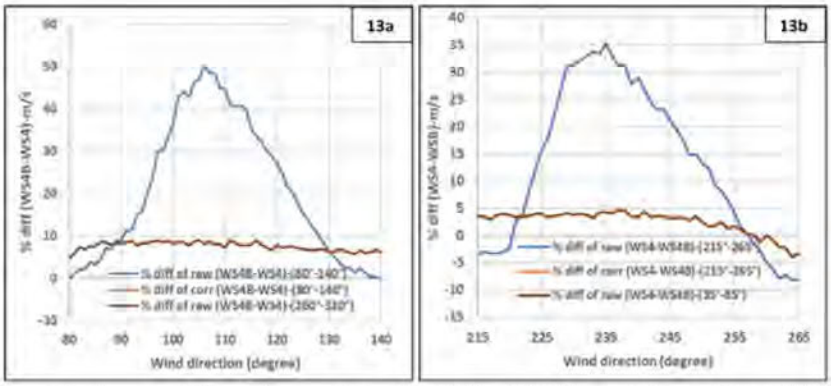

Figure 13a: Percentage Difference between Pairs of Raw WSB and WS4 Observed between (80° and 140°), Corrected WS4 Compared to raw WSB between (80° and 140°) and Undisturbed raw WS4B and WS4 Measured between 260° and 320°. Figure 13b. Percentage Difference between Pairs of raw WS4 and WS4b Observed between (215° and 265°), corrected WS4B Compared to raw WS4 between (215° and 265°) and Undisturbed Raw WS4 and WS4B Measured between 35° and 85°.

11. CONCLUSIONS

Local flow modification around the 3D complex geometry of two communication towers located at Amper-bo and Korabib in Namibia was performed using Ansys Fluent flow solver. The speed sensor to tower separation distance needed to keep the speed sensor out of the tower-induced flow defect was computed and the safe angle range based on the two major boom configurations often encountered in lattice triangular tower instrumentation from a wind measurement perspective was defined. With the IEC standard boom configuration ($\theta = 0°$), the tower is face-on to the wind and the incident wind is considered perpendicular to the same tower face, giving rise to velocity deficit values that are predicted using the upstream contour profiles of the modified flow. Similar flow analysis was performed on the second and most common boom arrangement, for a boom that is placed parallel to the face of the tower. For each of the boom configurations, a total of 36 incident wind angles were considered. The corresponding boom lengths for each incident wind angle were computed with respect to the reference direction ($\theta = 0°$), and the study concludes thus:

- At Amper-bo and Korabib, a boom length of 2.4 m and 1.76 m respectively, protruding from the tower face, is required to achieve 99 % of the freestream velocity using the IEC standard configuration ($\theta = 0°$). Similarly, when the direction of the booms placed parallel to the tower face is considered as the reference direction, the tower at Amper-bo and Korabib needed approximately 1.3 m boom length to achieve 99% of the free stream velocity. The shorter boom length reported was expected due to the minimum obstructions encountered because of the alignment of the tower legs when the tower face was parallel to the incident wind direction.
- For both boom arrangements on the two towers, boom lengths obtained based on the IEC standard boom configuration ($\theta = 0°$) are long enough to keep the speed sensors out of the tower wakes if winds arrive at the tower at incident angles $\theta = < \pm 70°$ with respect to each boom arrangements reference direction (i.e., $\theta = 0°$). This defines the safe or effective angle range.
- Winds that arrive at the tower between $\pm 90° \geq x < \pm 150°$ with respect to each boom arrangement reference direction will cast their full shadow on the speed sensors. A boom length of approximately $x \geq 7.5$ m and $x \geq 6.5$ m respectively at Amper-bo and Korabib are needed to keep the speed sensors out of the tower wakes. The suitability of a slender boom of this length which might be susceptible to vibration and introduce more errors to the readings of the speed sensors mounted on them is questionable.
- A shorter boom length of $x \geq 4.5$ m to $x \geq 3.5$ m or less for Amper-bo and Korabib towers, respectively, is needed to keep the sensors out of the tower wakes when the incident wind angles are within the range $\pm 150° \leq x \leq \pm 180°$. Although the boom length within this range of incident wind angles appears shorter, a good practice for wind measurement perspective may consider this arrangement, not the most appropriate because any slight shift in the upstream wind direction will completely cast a shadow of the tower on the speed sensors.
- The study further revealed that the boom length computed based on the two popular boom arrangements is independent of the scale and turbulence models used in the CFD flow analysis. Also, complex flow interference was reported within the regions very close to the tower structure with no appreciable increase in boom length due to the presence of the secondary support structures.

In the second section of the study, wind data observed from the collocated speed sensors and the LiDAR captured data were combined to derive a correction factor that accurately predicts the site representative wind speeds when applied

to the wake-affected direction sectors. The following conclusions are drawn from the corrected wake affected direction sector when the direction sector selection rule was applied:

- There is a tremendous improvement in the coefficient of determination R^2 when the corrected wind speed is compared with the reference wind speed. When the correction factor derived using WS4B is applied to WS4, the R^2 value improves from 0.1281 to 0.9901 whereas the Root Means Square Error (RMSE) decreases from 1.338 to 0.386 i.e. when the pair of the raw wind speed is compared with the corrected wind speed. For WS4B, R^2 improved to 0.9817 from 0.0449 after applying the correction factor based on WS4 whereas the RMSE decreases from 0.756 to 0.127.
- The LiDAR observed speed was used as a reference wind speed to derive the correction factor for WS4 and WS4B. The R^2 value obtained when the corrected WS4 is compared to the reference LiDAR wind speed is 0.8897 as against 0.0234 when the raw data were compared, and a corresponding decrease of RMSE from 1.4215 to 0.541. A similar analysis using LiDAR data as reference wind data shows that R_2 is 0.8646 after the correction factor is applied as against 0.0226 obtained when the pair of raw data was compared. The RMSE values also decreased from 0.923 to 0.189.

Finally, the speed sensor to tower separation distance needed to keep the speed sensor away from the tower-induced flow defect was thoroughly investigated using two lattice triangular towers of different construction details and different arrangements. A safe angle range ($\theta = < \pm 70^{o}$) was proposed. Winds that arrive at the tower at other angles outside this range will likely induce error reading on the speed sensor and this explains why towers instrument according to IEC standard still fall short of the 1 % speed deficit recommended. Therefore, accurate instrumentation of the tower from a wind measurement perspective requires a combination of physical modelling and CFD flow simulation at the desired incident wind angle. Thus, based on the accuracy of the correction method proposed, it may no longer be necessary to discard the tower-affected direction sectors in wind analysis.

ACKNOWLEDGMENTS

Initial funding for this project was provided by the Ministry of Foreign Affairs of Denmark, United Kingdom Department for International Development, Ministry of Foreign Affairs of Finland, Austrian Development Agency, and Namibia Power Corporation. Invaluable support is provided by Namibia Energy Institute under Namibia University of Science and Technology. Thanks to Mobile Telecommunication (LTD) Namibia for permitting the instrumentation of their communication towers for the NWRAP project.

REFERENCES

1. *International Electrotechnical Commission (IEC), "Wind energy generation systems – Part 12-1: Power performance measurements of electricity producing wind turbines," International Electrotechnical Commission (IEC), IEC Central Office 3 rue de Varembé CH-1211 Geneva 20, Switzerland, International Standard IEC 61400-12-1:2005(E), Dec. 2005.*
2. *International Electrotechnical Commission (IEC), "Wind energy generation systems – Part 12-1: Power performance measurements of electricity producing wind turbines," International Electrotechnical Commission (IEC), IEC Central Office 3 rue de Varembé CH-1211 Geneva 20, Switzerland, International Standard IEC 61400-12-1:2017-03(en-fr), Mar. 2017. Accessed: Oct. 15, 2018. [Online]. Available: https://webstore.iec.ch/publication/26603.*
3. *M. E. Okorie and F. Inambao, "Tower Wake Distortion Effect: A Comprehensive Review of Methods and Applications",*

International Journal of Engineering Research and Technology, Vol. 13, No. 12, 2020, p. 17, 2020.

4. *V. Bezrukovs, V. Bezrukovs, S. Upnere, L. Gulbe, and D. Bezrukovs, "The Use of Cellular Communication Masts for Wind Share Research," Energetika, Vol. 64, No. 2, 2018, doi: 10.6001/energetika. v64i2.3780.*
5. *M. Lotfi, "Atmospheric Wind Flow Distortion Effects of Meteorological Masts", Master's thesis, University of Porto, Porto, Portugal, 2015.*
6. *S. Fabre, M. Stickland, T. Scanlon, A. Oldroyd, D. Kindler, and F. Quail, "Measurement and Simulation of the Flow Field Around the FINO 3 Triangular Lattice Meteorological Mast," Journal of Wind Engineering and Industrial Aerodynamics, Vol. 130, 2014, pp. 99–107, doi: 10.1016/j.jweia.2014.04.002*
7. *M. Tusch, C. Masson, and P. Héraud, "Modeling of Turbulent Atmospheric Flow Around Tubular and Lattice Meteorological Masts," Journal of Solar Energy Engineering, Vol. 133, No. 1, 2011, p. 011011, 2011, doi: 10.1115/1.4003293*
8. *Jones, David A., and Hanzhen Liu. "Searching for the Tao? Reexamining Modern Changes in Asian Management: Characteristics and Significance." International Journal of Business & General Management 6.5 (2017): 119-134.*
9. *V. Bezrukovs, V. Bezrukovs, S. Upnere, D. Bezrukovs, and A. Sauhats, "The Assessment of Wind Speed Distortions in a Simulated Flow Around a Lattice Cellular Communication Mast," in 2017 European Conference on Electrical Engineering and Computer Science (EECS), Nov. 2017, pp. 421–428, doi: 10.1109/EECS.2017.84.*
10. *OFFIA OLUA, B. L., QC ELUWA, and C. ABUAJAH. "Incorporation of Papain into Ice Cream: Impact on Pawpaw (Carica Papaya) Ice Cream Quality." IASET: International Journal of Biology, Biotechnology and Food Science (IASET: IJBBFS) 1.1: 7-22.*
11. *M. E. Okorie and F. Inambao, "Identification of Tower and Boom-Wakes Using Collocated Anemometers and LiDAR Measurement," International Journal of Mechanical Engineering and Technology, Vol. 10, No. 6, 2019, pp. 72–94.*
12. *K. McCaffrey et al., "Identification of Tower-Wake Distortions Using Sonic Anemometer and LiDAR Measurements," Atmospheric Measurement Techniques, Vol. 10, No. 2, 2017, pp. 393–407, doi: http://dx.doi.org/10.5194/amt-10-393-2017*
13. *M. E. Okorie and F. Inambao, "Prediction of the Impact of Tower Shading on Resource Parameters and Performance by Using LiDAR", Building Services Engineering Research and Technology, Vol. 13, No. 11, 2020, p. 20.*

CHAPTER 7: IMPACT OF FREESTREAM TURBULENCE ON THE BOOM LENGTH

This chapter explores the impact of freestream turbulence on the boom length required to keep the speed sensor out of tower wakes by comparing the CFD flow simulation results that capture the site's realistic freestream turbulence parameters to the simulation results obtained from standard external flow analysis. Extreme cases of laminar flow were also computed and compared with the models that have different turbulence parameters. The chapter concludes that freestream turbulence does not have any significant impact on the boom but makes flow interference more complex within the regions near the wall of the tower. It also increases the drag on the tower and engenders visible inhomogeneity in the flow parameters in the wake of the tower.

Cite this article: M. E. Okorie and F. L. Inambao, "Impact of Freestream Turbulence on the Boom Length," International Journal of Mechanical and Production Engineering Research and Development, vol. 11, no. 4, pp. 341–354, 2021, doi:10.24247/ijmperdaug202126.

Link to the article:

http://www.tjprc.org/publishpapers/2-67-1626785833-IJMPERDAUG202126.pdf

International Journal of Mechanical and Production Engineering Research and Development (IJMPERD)
ISSN (P): 2249–6890; ISSN (E): 2249–8001
Vol. 11, Issue 4, Aug 2021, 341-354

TRANS STELLAR
•Journal Publications •Research Consultancy

Original Article

IMPACT OF FREESTREAM TURBULENCE ON THE BOOM LENGTH

MADUAKO E. OKORIE[1] & Professor FREDDIE L. INAMBAO[2*]

[1]Namibia University of Science and Technology, Windhoek, Namibia. PhD Student, Department of Mechanical Engineering, University of KwaZulu-Natal, Durban, 4041, South Africa

[2]Department of Mechanical Engineering, University of KwaZulu-Natal, Durban, 4041, South Africa*

ABSTRACT

Instrumented towers used for wind measurement are in the region of the atmosphere where atmospheric turbulence is expected to dominate the flow regime. Error readings captured by the speed sensors as a result of tower shadowing are expected to increase due to atmospheric turbulence. Although the understanding is that tower shadowing should be considered as an atmosphericrather than an arbitrary external flow problem, key issues are still unknown, such as the influence of freestream turbulence on the boom length needed to keep the anemometer out of tower wake distortions.This study sought to understand the exact effect of freestream turbulence on boom lengths by performing three-dimensional (3D) computational fluid dynamics (CFD) flow simulation around and through the 3D complex geometry of lattice triangular communication towers located at Amper-bo and Korabib in southern Namibia. The impact of freestream turbulence was investigated by comparing the simulation results that capture the site's realistic freestream turbulence parameters to the simulation results obtained from standard externalflow analysis (5 % turbulence intensity [TI] and 1 m length scale being the default setting in Ansys fluent) at three heights (10 m, 65 m, and 200 m).The shear stress transport (k-ωSST) turbulence model that uses the blending function to activate the k-ω model near the wall, and thek-e model in the free stream region, were adopted. Flow interferences near the tower wall with the boom length at the desired distance upstream from the tower surface were accurately captured. Results from laminar derived flow distortion using the same wind speeds observed at 10 m, 65 m, and 200 m as reference speeds were compared with the previous two approaches with different turbulence parameters. At Amper-bo, based on the International Electro technical Commission(IEC 6400-12-1) standard boom configuration, at 10 m, 65 m and 200 m, the anemometers should be positioned approximately at 1.6L, 1.9L and 2.3L from the tower surface to achieve 99 %, 99.5 % and 101 % of the freestream velocity, respectively. At Korabib, anemometers should be positioned approximately at 0.7L, 0.9L and 1.3L from the tower surface to achieve 99 %, 99.5 % and 101 % of the freestream velocity, respectively. The results show that freestream turbulence does not have a significant impact on the length of boom needed to keep the anemometer out of the tower wake. Speedup at the tower edges and around individual members was used as a measure of how complex the flow interference was. Higher percentage of speeds were computed at all heights using the simulation parameter that captured the sites'environment, while the laminar model generated the least speedup. Again, the results show that drag on each member of the tower increased with increase in turbulence levels. Finally, it is safe to conclude that freestream turbulence does not have any significant impact on the boom but makes flow interference more complex within the regions near the wall of the tower. It also increases the drag on the tower and engenders visible inhomogeneityin the flow parameters in the wake of the tower.

KEYWORDS: Freestream Turbulence, Boom Length, Drag Coefficient, Speedup & Wind Speed

Received: Jun 01 2021; **Accepted**: Jun 21, 2021; **Published**: Jul 20, 2021; **Paper Id.**: IJMPERDAUG202126

1. INTRODUCTION

Instrumented towers used for wind measurement are in the region of the atmosphere where atmospheric turbulence is expected to dominate the flow regime. Tower shadowing contributes a non-negligible error to anemometer readings. The error is expected to increase if the tower is exposed to atmospheric turbulence. Earliest reported literature (i.e.,Cermak, & Horn, 1968; Perrin et al., 2007)opined that turbulence increase does not increase the tower induced flow defect significantly.CFD derived flow distortion was performed on lattice and tubular towers that were modelled as actuator discs(Tusch et al., 2011).The authors reported an increase in tower induced flow distortion due to freestream turbulence increase when compared with International Electrotechnical Commission (IEC) (2005) and IEC (2017). In Fabre et al. (2014), a 3D CFD flow simulation around a complex 3D structure of a lattice triangular tower was performed using $k-\omega SST$ turbulence model in Open FOAM solver (Simple foam).With turbulence intensity (TI) of 5% and length scale (L) calculated as a function of the computational domain, the study showed that tower wake distortion increased due to freestream turbulence when compared with IEC (2005) and IEC (2017).Eidsvik (2014) and Richard and Hoxey (1993)provided a set of equations suitable for modeling atmospheric flow. Furthermore, Lofti (2015) conducted a comparative study on the choice of boundary conditions for modelling atmospheric turbulence. For each of the boundary conditions compared, the author reported an increase in tower wake distortion due to the increased level of turbulence and stated that the approach used in Fabre et al. (2014)leads to under prediction of the boom length at some incident wind angles. The study concluded that tower shadowing should be considered as an atmospheric problem rather than arbitrary external flow problem. Notably, no common approach was adopted for the previous studies. Also, application of the outcomes of previous studies are limited when towers of different configurations, located in different atmospheric conditions in the boundary layer are concerned. On this premise, continuous evaluation is needed, hence this study. This paper sought to understand the exact impact of free stream turbulence on boom length.It was aimed at finding out if it is justified to invest extra resources towards evaluating the phenomenon (tower shadowing) as an atmospheric problem.This vital detail is not found in previous literature. The results of the study will enable stakeholders to make an informed decision on whether or not to invest extra computational costs and other resources in treating towershadings asan atmospheric flow problem. Finally, the outcome of this study contributes to literature and further assists stake holders with required adjustments needed, if any, in order to account for the extra flow perturbations resulting from freestream turbulence influence.

2. BACKGROUND

Amper-bo (25.354°S, 18.313°E) and Schlip (24.030°S, 17.131°E) are the two National Wind Resource Assessment Project (NWRAP) sites selected for this study; they are 1152 m and 1381 m, respectively, above sea level. QinetiQ Ltd (UK) ZephIR Z300 LiDAR was placed near the foot of the instrumented communication towers for wind measurement. The tower construction and instrumentation details are found in Okorie and Inambao (2021a) and Okorie and Inambao (2019). The two tower modules used are equilateral triangular in nature and the construction details are reported in Okorie and Inambao (2021a). The width and height of the tower module at Amper-bo are 1.1 m and 0.89 m, respectively. The tower is constructed with vertical tubular rods (100 mm outer diameter) and a network of angular cross and horizontal bracings. The construction details of the tower at Schlip are the same as the tower at Amper-bo. The tower at Korabib has sharp edges. It has three vertical angle bars (70 mm x 70 mm x 6 mm) and a network of smaller angular cross and horizontal bracings. The width and height of the tower module are 1.320 m and 1.512 m, respectively.

3. GOVERNING EQUATIONS

Fluid flow was governed by the conservation of mass (continuity) and conservation of momentum (RANS equations), shown in Equation 1 and Equation 2, respectively.

$$\frac{\partial \overline{U}_i}{\partial x_i} = 0 \quad (1)$$

$$\frac{\partial(\overline{U}_i \overline{U}_j)}{\partial x_j} = -\frac{\partial \overline{P}}{\partial x_i} + \frac{\partial}{\partial x_j}\left\{\mu_l\left(\frac{\partial \overline{U}_i}{\partial x_j} + \frac{\partial \overline{U}_j}{\partial x_i}\right) - \rho\overline{u_i u_j}\right\} \quad (2)$$

Where $\bar{u}$ is the Reynolds-averaged velocity, $\bar{P}$ is the averaged pressure, μ is the eddy viscosity and $\overline{u_i u_j}$ is the Reynolds stress tensor.

The presence of the stress terms introduces more variables that cannot be fully resolved with the available equations, hence the closure problem. Turbulence modelsoften used in external aerodynamics flow simulationsare therefore employed to resolve the closure problem. The shear stress transport (k-ωSST) turbulence model adopted in this study uses the blending function to activate the k-ω model near the wall and k-e model within the freestream region(Fabre et al., 2014). With the chosen turbulence model, complex flow interference and drag near the tower wall are accurately captured.

The equations used are.

$$\frac{\partial(\rho k)}{\partial t} + \frac{\partial(\rho U_i k)}{\partial x_i} = \widetilde{P}_k - \beta^* \rho k\omega + \frac{\partial}{\partial x_i}\left[\left(\mu + \rho_k \mu_t\right)\frac{\partial k}{\partial x_i}\right] \quad (3)$$

$$\frac{\partial(\rho\omega)}{\partial t} + \frac{\partial(\rho U_i \omega)}{\partial x_i} = \alpha\rho S^2 - \beta\rho\omega^2 + \frac{\partial}{\partial x_i}\left[\left(\mu + \sigma_\omega \mu_t\right)\frac{\partial \omega}{\partial x_i}\right] + 2(1 - F_1)\rho\sigma_{w2}\frac{1}{\omega}\frac{\partial k}{\partial x_i}\frac{\partial \omega}{\partial x_i} \quad (4)$$

According to Fabre et al. (2014), the blending function F1 is defined by:

$$F_1 = \tanh\left\{\left\{\min\left[\max\left(\frac{\sqrt{k}}{\beta^*\omega y}, \frac{500\nu}{y^2\omega}\right), \frac{4\rho\sigma_{\omega 2} k}{CD_{k\omega} y^2}\right]\right\}^4\right\} \quad (5)$$

4. METHODS

The boundary conditions that capture the sites' realistic freestream turbulence parameters were used during flow simulation. In this regard, two sets of equations proposed by Eidsvik (2014) and Richard and Hoxey (1993)(Table 1)were used to compute the friction velocity ($u*$), turbulent kinetic energy(k) and turbulence dispassion rate (e).

Table 1: Equations for Capturing the Flow Variables.

P.J. Richards and R.J. Hoxey, 1993	Karl J. Eidsvik
$u_* = UK/ln(z/z_o)$	$u_* = UK/ln(z/z_o)$
$k = u_*^2/\sqrt{C_\mu}$	$k = u_*^2/\sqrt{C_\mu}\,(1 - z/\delta)^2$
$\varepsilon = u_*^3/Kz$	$\varepsilon = u_*^3/Kz\,(1 - z/\delta)^2$

Notes: where U is the upstream velocity, z is the reference height, z_o is the roughness length, K is Von Karman's constant= 0.4, C_μ = 0.09 and (δ = 1000 m) is the boundary layer thickness considered in (Eidsvik, 2008).

Based on the observed wind data, the site representative turbulence intensity was computed. InIEC (2005) the representative turbulence intensity is used to characterize the site's TI. The representative TI is the mean TI plus 1.28 standard deviation of the mean value, calculated from 15 m/s statistics. The representative TI is equal to the 90th percentile of the mean TI values. The turbulence intensity (TI), turbulence length scale (L) and the specific turbulence dispassion rate (ω) were computed using the equations shown in table 2.

Table 2: Recommended Equations for Computation of Turbulence Flow Parameters

$k = 3/2\,(\overline{U}I)^2$	$\varepsilon = \left(C_{\mu}^{0.75}.k^{1.5}\right)/l$	$\omega = \left(C_{\mu}^{0.75}k^{0.5}\right)/l$

5. BRIEF DESCRIPTION OF THE OBSERVED DATA

The observed data analyzed and reported in this work were captured using LiDAR and speed sensors placed on the communication towers at Amper-bo and Schlip. The LiDAR measured data at Amper-bo for a period of 8.4 months (16th Jan. 2014 to 30th Sept. 2014) and approximately 3 months (31st of Sept. to Dec. 2014) at SchlipOkorie and Inambao (2020).The detailed tower instrumentations at different hub heights and mean speeds captured by LiDAR and anemometers mounted on the towers at Amper-boand Schlip are found in Okorie and Inambao (2020).Apart from the site observed wind speed at each hub height, the roughness length is another parameter that plays a pivotal role in estimation of the friction velocity (u*) needed to compute the turbulent kinetic energy (k) and the turbulent dispassion rate (e). A multi-point fitted log law approach was adopted for computation of the z_0 and the result from both measurement techniques at both sites are summarized in Table 3. The mean and peak values of z_0 obtained from the in-situ measurement wereused in this study because the mean value captures the seasonal variation of z_0, and the monthly peak values indicate the maximum z_0 obtained from the sites (Table 3).

Table 3: Summary of the Mean and Peak values of z0 of at Amper-bo and Schlip in 2014

	Amper-bo		Schlip	
	Mean Value of z_0 (Annual-2014)	**Peak Value of z_0 (June-2014)**	**Mean Value of z_0 (Annual-2014)**	**Peak Value of z_0 (June-2014)**
Anemometers	0.494	1.51	0.0397	0.139
	Mean value of z_0 for 8.4 months	Peak value of z_0 (June-2014	Mean value of z_0 for 3 months	
LiDAR	0.626	1.06	0.0243	-

6. RESULTS AND DISCUSSIONS

6.1 TI and Length Scale Variations with Heights

Based on the models proposed inEidsvik (2008) and Richards and Hoxey (1993), the friction velocity (u*), turbulence kinetic energy (k), and the rate of dispersion of turbulence kinetic energy (e) were computed. Inputting these parameters in the set of equations in table 2, the TI, length scale (L), and turbulence dispersion rate (ω), were obtained. The TI values obtained from Eidsvik (2008) and Richards and Hoxey (1993), equations were compared to the mean and representative TI values obtained from the observed wind data. From Figure 1 it is evident that the TI values generally decrease with height at both sites, as expected. The computed TI values based onEidsvik (2008) and Richards and Hoxey (1993) equations predicted accurately the sites' mean TI values.

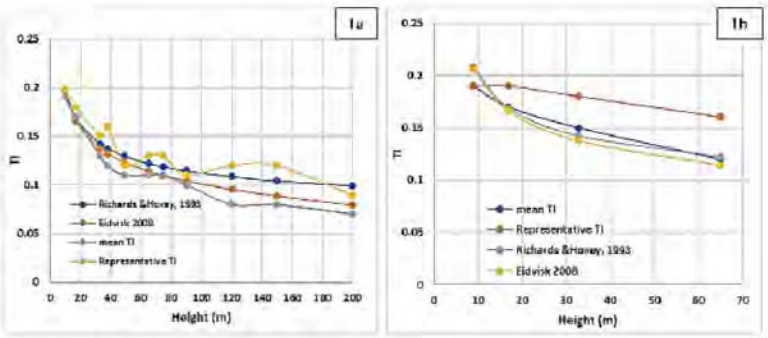

Figure 1a: Calculated TI as Function of Height for the LiDAR Observed Data at Amper-bo.
Figure 1b: Calculated TI as a Function of Height for the in-Situ Measurement at Amper-bo.

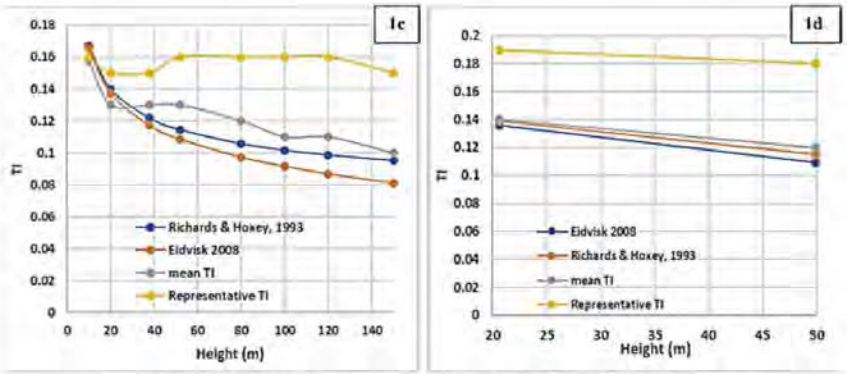

Figure 1c: Calculated TI as Function of Height for LiDAR Data Observed at Schlip.
Figure 1d: Calculated TI as a Function of Height for in-Situ Measured data at Schlip.

The representative TI values were higher than the rest at both sites and with both measurement techniques. The representative TI values were therefore used with other relevant parameters from the sites to calculate the length scale and turbulence dispersion rate. In general, the length scale increased with height (Figure 2) while turbulence dispersion rate (ω) decreased with height. Figures 2a and 2b illustrate the length scales drawn as a function of height for both the LiDAR observed and the in-situ measurement at Amper-bo. Also, Figures 2b and 2c show the variation of the length scale with height for LiDAR and in-situ observed data at Schlip. For both measurement techniques, and at both sites, the length scale computed using the representative TI is higher than the values predicted by Eidsvik (2008) and Richards and Hoxey (1993), models and was more pronounced at Schlip. The over prediction of the length scale at other heights when the representative TI was used as the input parameter was expected, as the representative TI value was obtained at 15 m/s. As a result, Richards and Hoxey (1993)which predicted highest values of TI and length scale among the two models, was adopted and used as simulation parameters.

Freestream turbulence impact was investigated by comparing the simulation results that captured the site's realistic freestream turbulence parameters to the simulation results obtained from standard external flow simulation (5 % turbulence intensity (TI) and 1 m length scale in Ansys default) at three heights (10 m, 65 m, and 200 m). Results from laminar derived flow distortion using the same wind speeds observed at 10 m, 65 m and 200 m as reference speeds were compared with the previous two flow simulations with different turbulence parameters.

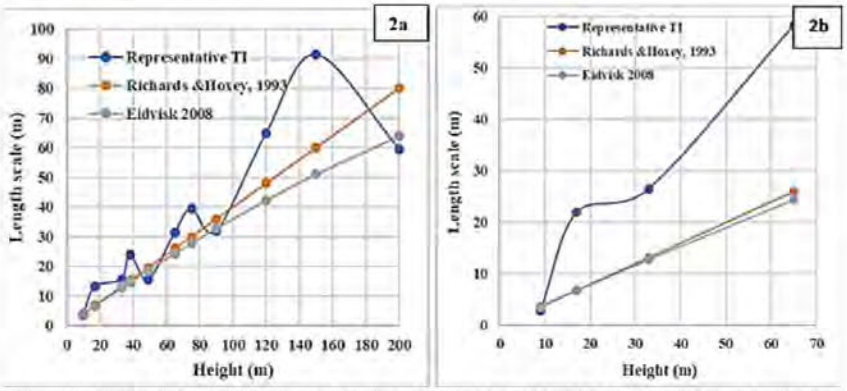

Figure 2a: Calculated Length Scale as a Function of Height for the LiDAR Observed Data at Amper-bo.
Figure 2b: Calculated Length Scale as a Function of Height for the in-Situ Measurement at Amper-bo.

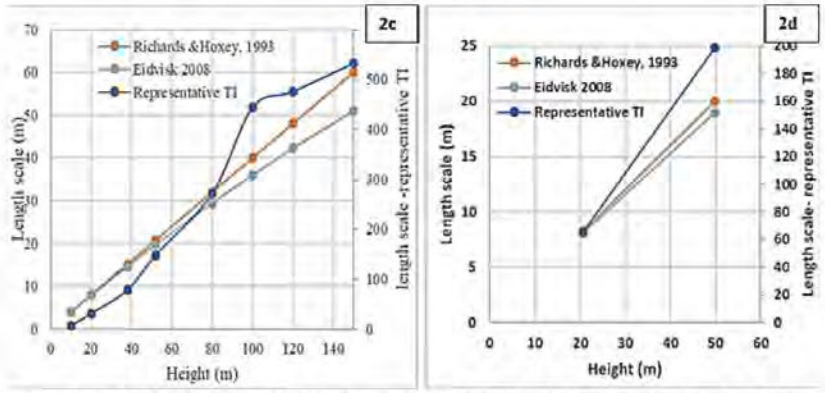

Figure 2c: Calculated Length Scale as a Function of Height for the LiDAR Observed Data at Schlip.
Figure 2d: Calculated Length Scale as a Function of Height for the in-Situ Measurement at Schlip.

6.2 Anemometer Separation Distance from the Tower

Evaluation of the freestream turbulence effect on anemometer separation distance from the tower surface, preferably referred to as the boom length, was the major objective of this paper. Figure 3a is the CFD derived flow distortion over the tower at Amper-bo. The boom length drawn as a function of the normalised velocity from the upstream contour, is

illustrated in figures 3b, 3c and 3d.

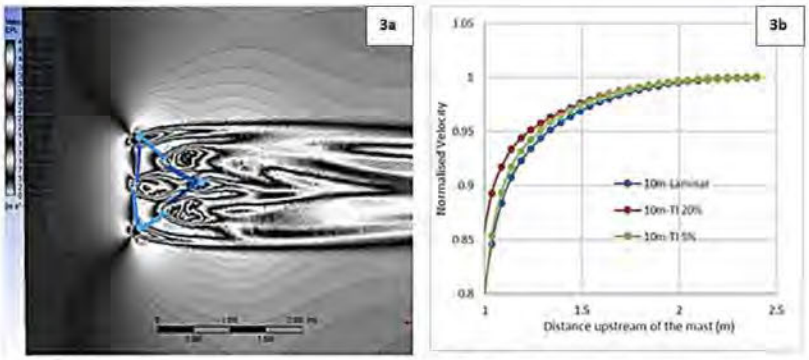

Figure 3a: A 3D CFD Derived Flow Distortion Around the Lattice Triangular Tower at Amper-bo. Figure 3b: The Boom Length from the Tower Surface Drawn as a Function of the Normalised Velocity at 10 m Hub Height of the Tower at Amper-bo.

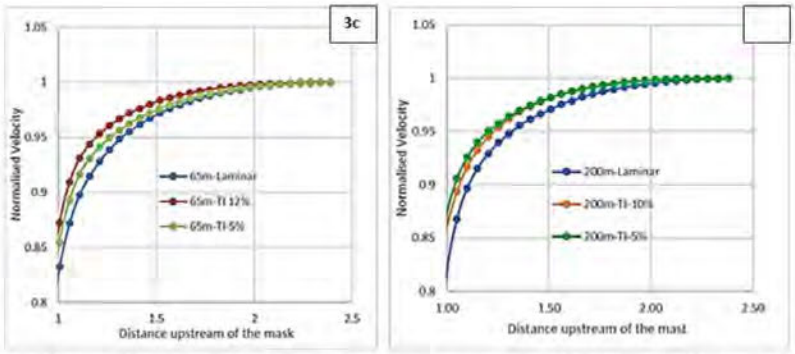

Figure 3c: The Boom Length from the Tower Surface Drawn as a Function of the Normalised Velocity at 65 m Hub Height based on the Tower at Amper-bo. Figure 3d. The Boom Length from the Tower Surface Drawn as a Function of the Normalised Velocity at 65 m Hub Height based on the Tower at Amper-bo.

The boom lengths computed are based on the IEC 6400-12-1 standard boom configuration, where the incident wind is assumed to be perpendicular to the tower face, giving rise to a velocity deficit value that is computed using the upstream contour profile, along the same axis with the incoming winds.

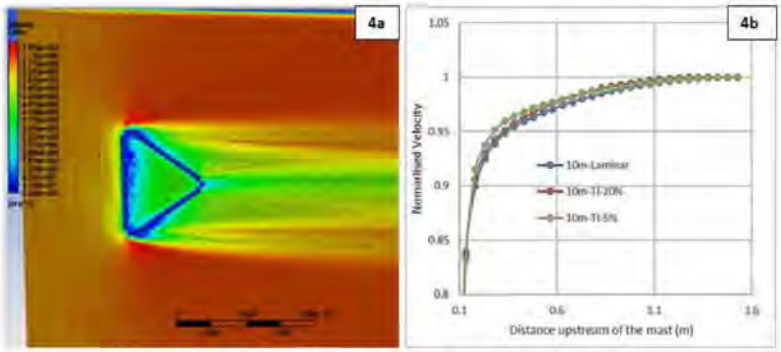

Figure 4a: A 3D CFD Derived flow Distortion around the Lattice Triangular Tower at Korabib.
Figure 4b: The Boom Length from the Tower Surface Drawn as a Function of the Normalised Velocity at 10 m Hub Height of the Tower at Korabib.

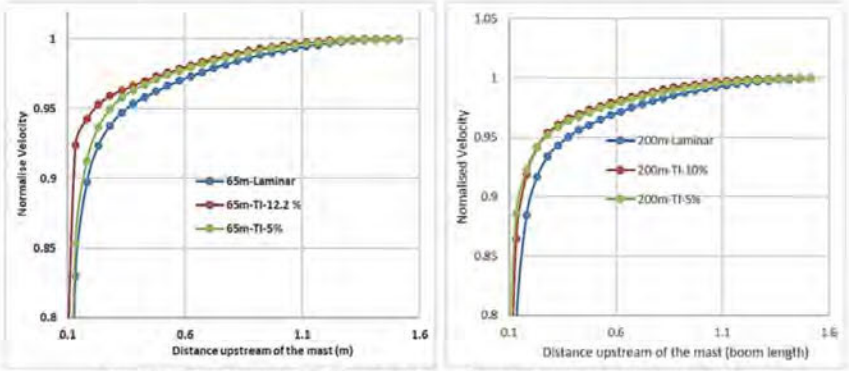

Figure 4c: The Boom Length from the Tower Surface Drawn as a Function of the Normalised Velocity at 65 m Hub Height based on the Tower at Korabib.
Figure 4d: The Boom Length from the Tower Surface Drawn as a Function of the Normalised Velocity at 65 m Hub Height based on the Tower at Korabib.

At Amper-bo the observed wind speeds were 3.7 m/s, 6.3 m/s and 7.5 m/s, at 10 m, 65 m, and 200 m, respectively. For the standard external flow, TI and length scale were 5% and 1 m respectively in Fluent solver. At 10 m height, the calculated TI was 20 %, and the length scale was 4 m. At 65 m height, the calculated TI reduced to 12 % while the length scale increased to 26 m. A further reduction of calculated TI to 10% and a length scale increase of 80 m was computed at 200 m. At the three heights considered, the laminar model appears to produce a more conservative result in the regions very close to the tower wall. The result obtained from the three sets of flow modelling approaches appears to achieve some sort of parity within the region of interest, i.e., at some distance away from the tower surface. The CFD derived flow simulation that captures the realistic site freestream turbulence, the standard external flow approach(5% TI and 1 m length scale) and their laminar counterparts predicted approximately the same boom length.At 10 m, 65 m and 200

m, anemometers should be positioned approximately at 1.6L, 1.9L and 2.3L from the tower surface to achieve 99 %, 99.5 % and 101 % respectively of the freestream velocity.

Again, similar flow modelling approaches and boundary conditions were used on the tower at Korabib (which has sharp edges). The laminar model also appears to produce a more conservative result in the regions nearer to the tower wall, though insignificant since there was no difference in the boom length reported within the region of interest. With this tower configuration (Figure 4), the three flow modelling approaches used at 10 m, 65 m and 200 m are illustrated in Figures 4b, 4e and 4c. Again, anemometers should be positioned approximately at 0.7L, 0.9L and 1.3L from the tower surface to achieve 99 %, 99.5 % and 101 % of the freestream velocity, respectively. The results obtained from the two towers of different configurations, using different simulation parameters, shows that freestream turbulence does not have a significant impact on the boom length required to keep the speed sensors out of the wake distortion effect of the tower. It is noted that the boom length obtained from this computational approach was more conservative when compared to its counterpart as obtained from the centreline velocity deficit expression described in IEC (2017) and Okorie and Inambao (2021a). However, the difference may not be attributed to the effect of freestream turbulence but rather to the numerical approach, coupled with the oversimplification of the complex 3D nature of an operational tower to a 2D actuator disc model. As reported in Okorie and Inambao (2021b)., proper instrumentation of the tower to reduce its shadowing effects requires a combination of physical and numerical modelling, a good understanding of the safe angle range for boom installation, and the prevailing wind pattern on the site.

6.3 Complex Flow Interference and Drag Coefficient

How complex the flow interference around an operational tower is, attributed to its discrete members(IEC, 2017; Okorie and Inambao, 2021a) i.e., horizontal bracings, cross bracings, and other secondary support structures unique to the parent tower's application. Complexflow interference in this context was ascertained by computing the maximum speed-ups at the edges and around other tower discrete members. Regarding the Amper-bo tower, at 10 m height, speed-ups of 34.6 %, 30.2 % and 29.2% were computed from the CFD derived flow distortion when TI of 20 %, TI of 5 % and the laminar models, respectively, were used as the computational parameters. Similarly, at 65 m, speed-ups of 31.1 %, 29.1 % and 27.5 % were obtained from the computation when TI of 12 %, TI of 5 % and the laminar models, respectively, were used. At 200 m height, 30.3 %, 28.9 % and 26.4 % were speed-ups computed from the CFD derived flow distortion when TI of 10 %, TI of 5 % and the laminar models, respectively were used as the computational parameters. Regarding the Korabib tower with sharp edges, at 10 m 30.2 %, 28.6 % and 26.5 % were obtained when TI of 20 %, TI of 5 % and the laminar models, respectively,were used as the computational parameters. Similarly, at 65 m, 28.6%, 27.5 % and 25.5 % respectively, were obtained when TI of 12 %, TI of 5 % and the laminar models, respectively, were used as the computational parameters. For similar computational parameters but for TI of 10%, at 200m, 27.4 %, 26.5 % and 24.3 % were obtained. The percentage speed-up values obtained from the three computational approaches differed. Higher percentage speed-ups were evident using the flow parameters that captured the site's realistic freestream turbulence, followed by the standard external flow approach (5% TI and 1 m turbulence length scale in Ansys fluent) and then the laminar model. The TI and speed-up values decreased with height. The results show that the flow interference was much more complex within the regions close to the tower wall due to the freestream turbulence effect. The percentage difference in speed-ups at each height using different simulation parameters was remarkable. Using Amper-bo tower, the percentage difference was approximately 14.1 % and approximately 11.8% with the Korabib tower, on the average. Though not an area of interest in this study, there was

notable inhomogeneity and a large spread of the flow parameters in the wake as result of freestream turbulence. It may be necessary to ascertain the impact of freestream turbulence on boom vibration and its associated errors in relation to the wind speed captured by the speed sensor. This remains a grey area for further research work since complex flow interference is evidently high within the regions that are very close to the tower surface.

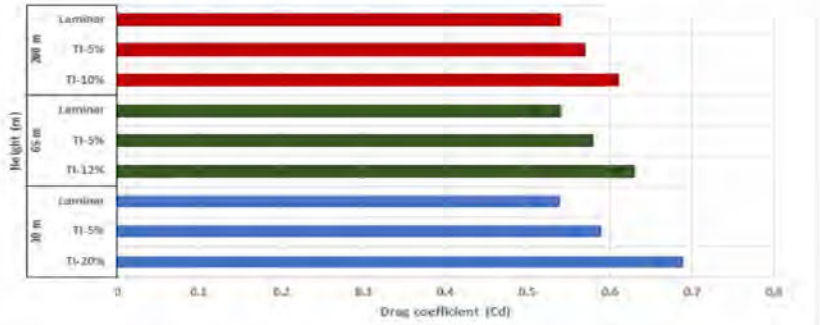

Figure 5: The Drag Coefficients (Cd) based on CFD Flow Simulation Around the Tower at Amperbo using TI and Length Scales Values Computed at Different Heights.

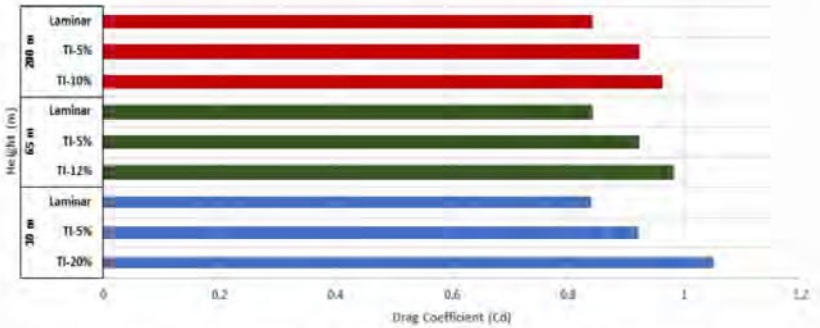

Figure 6: The Drag Coefficients (Cd) based on CFD Flow Simulation Around the Tower at Korabib using TI and Length scales Values Computed at Different Heights.

Figure 5 and Figure 6 are the drag coefficients drawn as a function of the height. The drag coefficient (Cd) obtained from laminar flow over the Amper-bo tower module was approximately 0.54 at all heights whereas a Cd of approximately 0.84 was recorded for the tower at Korabib. Again, based on the standard external flow approach (5% TI and 1 m length scale in Ansys fluent), Cds of approximately 0.59 and 0.92 were computed at all heights using the Amper-bo and Korabib tower modules, respectively. When the simulation parameters that captured the sites realistic freestream turbulence at the three heights were used, Cd values that were somewhat related to the TI values were obtained. Using the tower module at Amper-bo, Cd was 0.69 when TI was 20% at 10 m height, while it was 0.63 for TI value of 12 % at 64 m. At 200 m, Cd was 0.61 when TI was 10%. The Cd computed at 10 m height was 9.5 % and 11.6% higher than the values

obtained at 65 m and 200 m, respectively.

Similarly, using the tower module at Korabib, Cd was 1.05 when TI was 20% at 10 m height, while it was 0.98 for TI value of 12 % at 64 m. At 200 m, Cd was 0.96 when the TI was 10%. The Cd computed at 10 m height was 6.7 % and 8.9% higher than the values obtained at 65 m and 200 m, respectively. Applying the true site freestream characteristics leads to a higher value of Cd when compared to the standard external flow approach and the laminar model. Again, the result showed that increased levels of turbulence increase drag on the induvial members of the tower.

7. CONCLUSIONs

A 3D CFD simulation was performed around two lattice equilateral triangular tower modules of different configurations in order to evaluate the impact of atmospheric turbulence on the boom length needed to keep the anemometer out of the wake distortion effect of the tower. Freestream turbulence impact was investigated by comparing the simulation results that captured the site's realistic freestream turbulence parameters to the simulation results obtained from standard external flow analysis (5 % turbulence intensity [TI] and 1 m length scale in Ansys fluent) at the three heights (10 m, 65 m, and 200 m) considered. The shear stress transport ($k-\omega SST$) turbulence model that used the blending function to activate the $k-\omega$ model near the wall, and the$k-e$ model within the freestream region,were adopted. With the chosen turbulence model, complex flow interference and drag near the tower wall and the boom length at a desired distance upstream from the tower surface were accurately captured. Conclusions based on the derived flow distortion around the towers due to variation of the simulation parameters were as follows:

- The three modelling approaches which hinged on the variation of the CDF simulation parameters, predicted approximately the same length of boom that will keep the speed sensor out of the wake influence of the tower. At 10 m, 65 m and 200 m, anemometers should be positioned approximately at 1.6L, 1.9L and 2.3L from the tower surface to achieve 99 %, 99.5 % and 101 % respectively of the freestream velocity for the tower at Amper-bo. Similarly, at Korabib, anemometers should be positioned approximately at 0.7L, 0.9L and 1.3L from the tower surface to achieve 99 %, 99.5 % and 101 % of the freestream velocity, respectively. The study concludes that atmospheric turbulence does not have a significant impact on the boom length required to keep the speed sensors out of the wake distortion effect of the tower.
- The maximum speed-ups at the edges and around other tower discrete members were evaluated to gain insight into howcomplex the flow interference was within the vicinity of the towers. First, the study noted that this phenomenon was tower dependent. Second, there was evidence that flow interference was more complex due to atmospheric turbulence. Turbulence intensity decreased with height,as did the percentage speed-ups, irrespective of higher wind speed measured at such higher heights. The percentage difference in speed-ups at each height using different simulation parameters was remarkable. At Amper-bo tower the percentage difference was approximately 14.1 % and at Korabib tower it was approximately 11.8%. Notable inhomogeneity and large spread of the flow parameters in the wake as result of freestream turbulence were evident. Though it has no effect on the computed boom length, nonetheless, it may be necessary to ascertain the impact of freestream turbulence on boom vibration and its associated errors in relation to the wind speed captured by the speed sensor. This remains a grey area for further research work since flow interference appears more complex within the regions that are very close to the tower surface.
- The drag coefficients computed using different simulation parameters show that drag on the tower structures

increased due to atmospheric turbulence; hence the higher values of drag coefficients reported when the turbulence level was high.

Finally, this study investigated the effect of atmospheric turbulence on the boom length by using different simulation parameters to perform a 3D CFD flow analysis around two lattice triangular towers with different construction details. There is evidence that flow interference was more complex within the regions nearer to the tower wall due to the increase in turbulence levels. Drag on each member of the tower increased with increase in turbulence levels as well. However, the study concluded that atmospheric turbulence did not increase the length of booms needed to keep the speed sensor out of the tower wakes.

REFERENCES

1. *Cermak, J. E. & J. D. Horn, J. E. (1968). Tower shadow effect.Journal of Geophysical Research (1896-1977), 73(6), 1869–1876. doi: 10.1029/JB073i006p01869.*
2. *Eidsvik, K. (2008). Prediction errors associated with sparse grid estimates of flows over hills.Boundary-Layer Meteorology, 127, 153–172. doi: 10.1007/s10546-007-9247-9.*
3. *Fabre, S., Stickland, M., Scanlon, T., Oldroyd, A., Kindler, D.,& Quail, F. (2014). Measurement and simulation of the flow field around the FINO 3 triangular lattice meteorological mast. Journal of Wind Engineering and Industrial Aerodynamics, 130, 99–107. doi: 10.1016/j.jweia.2014.04.002.*
4. *International Electrotechnical Commission (IEC), (2005). Wind turbines - Part 1: Design requirements. International Standard IEC 61400-1:2005(E), Geneva, Switzerland: IEC.*
5. *International Electrotechnical Commission (IEC).(2005). Wind energy generation systems – Part 12-1: Power performance measurements of electricity producing wind turbines. International Standard IEC 61400-12-1:2005(E).Geneva, Switzerland: IEC.*
6. *International Electrotechnical Commission (IEC). (2017). Wind energy generation systems – Part 12-1: Power performance measurements of electricity producing wind turbines. International Standard IEC 61400-12-1:2017-03(en-fr) Accessed: Oct. 15, 2018. [Online]. Available: https://webstore.iec.ch/publication/26603*
7. *Lofti, M. F. (2015). Atmospheric wind flow distortion effects of meteorological masts. Master's dissertation, University of Porto, Porto, Portugal, 2015.*
8. *Okorie, M. E. & Inambao F. L. (2021b). Local wind flow modifications within the vicinity of a communication tower International Journal of Mechanical and Production Engineering Research and Development,11(3), 421–440. doi: 10.24247/ijmperdjun202135.*
9. *Okorie, M. E. & Inambao, F. L. (2020). Prediction of the impact of tower shading on resource parameters and performance by using LiDAR. Building Services Engineering Research and Technology, 13(11), 3125-3144.*
10. *Okorie, M. E.,& Inambao, F. L. (2019). Identification of tower and boom wakes using collocated anemometers and Lidar measurement. International Journal of Mechanical Engineering and Technology, 10(6), 72–94.*
11. *Okorie, M. E.,& Inambao, F. L. (2021a). Angle dependence of tower wake distortion: A parametric study. International Journal of Mechanical and Production Engineering Research and Development, 11(3), 481-498*
12. *Perrin, D., McMahon, N., Crane, M., Ruskin, H. J., Crane, L., & Hurley, B. (2007). The effect of a meteorological tower on its top-mounted anemometer. Applied Energy, 84, 413–424.*

13. *Richards, P. J.,& Hoxey, R. P. (1993). Appropriate boundary conditions for computational wind engineering models using the k-ε turbulence model.Journal of Wind Engineering and Industrial Aerodynamics, 46–47, 145–153. doi: 10.1016/0167-6105(93)90124-7.*

14. *Tuseh, M., Masson, C., & Héraud, P. (2011). Modeling of turbulent atmospheric flow around tubular and lattice meteorological masts,"Journal of Solar Energy Engineering, 133(1), 011011. doi: 10.1115/1.4003293.*

15. *Parmar, Jigar K., Sunny K. Darji, and Gajendra R. Patel. "Fuzzy Based MPPT Controller of Wind Energy Conversion System using PMSG." International Journal of Electrical and Electronics Engineering (IJEEE) 7.3: 17-30.*

16. *Isaac, Ann Maria, and K. Rathi. "Performance Analysis of Hybrid HVDC Transmission Systems for Connecting Offshore Wind Farm to Onshore Grid." International Journal of Innovative Research in Science, Engineering and Technology 3.5: 201-207.*

17. *Jai Kumar Sharma, Aman Goyal, Mukesh Pandey & Sateesh Kumar, "Design and Analysis of Vertical Axis Wind Turbine Booster at Low Wind Speed", International Journal of Mechanical and Production Engineering Research and Development (IJMPERD), Vol. 10, Issue 3, pp. 13823-13836.*

18. *S. Sivabalan, G. Sathishkumar, S. Sivaganesan & S. Raja, "Aerodynamic Analysis of Horizontal Axis win Turbine Blade for Low Wind Condition", International Journal of Mechanical and Production Engineering Research and Development (IJMPERD) ISSN (P): 2249-6890; ISSN (E): 2249-8001 Special Issue, pp. 316-328*

CHAPTER 8: CONCLUSION AND RECOMMENDATIONS

8.1 Conclusion

This thesis aimed at a combination of light detection and ranging (LiDAR) and in-situ measurements and computational fluid dynamics (CFD) simulations to evaluate the suitability of using mobile telecommunication towers for wind measurement in Namibia. This project falls under the National Wind Resource Assessment Project (NWRAP) of Namibia which is so far the most comprehensive wind measurement in the country. The lattice equilateral triangular communication towers of different configurations instrumented for this wind measurement, belong to the Mobile Telecommunication Limited (MTC) Namibia. Cost reduction and timely commencement of the project necessitated the choice of the available communication towers for this purpose. Holistic evaluation of the site's wind statistics and risks required placing some speed sensors at intermediate heights of the tower using booms. This type of boom arrangement inevitably exposes the speed sensors to tower wake distortion effects and introduces non-negligible errors in the readings of the speed sensors, even where a dedicated mast erected solely for wind measurement is used. The presence of other secondary support structures commonly found in operational towers of this type exacerbate tower induced flow defects due to complex interferences resulting from these discrete members. To take a spot check at each hub height where winds are measured and to also capture undisturbed freestream winds, the LiDAR was deployed at a proximity (2.4 m) to the foot of the tower. The placement of the LiDAR in a close range to the tower enabled comprehensive assessment, evaluation and comparison of the data sets captured by the two measurement techniques. To gain insight into the winds' interaction with the towers, a three-dimensional (3D) CFD derived flow distortion around and through the complex 3D nature of the triangular towers was performed in Ansys fluent solver using different turbulence models ($k-wSST$, k-ω standard equation, k-ε and one equation Spalart-Almaras). The results obtained from different approaches were combined where appropriate for the context of this study and the following conclusions were drawn:

- On the identification of the tower waked direction sectors/regions, the study revealed that the coefficient of determination (R^2) of turbulence intensities (TI) obtained from the collocated speed sensors and the LiDAR observed data appears to be a better descriptor of the wake boundaries when compared to the commonly used traditional speed ratio approach. This is because the perturbations resulting from the tower wakes are more accurately captured by the turbulence level they generate, hence a more

accurate description of the boundaries of the wake affected direction sectors. A new, simpler, and more useful approach to identifying and defining waked boundaries is proposed. The study established that time series wind shear coefficient (WSC) computed from wind data measured at two intermediated heights (binned in < 5° bin of the wind direction interval and drawn as a function of the wind direction), located at approximately the same azimuth from the north, is enough to describe accurately the wake boundaries without the need for a collocated speed sensor.

- The controlling parameters (thrust coefficient [C_T] and the tower leg lengths [L_m]) found in the centreline speed deficit expression provided in the International Electrotechnical Commission (IEC 61400-12-1) standard of which the derivation was based on the reference direction ($\theta = 0°$) are proven to be angle dependent. The boom length is calculated using this expression is based on the IEC 61400-12-1 standard boom configuration ($\theta = 0°$). As a result, the boom length computed thus, does not guarantee that wind observation is accomplished within the recommended industry-accepted accuracy of < 1 % errors between 0° and 360°. This study combined physical modelling and numerical simulations on two towers (at Amper-bo and at Korabib) of different construction details to derive the values of the thrust coefficient (C_{Ti}) and the leg length (L_i) at different incident wind angles. The derived values of the thrust coefficient (C_{Ti}) and the leg length (L_i) were incorporated into the IEC centreline velocity deficit expression to arrive at a modified speed deficit expression used to predict the booms lengths at incident wind angles other than the IEC reference direction ($\theta = 0°$). For each of the towers, a suitable expression for the thrust coefficient was proposed.
- Furthermore, the study proposed a safe angle range $x = \pm \leq \theta°$, i.e., the incident wind angles for which the boom length computed based on the IEC standard configuration ($\theta = 0°$) can effectively keep the speed sensors out of the tower wakes for winds that arrive at the tower within that defined angle range. The safe angle range $\theta = < \pm 70^o$ with respect to each boom configuration reference direction (i.e., $\theta = 0^o$). The proposed safe angle range is applicable to the IEC standard boom configuration and the common boom arrangement (locating the boom parallel to the tower face) found in operational towers.
- On the impact of atmospheric turbulence on the tower induced flow defect, the study concludes that freestream turbulence does not have any significant impact on the boom

such that it is required to keep the speed sensors out of the tower wakes. It rather makes flow interference more complex and tense within the regions near the wall of the tower. It also increases the drag on the tower and engenders visible inhomogeneity on the flow parameters in the wake of the tower. It is relevant to note at this point that considering tower wake distortion as an ordinary external flow problem rather than atmospheric problem is adequate if the emphasis is on the computation of the boom length. This approach will underpredict the drag on the individual tower members and the speedups around and through the tower.

- Physical modelling of the tower structure enabled accurate computation of the solidity ratio to an accuracy of 0.001m. This approach shows that the presence of secondary support structures increased the blockage to wind flow, giving rise to higher C_T which when used in the centreline speed deficit expression prescribed in IEC 61400-12-1 standard, produced longer boom lengths. The study concluded that overestimation of the boom lengths associated with the standard is traceable to how C_T is evaluated and used. In contrast, the computational approach illustrates a more complex flow interference around the towers structure due to secondary support structures with no appreciable increase in boom length. Accurate tower instrumentation for wind measurement perspectives will require a combination of physical and numerical modelling and knowledge of prevailing wind patterns at the site.
- An accurate correction method that removes the need to discard wind data in the wake affected direction sectors during wind analysis was proposed.
- In-situ measurements validated with light detecting and ranging (LiDAR) observations and computational fluid dynamics (CFD) simulations, coupled with physical modelling of the tower structure, were used to evaluate the suitability of using mobile telecommunication towers for accurate wind measurement in Namibia. Accurate tower instrumentation for wind measurement perspective requires a combination of physical and numerical modelling, a good understanding of the safe angle range for proper boom installation and knowledge of prevailing wind pattern at the site. The result obtained from this study will be applicable to towers of different configurations for accurate instrumentation.

8.2 Recommendations

Due to freestream turbulence effects, flow interference is observed to be more complex and tense within the regions close to the tower surface. Although, the study concluded that

freestream turbulence does not have significant effect on the boom length required to keep the speed sensor out of the tower wakes. However, it is expected that the resulting complex flow due to freestream turbulence will increase the vibration of booms mounted on the tower. If such vibration is significant, it will induce more error readings to the speed sensor fixed on the boom. Future research work therefore becomes necessary in other to understand the impact of freestream turbulence on the boom vibrations and how it affects the readings of the speed sensors fixed on them. This may be accomplished by comparing the flow induced perturbations (speed sensor error readings) due to boom vibration when standard external flow simulation is performed around the tower structure to the flow induced perturbations (speed sensor error readings) obtained from flow simulation that captures the effect of atmospheric turbulence on the site. Combination of wind tunnel test and computational flow simulation will generate enough data for validation and are hereby proposed for this future work.

Appendix A: Editing Certificates

The scope of work done by the editor shown in the editing certificates include language, layout and references checks for all the chapters and publications in this thesis.

DR RICHARD STEELE
BA, HDE, MTech(Hom)
HOMEOPATH
Registration No. A07309 HM
Practice No. 0807524
Freelance academic editor
Associate member: Professional Editors' Guild, South Africa

110 Cato Road
Glenwood, Durban 4001
031-201-6508/082-928-6208
Fax 031-201-4989
Postal: P.O. Box 30043, Mayville 4058
Email: rsteele@telkomsa.net

EDITING CERTIFICATE

Re: **Maduako E. Okorie**
Journal article: **Tower Wake Distortion Effect: A comprehensive Review of Methods and Applications**

I confirm that I have edited this article and the references for clarity, language and layout. I returned the document to the author with track changes so correct implementation of the changes and clarifications requested in the text and references is the responsibility of the author. I am a freelance editor specialising in proofreading and editing academic documents. My original tertiary degree which I obtained at the University of Cape Town was a B.A. with English as a major and I went on to complete an H.D.E. (P.G.) Sec. with English as my teaching subject. I obtained a distinction for my Master's dissertation in the Department of Homeopathy at Technikon Natal in 1999 (now the Durban University of Technology). During my 13 years as a part-time lecturer in the Department of Homoeopathy at the Durban University of Technology I supervised numerous Master's degree dissertations.

Dr Richard Steele
18 April 2020
per email

DR RICHARD STEELE
BA, HDE, MTech(Hom)
HOMEOPATH
Registration No. A07309 HM
Practice No. 0807524
Freelance academic editor
Associate member: Professional Editors' Guild, South Africa

110 Cato Road
Glenwood, Durban 4001
031-201-6508/082-928-6208
Fax 031-201-4989
Postal: P.O. Box 30043, Mayville 4058
Email: rsteele@telkomsa.net

EDITING CERTIFICATE

Re: **Maduako E. Okorie**
Journal article: **IDENTIFICATION OF TOWER AND BOOM-WAKES USING COLLOCATED ANEMOMETERS AND LIDAR MEASUREMENT**

I confirm that I have edited this article and the references for clarity, language and layout. I returned the document to the author with track changes so correct implementation of the changes and clarifications requested in the text and references is the responsibility of the author. I am a freelance editor specialising in proofreading and editing academic documents. My original tertiary degree which I obtained at the University of Cape Town was a B.A. with English as a major and I went on to complete an H.D.E. (P.G.) Sec. with English as my teaching subject. I obtained a distinction for my Master's dissertation in the Department of Homeopathy at Technikon Natal in 1999 (now the Durban University of Technology). During my 13 years as a part-time lecturer in the Department of Homoeopathy at the Durban University of Technology I supervised numerous Master's degree dissertations.

Dr Richard Steele
14 March 2019
per email

DR RICHARD STEELE
BA, HDE, MTech(Hom)
HOMEOPATH
Registration No. A07309 HM
Practice No. 0807524
Freelance academic editor
Associate member: Professional Editors' Guild, South Africa

110 Cato Road
Glenwood, Durban 4001
031-201-6508/082-928-6208
Fax 031-201-4989
Postal: P.O. Box 30043, Mayville 4058
Email: rsteele@telkomsa.net

EDITING CERTIFICATE

Re: **Maduako E. Okorie**
Journal article: **Prediction of the Impact of Tower Shading on Resource Parameters and Performance by Using LiDAR**

I confirm that I have edited this article and the references for clarity, language and layout. I returned the document to the author with track changes so correct implementation of the changes and clarifications requested in the text and references is the responsibility of the author. I am a freelance editor specialising in proofreading and editing academic documents. My original tertiary degree which I obtained at the University of Cape Town was a B.A. with English as a major and I went on to complete an H.D.E. (P.G.) Sec. with English as my teaching subject. I obtained a distinction for my Master's dissertation in the Department of Homeopathy at Technikon Natal in 1999 (now the Durban University of Technology). During my 13 years as a part-time lecturer in the Department of Homoeopathy at the Durban University of Technology I supervised numerous Master's degree dissertations.

Dr Richard Steele
23 April 2020
per email

DR RICHARD STEELE
BA, HDE, MTech(Hom)
HOMEOPATH
Registration No. A07309 HM
Practice No. 0807524
Freelance academic editor
Associate member: Professional Editors' Guild, South Africa

110 Cato Road
Glenwood, Durban 4001
031-201-6508/082-928-6208
Postal: P.O. Box 30043, Mayville 4058
Email: rsteele@vodamail.co.za

EDITING CERTIFICATE

Re: **Maduako E. Okorie**
For editing journal article: **Angle Dependence of Tower Wake Distortion: A Parametric Study**

I confirm that I have edited this article and the references for clarity, language and layout. I returned the document to the author with track changes so correct implementation of the changes and clarifications requested in the text and references is the responsibility of the author. I am a freelance editor specialising in proofreading and editing academic documents. My original tertiary degree which I obtained at the University of Cape Town was a B.A. with English as a major and I went on to complete an H.D.E. (P.G.) Sec. with English as my teaching subject. I obtained a distinction for my M.Tech. dissertation in the Department of Homoeopathy at Technikon Natal in 1999 (now the Durban University of Technology). I was a part-time lecturer in the Department of Homoeopathy at the Durban University of Technology for 13 years and supervised many master's degree dissertations during that period.

Dr Richard Steele
13 February 2021
per email

DR RICHARD STEELE
BA, HDE, MTech(Hom)
HOMEOPATH
Registration No. A07309 HM
Practice No. 0807524
Freelance academic editor
Associate member: Professional Editors' Guild, South Africa

110 Cato Road
Glenwood, Durban 4001
031-201-6508/082-928-6208
Postal: P.O. Box 30043, Mayville 4058
Email: rsteele@vodamail.co.za

EDITING CERTIFICATE

Re: **Maduako E. Okorie**
For editing journal article: **Local Wind Flow Modifications Within the Vicinity of a Communication Tower**

I confirm that I have edited this article and the references for clarity, language and layout. I returned the document to the author with track changes so correct implementation of the changes and clarifications requested in the text and references is the responsibility of the author. I am a freelance editor specialising in proofreading and editing academic documents. My original tertiary degree which I obtained at the University of Cape Town was a B.A. with English as a major and I went on to complete an H.D.E. (P.G.) Sec. with English as my teaching subject. I obtained a distinction for my M.Tech. dissertation in the Department of Homoeopathy at Technikon Natal in 1999 (now the Durban University of Technology). I was a part-time lecturer in the Department of Homoeopathy at the Durban University of Technology for 13 years and supervised many master's degree dissertations during that period.

Dr Richard Steele
24 March 2021
per email

DR RICHARD STEELE
BA HDE MTech(Hom)
HOMEOPATH
Registration No. A07309 HM
Practice No. 0807524
Freelance academic editor
Associate member: Professional Editors' Guild, South Africa

110 Cato Road
Glenwood, Durban 4001
031-201-6508/082-928-6208
Postal: P.O. Box 30043, Mayville 4058
Email: rsteele@vodamail.co.za

EDITING CERTIFICATE

Re: **Maduako E. Okorie**

Journal article: **IMPACT OF FREESTREAM TURBULENCE ON THE BOOM LENGTH REQUIRED TO KEEP ANEMOMETER OUT OF TOWER WAKE DISTORTION**

I confirm that I have edited this article and the references for clarity, language and layout. I returned the document to the author with track changes so correct implementation of the changes and clarifications requested in the text and references is the responsibility of the author. I am a freelance editor specialising in proofreading and editing academic documents. My original tertiary degree which I obtained at the University of Cape Town was a B.A. with English as a major and I went on to complete an H.D.E. (P.G.) Sec. with English as my teaching subject. I obtained a distinction for my M.Tech. dissertation in the Department of Homoeopathy at Technikon Natal in 1999 (now the Durban University of Technology). I was a part-time lecturer in the Department of Homoeopathy at the Durban University of Technology for 13 years and supervised many master's degree dissertations during that period.

Dr Richard Steele
19 June 2021
per email

Appendix B: Journal Acceptance Letters and Publication Certificates

Appendix B contains the Journal acceptance letters and Publication certificates issued by the publishers.

IAEME Publication

(Publishers of High Quality Peer Reviewed Refereed Scientific, Engineering & Technology, Medicine and Management International Journals)

www.iaeme.com
editor@iaeme.com
iaemedu@gmail.com

INTERNATIONAL JOURNAL OF MECHANICAL ENGINEERING AND TECHNOLOGY (IJMET)

www.iaeme.com/ijmet/index.asp

SCOPUS INDEXED JOURNAL

http://iaeme.com/IJMET/IJMET_Scopus.asp

Journal Impact Factor (2019): 10.6879 Calculated by GISI (www.jifactor.com)

ISSN Print: 0976 - 6340 ISSN Online: 0976 - 6359

Official Acceptance of Research Paper

Paper ID: IJMET/10/04/2019/IJMET_42637 **Date:** 21-March-2019

Dear **Maduako E. Okorie and Freddie Inambao**

We would like to inform you that your paper titled **"IDENTIFICATION OF TOWER AND BOOM-WAKES USING COLLOCATED ANEMOMETERS AND LIDAR MEASUREMENT"** has been accepted for publication in **International Journal of Mechanical Engineering and Technology (IJMET),** Volume 10, Issue 04, (April 2019) issue of the journal based on the Recommendation of the Editorial Board without any major corrections in the content submitted by the researcher.

This letter is the official confirmation of acceptance of your research paper.

Your research paper will be appearing in IJMET, Volume 10, Issue 04, April 2019.

International Journal of Mechanical Engineering and Technology (IJMET)
Journal Impact Factor (2019): 10.6879 Calculated by GISI
ISSN Print: 0976 – 6340
ISSN Online: 0976 – 6359

Review Comments are attached along with the mail.

Kindly send the Publication fee of **$ 575/- (Online only).** The Online Only mode includes online publication of paper, indexing of paper in more than 20 search engines and soft copy of the publication certificate.

You can transfer the money and send the scan copy of payment made evidence through e-mail.

Plot: 03, Flat- S 1, Poomalai Santosh Pearls Apartment, Plot No. 10, Vaiko Salai 6th Street, Jai Shankar Nagar, Palavakkam, Chennai - 600 041, Tamilnadu, India. Mobile: +91-9884798314, E-mail: editor@iaeme.com

Account Details

Account Number	1911683597
Name of the Account	IAEME Publication
Bank	Kotak Mahindra Bank Ltd
Branch	T. Nagar Branch
Address of the Bank	Ground Floor, Shree Essarar Towers, 41 Venkatnarayana Road, T.Nagar, Chennai - 600017, Tamil Nadu, India
Type of Account	Current
Swift Code	KKBKINBBXXX
IFSC CODE	KKBK0000468
MICR CODE	600485008

Kindly acknowledge the Paper acceptance. Thanks and looking to receive the payment from your side at the earliest.

Thank you.
Yours Sincerely,

Prof. Dr. S. Balasubramanian, Ph.D, DSc
Chief Editor
IAEME Publication
Plot: 03, Flat- S 1,
Poomalai Santosh Pearls Apartment
Plot No. 10, Vaiko Salai 6th Street
Jai Shankar Nagar
Palavakkam, Chennai- 600 041
Tamilnadu, India, Mobile: 09884798314
E-mail: iaemedu@gmail.com
Website: www.iaeme.com

TRANS STELLAR
• Journal Publications • Research Consultancy

Mar 02, 2021

To

Professor Freddie L. Inambao,
UNIVERSITY OF KWAZULU NATAL
PRIVATE BAG X54001
DURBAN
4000
SOUTH AFRICA
VAT NUMBER – 4860209305

Dear Professor Freddie L. Inambao,

Greetings.

Subject: Acceptance of research paper for publication in our International Journal

It's our pleasure to inform you that, after the peer review of your paper, **Titled: "ANGLE DEPENDENCE OF TOWER WAKE DISTORTION: A PARAMETRIC STUDY"** authored by **"Maduako E. Okorie & Freddie L. Inambao"** submitted to us for an evaluation by you on **24th Feb 2021** has been accepted by the Review Board for publishing in **"International Journal of Mechanical and Production Engineering Research and Development (IJMPERD) Journal with ISSN (Print): 2249-6890; ISSN (Online): 2249-8001; Impact Factor (JCC): 9.6246; NAAS Rating: 3.11; IBI Factor: 3.2; ICV 2015:60.6"**

Again, thank you for working with TRANSSTELLAR. We believe that our collaboration will help to accelerate the global knowledge creation and sharing one step further. TRANSSTELLAR looks forward to your final publication package. Please do not hesitate to contact us if you have any further questions.

Thanking you,
Yours sincerely,

Associate Editor
TJPRC Pvt Ltd.

TRANS STELLAR
- Journal Publications - Research Consultancy

Mar 29, 2021

To

Professor Freddie Inambao
University of Kwazulu Natal
Private Bag X54001
Durban
4000
South Africa
Vat Number – 4860209305

Dear Scholar. Professor Freddie Inambao,

Subject: Acceptance of research paper for publication in our International Journal

Greetings.

It's our pleasure to inform you that, after the peer review of your paper, **Titled: "LOCAL WIND FLOW MODIFICATIONS WITHIN THE VICINITY OF A COMMUNICATION TOWER"** authored by **"Maduako E. Okorie & Freddie L. Inambao"** submitted to us for an evaluation by you on **Mar 27, 2021** has been provisionally accepted by the Review Board for publishing in **"International Journal of Mechanical and Production Engineering Research and Development (IJMPERD) journal with ISSN (Print): 2249-6890; ISSN (Online): 2249-8001; Impact Factor (JCC): 9.6246; NAAS Rating: 3.11; IBI Factor: 3.2; Scopus Indexed Journal; ICV 2015:60.6.**

Again, thank you for working with TRANSSTELLAR. We believe that our collaboration will help to accelerate the global knowledge creation and sharing one step further. TRANSSTELLAR looks forward to your final publication package. Please do not hesitate to contact us if you have any further questions.

Thanking you,
Yours sincerely,

For Transstellar Journal Publications & Research Consultancy Pvt. Ltd.
[redacted]
Authorized Signatory

Associate Editor
TJPRC Pvt Ltd.

TRANS STELLAR
- Journal Publications - Research Consultancy

Jun 23, 2021

To

Professor Freddie Inambao
University of Kwazulu Natal
Private Bag X54001
Durban
4000
South Africa
Vat Number – 4860209305

Dear Scholar. Professor Freddie Inambao,

Subject: Acceptance of research paper for publication in our International Journal

Greetings.

It's our pleasure to inform you that, after the peer review of your paper, **Titled: "IMPACT OF FREESTREAM TURBULENCE ON THE BOOM LENGTH"** authored by **"Maduako E. Okorie 1 And Professor Freddie L. Inambao"** submitted to us for an evaluation by you on **Jun 21, 2021** has been provisionally accepted by the Review Board for publishing in **"International Journal of Mechanical and Production Engineering Research and Development (IJMPERD) journal with ISSN (Print): 2249-6890; ISSN (Online): 2249-8001; Impact Factor (JCC): 9.6246; NAAS Rating: 3.11; IBI Factor: 3.2; ICV 2015:60.6.**

Again, thank you for working with TRANSSTELLAR. We believe that our collaboration will help to accelerate the global knowledge creation and sharing one step further. TRANSSTELLAR looks forward to your final publication package. Please do not hesitate to contact us if you have any further questions.

Thanking you,
Yours sincerely,

Associate Editor
TJPRC Pvt Ltd.

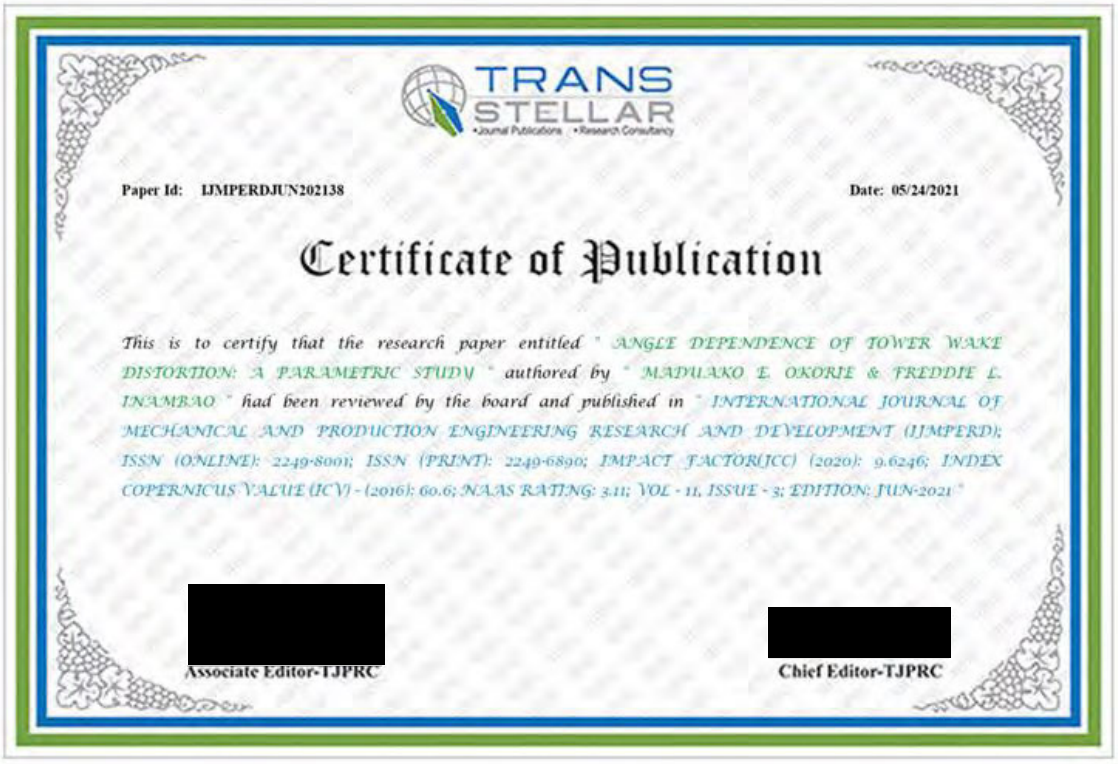

TRANS STELLAR
•Journal Publications •Research Consultancy

Paper Id: IJMPERDJUN202138

Date: 05/24/2021

Certificate of Publication

This is to certify that the research paper entitled " ANGLE DEPENDENCE OF TOWER WAKE DISTORTION: A PARAMETRIC STUDY " authored by " MADUAKO E. OKORIE & FREDDIE L. INAMBAO " had been reviewed by the board and published in " INTERNATIONAL JOURNAL OF MECHANICAL AND PRODUCTION ENGINEERING RESEARCH AND DEVELOPMENT (IJMPERD); ISSN (ONLINE): 2249-8001; ISSN (PRINT): 2249-6890; IMPACT FACTOR(JCC) (2020): 9.6246; INDEX COPERNICUS VALUE (ICV) - (2016): 60.6; NAAS RATING: 3.11; VOL - 11, ISSUE - 3; EDITION: JUN-2021 "

[redacted]
Associate Editor-TJPRC

[redacted]
Chief Editor-TJPRC

IAEME Publication

(Publishers of High Quality Peer Reviewed Refereed Scientific, Engineering & Technology, Medicine and Management International Journals)

www.iaeme.com
editor@iaeme.com
iaemedu@gmail.com

INTERNATIONAL JOURNAL OF MECHANICAL ENGINEERING & TECHNOLOGY (IJMET)

www.iaeme.com/ijmet/index.asp

Paper ID: IJMET_10_06_005

Date: 13-June-2019

Certificate of Publication

This is to certify that the research paper entitled "IDENTIFICATION OF TOWER AND BOOM-WAKES USING COLLOCATED ANEMOMETERS AND LIDAR MEASUREMENT" authored by "Maduako E. Okorie and Freddie Inambao" had been reviewed by the Editorial Board and published in "International Journal of Mechanical Engineering & Technology (IJMET), Volume 10, Issue 06, June 2019, pp. 72-94; ISSN Print: 0976-6340 and ISSN Online: 0976-6359; Journal Impact Factor (2019): 10.6879 Calculated by GISI (www.jifactor.com); InfoBase Index IBI Factor for the year 2015–16 is 3.46; Thomson Reuters' Researcher ID: B-7384-2016".

Chief Editor

[redacted]

Plot: 03, Flat- S 1, Poomalai Santosh Pearls Apartment, Plot No. 10, Vaiko Salai 6th Street, Jai Shankar Nagar, Palavakkam, Chennai - 600 041, Tamilnadu, India.
E-mail: editor@iaeme.com